ESKOM

NUCLEAR SITES
SITE SAFETY REPORTS

NUMERICAL MODELLING OF COASTAL PROCESSES

BANTAMSKLIP

Report No. 1010/3/101

SEPTEMBER 2009

PRESTEDGE RETIEF DRESNER WIJNBERG (PTY) LTD
CONSULTING PORT AND COASTAL ENGINEERS

Numerical Modelling of Coastal Processes - Bantamsklip Report 1010/3/101					
Revision	**Date**	**Author**	**Checked**	**Status**	**Approved**
00	March 2008	SAL	AAM/GKP	Draft for Comment	AAM
01	March 2008	SAL	AAM/GKP	For Use	AAM
02	March 2008	SAL	AAM/GKP	For Use	AAM
03	September 2009	SAL	AAM/GKP	For Use	
Keywords: Numerical modelling, waves, water levels, currents, thermal plume, sediment transport, tsunami, Bantamsklip					

ESKOM

NUCLEAR SITES
SITE SAFETY REPORTS

NUMERICAL MODELLING OF COASTAL PROCESSES
BANTAMSKLIP

TABLE OF CONTENTS

PAGE NO.

1. INTRODUCTION 1

1.1 Background 1
1.2 Scope of work 1
1.3 Limitations 2
1.4 Conventions and terminology 2

2. DESCRIPTION OF NUMERICAL MODELS 3

2.1 Introduction 3
2.2 Wave refraction model 3
2.3 Cross-shore hydrodynamic model 4
2.4 Two-dimensional hydrodynamic model 5
2.5 Three-dimensional hydrodynamic model 5
2.6 Two-dimensional sediment transport model 6
2.7 Suspended sediment model 6
2.8 Extreme value analysis 7
2.9 CORMIX near-field dilution model 7

3. FIELD MEASUREMENTS 8

4. WATER LEVELS 10

4.1 Tides 10
4.2 Extraction of storm surge 10
4.3 Extreme value analysis of storm surge 11

5. TSUNAMI FLOODING 13

5.1 Background 13
5.2 Distant tsunamis 13
5.2.1 Sources 13
5.2.2 Model setup 16
5.2.3 Model calibration 16
5.2.4 Results 17
5.3 Local tsunamis 18
5.3.1 Sources 18
5.3.2 Modelling approach 19
5.3.3 Model setup 19
5.3.4 Slumps modelled 20
5.3.5 Results 21
5.3.6 Discussion 21
5.4 Conclusions 22
5.5 Recommendations 22

6. WAVES 23

6.1 Waves measured at the site 23
6.2 Offshore hindcast data 23
6.3 Model setup 24

6.4 Model calibration 24
6.5 Extreme value analysis of wave height 25
6.6 Wave transformation across surf-zone 26

7. SEAWATER TEMPERATURE 27

7.1 Temperature measured at site 27
7.2 Extreme value analysis of temperature 28

8. CURRENTS 30

8.1 Background 30
8.2 Currents measured at site 30
8.3 Hydrodynamic modelling 31
8.3.1 Model setup 31
8.3.2 Model calibration 32
8.3.3 Selection of representative hydrodynamic conditions 33

9. THERMAL PLUME DISPERSION 35

9.1 Background 35
9.2 Discharge characteristics 35
9.3 Intake and outfall layouts tested 36
9.3.1 Background 36
9.3.2 Layout 1: Offshore tunnel intake (45 m depth) and offshore tunnel outfall (25 m depth) 36
9.3.3 Layout 2: Basin intake and offshore tunnel outfall (40 m depth) 37
9.3.4 Layout 3: Offshore tunnel intake (45 m depth) and nearshore channel outfall (2 m depth) 38
9.3.5 Layout 4: Basin intake and nearshore channel outfall (2 m depth) 38
9.3.6 Layout 5: Offshore tunnel intake (30 m depth) and nearshore channel outfall (5 m depth) 38
9.3.7 Layout 6: Basin intake and nearshore channel outfall (5 m depth) 38
9.4 Model setup 39
9.4.1 Near-field model 39
9.4.2 Far-field model 40
9.5 Results 40
9.5.1 Near-field dilution 40
9.5.2 Far-field temperature and dilution 42
9.5.3 Recirculation 43

10. SEDIMENT TRANSPORT 45

10.1 Background 45
10.2 Sediment grain size 45
10.3 Sediment transport rates 47
10.3.1 Model setup 47
10.3.2 Schematisation of wave and wind climate 47
10.3.3 Model calibration 47
10.3.4 Results 48
10.4 Suspended sediment concentrations 49
10.4.1 Background 49
10.4.2 Measured suspended sediment concentrations 50
10.4.3 Model setup 51
10.4.4 Conditions modelled 52
10.4.5 Results 52

11. CONCLUSIONS AND RECOMMENDATIONS 54

REFERENCES
FIGURES

APPENDIX A: Reference list of DHI applications of the MIKE model to power plants and marine outfalls
APPENDIX B: Report on calibration of wave hindcast data by Fugro Oceanor

APPENDIX C: Council for Geoscience Report: A Probabilistic Tsunami Hazard Assessment for Coastal South Africa from Distant Tsunamogenic Areas

APPENDIX D: Council for Geoscience Report: Potential Sources of Tsunami Along the South African Coast

APPENDIX E: Data Reports on Oceanographic Measurements by Lwandle Technologies

LIST OF TABLES

Table 3.1: Data collection programme 8
Table 3.2: Data measurement sites 9
Table 4.1: Predicted tidal levels at Hermanus 10
Table 4.2: Extreme tidal residuals at Cape Town 11
Table 4.3: Extreme tidal residuals at Mossel Bay 12
Table 5.1: Distant tsunami sources modelled 14
Table 5.2: Fault parameters and vertical seabed displacement 15
Table 5.3: Modelled water levels at Bantamsklip due to distant tsunamis 18
Table 5.4: Slump parameters modelled 20
Table 5.5: Modelled water levels at Bantamsklip due to a theoretical 80 km^3 slump 21
Table 6.1: Extreme wave climate at -30 m CD 26
Table 7.1: Summary statistics of seawater temperatures measured at Bantamsklip Site 28
Table 7.2: Extreme seawater temperatures at three locations in the vicinity of Bantamsklip 29
Table 8.1: Summary statistics of current speeds measured at the Bantamsklip Site 30
Table 9.1: Seawater cooling requirements 35
Table 9.2: Near-field dilution model inputs for Layout 1 39
Table 9.3: Near-field dilution model inputs for Layout 2 40
Table 9.4: Near-field dilution results for Layout 1 41
Table 9.5: Near-field dilution results for Layout 2 41
Table 9.6: Thermal recirculation results 43
Table 10.1: Sediment grain size analysis for Bantamsklip 46
Table 10.2: Measured total suspended solids (TSS) at Bantamsklip Site 50
Table 10.3: Preliminary estimate of sand volume drawn into cooling water intake 53

LIST OF FIGURES

Figure 1.1 : Locality map for Bantamsklip site.
Figure 1.2 : Multi-beam bathymetric survey showing seabed features.
Figure 3.1 : Bathymetry and location of instruments deployed at Bantamsklip.
Figure 4.1 : Analysis of storm surge: Measured tide, predicted tide and residual at Cape Town. Full 40 year dataset.
Figure 4.2 : Analysis of storm surge: Measured tide, predicted tide and residual at Cape Town. Fourteen days including the May 1984 storm event.
Figure 4.3 : Extreme value analysis of positive storm surge at Cape Town.
Figure 4.4 : Extreme value analysis of negative storm surge at Cape Town.
Figure 4.5 : Analysis of storm surge: Measured tide, predicted tide and residual at Mossel Bay. Full 43 year dataset.
Figure 4.6 : Analysis of storm surge: Measured tide, predicted tide and residual at Mossel Bay. Fourteen days including the May 1984 storm event.
Figure 4.7 : Extreme value analysis of positive storm surge at Mossel Bay.
Figure 4.8 : Extreme value analysis of negative storm surge at Mossel Bay.
Figure 5.1 : Model bathymetry used for tsunami modelling of Sumatra and Karachi earthquake events.
Figure 5.2 : Calibration of tsunami model: Measured and modelled water levels due to the tsunami in the Port of Port Elizabeth for the 26 December 2004 Sumatra event.
Figure 5.3 : Maximum water levels predicted during tsunami event. Source is Sumatra A: 26 December 2004 earthquake, $M_w = 9.2$.
Figure 5.4 : Minimum water levels predicted during tsunami event. Source is Sumatra A: 26 December 2004 earthquake, $M_w = 9.2$.
Figure 5.5 : Maximum water levels predicted during tsunami event. Source is Sumatra B: maximum credible earthquake determined by the Council for Geoscience, $M_w = 9.2$.
Figure 5.6 : Minimum water levels predicted during tsunami event. Source is Sumatra B: maximum credible earthquake determined by the Council for Geoscience, $M_w = 9.2$.
Figure 5.7 : Maximum water levels predicted during tsunami event. Source is a Sumatra C: maximum plausible event from Borrero et al (2006), $M_w = 9.3$.
Figure 5.8 : Minimum water levels predicted during tsunami event. Source is a Sumatra C: maximum plausible event from Borrero et al (2006), $M_w = 9.3$.
Figure 5.9 : Maximum water levels predicted during tsunami event. Source is Karachi A: maximum credible earthquake determined by the Council for Geoscience, $M_w = 8.4$.
Figure 5.10 : Minimum water levels predicted during tsunami event. Source is Karachi A: maximum credible earthquake determined by the Council for Geoscience, $M_w = 8.4$.
Figure 5.11 : Model bathymetry used for tsunami modelling of the South Sandwich Islands earthquake events.
Figure 5.12 : Maximum water levels predicted during tsunami event. Source is South Sandwich Islands A: maximum credible earthquake determined by the Council for Geoscience, $M_w = 7.6$.
Figure 5.13 : Minimum water levels predicted during tsunami event. Source is South Sandwich Islands A: maximum credible earthquake determined by the Council for Geoscience, $M_w = 7.6$.
Figure 5.14 : Maximum water levels predicted during tsunami event. Source is South Sandwich Islands B: magnitude increased to $M_w = 8.0$.
Figure 5.15 : Minimum water levels predicted during tsunami event. Source is South Sandwich Islands B: magnitude increased to $M_w = 8.0$.
Figure 5.16 : Top: Main morphological and structural features of submarine slumps (Dingle, 1977). Bottom: Parameters defining slump model (Watts et al, 2003).
Figure 5.17 : Location of slump zones around Southern Africa shown in pink (Dingle et al, 1987).
Figure 5.18 : Model bathymetry used for tsunami modelling due to slumps on the South African shelf margin. Locations of the three slumps modelled are indicated.
Figure 5.19 : Details of the Agulhas Slump (Dingle, 1977).

Figure 5.20 : Maximum water levels predicted during tsunami event. Source is theoretical Agulhas Slump with volume of slumped sediment = 80 km^3.

Figure 5.21 : Minimum water levels predicted during tsunami event. Source is theoretical Agulhas Slump with volume of slumped sediment = 80 km^3.

Figure 5.22 : Maximum water levels predicted during tsunami event. Source is theoretical Cape Town Slump (South) with volume of slumped sediment = 80 km^3.

Figure 5.23 : Minimum water levels predicted during tsunami event. Source is theoretical Cape Town Slump (South) with volume of slumped sediment = 80 km^3.

Figure 5.24 : Maximum water levels predicted during tsunami event. Source is theoretical Cape Town Slump (North) with volume of slumped sediment = 80 km^3.

Figure 5.25 : Minimum water levels predicted during tsunami event. Source is theoretical Cape Town Slump (North) with volume of slumped sediment = 80 km^3.

Figure 6.1 : Wave measurements at Bantamsklip Sites A and B. Time-series of wave parameters (refer to Figure 3.1 for instrument positions).

Figure 6.2 : Wave measurements at Bantamsklip Site B during two storm events. Time-series of wave parameters (refer to Figure 3.1 for instrument positions).

Figure 6.3 : Wave measurements at Bantamsklip Site A (refer to Figure 3.1 for instrument position). Wave rose and histogram of wave heights.

Figure 6.4 : Wave measurements at Bantamsklip Site B (refer to Figure 3.1 for instrument position). Wave rose and histogram of wave heights.

Figure 6.5 : Time-series of offshore wave hindcast parameters. Position is 60 km south-west of Bantamsklip in 180 m depth at position E 19.0°, S 35.0° (refer to Figure 6.7).

Figure 6.6 : Rose and histogram of offshore wave hindcast data. Position is 60 km south-west of Bantamsklip in 180 m depth at position E 19.0°, S 35.0° (refer to Figure 6.7).

Figure 6.7 : Numerical mesh used for wave refraction modelling.

Figure 6.8 : Calibration of wave model. Measured and modelled time-series of wave parameters at Site A (refer to Figure 3.1 for location).

Figure 6.9 : Calibration of wave model. Measured and modelled time-series of wave parameters at Site B (refer to Figure 3.1 for location).

Figure 6.10 : Example of wave refraction from offshore to Bantamsklip site. Deepwater wave condition: H_{m0} = 9.2 m, T_p = 16.4 s, Mean direction = 221°.

Figure 6.11 : Example of wave refraction from offshore to Bantamsklip site. Deepwater wave condition: H_{m0} = 9.2 m, T_p = 16.4 s, Mean direction = 221°.

Figure 6.12 : Characterisation of storm waves refracted to -30 m CD depth contour at Bantamsklip site. Position is Point 1 (see Fig 6.11). Includes only storms where the offshore H_{m0} > 4.5 m.

Figure 6.13 : Extreme value analysis of waves at -30 m CD depth at Bantamsklip. Position is Point 1 (see Fig 6.11).

Figure 6.14 : Example of cross-shore wave transformation modelling from -30 m CD depth to shoreline.

Figure 7.1 : Seawater temperatures measured at Bantamsklip for SSR. (Refer to Figure 3.1 for instrument positions).

Figure 7.2 : Seawater temperatures measured at Bantamsklip by Bayworld (2008, 2009). (Refer to Figure 3.1 for instrument positions).

Figure 7.3 : Seawater temperatures measured in surf-zone at Cape Agulhas, Gansbaai and Hermanus (refer to Figure 1.1 for locations).

Figure 7.4 : Histograms of measured seawater temperatures in surf-zone at Cape Agulhas, Gansbaai and Hermanus (refer to Figure 1.1 for locations).

Figure 7.5 : Extreme Value Analysis of measured seawater temperatures in surf-zone at Cape Agulhas.

Figure 7.6 : Extreme Value Analysis of measured seawater temperatures in surf-zone at Gansbaai.

Figure 7.7 : Extreme Value Analysis of measured seawater temperatures in surf-zone at Hermanus.

Figure 8.1 : Current measurements at Site A (refer to Figure 3.1 for position). Time-series of near surface and near bottom currents.

Figure 8.2 : Current measurements at Site B (refer to Figure 3.1 for position). Time-series of near surface and near bottom currents.

Figure 8.3 : Current measurements at Sites A and B (refer to Figure 3.1 for locations). Near surface and near seabed current rose plots.

Figure 8.4 : Numerical mesh and bathymetry used for hydrodynamic modelling.

Figure 8.5 : Calibration of hydrodynamic model: current speed and direction. Measured and modelled time-series of currents at Bantamsklip Site B for period April and May 2008. (refer to Figure 3.1 for location).

Figure 8.6 : Calibration of hydrodynamic model: current speed and direction. Measured and modelled time-series of currents at Bantamsklip Site A for period April and May 2008. (refer to Figure 3.1 for location).

Figure 8.7 : Calibration of hydrodynamic model: current speed and direction. Measured and modelled time-series of currents at Bantamsklip Site A for period July 2008. (refer to Figure 3.1 for location).

Figure 8.8 : Calibration of hydrodynamic model: thermal plume dispersion at Koeberg. Modelled surface temperatures at 11:00 and measured surface temperatures between 11:20 and 11:50 on 14 October 1985. Vectors show modelled currents.

Figure 8.9 : Calibration of hydrodynamic model: thermal plume dispersion at Koeberg. Modelled surface temperatures at 12:00 and measured surface temperatures between 11:30 and 12:15 on 16 October 1985. Vectors show modelled currents.

Figure 8.10 : Calibration of hydrodynamic model: thermal plume dispersion at Koeberg. Modelled surface temperatures at 12:00 and measured surface temperatures between 11:18 and 12:10 on 18 October 1985. Vectors show modelled currents.

Figure 8.11 : Wave and wind time-series used in hydrodynamic and plume modelling. 14 day summer simulation period.

Figure 8.12 : Wave and wind time-series used in hydrodynamic and plume modelling. 14 day winter simulation period.

Figure 8.13 : Wave and wind time-series used in hydrodynamic and plume modelling. 14 day calm simulation period.

Figure 9.1 : Layout 1: Offshore tunnel intake (45 m depth) and offshore tunnel outfall (25 m depth).

Figure 9.2 : Layout 2: Basin intake and offshore tunnel outfall (40 m depth).

Figure 9.3 : Layout 3: Offshore tunnel intake (45 m depth) and nearshore channel outfall (2 m depth).

Figure 9.4 : Layout 4: Basin intake and nearshore channel outfall (2 m depth).

Figure 9.5 : Layout 5: Offshore tunnel intake (30 m depth) and nearshore channel outfall (5 m depth).

Figure 9.6 : Layout 6: Basin intake and nearshore channel outfall (5 m depth).

Figure 9.7 : Near-field dilution modelling results. Layout 1: Offshore tunnel outfall in 25 m depth.

Figure 9.8 : Near-field dilution modelling results. Layout 2: Offshore tunnel outfall in 40 m depth.

Figure 9.9 : Example of modelled currents and thermal plume near water surface at a time when the currents are northward. Layout 6: Basin intake and nearshore channel outfall (5 m depth).

Figure 9.10 : Example of modelled currents and thermal plume near water surface at a time when the currents are southward. Layout 6: Basin intake and nearshore channel outfall (5 m depth).

Figure 9.11 : Thermal plume modelling: Mean increase in temperature due to power station. Layout 1: Offshore tunnel intake (45 m depth) and offshore tunnel outfall (25 m depth). Power output: 10 000 MWe.

Figure 9.12 : Thermal plume modelling: Maximum increase in temperature due to power station. Layout 1: Offshore tunnel intake (45 m depth) and offshore tunnel outfall (25 m depth). Power output: 10 000 MWe.

Figure 9.13 : Thermal plume modelling: Mean increase in temperature due to power station. Layout 2: Basin intake and offshore tunnel outfall (40 m depth). Power output: 10 000 MWe.

Figure 9.14 : Thermal plume modelling: Maximum increase in temperature due to power station. Layout 2: Basin intake and offshore tunnel outfall (40 m depth). Power output: 10 000 MWe.

Figure 9.15 : Thermal plume modelling: Mean increase in temperature due to power station. Layout 3: Offshore tunnel intake (45 m depth) and nearshore channel outfall (2 m depth). Power output: 10 000 MWe.

Figure 9.16 : Thermal plume modelling: Maximum increase in temperature due to power station. Layout 3: Offshore tunnel intake (45 m depth) and nearshore channel outfall (2 m depth). Power output: 10 000 MWe.

Figure 9.17 : Thermal plume modelling: Mean increase in temperature due to power station. Layout 4: Basin intake and nearshore channel outfall (2 m depth). Power output: 10 000 MWe.

Figure 9.18 : Thermal plume modelling: Maximum increase in temperature due to power station. Layout 4: Basin intake and nearshore channel outfall (2 m depth). Power output: 10 000 MWe.

Figure 9.19 : Thermal plume modelling: Mean increase in temperature due to power station. Layout 5: Offshore tunnel intake (30 m depth) and nearshore channel outfall (5 m depth). Power output: 10 000 MWe.

Figure 9.20 : Thermal plume modelling: Maximum increase in temperature due to power station. Layout 5: Offshore tunnel intake (30 m depth) and nearshore channel outfall (5 m depth). Power output: 10 000 MWe.

Figure 9.21 : Thermal plume modelling: Mean increase in temperature due to power station. Layout 6: Basin intake and nearshore channel outfall (5 m depth). Power output: 10 000 MWe.

Figure 9.22 : Thermal plume modelling: Maximum increase in temperature due to power station. Layout 6: Basin intake and nearshore channel outfall (5 m depth). Power output: 10 000 MWe.

Figure 9.23 : Thermal plume modelling: Mean increase in temperature due to power station. Layout 1: Offshore tunnel intake (45 m depth) and offshore tunnel outfall (25 m depth). Power output: 4000 MWe.

Figure 9.24 : Thermal plume modelling: Maximum increase in temperature due to power station. Layout 1: Offshore tunnel intake (45 m depth) and offshore tunnel outfall (25 m depth). Power output: 4000 MWe.

Figure 9.25 : Thermal plume modelling: Mean increase in temperature due to power station. Layout 6: Basin intake and nearshore channel outfall (5 m depth). Power output: 4000 MWe.

Figure 9.26 : Thermal plume modelling: Maximum increase in temperature due to power station. Layout 6: Basin intake and nearshore channel outfall (5 m depth). Power output: 4000 MWe.

Figure 9.27 : Thermal plume modelling: time-series of recirculation results showing the increase in temperature at the intakes for the various layouts and power outputs modelled.

Figure 10.1 : Sediment transport modelling. Measured D_{50} grain size.

Figure 10.2 : Sediment transport modelling. Testing of wave and current modules in a simplified model comprising a uniform 1:67 beach slope with a wave approaching 30° from normal.

Figure 10.3 : Sediment transport modelling. Testing of the coupled wave, current and sediment transport model for a simplified case with a uniform 1:67 beach slope and a wave approaching 30° from normal.

Figure 10.4 : Sediment transport modelling: Model calibration. Sediment transport entering the intake basin at the existing Koeberg power station.

Figure 10.5 : Sediment transport modelling: Potential net sediment transport rate. Layout 1: Offshore tunnel intake and offshore tunnel outfall. D_{50} = 0.2 mm. Overview plot.

Figure 10.6 : Sediment transport modelling: Potential net sediment transport rate. Layout 1: Offshore tunnel intake and offshore tunnel outfall. D_{50} = 0.2 mm. Detailed view.

Figure 10.7 : Sediment transport modelling: Potential net sediment transport rate. Layout 2: Basin intake and offshore tunnel outfall. D_{50} = 0.2 mm. Detailed view.

Figure 10.8 : Sediment transport modelling: Potential net sediment transport rate. Layout 5: Offshore tunnel intake and nearshore channel outfall. D_{50} = 0.2 mm. Detailed view.

Figure 10.9 : Sediment transport modelling: Potential net sediment transport rate. Layout 6: Basin intake and nearshore channel outfall. D_{50} = 0.2 mm. Detailed view.

Figure 10.10 : Sediment transport modelling: Potential net sediment transport rate. Layout 1: Offshore tunnel intake and offshore tunnel outfall. D_{50} = 0.15 mm. Detailed view.

Figure 10.11 : Sediment transport modelling: Potential net sediment transport rate. Layout 1: Offshore tunnel intake and offshore tunnel outfall. D_{50} = 0.3 mm. Detailed view.

Figure 10.12 : Measured total suspended solids.

Figure 10.13 : Example of modelled vertical profile of suspended sand concentration.

1. INTRODUCTION

1.1 Background

Eskom have embarked on a Nuclear Sites Programme as part of their overall Nuclear Programme. The purpose of the programme is to identify the most suitable nuclear sites to meet the requirements of sufficiency for a "Strategic reserve of banked potential sites" through a Nuclear Siting Investigation Programme implemented to internationally accepted standards, according to best practice and in line with authority requirements (e.g. the National Nuclear Regulator) as appropriate.

To this end, Eskom have embarked on a programme to prepare licenceable Site Safety Reports (SSR's) for three sites, namely Duynefontein, Bantamsklip and Thyspunt. SSR's are licensing documents that are submitted to the national nuclear regulatory authority in support of obtaining a site licence. The data incorporated into the SSR's contain site-related information spanning the site life-cycle phases from Nuclear Siting Investigations through construction, commissioning, operation, decommissioning, to site reuse and thereafter.

Prestedge Retief Dresner Wijnberg (Pty) Ltd (PRDW), as part of a multi-disciplinary team preparing the SSR's, are responsible for the Oceanography and Coastal Engineering Chapters of the Site Safety Report, which are required to be prepared in accordance with Eskom's Technical Specification for this work. This report on the Numerical Modelling of Coastal Processes, along with the Coastal Engineering Investigations Report (PRDW, 2009a), detail the studies undertaken in support of the SSR Chapter on Oceanography and Coastal Engineering. Due to space constraints the SSR contains a summary of the methodology and results, whilst these two supporting reports provide additional details on the studies undertaken. This report describes the Bantamsklip site (see Figures 1.1 and 1.2 for location), whilst similar reports have been prepared for the Duynefontein and Thyspunt sites.

1.2 Scope of work

The scope of work is to characterise the following parameters at the Bantamsklip site:

- Water levels
- Tsunami flooding
- Wave height, period and direction
- Seawater temperatures
- Currents
- Thermal plume dispersion and recirculation for typical intake and outfall configurations
- Sediment transport
- Suspended sediment concentrations.

1.3 Limitations

As required by Eskom's Technical Specification for this work, this study analyses return periods up to $1:10^6$ years for water levels, waves and sea temperatures. Since these predictions are based on the available measured or hindcast datasets covering only the last 13 to 30 years, the predictions for return periods longer than 50 to 100 years need to be interpreted with caution.

1.4 Conventions and terminology

The following conventions and terminology are used in this report:

- Wave direction is the direction from which the wave is coming, measured clockwise from true north.
- Wind direction is the direction from which the wind is coming, measured clockwise from true north.
- Current direction is the direction towards which the current is flowing, measured clockwise from true north.
- H_{m0} is the significant wave height, determined from the zeroth moment of the wave energy spectrum. It is approximately equal to the average of the highest one-third of the waves in a given sea state.
- T_p is the peak wave period, defined as the wave period with maximum wave energy density in the wave energy spectrum.
- Mean wave direction is defined as the mean direction calculated from the full two-dimensional wave spectrum by weighting the energy at each frequency.
- D_N is the diameter for which N% of the sediment, by mass, has a smaller diameter, e.g. D_{50} is the median grain diameter.
- Time is South African Standard Time (Time Zone -2).
- Seabed and water levels are measured relative to Chart Datum, which corresponds to Lowest Astronomical Tide (LAT) for Hermanus. Chart Datum is 0.788 m below Mean Sea Level or Land Levelling Datum (South African Tide Tables, 2008).
- The map projection system is as follows:

Map projection:	Gauss Conformal
Datum:	Hartebeesthoek 94
Spheroid:	WGS84
Scale factor:	1
Central meridian:	19°E
Reference system:	WG19
Co-ordinates:	Eastings (X, increasing eastwards)
	Northings (Y, increasing northwards)
Distance units:	International metre

2. DESCRIPTION OF NUMERICAL MODELS

2.1 Introduction

The numerical modelling has been undertaken using the MIKE suite of models developed by Danish Hydraulics Institute (DHI). The MIKE suite of models is the most comprehensive professional coastal engineering software suite currently available. This means that all the modelling for this project is being conducted using the same suite of integrated models, thus employing the same pre- and post-processing tools, numerical grids, data structures, and allowing direct coupling of the output of one model with the input to the next model. This increases the reliability of the results by minimising any errors associated with interfacing models and data structures from different sources.

The software is under continual development, testing and application by Danish Hydraulic Institute's more than 750 employees based in more than 25 countries worldwide. Major software updates occur annually and minor updates occur quarterly on average. The latest version is Release 2008 Service Pack 3, which is being used for the modelling described below. The software has been employed by DHI alone on more than 80 power, desalination and industrial plants worldwide.

A reference list of DHI applications of the MIKE model to power plants and marine outfalls is included in Appendix A. Validation documents, user manuals and scientific documentation for each model is available on request.

2.2 Wave refraction model

The MIKE 21 Spectral Waves Flexible Mesh model (DHI, 2008a) is used for wave refraction modelling. The model simulates the growth, decay and transformation of wind-generated waves and swell in offshore and coastal areas using unstructured meshes.

MIKE 21 SW includes two different formulations:

- Directional decoupled parametric formulation
- Fully spectral formulation.

The directional decoupled parametric formulation is based on a parameterization of the wave action conservation equation. The parameterization is made in the frequency domain by introducing the zeroth and first moment of the wave action spectrum as dependent variables.

The fully spectral formulation is based on the wave action conservation equation, where the directional-frequency wave action spectrum is the dependent variable.

MIKE 21 SW includes the following physical phenomena:

- Wave growth by action of wind
- Non-linear wave-wave interaction
- Dissipation due to white-capping
- Dissipation due to bottom friction
- Dissipation due to depth-induced wave breaking
- Refraction and shoaling due to depth variations
- Wave-current interaction
- Effect of time-varying water depth and flooding and drying.

The discretization of the governing equation in geographical and spectral space is performed using cell-centred finite volume method. In the geographical domain, an unstructured mesh technique is used. The time integration is performed using a fractional step approach where a multi-sequence explicit method is applied for the propagation of wave action.

MIKE 21 SW is also used in connection with the calculation of the sediment transport, which for a large part is determined by wave conditions and associated wave-induced currents. The wave-induced current is generated by the gradients in radiation stresses that occur in the surf zone. MIKE 21 SW can be used to calculate the wave conditions and associated radiation stresses. Subsequently the wave-induced flow is calculated using the MIKE 21 Flow Model FM.

2.3 Cross-shore hydrodynamic model

The cross-shore hydrodynamic engine of the LITPACK model (DHI, 2008b) has been applied to model wave set-up and the transformation of wave heights across the surf-zone.

The hydrodynamic model includes a description of propagation, shoaling and breaking of waves, calculation of the driving forces due to radiation stress gradients, momentum balance for the cross-shore and longshore direction giving the wave set-up and the longshore current velocities. The model can be applied on complex coastal profiles with longshore bars. In the case of a longshore bar the broken waves can reform in the trough onshore of the bar. The waves can be treated as regular or irregular, and the effect of directional spreading can be included in the description.

For irregular waves, the Battjes and Janssen approach is applied in this study. The statistical description of the wave heights is a truncated Rayleigh distribution where the upper bound is the local maximum wave height. The mean wave energy balance equation is applied to calculate the RMS-value of the wave heights across the coastal/beach profile. The wave period is fixed.

2.4 Two-dimensional hydrodynamic model

The two-dimensional hydrodynamic model used is the MIKE 21 Flow Model (DHI, 2008c). The model is used to simulate tsunami propagation and transformation. MIKE 21 is a general purpose numerical modelling system for the simulation of water levels and flows in estuaries, bays and coastal areas. The model solves the two-dimensional shallow water equations (conservation of mass and vertically-integrated momentum) on a series of dynamically-nested rectangular grids using the Alternating Direction Implicit (ADI) technique. The solver is second to third-order accurate in the convective momentum terms.

MIKE 21 Flow includes the following physical phenomena relevant to tsunami simulations:

- Bottom friction
- Flooding and drying, i.e. tsunami run-up on a beach
- Coriolis forcing.

2.5 Three-dimensional hydrodynamic model

The three-dimensional hydrodynamic model used is the MIKE 3 Flow Flexible Mesh Model (DHI, 2008d). The model is used to simulate the three-dimensional tidal, wind and wave-driven currents and the thermal plume dispersion. The model is based on the numerical solution of the three-dimensional incompressible Reynolds averaged Navier-Stokes equations invoking the assumptions of Boussinesq and of hydrostatic pressure. The model consists of the continuity, momentum, temperature, salinity and density equations and is closed by a k-ε vertical turbulence closure scheme. Horizontal eddy viscosity is modelled with the Smagorinsky formulation.

The time integration of the shallow water equations and the transport equations is performed using a semi-implicit scheme, where the horizontal terms are treated explicitly and the vertical terms are treated implicitly. In the vertical direction a structured mesh, based on a sigma-coordinate transformation is used, while the geometrical flexibility of the unstructured flexible mesh comprising triangles or rectangles is utilised in the horizontal plane.

MIKE 3 Flow Model includes the following physical phenomena:

- Currents due to tides
- Currents due to wind stress on the water surface
- Currents due to waves: the second order stresses due to breaking of short period waves can be included using the radiation stresses computed in the MIKE 21 SW model
- Coriolis forcing
- Bottom friction
- Flooding and drying

- Advection and dispersion of heat, salt and other constituents
- Effect of water temperature and salinity on density and turbulence (baroclinic mode)
- Heat exchange with the atmosphere: the exchange is calculated for the processes of long wave radiation, sensible heat flux (convection), short wave radiation and latent heat flux (evaporation).

2.6 Two-dimensional sediment transport model

The sediment transport model used is the MIKE 21 Flow Model FM, Sand Transport Model (DHI, 2008e). The model comprises a dynamic coupling between the following modules:

- Spectral wave module
- Hydrodynamic module
- Sand transport module.

The spectral wave module is MIKE 21 SW as described in Section 2.2. The hydrodynamic module is the MIKE 21 Flow Flexible Mesh Model, which is the two-dimensional version of the model described in Section 2.5.

The Sand Transport Module calculates the transport of non-cohesive sediment based on the combination of flow conditions from the hydrodynamic module and wave conditions from the wave module. For the case of combined wave and currents, sediment transport rates are derived by linear interpolation in a sediment transport lookup table. The values in the table are calculated by the quasi three-dimensional sediment transport model (STPQ3D). STPQ3D calculates instantaneous and time-averaged hydrodynamics and sediment transport in two horizontal directions. As the model calculates the bed load and the suspended load separately, the values in the sediment transport table are the total load.

The temporal and vertical variations of shear stress, turbulence, flow velocity and sediment concentrations are resolved. The time evolution of the boundary layer due to combined wave/current motion is solved by means of an integrated momentum approach. The force balance includes contributions from the near bed wave orbital motion, forces associated with wave breaking (gradients of radiation stresses) and the sloping water surface. Note that equilibrium sediment transport conditions are assumed, i.e. the sediment transport reacts instantaneously to the wave and current conditions.

2.7 Suspended sediment model

The LITSTP engine of the LITPACK model (DHI, 2008b) has been applied to model the suspended sediment concentration profiles for estimating the volume of sediment drawn into the cooling water intake. The model solves the vertical diffusion equation on an intrawave period grid to provide a detailed description of the suspended sediment concentration both vertically and over the wave period.

The model accounts for waves and currents at arbitrary angles, breaking/non-breaking waves, plane/ripple-covered bed, uniform/graded bed material, effect of bed slope and the effect of streaming. The sediment is divided into 30 size fractions based on a log-normal grading curve characterized by the median grain diameter D_{50} and the sediment grading defined by $(D_{84}/D_{16})^{0.5}$. The model output is the time-averaged vertical profile of suspended sediment concentration. The model only simulates non-cohesive sediments with grain sizes greater than 0.063 mm, i.e. sand particles.

2.8 Extreme value analysis

The EVA toolbox (DHI, 2008f) comprises a comprehensive suite of routines for performing extreme value analysis. These include:

- A pre-processing facility for extraction of the extreme value series from the record of observations.
- Support of two different extreme value models, the annual maximum series model and the partial duration series model.
- Support of a large number of probability distributions, including exponential, generalised Pareto, Gumbel, generalised extreme value, Weibull, Frechét, gamma, Pearson Type 3, Log-Pearson Type 3, log-normal, and square-root exponential distributions.
- Three different estimation methods: method of moments, maximum likelihood method, and method of L-moments.
- Three validation tests for independence and homogeneity of the extreme value series.
- Calculation of five different goodness-of-fit statistics.
- Support of two different methods for uncertainty analysis, Monte Carlo simulation and Jackknife resampling.
- Comprehensive graphical tools, including histogram and probability plots.

2.9 CORMIX near-field dilution model

The CORMIX Ver 5.0 GTS model (Doneker *et al*, 2007) has been used to simulate the near-field dilution of the thermal plume, i.e. the dilution that occurs as the plume rises from the diffuser ports towards the water surface. CORMIX employs an expert system approach based on flow classification using length scales to determine the discharge/environment interaction and the flow processes that control initial near-field mixing and the transition to far-field plume behaviour. Note that CORMIX is not part of the MIKE suite of models from DHI.

3. FIELD MEASUREMENTS

A comprehensive data collection programme has been developed and implemented at the Bantamsklip site. The objective of this programme is to provide baseline data for:

- Evaluation of the site and Nuclear Power Plant (NPP) safety
- Design of coastal structures at the site
- Calibrating the numerical models to confirm the accuracy of the numerical models used for estimation of both frequent and rare events.

The data collection programme is summarised in Table 3.1. The programme commenced in February 2008 and is scheduled to be completed in August 2010. The data measured until July 2009 is presented in this report, under the relevant report section as indicated in Table 3.1. Owing to instrumentation firmware problems and vandalism the datasets are not continuous. Technical details of the instrumentation employed and additional results are provided in Appendix E.

TABLE 3.1: DATA COLLECTION PROGRAMME

Parameter	**Description**	**Results (in this report unless indicated)**
Bathymetry	Multi-beam bathymetric survey	Section 6.3
Beach Profiles	Measured quarterly since April 2008	Coastal Engineering Report (PRDW, 2009a)
Sediment Grain Sizes	Beach and nearshore samples in March 2008	Section 10.2
Wave Data	Measured at the site since March 2008. Also 15 years of offshore hindcast data.	Section 6.1
Water Levels	Measured at the site since March 2008 28.9 years of tidal data from Cape Town 30.2 years of tidal data from Mossel Bay	Section 4.2
Currents	Measured at the site since March 2008	Section 8.2
Seawater Temperature	Measured at the site since February 2008	Section 7.1
Salinity	Measured at the site since February 2008	Section 7.1
Turbidity	Measured at the site since February 2008	Section 10.4.2
Biofouling	Measured at the site since February 2008	Coastal Engineering Report (PRDW, 2009a)

The sites at which data has been measured are plotted in Figure 3.1 and tabulated in Table 3.2. Sites A to D have been established specifically for this SSR and the measurements are being conducted by Lwandle Technologies (Pty) Ltd under sub-contract to PRDW. Sites 1 to 4 were used for seawater temperature measurements in 2008 by Bayworld on behalf of Eskom (Bayworld, 2008 and 2009).

TABLE 3.2: DATA MEASUREMENT SITES

Site name	Oceanographic parameters measured	Measurement agency	Water depth [m]	Position in degrees WGS84 [longitude, latitude]	Position in meters WG19 [X, Y]
Site A	Waves, currents, seawater temperature, salinity	Lwandle Technologies	12	19.5606, -34.7198 (1)	51350, -3843651 (1)
Site B	Waves, currents, seawater temperature, salinity	Lwandle Technologies	30	19.5111, -34.7101 (1)	46822, -3842551 (1)
Site C	Water level	Lwandle Technologies	1.75	19.5513, -34.7077 (2) 19.5517, -34.7040 (3)	50506, -3842304 (2) 50545, -3841894 (3)
Site D	Seawater temperature	Lwandle Technologies	30	19.5111, -34.7101 (1)	46822, -3842551 (1)
Site 1	Seawater temperature	Bayworld	30	19.5467, -34.7302	50071, -3844798
Site 2	Seawater temperature	Bayworld	26	19.5183, -34.7068	47483, -3842188
Site 3	Seawater temperature	Bayworld	30	19.5820, -34.7482	53292, -3846813
Site 4	Seawater temperature	Bayworld	51	19.5339, -34.7386	48893, -3845723
Site 5	Seawater temperature	Bayworld	78	19.5026, -34.7664	46012, -3848793

Notes:

(1) These site positions have moved by up to a few hundred metres between instrument deployments, but since this is unlikely to influence the measured data, only the most recent position is reported here. Refer to Figure 3.1 and Appendix E for further details.

(2) Position from February to August 2008

(3) Position from January 2009 onwards

4. WATER LEVELS

4.1 Tides

The closest port to the Bantamsklip site for which tidal predictions are available is Hermanus (see Figure 1.1 for location). The predicted tidal levels at Hermanus are as follows (South African Tide Tables, 2008):

TABLE 4.1: PREDICTED TIDAL LEVELS AT HERMANUS

Parameter	Level [m CD]
Highest Astronomical Tide (HAT)	2.07
Mean High Water Springs (MHWS)	1.78
Mean High Water Neaps (MHWN)	1.29
Mean Level (ML)	1.02
Mean Low Water Neaps (MLWN)	0.75
Mean Low Water Springs (MLWS)	0.27
Lowest Astronomical Tide (LAT)	0.00

These levels are relative to Chart Datum, which is 0.788 m below Mean Sea Level or Land Levelling Datum (South African Tide Tables, 2008).

4.2 Extraction of storm surge

The actual water level at a coastal site will differ from the predicted tidal level due to changes in atmospheric pressure and wind effects (collectively referred to as storm surge), as well as other factors including shelf waves, edge waves, wave set-up, wave run-up, seiche and tsunami. In this section only the storm surge component of the water level is estimated based on long-term hourly water level measurements. Tsunamis are considered in Section 5, while shelf waves, edge waves, wave set-up and wave run-up are considered in the Coastal Engineering Investigations Report (PRDW, 2009a), along with the combination of all the relevant components to obtain the extreme water levels.

The closest port to the Bantamsklip site for which tidal data is available is Hermanus, and the predicted tidal levels for Hermanus are given in Section 4.1. However, the tidal predictions for Hermanus are based on only limited historical measurements by the South African Navy (Ms R E Farr, Superintendent Tidal Information, S A Navy, *pers.comm.*). The two closest ports to the Bantamsklip site for which long-term tidal measurements exist are Cape Town and Mossel Bay.

The procedure described below is used to analyse the storm surge. The hourly measured tide for Cape Town for the period 1967 to 2007 and Mossel Bay for the period 1964 to 2006 was kindly provided by the Hydrographer of the South African Navy (who is not responsible for any transcription errors or errors due to calculations using the data). The data is then corrected to the present Chart Datum level taking into account the changes in Chart Datum level in use between 1978 and 2003 (South African Tide Tables, 2008). The data is ‘cleaned’ by removing obviously incorrect spikes and other errors. The

MIKE tidal analysis toolkit (DHI, 2008g) is then used to perform a tidal analysis on the data to obtain the tidal constituents and to subsequently perform a tidal prediction for the full period.

The measured tide is then subtracted from predicted tide to obtain the tidal residuals. These residuals are again 'cleaned' to remove additional spikes and other errors in the data. Attention is paid to removing as far as possible errors caused by timing errors in the measurements, since these can significantly corrupt the residual signal. The resulting dataset comprises 28.9 years of residual data for Cape Town and 30.2 years for Mossel Bay.

The measured tide, predicted tide and residuals for Cape Town are plotted in Figure 4.1 (the full time-series) and Figure 4.2 (fourteen days including the May 1984 storm when one of the largest residuals was recorded). The equivalent plots for Mossel Bay are Figures 4.5 and 4.6.

4.3 Extreme value analysis of storm surge

The residuals are analysed to estimate the positive storm surge (actual water level higher than predicted tide) and negative storm surge (actual water level higher lower than predicted tide) with return periods of 1:1, 1:10, 1:100 and $1:10^6$ years. As discussed in Section 1.3, the results for the $1:10^6$ year return period need to be interpreted with caution due to the available data comprising only approximately 30 years.

The analysis is performed using the EVA (Extreme Value Analysis) toolbox (as described in Section 2.8). The analysis comprises fitting a three parameter Weibull distribution using the Method of Moments to an extreme value series extracted from the input time-series. The extreme value series is selected using the 'peaks over threshold' or 'partial duration series' method, with the threshold defined as the value that is exceeded 8 times per year on average. To ensure independence, two successive events are extracted only if the time between the events exceeds 24 hours. The 95% confidence level to the best estimate is calculated using the Monte Carlo method. The results of the extreme value analysis for Cape Town are presented in Figures 4.3 and 4.4, and Table 4.2.

TABLE 4.2: EXTREME TIDAL RESIDUALS AT CAPE TOWN

Return Period [years]	Best estimate positive residual [m]	Upper 95% confidence positive residual [m]	Best estimate negative residual [m]	Upper 95% confidence negative residual [m]
1	0.44	0.46	-0.42	-0.44
10	0.59	0.64	-0.59	-0.65
100	0.74	0.84	-0.76	-0.87
10^6	1.31	1.67	-1.46	-1.89

The results of the extreme value analysis for Mossel Bay are presented in Figures 4.7 and 4.8, and Table 4.3.

TABLE 4.3: EXTREME TIDAL RESIDUALS AT MOSSEL BAY

Return Period [years]	Best estimate positive residual [m]	Upper 95% confidence positive residual [m]	Best estimate negative residual [m]	Upper 95% confidence negative residual [m]
1	0.61	0.63	-0.62	-0.65
10	0.78	0.83	-0.84	-0.92
100	0.94	1.04	-1.07	-1.21
10^6	1.51	1.86	-1.93	-2.46

Since the residuals for Mossel Bay are larger than those for Cape Town, the conservative approach is to apply the Mossel Bay results for the Bantamsklip site.

5. TSUNAMI FLOODING

5.1 Background

A tsunami is a train of water waves generated by impulsive disturbances of the water surface due to non-meteorological but geophysical phenomena such as submarine earthquakes, volcanic eruptions, submarine slumps and landslides or ice falls into a body of water. A conservative analysis of the potential effects produced by tsunamis should be performed and the nuclear installation should be designed for a design basis flood with a probable maximum tsunami taken into consideration (IAEA, 2003).

The approach adopted in this study is for the Council for Geoscience to define the distant and local tsunamigenic sources and for PRDW to then model the propagation of the tsunami from the source to the nuclear installation site.

5.2 Distant tsunamis

5.2.1 Sources

The Council for Geoscience compiled a report (CGS, 2008a) titled 'A Probabilistic Tsunami Hazard Assessment for Coastal South Africa from Distant Tsunamogenic Areas', which is included as Appendix C of this report. The report identifies Sumatra, Karachi and the South Sandwich Islands as tsunamigenic regions which can affect the coastal areas of South Africa. For each region the report provides the maximum credible earthquake magnitude and the corresponding fault parameters.

Given the fault parameters (origin, strike, length, width, dislocation, depth and dip), the vertical displacement of the seabed caused by the earthquake is estimated using the method of Okada (1985). This method assumes that the displacement of the seabed is a result of the fault movement in a semi-infinite elastic homogeneous body. The vertical displacement of the seabed induces a corresponding displacement of the water surface, which is applied as the initial condition for the hydrodynamic model.

For each source region, a number of tests were performed using the hydrodynamic model to investigate which combination of fault parameters resulted in the worst tsunami reaching the nuclear site. Based on these tests, the six tsunami events described in Table 5.1 are presented in this report. The fault parameters and the resulting maximum vertical seabed displacements for each tsunami event are provided in Table 5.2.

TABLE 5.1: DISTANT TSUNAMI SOURCES MODELLED

Earthquake event	Description
Sumatra A	This is the actual tsunami event of 26 December 2004. It is used to calibrate the numerical model. The fault parameters applied are those from Grilli *et al* (2007).
Sumatra B	This is the maximum credible Sumatra earthquake as determined by CGS (2008a). The fault dip is set to the maximum value and the fault depth to the minimum value recommended in CGS (2008a), since model tests indicated that these values resulted in the largest tsunami. As recommended by CGS (2008a), the fault position and strike were selected to result in the highest tsunami reaching South Africa, as determined from model sensitivity tests. This results in the position being moved south of the 26 December 2004 event to near the Mentawai Islands.
Sumatra C	This is a maximum plausible future rupture of the Mentawai section of the Sundra megathrust, as described by Borrero *et al* (2006).
Karachi A	This is the maximum credible Karachi earthquake as determined by CGS (2008a). The fault dip is set to the maximum value and the fault depth to the minimum value recommended by CGS (2008a), since model tests indicated that these values resulted in the largest tsunami. As recommended by CGS (2008a), the fault position and strike were selected to result in the highest tsunami reaching South Africa, as determined from model sensitivity tests.
South Sandwich Islands A	This is the maximum credible South Sandwich Islands earthquake determined by CGS (2008a). The fault dip is set to 70° and the fault depth to 1 km, since model sensitivity tests indicated that these values resulted in the largest tsunami. As recommended by CGS (2008a), the fault position and strike were selected to result in the highest tsunami reaching South Africa, as determined from model sensitivity tests.
South Sandwich Islands B	This has the same location as South Sandwich Islands A, but the moment magnitude is increased from 7.6 to 8.0 as a sensitivity test.

TABLE 5.2: FAULT PARAMETERS AND VERTICAL SEABED DISPLACEMENT

Fault parameter	**Segment number** [1]	**Sumatra A (26 Dec 2004 event)**	**Sumatra B (max credible CGS)**	**Sumatra C (max plausible Borrero)**	**Karachi A (max credible CGS)**	**South Sandwich A (max credible CGS)**	**South Sandwich B (M_w = 8.0)**
Origin longitude [2]	1	94.10	98.55	98.30	63.00	-26.00	-26.00
[degrees,	2	93.33	-	100.00	-	-	-
+ve East, -ve West]	3	92.71	-	101.40	-	-	-
	4	92.17	-	-	-	-	-
	5	92.44	-	-	-	-	-
Origin latitude [2]	1	3.48	-2.08	-2.00	24.5	-56.00	-56.00
[degrees,	2	5.10	-	-4.20	-	-	-
+ve North, -ve South]	3	7.21	-	-6.00	-	-	-
	4	9.68	-	-	-	-	-
	5	11.78	-	-	-	-	-
Strike [degrees] [3]	1	323	321	321	270	160	160
	2	348	-	321	-	-	-
	3	338	-	321	-	-	-
	4	356	-	-	-	-	-
	5	10	-	-	-	-	-
Length [km]	1	220	741.3	260	283.1	102.8	162
	2	150	-	360	-	-	-
	3	390	-	140	-	-	-
	4	150	-	-	-	-	-
	5	350	-	-	-	-	-
Width [km]	1	130	166.72	130	96.92	54.75	71
	2	130	-	180	-	-	-
	3	120	-	70	-	-	-
	4	95	-	-	-	-	-
	5	95	-	-	-	-	-
Mean dislocation [m]	1	18	12.82	20	4.18	1.29	2.2
	2	23	-	20	-	-	-
	3	12	-	20	-	-	-
	4	12	-	-	-	-	-
	5	12	-	-	-	-	-
Depth [km] [4]		25	25	15	25	1	1
Dip [degrees]		12	15	15	27	70	70
Seismic moment M_o [N/m] [5]		8.3×10^{22}	6.4×10^{22}	8.7×10^{22}	4.6×10^{21}	2.9×10^{20}	1.0×10^{21}
Moment magnitude M_w [-] [6]		9.2	9.2	9.3	8.4	7.6	8.0
Max displacement up [m] [7]		9.6	5.4	9.0	1.8	0.8	1.3
Max displacement down [m]		-5.7	-2.3	-3.6	-0.4	-0.4	-0.7

Notes: (1) The fault may comprise between 1 and 5 fault segments
(2) The origin is defined as the mid-point of the upper border of the fault
(3) An observer facing along strike should see the fault dip to the right (degrees clockwise from north)
(4) Depth is defined as depth from the seabed to the upper border of the fault
(5) $M_o = \mu LWD$, with μ = shear modulus $\approx 4 \times 10^{10}$ Pa, L = Fault Length, W = Width, D = Dislocation
(6) $M_w = (\log_{10} M_o - 9) / \log_{10} 32$
(7) The seabed displacement modelled has a complex three-dimensional shape - only the maximum upward and downward displacements are given here.

5.2.2 Model setup

The MIKE 21 HD hydrodynamic model (as described in Section 2.4) is used to simulate the propagation of the tsunami wave from the source to the nuclear site. The model solves the two-dimensional shallow water equations (conservation of mass and vertically-integrated momentum) on a series of dynamically-nested rectangular grids using an implicit time scheme. Processes simulated include Coriolis force, bottom shear stress, flooding and drying. The waves are assumed to be non-breaking and the loss of energy and momentum by wave breaking is not simulated.

Nine nested grids were used, with the grid spacing varying from 120 m near the nuclear site to 9720 m at the model boundaries. The model bathymetry is obtained from the following sources:

- ETOPO 2 minute global bathymetry dataset for depths greater than approximately 200 m.
- MIKE C-MAP electronic hydrographic charts (DHI, 2008h) for depths from 200 m to 75 m.
- Multi-beam bathymetric surveys by the Council for GeoScience for depths from 75 m to 20 m.
- Multi-beam bathymetric survey of the inshore zone by Tritan Survey cc for depths from 30 m to 5 m.
- Beach profiles by Tritan Survey cc
- Lidar survey by Southern Mapping Company for land.

The model domain and bathymetry used to simulate tsunamis from the Sumatra and Karachi regions is shown in Figure 5.1, while the bathymetry for the South Sandwich Islands tsunamis is shown in Figure 5.11.

The model time step is 6 s, which ensures a Courant Number of less than 1.0 (although a Courant number up to 20 may be acceptable for stability of the implicit solver, in this case a value of 1 is required for model accuracy). The grid spacings are selected to ensure at least 20 to 30 grid points per tsunami wavelength. The drying depth is set at 0.2 m and the flooding depth is 0.3 m. Bed resistance is specified by a Manning number of 32 $m^{1/3}/s$. Eddy viscosity is found to have an insignificant influence on these simulations and is set to zero. The still water level modelled is Mean Sea Level.

The fault parameters (Table 5.2) are used to calculate the vertical displacement of the seabed caused by the earthquake, which induces a corresponding displacement of the water surface and is applied as the initial condition for the hydrodynamic model.

5.2.3 Model calibration

The model is calibrated by simulating the Sumatra tsunami of 26 December 2004. The fault parameters and associated maximum vertical seabed displacement are shown in Table 5.2.

The 26 December 2004 event was measured at a number of tidal stations along the South African coastline, with the largest water level variation measured in the Port of Port Elizabeth (Rabinovich and Thomson, 2007). The measured tidal data for Port Elizabeth was kindly provided by the Hydrographer of the South African Navy. The measured tide is subtracted from predicted tide and then adjusted for the average storm surge of 0.18 m measured during the tsunami. The resulting tsunami signal is shown in Figure 5.2. It should be noted that the maximum crest of the tsunami was not recorded due to an instrument problem. Hartnady and Okal (2007) estimate the maximum crest level to have been approximately 2.11 m above the predicted tidal level. If the 0.18 m average storm surge is taken into account the maximum crest level reduces to 1.93 m.

The modelled tsunami levels inside the Port of Port Elizabeth compare well to the measurements (Figure 5.2). In this case the model slightly under-predicts the maximum water level (model: 1.7 m, measured: approximately 1.9 m) while over-predicting the minimum water level (model: -2.0 m, measured: -1.5 m). The tsunami has a period of between 30 and 40 minutes. These results provide confidence that the model is capable of simulating the tsunami propagation and transformation processes from distant sources.

5.2.4 Results

Results are presented for each of the six tsunami events described in Table 5.1 and Table 5.2. Each simulation continues for approximately 24 hours after the tsunami wave reaches the site, to ensure that the maximum and minimum water levels are simulated. For each tsunami, the results are presented as two figures showing the maximum and minimum water levels relative to Still Water Level at any time during the simulation. Each figure includes a plot of the larger model domain as well as a zoomed-in view near each of the three proposed nuclear sites (Thyspunt, Bantamsklip and Duynefontein). For reference purposes, Port Elizabeth is also shown. The maximum and minimum water levels in the larger model domain are calculated from model output intervals of 10 minutes, which allows the tsunami wave crests to be visualised in the plots. The maximum and minimum water levels in the zoomed-in views are calculated from model output intervals of 1 minute, which ensures that the maximum levels are accurately detected.

The contour plots are presented in Figures 5.3 to 5.15. It can be seen that for tsunamis in the Indian Ocean, the Bantamsklip site is relatively sheltered compared to Port Elizabeth. The Mentawai Islands earthquakes (Sumatra B and C) are seen to direct the tsunami south-westwards towards South Africa, compared to the 26 December 2004 event, which directed more energy westwards towards Sri Lanka.

The maximum and minimum water levels at any position within a 3 km radius of the Bantamsklip site have been extracted from the results and are presented below. The 3 km radius accounts for uncertainty regarding the exact location of the nuclear installation, as well as the possibility of flooding from a flank rather than frontally. The maximum and minimum levels generally occur along the shoreline rather than offshore, due to shoaling and run-up/run-down effects.

TABLE 5.3: MODELLED WATER LEVELS AT BANTAMSKLIP DUE TO DISTANT TSUNAMIS

Earthquake event	Maximum water level [m above SWL]	Minimum water level [m below SWL]
Sumatra A	0.7	-0.7
Sumatra B	1.5	-1.0
Sumatra C	1.5	-1.5
Karachi A	0.1	-0.2
South Sandwich Islands A	0.7	-0.5
South Sandwich Islands B	1.2	-1.2

The Sumatra C tsunami is seen to result in the most extreme water levels. To account for uncertainties in the source parameters as well as in the modelled tsunami propagation and transformation (see the model calibration in Section 5.2.3), it is recommended to increase the modelled results by 0.5 m. This results in a recommended maximum level of 2.0 m and a minimum level of -2.0 m. These are the maximum tsunami-induced water levels relative to Still Water Level. The total water level will additionally include the effect of tide, wave run-up, wave set-up and storm surge, as described in PRDW (2009a).

5.3 Local tsunamis

5.3.1 Sources

The Council for Geoscience compiled a report (CGS, 2008b) titled 'Potential Sources of Tsunami Along the South African Coast', which is included as Appendix D of this report. The possible tsunamigenic sources identified include: cosmic impact, remote submarine seismicity, submarine slides and slumps, meteotsunami, volcanic activity, terrestrial landslides and rockfalls. The summary and recommendations section of the report (CGS, 2008b) is reproduced below:

- The report provides a qualitative account of possible tsunamigenic sources that could threaten the South African coastline. To adequately assess the risk, a quantitative assessment of each source category is required.
- Offshore slump generated tsunami are considered the largest unknown risk factor. Holocene and recent historical records provide graphic evidence of their destructive capability on regional scales. Further research including all available stratigraphic/sedimentological/geomorphological data should be undertaken to better define the risk.
- Meteotsunami (edge waves) may well have been responsible for the 1969 and 2008 tsunami events along the southern African west coast. In depth research into the global frequency, locality and magnitude of meteotsunami should be undertaken to further quantify the risk. In particular, the atmospheric conditions along the west coast prior to the 1969 event should be compared with those of its 2008 counterpart.
- Worst case scenarios need to be defined. For instance, the potential impacts of the coincidence of maximum storm waves, storm surge, astronomical tides and meteotsunami should be modelled.

- Because of the relatively short history of tsunami records along the South African coast, the database should be extended by conducting an investigation of palaeotsunami in the stratigraphic record. No systematic work has yet been conducted along this coast. Areas of focus should be in the vicinity of planned nuclear installations.

5.3.2 Modelling approach

The Council for Geoscience report (CGS, 2008b) considers offshore slump generated tsunamis as the largest unknown risk factor for the South African coast. A number of slump regions have been documented where historical slumping has occurred on massive scales in various phases including late Mesozoic (148 million years ago to 65 million years ago), early to late Tertiary (65 Ma to 1.8 Ma) and possibly Quaternary (1.8 Ma to present). However, a quantitative assessment of the risk of occurrence and geometry of future slump events along the South African shelf margin is not available at present. This is in contrast to the distant tsunamigenic sources which are comparatively well defined (Section 5.2).

After discussion with the external reviewer for this study (Prof. C A Fleming), the modelling approach adopted in this study is to simulate the tsunamis generated by a number of theoretical offshore slumps in order to estimate the slump volume required to generate a tsunami at the nuclear installation sites of comparable size to that from the maximum credible distant earthquake described in Section 5.2.

5.3.3 Model setup

The MIKE 21 HD hydrodynamic model (as described in Section 2.4) is used to simulate the propagation of the tsunami wave from the source to the nuclear site. The model grid and parameters are the same as used for the distant earthquake sources (Section 5.2.2), except that the time-step is reduced from 6 to 3 s, and for numerical stability the eddy viscosity is increased from 0 to 20 m^2/s.

Submarine mass failures can be categorised as either slip events, which are typically large translations in landslide masses, or rotational failure leading to a slump event. Since most of the South African events are categorised as slumps (CGS, 2008b), only slumps will be considered in this study. Unlike tsunami generation by earthquakes, which can be accurately modelled using the instantaneous co-seismic displacement of the water surface as an initial condition, submarine slumps or slides typically take place over a number of minutes. To simulate slumps or slides the MIKE 21 HD hydrodynamic model has the facility to dynamically change the seabed level as a function of time.

A numerical routine is developed to define the dynamic changes in seabed level arising from a slump. The submarine slump is simulated as a rigid body moving down a slope (Figure 5.16). The body has a Gaussian shape as specified in Grilli and Watts (2005). The equation describing the slump motion follows Watts *et al* (2003), where the slump motion is modelled as a rigid body undergoing a rotation around a point described as the centre of rotation of a circle prescribed by the arc of the circular failure

plane. The rigid body is subject to external moments due to gravity, added mass and shear stress summed over the failure plane. The slump motion is described with a cosine function and as such experiences an initial angular acceleration, relatively constant maximum angular velocity and a subsequent deceleration before coming to rest in a position such that the centre of mass of the slump is vertically under the axis of rotation. The input parameters required for the slump model are described in the following section.

5.3.4 Slumps modelled

CGS (2008b) describes two historical slump regions relevant to the proposed nuclear sites: the Cape Town and Agulhas Slumps, shown in Figure 5.17. Three theoretical slumps have been modelled, with each slump located within one of the historical slumping regions and directly opposite one of the three proposed nuclear sites, as shown in Figure 5.18.

The magnitude of tsunami generated by a slump depends on a number of parameters, including slump volume, water depth, slump thickness, initial acceleration and maximum velocity of the slump. The geometry of the slumps which have been modelled is based on the measured geometry of the upper or proximal part of the Agulhas Slump, as indicated in Figure 5.19. Setting the slump width equal to the slump length gives a slump volume of 80 km^3. The slump parameters modelled are given in Table 5.4.

TABLE 5.4: SLUMP PARAMETERS MODELLED

Parameter	Agulhas Slump	Cape Town Slump (South)	Cape Town Slump (North)
Volume [km^3] (1)	80	80	80
Length [km] (2)	18	18	18
Width [km] (3)	18	18	18
Thickness [km] (4)	0.3	0.3	0.3
Rotation [deg] (5)	0.4	0.4	0.4
Radius [km] (6)	135	135	135
Displacement [km] (7)	1.0	1.0	1.0
Centroid longitude [deg]	24.89	18.38	17.18
Centroid latitude [deg]	-35.22	-35.44	-34.37
Strike [deg] (8)	75	140	160
Water depth [m]	2000	2000	2000
Initial acceleration [m/s^2]	0.011	0.011	0.011
Maximum velocity [m/s]	2.3	2.3	2.3
Duration [minutes] (9)	11.3	11.3	11.3

Notes: (1) Since the slump is elliptic, the volume = π/4 x length x width x thickness
(2) Length of the slump is measured down the slope, see 'b' in Figure 5.16
(3) Width of the slump is measured across the slope.
(4) See 'T' in Figure 5.16
(5) See 'φ' in Figure 5.16
(6) See 'R' in Figure 5.16
(7) See 'S' in Figure 5.16
(8) An observer facing along the strike will see the slump moving down to the right (degrees clockwise from north)
(9) This is the total duration of the slump movement

5.3.5 Results

Results are presented for each of the three slump-generated tsunamis described in Table 5.4. Each simulation continues for approximately 10 hours after the tsunami wave reaches the site, to ensure that the maximum and minimum water levels are simulated. For each tsunami, the results are presented as two figures showing the maximum and minimum water levels relative to Still Water Level at any time during the simulation. Each figure includes a plot of the larger model domain as well as a zoomed-in view near each of the three proposed nuclear sites (Thyspunt, Bantamsklip and Duynefontein). The maximum and minimum water levels in the larger model domain are calculated from model output intervals of 10 minutes, which allows the tsunami wave crests to be visualised in the plots. The maximum and minimum water levels in the zoomed-in views are calculated from model output intervals of 1 minute, which ensures that the maximum levels are accurately detected. The contour plots are presented in Figures 5.20 to 5.25.

The maximum and minimum water levels at any position within a 3 km radius of the Bantamsklip site have been extracted from the results and are presented below. The 3 km radius accounts for uncertainty regarding the exact location of the nuclear installation, as well as the possibility of flooding from a flank rather than frontally. The maximum and minimum levels generally occur at the shoreline due to shoaling and run-up/run-down effects.

TABLE 5.5: MODELLED WATER LEVELS AT BANTAMSKLIP DUE TO A THEORETICAL 80 KM^3 SLUMP

Slump event	Maximum water level [m above SWL]	Minimum water level [m below SWL]
Agulhas Slump	0.5	-0.5
Cape Town Slump (South)	2.0	-2.0
Cape Town Slump (North)	0.5	-0.5

5.3.6 Discussion

The hydrodynamic modelling indicates that a theoretical 80 km^3 slump in the historical Cape Town Slump region is likely to result in a tsunami amplitude of up to 2.0 m at the Bantamsklip site, while the same sized slump in the historic Agulhas Slump region results in a 0.5 m amplitude tsunami at Bantamsklip.

Compared to the theoretical 80 km^3 slump that has been modelled, the historical Agulhas Slump is one of the largest identified world-wide with an estimated length of 750 km, width of 106 km and volume of 20 000 km^3 (Dingle, 1977). According to Dingle (1977), the slump involved Pliocene sediments and may therefore be Quaternary (1.8 million years to present) in age. The volume of this slump is 250 times larger than the slump that has been modelled, implying a devastating tsunami for which evidence should presumably be contained in the stratigraphic record.

An important factor, however, is whether the slump occurred as a single unit or as a number of smaller events over time. Preliminary numerical modelling indicates that for the Agulhas and Cape Town slump regions, the duration of the tsunami-induced water level disturbance at the shore is 1 to 2 hours, implying that individual slumps separated by longer than this time are effectively separate smaller events rather than one large event.

5.4 Conclusions

The maximum tsunami risk from distant earthquake sources is found to be from the Sumatra region, which results in a maximum tsunami level of 2.0 m and a minimum level of -2.0 m (including a 0.5 m safety allowance) at the Bantamsklip site.

The maximum risk to the Bantamsklip site from local sources is likely to be a submarine slump in the historical Cape Town Slump region. The hydrodynamic modelling indicates that a slump volume of 80 km^3 is required to generate a tsunami at the Bantamsklip site that exceeds the tsunami from the distant Sumatra earthquake. However, a quantitative assessment of the risk of occurrence and geometry of future slump events along the South African shelf margin is not available at present.

Until further geological research is undertaken, it is proposed to base the tsunami risk on the relatively well defined distant earthquake sources. This results in a recommended maximum level of 2.0 m and a minimum level of -2.0 m. These are the maximum tsunami-induced water levels relative to Still Water Level. The total water level will additionally include the effect of tide, wave run-up, wave set-up and storm surge, as described in PRDW (2009a).

5.5 Recommendations

Additional research is required to better define the risk from local tsunamigenic sources. The CGS (2008b) report recommends the following approach:

- Further research including all available stratigraphic/sedimentological/geomorphological data should be undertaken to better define the risk from offshore slump generated tsunami.

- In depth research into the global frequency, locality and magnitude of meteotsunami should be undertaken to further quantify the risk. In particular, the atmospheric conditions along the west coast prior to the 1969 event should be compared with those of its 2008 counterpart.

- Because of the relatively short history of tsunami records along the South African coast, the database should be extended by conducting an investigation of palaeotsunami in the stratigraphic record. No systematic work has yet been conducted along this coast. Areas of focus should be in the vicinity of planned nuclear facilities.

6. WAVES

6.1 Waves measured at the site

Waves have been measured at the Bantamsklip site at Site A (water depth of 12 m) and Site B (water depth of 30 m) starting in March 2008. The locations of the two sites are shown in Figure 3.1 and the coordinates are given in Table 3.2. A number of problems including instrument firmware issues and third party interference have reduced the data return to date. The firmware issues have now been addressed by the instrument manufacturer and the instrument locations have been shifted to reduce third party interference. Full details of the measurements are given in Appendix E.

The measured wave parameter time-series are plotted in Figure 6.1. The two significant storms measured to date are plotted in more detail in Figure 6.2. The measurement interval is one hour. Unfortunately in both cases only the instrument at Site B was operational. The storm of 24 June 2009 shows a steady increase in H_{m0} peaking at 7.5 m, while the H_{m0} level that is exceeded for 6 hours during the storm event is 7.2 m. At the peak of the storm the T_p is 17 s and the mean wave direction is 220°.

In contrast, the storm of 9 August 2008 shows an erratic increase in H_{m0} reaching a peak of 8.6 m, while the H_{m0} level that is exceeded for 6 hours during the storm event is significantly lower at 5.8 m. The abrupt change in the measured H_{m0} (2.8 m increase in 1 hour) and wave direction (28° decrease in 1 hour) at the peak of the storm, along with the subsequent failure of the instrument, cast doubt on the accuracy of the peak values measured during this storm event.

Wave roses and wave height histograms for Sites A and B are shown in Figures 6.3 and 6.4, respectively. The most frequent wave direction at Site A is 220°, while at Site B the most frequent wave direction is 200°, although the larger waves have a direction of 220°.

These data have been used to calibrate the wave models, as described in Section 6.4. Since the currently available datasets (up to August 2009) have durations of only 5 months, a 15 year wave hindcast dataset has been refracted inshore and then used for the extreme value analysis of wave height. The wave measurements are ongoing until August 2010 and will continue to provide valuable design data.

6.2 Offshore hindcast data

Fifteen years of offshore wave hindcast data was purchased from Fugro Oceanor in Norway. The data covers the period from November 1990 to October 2007, but excluding the period June 1991 to May 1993 (during which the data quality is lower). The data position is approximately 60 km south-west of Bantamsklip in 180 m water depth at coordinates E 19.0°, S 35.0° (see Figure 6.7). The data comprises two-dimensional wave spectra and wave parameters (H_{m0}, T_p, mean direction) at 6 hourly intervals.

The source of the data are directional wave spectra from the WAM (WAve Model) numerical model run at the European Centre for Medium Range Weather Forecasting (ECMWF). The model data has been calibrated by Fugro Oceanor against available satellite altimeter data. A full description of the data sources and the calibration and verification procedure is provided in Appendix B.

The full dataset is plotted in the form of a time-series (Figure 6.5), wave rose and wave height histogram (Figures 6.6). The dominant wave direction is 230°, the median H_{m0} is 2.8 m and the maximum H_{m0} is 10.8 m.

6.3 Model setup

The wave modelling has been conducted using the MIKE Spectral Waves model (as described in Section 2.2). The objective is to transform the hindcast data from offshore to nearshore where it will be used for a number of applications including wave heights for design of coastal structures, wave run-up, wave-driven currents for plume dispersion and sediment transport.

The model mesh extends from the offshore wave hindcast position in 180 m depth to the shoreline. The mesh size varies from 50 m in the area of interest to 2000 m at the offshore boundary (Figure 6.7).

The model bathymetry is obtained from the following sources:

- MIKE C-MAP electronic hydrographic charts (DHI, 2008h) for depths from 200 m to 75 m.
- Multi-beam bathymetric surveys by the Council for GeoScience for depths from 75 m to 20 m.
- Multi-beam bathymetric survey of the inshore zone by Tritan Survey cc for depths from 30 m to 5 m.
- Beach profiles by Tritan Survey cc
- Lidar survey by Southern Mapping Company for land.

6.4 Model calibration

The model is calibrated by refracting the offshore hindcast data to the inshore measurement positions (Sites A and B, see Figure 3.1) for the period February to July 2008. The model parameter settings based on this calibration are described below.

The directionally decoupled parametric formation is found to give comparable results to the fully spectral formulation and is adopted due to its lower computational cost. For the directional spreading a $\cos^n(\theta-\theta_m)$ distribution is used, where n is the directional spreading index and θ_m is the mean wave direction. A constant spreading index of n = 1.0 (directional standard deviation = 40°) gave superior results to more complex formations where the spreading is made a function of wave period or

direction. The directional discretization in the model is 10°. The wave breaking index is 0.8. Bottom friction is modelled with a constant friction factor f_w equal to the default value of 0.02.

The resulting model calibration is considered to be good (Figures 6.8 and 6.9). Since the boundary condition used for the calibration is the offshore wave hindcast data and not measured data, the calibration also confirms the accuracy of these hindcast data.

Figure 6.10 shows an example of the wave refraction from offshore towards the site, while Figure 6.11 shows a more detailed view near the Bantamsklip site.

6.5 Extreme value analysis of wave height

The calibrated wave model is used to transform the offshore hindcast data inshore to five positions along the -30 m CD depth contour. Since the objective is to determine the extreme inshore wave climate, the refraction has been performed only at the times in the 15 year record when the offshore H_{m0} exceeded 4.5 m.

Results are extracted at the five points along the -30 m CD depth contour shown in Figure 6.11. The wave rose for the storm waves refracted to Point 1 is shown in Figure 6.12, as well as the H_{m0}-T_p relationship.

The wave data refracted to the -30 m CD positions have been analysed to estimate the H_{m0} with return periods of 1:1, 1:10, 1:100 and $1:10^6$ years. As discussed in Section 1.3, the results for the $1:10^6$ year return period need to be interpreted with extreme caution, since it is based on only 15 years of data.

The analysis is performed using the EVA (Extreme Value Analysis) toolbox (as described in Section 2.8). The analysis comprises fitting a three parameter Weibull distribution using the Method of Moments to an extreme value series extracted from the input time-series. The extreme value series is selected using the 'peaks over threshold' or 'partial duration series' method, with the threshold defined as the value that is exceeded 8 times per year on average. To ensure independence, two successive events are extracted only if the time between the events exceeds 48 hours. The 95% confidence level to the best estimate is calculated using the Monte Carlo method. The results of the extreme value analysis are presented in Figure 6.13 and Table 6.1.

Included in Table 6.1 are the increased wave heights taking climate change into account, which is assumed to increase the heights by 17% - refer to PRDW (2009a) for details on climate change. Also included in Table 6.1 is the estimated T_p for each wave height, based on the relationship between T_p and H_{m0} at -30 m CD (refer to Figure 6.12).

TABLE 6.1: EXTREME WAVE CLIMATE AT -30 M CD

	Return Period [years]	No climate change				Climate change (17% increase in H_{m0})			
		H_{m0} best estimate [m]	T_p [s]	H_{m0} upper 95% confidence [m]	T_p [s]	H_{m0} best estimate [m]	T_p [s]	H_{m0} upper 95% confidence [m]	T_p [s]
Point 1	1	5.8	15.1	6.0	15.3	6.7	16.2	7.0	16.5
	10	7.1	16.6	7.6	17.2	8.3	17.9	8.9	18.5
	100	8.3	18.0	9.2	18.9	9.7	19.4	10.8	20.4
	10^6	13.0	22.4	16.0	24.8	15.2	24.1	18.8	26.7
Point 2	1	5.7	15.0	5.9	15.3	6.7	16.1	6.9	16.5
	10	7.0	16.5	7.5	17.1	8.2	17.8	8.7	18.4
	100	8.2	17.8	9.1	18.7	9.6	19.3	10.6	20.2
	10^6	12.8	22.2	15.7	24.5	15.0	23.9	18.4	26.5
Point 3	1	5.5	14.7	5.7	15.0	6.4	15.9	6.7	16.2
	10	6.8	16.3	7.3	16.8	7.9	17.5	8.5	18.1
	100	8.0	17.6	8.9	18.5	9.3	19.0	10.4	20.0
	10^6	12.6	22.0	15.6	24.4	14.8	23.8	18.2	26.4
Point 4	1	5.3	14.5	5.6	14.8	6.3	15.7	6.5	16.0
	10	6.6	16.0	7.0	16.6	7.7	17.3	8.2	17.9
	100	7.8	17.4	8.6	18.3	9.1	18.7	10.1	19.7
	10^6	12.3	21.8	15.2	24.2	14.4	23.5	17.8	26.1
Point 5	1	5.4	14.6	5.6	14.8	6.3	15.7	6.6	16.0
	10	6.6	16.1	7.1	16.6	7.8	17.4	8.3	18.0
	100	7.8	17.4	8.7	18.3	9.1	18.8	10.1	19.8
	10^6	12.4	21.8	15.3	24.2	14.5	23.5	17.9	26.1

These extreme values can be compared to the storms measured at the site. The storm of 24 June 2009 peaked with an H_{m0} of 7.5 m for 1 hour and exceeded 7.2 m for 6 hours during the storm event (see Figure 6.2). Since the extreme values in Table 6.1 are based on 6 hourly hindcast data, the measured H_{m0} of 7.2 m can be seen to have a return period of approximately 10 years at Position 1, which is the closest point to Site B. The fact that 5 months of measured data contain the 1:10 year event suggests that either this was an extreme event, or that the hindcast data may be under-predicting these storm events. The ongoing wave measurements will assist to clarify this issue.

6.6 Wave transformation across surf-zone

The cross-shore hydrodynamic engine of the LITPACK model (as described in Section 2.3) is used to transfer each of the extreme wave conditions at the -30 m CD position (Table 6.1) inshore to the -5 m CD position, where the resulting wave conditions are required as input to the wave set-up and run-up computations as described in the Coastal Engineering Investigations Report (PRDW, 2009a). An example of the model output is shown in Figure 6.14.

7. SEAWATER TEMPERATURE

7.1 Temperature measured at site

As part of this SSR, seawater temperature has been measured at Bantamsklip at Sites A to D starting in February 2008. The locations of the sites are shown in Figure 3.1 and the coordinates are given in Table 3.2. Full details of the measurements are given in Appendix E. These measurements are ongoing until August 2010 and provide valuable data for the design of the seawater cooling system. The data measured to date is plotted in Figure 7.1. The data shows that the water column tends to be vertically mixed in winter, while in summer the water temperature at 1.75 m depth may be up to 7°C warmer than at 30 m depth.

Seawater temperature data at Bantamsklip was also obtained from Eskom/Bayworld at Sites 1 to 5 for the period September 2008 to January 2009 (Bayworld, 2008 and 2009). The location of these sites is shown in Figure 3.1 and the coordinates are given in Table 3.2. The data is plotted in Figure 7.2.

The South African Weather Service maintains a database of sea temperatures measured daily in the surf-zone at a number of locations along the South African coastline. The closest measurement locations to the Bantamsklip site are Cape Agulhas, Gansbaai and Hermanus (refer to Figure 1.1 for locations) and these datasets were purchased from the South African Weather Service. The datasets have durations of 13.1, 17.8 and 25.1 years for Cape Agulhas, Gansbaai and Hermanus, respectively. The data is presented as time-series plots in Figure 7.3 and as histogram plots in Figure 7.4.

Summary statistics of the available seawater temperature datasets are provided in Table 7.1 (listed in order of increasing instrument depth). In some cases more than one instrument was deployed at one site, e.g. an ADCP with an onboard temperature sensor was deployed at the seabed along with a mooring with temperature loggers near the seabed and also higher up in the water column.

TABLE 7.1: SUMMARY STATISTICS OF SEAWATER TEMPERATURES MEASURED AT BANTAMSKLIP SITE

Location	Total water depth [m]	Instrument depth [m]	Sampling interval	Length of dataset	Minimum temperature [°C]	Mean temperature [°C]	Maximum temperature [°C]
Cape Agulhas	Surf-zone	Surf-zone	Daily	13.1 years	11.0	17.3	25.0
Gansbaai	Surf-zone	Surf-zone	Daily	17.8 years	11.0	15.9	23.0
Hermanus	Surf-zone	Surf-zone	Daily	25.1 years	9.0	15.6	25.6
Site C	1.75	1.75	10 min	6.8 months	11.3	15.0	20.6
Site D	30	4	10 min	1.3 months	14.2	15.0	15.9
Site D	30	8	10 min	7.6 months	9.5	13.9	19.8
Site A	12	12	10 min	4.6 months	9.5	14.0	17.5
Site D	30	13	10 min	2.7 months	10.0	13.1	17.9
Site D	30	30	10 min	11.2 months	9.4	12.3	19.2
Site B	30	30	10 min	5.3 months	9.4	12.5	16.8
Site 1	30	30	1 hour	5.4 months	10.1	12.9	18.7
Site 2	26	26	1 hour	5.4 months	10.2	13.0	19.2
Site 3	30	30	1 hour	5.4 months	10.2	12.9	18.5
Site 4	51	51	1 hour	5.4 months	10.1	12.3	19.2
Site 5	78	78	1 hour	5.4 months	9.8	11.8	15.1

7.2 Extreme value analysis of temperature

Of the available datasets shown in Table 7.1, only the Cape Agulhas, Gansbaai and Hermanus datasets are long enough (>10 years) to allow an extreme value analysis. These datasets have been analysed to estimate the temperatures with return periods of 1:1, 1:10, 1:100 and 1: 10^6 years. As discussed in Section 1.3, the results for the 1: 10^6 year return period need to be interpreted with caution due to the limited length of the datasets.

The analysis is performed using the EVA (Extreme Value Analysis) toolbox (as described in Section 2.8). The analysis comprises fitting a three parameter Weibull distribution using the Method of Moments to an extreme value series extracted from the input time-series. The extreme value series is selected using the 'peaks over threshold' or 'partial duration series' method, with the threshold defined as the value that is exceeded 8 times per year on average. To ensure independence, two successive events are extracted only if the time between the events exceeds 48 hours. The 95% confidence level to the best estimate is calculated using the Monte Carlo method. The results of the extreme value analysis are presented in Figures 7.5 to 7.7 and Table 7.2.

TABLE 7.2: EXTREME SEAWATER TEMPERATURES AT THREE LOCATIONS IN THE VICINITY OF BANTAMSKLIP

	Cape Agulhas		Gansbaai		Hermanus	
Return period [years]	**Best estimate [°C]**	**Upper 95% confidence [°C]**	**Best estimate [°C]**	**Upper 95% confidence [°C]**	**Best estimate [°C]**	**Upper 95% confidence [°C]**
1	23.6	23.8	20.6	20.9	21.0	21.3
10	24.6	24.9	22.5	23.2	23.1	23.8
100	25.3	25.9	24.3	25.5	25.2	26.5
10^6	27.6	29.0	30.4	34.2	33.0	37.8

For return periods of 1:100 years and less, the highest temperatures occur at the Cape Agulhas location, while Hermanus has the highest temperature for the $1:10^6$ year return period. To be conservative, the recommended approach is to use the higher Cape Agulhas results for return periods of 1:100 and less, and the Hermanus results for the $1:10^6$ return period.

The temperatures in Table 7.2 are based on water measurements in the shallow surf-zone and are thus applicable to a basin cooling water intake design. The intake temperature is likely to be lower for tunnel intakes located in depths of 25 to 45 m (see Section 9.3), although the available seawater temperature measurements are insufficient to quantify this decrease. The ongoing measurements will provide a longer dataset to establish the decrease in extreme temperatures with depth.

8. CURRENTS

8.1 Background

Currents are important for thermal plume dispersion (Section 9), sediment transport (Section 10) and also for the design of coastal structures such as intakes and outfalls. Currents have thus been measured at the site and a hydrodynamic model has been set up and calibrated to simulate the currents at the site for various environmental forcings and intake/outfall layouts.

8.2 Currents measured at site

Currents have been measured at the Bantamsklip site at Site A (water depth of 12 m) and Site B (water depth of 30 m) starting in March 2008. The locations of the two sites are shown in Figure 3.1 and the coordinates are given in Table 3.2. The instruments are Acoustic Doppler Current Profilers (ADCPs) which measure the current speed and direction at 0.5 m depth intervals from the surface to the seabed at 10 minute intervals. A number of problems including instrument firmware issues and third party interference have reduced the data return to date. The firmware issues have now been addressed by the instrument manufacturer and the instrument locations have been shifted to reduce third party interference. Full details of the measurements are given in Appendix E.

The data measured to date are plotted as time-series in Figures 8.1 and 8.2, and current roses in Figure 8.3. The currents show evidence of forcing by winds, waves and tides. The current speeds are moderate with a maximum speed of 0.73 m/s measured to date. Currents near the seabed are approximately half as strong as near the surface. The current directions show a high degree of variability, including a predominantly north-westerly current near the surface at Site B and an easterly current near the seabed at Site A. Summary statistics are presented in Table 8.1.

TABLE 8.1: SUMMARY STATISTICS OF CURRENT SPEEDS MEASURED AT THE BANTAMSKLIP SITE

	Site A (water depth 12 m)		**Site B (water depth 30 m)**	
	Near surface (-1.2 m)	Near seabed (-8.2 m)	Near surface (-3.8 m)	Near seabed (-23.8 m)
Mean current speed [m/s]	0.12	0.05	0.14	0.06
Maximum current speed [m/s]	0.73	0.60	0.62	0.41

These data have been used to calibrate the hydrodynamic model, as described in Section 8.3.2. The current measurements are ongoing and will provide valuable design data in the future.

8.3 Hydrodynamic modelling

8.3.1 Model setup

The MIKE 3 Flow Flexible Mesh three-dimensional hydrodynamic model (as described in Section 2.5) has been set up to simulate the currents and the dispersion of the thermal plume due to winds, waves, tides and buoyancy effects.

The model bathymetry is obtained from the following sources:

- MIKE C-MAP electronic hydrographic charts (DHI, 2008h) for depths from 200 m to 75 m.
- Multi-beam bathymetric surveys by the Council for GeoScience for depths from 75 m to 20 m.
- Multi-beam bathymetric survey of the inshore zone by Tritan Survey cc for depths from 30 m to 5 m.
- Beach profiles by Tritan Survey cc
- Lidar survey by Southern Mapping Company for land.

The horizontal model grid comprises both triangular and quadrilateral elements with sizes ranging from 50 m in the surf-zone to 1000 m at the offshore boundaries (see Figure 8.4). The vertical grid has five layers having thicknesses from seabed to surface of 20%, 30%, 20%, 20% and 10% of the local water depth.

The predicted tide is applied along the three open boundaries of the model. Since a weak tidal signal is evident in the measured currents, the tidal levels applied in the model are varied along the boundaries. The tidal levels are obtained from a global tide model including the major diurnal (K_1, O_1, P_1 and Q_1) and semidiurnal tidal constituents (M_2, S_2, N_2 and K_2) with a spatial resolution of 0.25° × 0.25° based on TOPEX/POSEIDON altimetry data (DHI, 2008c).

A wind that varies in time but is constant over the model domain is applied. The wind used for the hydrodynamic calibration is the wind measured locally at the Bantamsklip site by Airshed Planning Professionals (Pty) Ltd. The wind used for the thermal plume and sediment transport simulations is the offshore Oceanor hindcast dataset (Section 6.2). As part of the model calibration process, the offshore winds were compared to the local winds and it was found that the offshore wind speed should be scaled by 0.7 in order to realistically simulate the measured wind-driven currents. The default wind drag coefficient C_d is used, which is a linear variation from 0.001255 at 7 m/s to 0.002425 at 25 m/s.

Wave-driven currents are included by first running the calibrated MIKE Spectral Waves model (refer to Section 6.4) and saving the radiation stresses at three hour intervals. The numerical grid for the wave refraction model corresponds to the hydrodynamic grid in the hydrodynamic domain, but extends further offshore to the 200 m contour (Figure 6.7).

For bed resistance the default roughness height k_s of 0.05 m is applied. Horizontal eddy viscosity and dispersion are computed using the Smagorinsky formulation with a default constant of 0.28. Vertical eddy viscosity is computed using the k-ε vertical turbulence closure scheme, while the vertical eddy dispersion is set to 0.1 times the vertical eddy viscosity. This scaling factor is applied to compensate for additional vertical mixing caused by the use of only 5 vertical layers and the potential smoothing of the vertical density gradient between the buoyant thermal plume and the ambient water. Model sensitivity tests confirm that using a scaling factor of 0.1 results in a measureable decrease in the vertical mixing compared to the default factor of 1.0.

Model sensitivity tests were performed in which ambient thermal stratification as well as heat exchange between the atmosphere and the sea surface were included in the simulation. These two processes were found to have only a small influence on the modelled currents and the temperature increase due to the plume above the background temperature. The simulations have thus been performed using a constant background temperature. It should be borne in mind that the background sea temperature varies on a seasonal, synoptic and diurnal time-scale (refer to Figures 7.1 to 7.3) and the temperature increase due to the thermal plume will be superimposed on this background variability. A constant salinity of 35.0 psu is specified.

8.3.2 Model calibration

The hydrodynamic model is first calibrated against measured currents at the Bantamsklip site. In addition, the thermal plume dispersion capabilities of the model have been calibrated against measured thermal plume temperatures. In the absence of an existing thermal plume at Bantamsklip, the plume at the existing Koeberg Nuclear Power Station is employed.

The model is first calibrated by comparing the modelled current speed and direction to those measured over a two month period at Sites A and B (see Figure 3.1 for the instrument locations). The calibration results are shown in Figures 8.5 to 8.7. The model is seen to reproduce the main features of measured currents, indicating that the key hydrodynamic forcing mechanisms, i.e. wind, wave and tides, are realistically simulated by the model.

The model is then calibrated by comparing the thermal plume predicted by the model to historical measurements of the plume from the existing Koeberg Nuclear Power Station (in the absence of an existing thermal plume at Bantamsklip). The historical Koeberg measurements were conducted using a skiboat and a helicopter (Rattey and Potgieter, 1987). The skiboat was equipped with a temperature probe mounted 30 cm below the water surface and traversed the study area on a grid pattern in order to measure the ambient water temperature and define the surface extent of the thermal plume. A helicopter equipped with an infrared sea surface temperature recorder was also used and took measurements on a grid pattern from a height of 100 m above the sea surface. Both sets of measurements were then combined to obtain an average picture of the thermal plume over the survey period of approximately 1 hour.

The surveys conducted on 14, 16 and 18 October 1985 were selected for model calibration. During all these surveys both reactors were operational and the discharge rate was 80 m^3/s, the intake temperature was approximately 13°C and the outfall temperature was approximately 23°C, i.e. a ΔT of 10°C. To allow a "spin-up" period, the model was run from 10 October to 19 October 1985, with an initial background temperature of 13°C. The wind applied in the model was the hourly data measured at 10 m height at Koeberg (Eskom, 1985), with the wind speed increased by a factor 1.65 to account for the increase in wind speed offshore (PRDW, 2009b). The wave height and period applied on the offshore boundary of the model were the 6 hourly values measured by a Waverider buoy in 170 m water depth approximately 15 km west of Slangkop (PRDW, 2009b). Since the wave direction was not measured, a constant direction of 230° was assumed, corresponding to the average wave direction obtained from wave hindcast data in this area.

The plume calibration results are plotted in Figures 8.8 to 8.10. Considering the uncertainties in the measurements (e.g. due to the averaging of the plume over the hour long survey period) and the uncertainties in the model inputs (e.g. the assumed wave direction and the constant background temperature field), the model results correspond well to the measurements and thus provide confidence in the predictive capability of the model.

8.3.3 Selection of representative hydrodynamic conditions

The Oceanor hindcast dataset (Section 6.2) includes 10 years of simultaneous wave and wind data which are required as input forcing to the hydrodynamic model, along with tidal forcing. However, the computer run-times for the three-dimensional hydrodynamic model limit the period that can be simulated to a number of months. A rigorous procedure was thus developed to select the following periods from the 10 year dataset:

- A 14 day period with typical summer conditions
- A 14 day period with typical winter conditions
- A 14 day period with calm conditions (low waves and wind).

The procedure first calculates the following parameters for each consecutive 14 day period in the 10 year dataset (values in brackets are the weighting factor applied in the cost function):

- The mean wave height (1.0)
- The standard deviation of the wave height (0.2)
- The mean wave direction, weighted by the wave height (1.0)
- The mean peak period (0.4)
- The mean wind speed (1.0)
- The standard deviation of the wind speed (0.2)
- The mean wind direction, weighted by the wind speed (1.0).

The procedure then uses a cost function (i.e. a function that minimises the difference between two values) to locate the 14 day period having parameters closest to the average conditions for each season. The calmest 14 day period was located using a weighting factor of 2.0 for mean wave height and 1.0 for mean wind speed, with all other weights set to zero. The periods located by this process are given below, and the wind and wave conditions for each period are plotted in Figures 8.11 to 8.13.

- 14 day summer period: 2006-01-05 to 2006-01-19
- 14 day winter period: 2001-06-21 to 2001-07-05
- 14 day calm period: 1997-04-08 to 1997-04-22

For the plume dispersion modelling, these three periods have been run sequentially giving a total simulation time of 42 days.

9. THERMAL PLUME DISPERSION

9.1 Background

The advantage of locating the power station at the coast is that it allows a once-through seawater cooling system to be used. However, the intake and outfall structures need to be designed to minimize recirculation between the outfall and the intake, and to ensure that the potential ecological impacts due to the discharge of heated water and other co-discharges such as chlorine and nuclides are acceptable.

9.2 Discharge characteristics

The Site Safety Report is based on a Plant Parameter Envelope (PPE) of 10 000 MWe, which according to Eskom (2008a) may include various combinations of conventional nuclear reactors and/or Pebble Bed Modular Reactors (PBMRs). Since the thermal plume modelling results described in this report will also be used for the Nuclear-1 EIA, the plume due to Nuclear-1 (maximum output of 4000 MWe) has also been modelled.

The cooling water requirements are characterised by the seawater flow rate and the temperature increase between the intake and the outfall (ΔT). The seawater cooling water requirement for the conventional nuclear reactors is based on information provided by Eskom (2008b), which indicates that a Pressurised Water Reactor (PWR) with a power of 1 650 MWe requires 76 m^3/s of cooling water and increases the water temperature by 12°C. It is assumed that for other power outputs the flow rate can be scaled linearly in proportion to the power while the temperature increase remains constant, i.e. the flow rate is 0.0460 $m^3/s/MWe$.

The estimated cooling water requirements for the PBMR have been provided by PBMR (2009), which indicate that a power of 400 MWt (delivering 160 MWe) requires 6 000 kg/s (approximately 6 m^3/s) of cooling water with a ΔT of 12°C, i.e. 0.0375 $m^3/s/MWe$. Since the PBMR has the same ΔT as the conventional reactor but a lower flow rate per MWe, it is conservative to base the site cooling water requirements on those for a conventional reactor, as given in Table 9.1.

TABLE 9.1: SEAWATER COOLING REQUIREMENTS

Power output [MWe]	Seawater flow rate [m^3/s]	ΔT [°C]	Comment
10 000	456	12	Site Safety Report
4 000	184	12	Nuclear-1 EIA Study

In addition to the increased temperature, the cooling water discharge may also contain co-discharges such as chlorine, nuclides, etc. Since these co-discharges have not yet been quantified, for this modelling study these are treated as conservative tracers, i.e. they undergo dilution by physical mixing only and any additional biochemical or physical processes are not modelled. The model results provide

the achievable dilutions for any discharged constituent. Once the concentration of these constituents has been quantified, the potential impact of these constituents can be assessed by comparing the achievable dilutions from the model results to the dilution required to reduce the concentration at discharge to a level at which no impacts occur.

Reverse Osmosis desalination is being considered to provide fresh water during the earthworks, construction and operation stages of the power station (Eskom, 2008b). During operation of the power installation, the brine discharge from the desalination plant will be mixed with the once-through cooling water discharge from the power station and discharged at the cooling water outfall. The operational stage desalination plant fresh water output is 4000 m^3/day (Eskom, 2008b). The brine output flow associated with this is 6000 m^3/day (or 0.069 m^3/s), while the cooling water discharge rate for Nuclear-1 with an expected power output of 3300 MWe will be approximately 152 m^3/s (Eskom 2008b). This means that the brine will be diluted 2 200 times in the pipe prior to discharge into the sea, making the brine effectively undetectable.

During the earthworks and construction stages, however, the cooling water outfall structure will not be completed and the brine will have to be discharged independently of the cooling water. The dilution of the construction stage brine has been modelled in PRDW (2008). Since the brine is not considered to be a site safety issue, it is not considered further in this report.

9.3 Intake and outfall layouts tested

9.3.1 Background

Since no engineering feasibility studies on the intake and outfall structures have been completed, six conceptual layouts were developed which serve to illustrate the thermal plumes and recirculation that can be anticipated for typical combinations of intake and outfall types. General design considerations for the intake and outfall are discussed in PRDW (2009a).

The intakes considered are basins and offshore tunnels, while the outfalls considered are nearshore channels and offshore tunnels. The layouts that were modelled are described below. Note that these are conceptual layouts that will need to be refined based on geotechnical and engineering considerations. All layouts are tested for a power output of 10 000 MWe as required for the Site Safety Report. In addition, Layouts 1 and 6 are also tested for a 4000 MWe output as required for the Nuclear-1 EIA study (refer to Table 9.1 for the cooling water requirements).

9.3.2 Layout 1: Offshore tunnel intake (45 m depth) and offshore tunnel outfall (25 m depth)

The intakes comprise submarine tunnels extending to a depth of approximately 45 m approximately 3.3 km offshore (see Figure 9.1). Intake structures will be positioned at the end of each intake tunnel with the intake openings positioned 3 to 5 m above the sea bed to prevent the drawing in of large

quantities of sediment. To reduce fish entrainment the intake openings should be designed to draw in water horizontally with a velocity of less than 0.3 m/s.

For the purposes of these tests, it is assumed that each reactor unit has a power output of 1 650 MWe and that there is one intake tunnel per reactor unit. This requires six tunnels for a power output of 10 000 MWe. Each tunnel has a flow of 76 m^3/s. The diameter of the tunnels is designed to avoid the risk of sediments settling in the tunnel (minimum velocity of 2.5 m/s). On the other hand, the velocity in the tunnels needs to be limited in order to reduce head losses in the tunnel. On this basis a tunnel diameter of 6.5 m is selected. Other configurations (reactor units with a different power outputs or a different number of tunnels) are possible, but the resulting thermal plumes are expected to be similar, provided the total power output remains at 10 000 MWe.

The outfalls comprise submarine tunnels extending to a depth of approximately 25 m approximately 2.5 km offshore. Following the same reasoning as the intake tunnels, there are six outfall tunnels each with a diameter of 6.5 m. Each outfall ends in a 200 m long diffuser with 5 ports at 50 m spacing. The ports have a diameter of 2 m and discharge vertically upwards from a height of 2 m above the seabed. The diffuser layout was selected to achieve an initial dilution of at least 10 and to ensure that the plume surfaces under all current and ambient stratification conditions. It is preferable that the plume is not trapped near the seabed as there is then an increased risk of ecological impacts at the seabed and also of recirculation back to the intakes. Further details of the diffuser and the near-field modelling is provided in Section 9.5.1. The lengths of the outfall tunnels are staggered to reduce interaction between thermal plumes from adjacent tunnels (see Figure 9.1).

In addition to the 10 000 MWe power output tested for the Site Safety Report, this layout is also tested for a 4000 MWe output as required for the Nuclear-1 EIA study (refer to Table 9.1 for the cooling water requirements). In this case only two intake tunnels and two outfall tunnels were modelled, with a flow of 92 m^3/s in each tunnel.

9.3.3 Layout 2: Basin intake and offshore tunnel outfall (40 m depth)

The intake is a basin which is conceptually modelled as an upscaled version of the existing Koeberg basin (see Figure 9.2). The basin has the following dimensions (refer to PRDW (2009a) for the design criteria used to derive these dimensions):

- Entrance width (measured to centre-line of breakwater): 145 m
- Entrance depth: -12 m CD
- Settling basin width: 530 m
- Settling basin length: 750 m
- Settling basin depth: -7.5 m
- Intake depth: -5 m CD.

Six intake pump houses are evenly distributed along the landward wall of the basin.

The outfall comprises six tunnels extending to a depth of approximately 40 m approximately 3.5 km offshore. Each outfall ends in a 200 m long diffuser with the same configuration described for Layout 1.

9.3.4 Layout 3: Offshore tunnel intake (45 m depth) and nearshore channel outfall (2 m depth)

The intakes are the same as Layout 1, i.e. six tunnels extending to a depth of approximately 45 m approximately 3.3 km offshore with intake openings positioned 3 to 5 m above the seabed (see Figure 9.3).

The outfall is a nearshore channel located on the north-west corner of the site (Figure 9.3) which is conceptually modelled as an upscaled version of the existing Koeberg outfall channel. The channel is 120 m wide and is divided into three sub-channels each 40 m wide (one channel per two reactor units). The offshore end of the channel extends 200 m offshore to a depth of approximately -2 m CD and the invert level at the offshore end of the channel is -1 m CD.

9.3.5 Layout 4: Basin intake and nearshore channel outfall (2 m depth)

The basin intake is the same as described for Layout 2. The nearshore channel outfall is the same as described for Layout 3 (Figure 9.4).

9.3.6 Layout 5: Offshore tunnel intake (30 m depth) and nearshore channel outfall (5 m depth)

This is a refinement of Layout 3. The tunnel intakes have been shortened and now extend to a depth of 30 m approximately 2.5 km offshore (Figure 9.5). The channel outfall has been extended to direct the thermal plume beyond the surf-zone. The offshore end of the channel is now 600 m offshore in a depth of approximately -5 m CD and the invert level at the offshore end of the channel is -1 m CD.

9.3.7 Layout 6: Basin intake and nearshore channel outfall (5 m depth)

The basin intake is the same as described for Layout 2. The nearshore channel outfall is the same as described for Layout 5, i.e. compared to Layout 4 the only difference is the extension of the channel outfall from 200 m to 600 m long (Figure 9.6).

In addition to the 10 000 MWe power output tested for the Site Safety Report, this layout is also tested for a 4000 MWe output as required for the Nuclear-1 EIA study (refer to Table 9.1 for the cooling water requirements). In this case the discharge was released into only one of the three 40 m wide sub-channels.

9.4 Model setup

9.4.1 Near-field model

Layouts 1 and 2 include an offshore tunnel outfall with a diffuser. In these cases the near-field dilutions (i.e. the dilution that occurs as the plume rises from the diffuser ports toward the water surface) and plume geometry has been modelled using the CORMIX model (see Section 2.9).

In this case it is preferable to design the diffuser to ensure that the plume rises to the surface instead of being trapped near the seabed, since there is then an increased risk of ecological impacts at the seabed and also since the tunnel intakes are located near the seabed and there would then be an increased risk of recirculation.

The CORMIX model inputs are the diffuser characteristics, the discharge characteristics and the ambient currents and stratification. The thermal stratification cases modelled are a well-mixed (i.e. unstratified) winter case and a strongly stratified summer case, based on the seawater temperature measurements at the site (see Figures 7.1 and 7.2). The inputs for Layouts 1 and 2 are given in Table 9.2 and Table 9.3, respectively.

TABLE 9.2: NEAR-FIELD DILUTION MODEL INPUTS FOR LAYOUT 1

Parameter	Value
Water depth	25 m
Diffuser length	200 m
Number of ports	5
Port height above seabed	2 m
Port diameter	2 m
Port orientation	Vertical
Discharge flow rate (total for all 5 ports)	76 m^3/s
Salinity	35 psu
Ambient current speeds	0.05, 0.1, 0.2, 0.4, 0.8 m/s
Ambient temperature at outfall at surface (unstratified | stratified)	15°C | 18°C
Ambient temperature at outfall at seabed, depth is 25 m (unstratified | stratified)	15°C | 12°C
Ambient temperature at intake, depth is 45 m (unstratified | stratified)	15°C | 11°C
Discharge temperature (unstratified | stratified)	27°C | 23°C

TABLE 9.3: NEAR-FIELD DILUTION MODEL INPUTS FOR LAYOUT 2

Parameter	Value
Water depth	40 m
Diffuser length	200 m
Number of ports	5
Port height above seabed	2 m
Port diameter	2 m
Port orientation	Vertical
Discharge flow rate (total for all 5 ports)	76 m^3/s
Salinity	35 psu
Ambient current speeds	0.05, 0.1, 0.2, 0.4, 0.8 m/s
Ambient temperature at outfall at surface (unstratified | stratified)	15°C | 18°C
Ambient temperature at outfall at seabed, depth is 40 m (unstratified | stratified)	15°C | 11°C
Ambient temperature at intake, depth is 5 m (unstratified | stratified)	15°C | 14°C
Discharge temperature (unstratified | stratified)	27°C | 26°C

9.4.2 Far-field model

The MIKE 3 Flow Flexible Mesh three-dimensional hydrodynamic model (as described in Section 2.5) has been set up to simulate the currents and the far-field dispersion of the thermal plume due to winds, waves, tides and buoyancy effects. The setup and calibration of the model is described in Sections 8.3.1 and 8.3.2, respectively. The selection of a 42 day simulation period comprising typical summer conditions, typical winter conditions and extreme calm conditions (low waves and wind) is described in Section 8.3.3.

As discussed in Section 8.3.2, the simulations have been performed using a constant background temperature of 15°C. At the intake point water is withdrawn from the model at the appropriate flow rate (refer to the cooling water requirements in Table 9.1) and then discharged at the outfall point at a temperature ΔT higher than the intake temperature. This means that temperature build-up due to recirculation is simulated explicitly.

In cases where the intake is located in deep water and the outfall is near the surface, the effective ΔT will be reduced, since the available measurements (Section 7.1) indicate that the temperature at depths of 30 to 45 m are on average 2 to 3°C colder than near the surface. This difference has not been included in the far-field modelling, which makes the model results for Layouts 3 and 5 somewhat conservative.

9.5 Results

9.5.1 Near-field dilution

Layouts 1 and 2 include an offshore tunnel outfall with a diffuser. In these cases the near-field dilutions (i.e. the dilution that occurs as the plume rises from the diffuser ports toward the water surface) and plume geometry has been modelled using the CORMIX model. The model set-up is described in Section 9.4.1.

The near-field model results include the initial dilutions, the horizontal plume width (reported here as the full width and not the half-width as given in the model output files), and the upper and lower plume boundary (measured upwards from the seabed). The results are extracted at the end of the near-field (i.e. once the vertical rise phase is complete) as well as at fixed distances of 500 m and 1000 m down current of the discharge point. These results are tabulated below and are plotted in Figures 9.7 and 9.8.

TABLE 9.4: NEAR-FIELD DILUTION RESULTS FOR LAYOUT 1

Parameter	Current speed [m/s]				
	0.05	0.1	0.2	0.4	0.8
End of near-field					
Dilution [-]	15.2 | 12.5	13.2 | 11.3	15.8 | 15.0	27.8 | 27.0	53.1 | 53.0
Horizontal plume width [m]	5778 | 4094	976 | 658	278 | 250	220 | 206	202 | 202
Upper plume boundary [m]	25.0 | 25.0	25.0 | 25.0	25.0 | 25.0	25.0 | 25.0	25.0 | 25.0
Lower plume boundary [m]	21.0 | 20.3	14.7 | 12.0	3.5 | 2.2	1.2 | 0.0	0.0 | 0.0
After 500 m					
Dilution [-]	9.7 | 10.0	13.9 | 12.4	19.2 | 17.7	31.5 | 31.2	59.4 | 59.5
Horizontal plume width [m]	5382 | 3894	1164 | 956	594 | 484	360 | 352	272 | 258
Upper plume boundary [m]	25.0 | 25.0	25.0 | 25.0	25.0 | 25.0	25.0 | 25.0	25.0 | 25.0
Lower plume boundary [m]	22.1 | 20.9	16.0 | 15.2	12.8 | 11.1	8.3 | 8.1	4.3 | 3.1
After 1000 m					
Dilution [-]	13.7 | 12.2	15.9 | 14.3	22.0 | 20.6	35.7 | 35.4	68.6 | 70.4
Horizontal plume width [m]	5592 | 4032	1982 | 1648	998 | 854	550 | 514	360 | 328
Upper plume boundary [m]	25.0 | 25.0	25.0 | 25.0	25.0 | 25.0	25.0 | 25.0	25.0 | 25.0
Lower plume boundary [m]	21.3 | 20.4	18.9 | 18.4	16.6 | 15.8	12.7 | 11.9	6.8 | 4.6

Notes: All results are given for two thermal stratification cases: unstratified | stratified

TABLE 9.5: NEAR-FIELD DILUTION RESULTS FOR LAYOUT 2

Parameter	Current speed [m/s]				
	0.05	0.1	0.2	0.4	0.8
End of near-field					
Dilution [-]	24.3 | 23.6	21.3 | 20.6	25.5 | 25.3	43.7 | 43.6	85.0 | 77.7
Horizontal plume width [m]	5896 | 5658	990 | 922	286 | 283	208 | 208	202 | 202
Upper plume boundary [m]	40.0 | 40.0	40.0 | 40.0	40.0 | 40.0	40.0 | 40.0	40.0 | 40.0
Lower plume boundary [m]	33.7 | 33.7	23.7 | 23.0	6.2 | 6.1	0.0 | 0.0	0.0 | 0.0
After 500 m					
Dilution [-]	15.6 | 15.1	22.2 | 21.6	30.7 | 29.9	50.5 | 50.2	92.3 | 84.6
Horizontal plume width [m]	5268 | 5486	1178 | 1110	600 | 554	366 | 360	264 | 270
Upper plume boundary [m]	40.0 | 40.0	40.0 | 40.0	40.0 | 40.0	40.0 | 40.0	40.0 | 40.0
Lower plume boundary [m]	35.3 | 35.1	25.7 | 25.2	20.6 | 19.5	13.8 | 13.5	6.8 | 7.4
After 1000 m					
Dilution [-]	22.0 | 21.3	25.4 | 24.9	35.0 | 34.6	56.7 | 56.4	102.6 | 93.9
Horizontal plume width [m]	5704 | 5474	2000 | 1924	1002 | 978	560 | 548	348 | 360
Upper plume boundary [m]	40.0 | 40.0	40.0 | 40.0	40.0 | 40.0	40.0 | 40.0	40.0 | 40.0
Lower plume boundary [m]	34.2 | 34.1	30.3 | 30.2	26.7 | 26.5	20.7 | 20.5	12.0 | 13.0

Notes: All results are given for two thermal stratification cases: unstratified | stratified

Layout 2 achieves higher initial dilutions than Layout 1 due to the increased water depth available for dilution. The increase is approximately proportional to the water depth, i.e. 40 m/25 m = 60% increase in dilution. For all conditions tested the initial dilution exceeds 9.7 for Layout 1 and 15.6 for Layout 2. In all cases tested the plume reaches the water surface. There is little difference between the

unstratified and the stratified cases, which indicates that for this diffuser configuration the buoyancy and momentum fluxes of the discharge dominate the ambient stratification.

The results show that a realistic coupling between the near- and far-field models can be achieved if the discharge is released into the far-field model over a horizontal width of 400 m (directly above the 200 m long diffuser) and into the upper half of the water column, i.e. for Layout 1 the upper plume boundary at 25 m and lower plume boundary at 12.5 m above the seabed, and for Layout 2 the upper plume boundary at 40 m and lower plume boundary at 20 m. The resulting far-field approximation of the near-field dilution is shown in Figures 9.7 and 9.8.

9.5.2 Far-field temperature and dilution

The thermal plume from the outfall is advected and dispersed by the ambient currents. The currents are seen to be predominantly wave-driven in the surf-zone and wind- and tidally-driven beyond the surf-zone. Figure 9.9 illustrates an example of the modelled currents and thermal plume at a time when the currents are going north, while Figure 9.10 shows an example of a time when the currents are southward. Since the currents are continually changing as the wave, wind and tidal conditions change, the position and size of the plume shows corresponding changes.

The model results for each layout have been post-processed to determine the maximum and mean (i.e. time-averaged) increase in temperature above background over the full 42 day simulation period. This has been done for both the surface and seabed layers of the model. The results are presented in Figures 9.11 to 9.26. Since the background sea temperature varies on a seasonal, synoptic and diurnal time-scale (refer to Figures 7.1 to 7.3), the temperature increase due to the thermal plume will be superimposed on this background variability.

These model results show the following:

- The maximum increase in temperature is significantly higher and more extensive than the mean increase in temperature (compare for example Figures 9.11 and 9.12). This is due to the dynamic plume behaviour which results in the plume remaining at one position for short periods of time only.
- The buoyancy of the plume due to the increased temperature tends to keep the plume near the water surface rather than the seabed, particularly as the plume is advected into deeper water. In the shallow water (less than 5 m) the plume tends to be mixed throughout the water column by vertical turbulence.
- Layout 2 results in a smaller thermal plume than Layout 1, due to the longer outfall tunnels which discharge into deeper water (40 m versus 25 m). Compare Figures 9.12 and 9.14.
- The nearshore channel outfall design (Layouts 3 to 6) results in a significantly larger thermal plume than the offshore tunnel outfalls (Layouts 1 and 2). This is due to the nearshore channel outfall discharging into shallow water with a limited volume of ambient water available for

mixing, rather than a deep offshore tunnel with a diffuser and high near-field mixing. Compare for example Figures 9.14 and 9.16.

- Extending the length of the nearshore channel outfall (Layouts 5 and 6) directs the plume offshore and reduces the temperatures at the shoreline. Compare for example Figures 9.16 and 9.20.
- The nearshore (<10 m depth) currents to the north of the site predominantly flow in a north-westerly direction (see for example Figure 9.15). For this reason the nearshore channel outfall is located to the north of the intake in order to reduce the risk of re-circulation.
- Reducing the flow rate from 456 to 184 m^3/s (i.e. from the 10 000 MWe power output tested for the Site Safety Report to a 4000 MWe output as required for the Nuclear-1 EIA study) reduces the extent of the plume by approximately half. Compare for example Figures 9.12 and 9.24, and Figures 9.22 and 9.26.

These results can also be interpreted as dilution factors for any co-discharges such as chlorine, nuclides, etc. as follows: divide 12 (the initial temperature increase) by the temperature increase shown in the plots, e.g. the 2°C contour in the plots represents a dilution factor of 12/2 = 6. If the co-discharge is mixed with the cooling water prior to discharge into the sea, the co-discharge will undergo a pre-dilution in the pipe in addition to the subsequent dilution in the sea.

These model results can be used to assess the potential ecological impacts due to the discharge of heated water and other co-discharges such as chlorine and nuclides.

9.5.3 Recirculation

The model results have been analysed to determine the recirculation of the thermal plume from the outfalls back to the intakes. Note that the hydrodynamic model automatically accounts for recirculation by constantly adjusting the outfall temperature to be 12°C above the intake temperature at each time-step. The results are plotted in Figure 9.27 and tabulated below.

TABLE 9.6: THERMAL RECIRCULATION RESULTS

Layout	Power output [MWe]	Mean temperature increase at intake [°C]	Maximum temperature increase at intake [°C]
Layout 1	10 000	0.4	1.0
Layout 2	10 000	0.9	2.0
Layout 3	10 000	0.4	1.2
Layout 4	10 000	0.7	3.2
Layout 5	10 000	0.6	2.1
Layout 6	10 000	0.8	3.4
Layout 1	4 000	0.2	0.8
Layout 6	4 000	0.4	2.2

These results indicate no significant recirculation problems for any of the layouts tested. The maximum recirculation temperatures occur for the layouts with a nearshore channel outfall and a basin intake (Layouts 4 and 6).

Although recirculation is generally undesirable as it may decrease the efficiency of the cooling system, the allowable recirculation depends on the ambient temperatures (see Section 7.2) as well as the maximum allowable intake temperatures. For the existing Koeberg units, a shut-down of the reactor will be necessary if the intake temperature exceeds 23°C (Eskom, 2006). It is expected that the cooling water system for future nuclear installations at the site will be designed to allow higher intake temperatures, e.g. one type of Pressurised Water Reactor (PWR) allows a maximum cooling water temperature of 30°C, as well as an extreme temperature of 34.5°C for the safety assessment (Eskom, 2007).

Making the very conservative assumption that the maximum recirculation event corresponds to the maximum ambient temperature, then for Layout 6 the maximum intake temperature for the 1:100 year return period would be 25.3°C (see Table 7.2) + 3.4°C (see Table 9.6) = 28.7°C. The other layouts would have lower intake temperatures due to lower recirculation and/or due to the intake being located in deeper water, e.g. tunnel intakes instead of the basin intake for Layout 6.

10. SEDIMENT TRANSPORT

10.1 Background

The aim of this section is to assess the sediment transport regime in the vicinity of the Bantamsklip site. In addition, the concentration of suspended sediment in the water column is modelled for various intake depths and wave conditions.

Additional sediment related studies are described in the Coastal Engineering Report (PRDW, 2009a). These include the analysis of historical beach plan shapes, beach erosion by storms, set-back due to sea level rise and sediment movement by tsunamis.

10.2 Sediment grain size

Sediment samples were taken on the beaches near the high and low water marks on 25 March 2008. Samples were also taken from the nearshore (10 to 30 m depth) using a Van Veen grab on 26 and 27 March 2008. Of the 20 nearshore stations sampled, 13 were found to be located on rocky reef and sand samples were thus obtained from only 7 nearshore stations. The grain size analysis is given in Table 10.1 and the spatial variation of the D_{50} grain size is plotted in Figure 10.1. D_N is the diameter for which N% of the sediment, by weight, has a smaller diameter. The sediment grading is defined as $(D_{84}/D_{16})^{0.5}$.

The results indicate that the sand on the beach at Pearly Beach is uniform with an average D_{50} of 0.20 mm and an average grading of 1.3. The sand on the beach in front of the Nuclear Plant Corridor is variable, with D_{50} varying from 0.14 to 0.61 mm, and the grading from 1.3 to 1.5. The 7 nearshore samples had a D_{50} ranging from 0.14 to 0.61 mm and a grading from 1.2 to 1.6. The nearshore sampling indicates extensive rocky reef offshore of the site, see also Figure 1.2.

TABLE 10.1: SEDIMENT GRAIN SIZE ANALYSIS FOR BANTAMSKLIP

Longitude [deg]	Latitude [deg]	D_{95} [mm]	D_{90} [mm]	D_{84} [mm]	D_{75} [mm]	D_{50} [mm]	D_{25} [mm]	D_{16} [mm]	D_{10} [mm]	D_5 [mm]	Grading [-]	Gravel [%]	Sand [%]	Silt [%]
19.583883	-34.730867	0.47	0.36	0.32	0.27	0.22	0.18	0.17	0.16	0.14	1.4	0.0	100.0	0.0
19.583450	-34.735117	0.28	0.22	0.20	0.18	0.15	0.13	0.12	0.11	0.10	1.3	0.0	100.0	0.0
19.560317	-34.717983	0.76	0.62	0.53	0.46	0.34	0.25	0.21	0.17	0.15	1.6	0.4*	99.6	0.0
19.533517	-34.697817	1.10	0.95	0.86	0.76	0.61	0.50	0.46	0.42	0.39	1.4	0.2	99.6	0.2
19.531267	-34.696500	0.63	0.30	0.20	0.17	0.15	0.13	0.12	0.11	0.10	1.3	1.2*	98.8	0.0
19.517983	-34.681733	0.21	0.18	0.17	0.16	0.14	0.13	0.12	0.11	0.11	1.2	0.0	100.0	0.0
19.516367	-34.680833	0.20	0.18	0.17	0.16	0.14	0.13	0.12	0.11	0.11	1.2	0.0	100.0	0.0
19.491950	-34.665733	0.41	0.35	0.32	0.29	0.22	0.17	0.16	0.15	0.14	1.4	0.0	100.0	0.0
19.518133	-34.670650	0.47	0.42	0.39	0.35	0.28	0.21	0.19	0.18	0.16	1.4	0.0	100.0	0.0
19.521633	-34.672450	0.35	0.31	0.29	0.26	0.21	0.18	0.16	0.16	0.14	1.3	0.0	100.0	0.0
19.525267	-34.674350	0.30	0.27	0.24	0.22	0.18	0.16	0.15	0.15	0.14	1.3	0.0	100.0	0.0
19.528633	-34.676967	0.26	0.23	0.22	0.20	0.18	0.16	0.15	0.15	0.14	1.2	0.0	100.0	0.0
19.531233	-34.679533	0.29	0.25	0.23	0.21	0.18	0.16	0.15	0.15	0.14	1.2	0.0	100.0	0.0
19.532483	-34.684150	0.36	0.32	0.29	0.25	0.21	0.17	0.16	0.16	0.15	1.3	0.0	100.0	0.0
19.542050	-34.691883	0.40	0.36	0.34	0.31	0.26	0.22	0.21	0.19	0.18	1.3	0.0	100.0	0.0
19.546133	-34.696283	0.41	0.37	0.34	0.32	0.28	0.24	0.22	0.21	0.19	1.3	0.0	100.0	0.0
19.552250	-34.702600	0.00	1.33	0.70	0.56	0.45	0.39	0.37	0.34	0.31	1.4	6.8*	93.2	0.0
19.558867	-34.710767	0.46	0.41	0.38	0.35	0.29	0.24	0.22	0.21	0.19	1.3	0.0	100.0	0.0
19.561750	-34.712033	0.50	0.45	0.42	0.38	0.31	0.26	0.24	0.23	0.21	1.3	0.0	100.0	0.0
19.564550	-34.713483	0.91	0.72	0.63	0.54	0.42	0.34	0.31	0.28	0.25	1.4	0.4*	99.6	0.0
19.566783	-34.715250	0.64	0.55	0.49	0.45	0.37	0.31	0.28	0.26	0.23	1.3	0.0	100.0	0.0
19.568867	-34.717650	0.89	0.76	0.67	0.59	0.46	0.38	0.35	0.33	0.30	1.4	0.0	100.0	0.0
19.571983	-34.718900	1.09	0.96	0.89	0.82	0.69	0.57	0.53	0.49	0.43	1.3	0.0	100.0	0.0
19.589500	-34.724583	0.63	0.55	0.49	0.44	0.36	0.30	0.27	0.26	0.23	1.3	0.0	100.0	0.0
19.595750	-34.728617	0.38	0.33	0.30	0.27	0.23	0.20	0.19	0.18	0.17	1.3	0.0	100.0	0.0
19.596467	-34.730183	0.35	0.32	0.29	0.26	0.22	0.19	0.18	0.17	0.16	1.3	0.0	100.0	0.0
19.631967	-34.754317	0.33	0.29	0.26	0.24	0.20	0.17	0.16	0.15	0.14	1.3	0.0	100.0	0.0
19.491800	-34.665800	0.41	0.36	0.33	0.29	0.22	0.17	0.16	0.15	0.14	1.4	0.0	100.0	0.0
19.518100	-34.670733	0.39	0.34	0.31	0.27	0.21	0.18	0.16	0.15	0.14	1.4	0.0	100.0	0.0
19.521567	-34.672567	0.43	0.37	0.33	0.28	0.20	0.17	0.15	0.15	0.14	1.5	0.0	100.0	0.0
19.525050	-34.674617	0.29	0.25	0.24	0.22	0.19	0.17	0.16	0.15	0.14	1.2	0.0	100.0	0.0
19.528417	-34.677117	0.30	0.25	0.23	0.21	0.18	0.16	0.15	0.14	0.14	1.2	0.0	100.0	0.0
19.531150	-34.679617	0.33	0.28	0.25	0.23	0.19	0.17	0.16	0.15	0.14	1.2	0.0	100.0	0.0
19.532333	-34.684267	0.35	0.30	0.27	0.24	0.19	0.17	0.16	0.15	0.14	1.3	0.0	100.0	0.0
19.542000	-34.691917	0.47	0.41	0.36	0.33	0.28	0.23	0.21	0.20	0.18	1.3	0.0	100.0	0.0
19.546050	-34.696333	0.57	0.48	0.44	0.39	0.32	0.27	0.25	0.23	0.21	1.3	0.0	100.0	0.0
19.552233	-34.702650	1.79	1.16	0.87	0.68	0.49	0.43	0.40	0.38	0.36	1.5	4.2*	95.8	0.0
19.558783	-34.710917	0.43	0.37	0.34	0.31	0.26	0.21	0.20	0.18	0.16	1.3	0.0	100.0	0.0
19.561733	-34.712083	0.49	0.44	0.40	0.36	0.30	0.25	0.23	0.21	0.19	1.3	0.0	100.0	0.0
19.564533	-34.713550	0.62	0.53	0.48	0.44	0.36	0.29	0.27	0.25	0.22	1.3	0.0	100.0	0.0
19.566767	-34.715317	0.65	0.55	0.48	0.44	0.35	0.28	0.26	0.24	0.21	1.4	0.0	100.0	0.0
19.568883	-34.717700	1.18	0.99	0.87	0.75	0.55	0.43	0.39	0.36	0.31	1.5	0.4*	99.6	0.0
19.572017	-34.718967	1.30	1.08	0.96	0.87	0.70	0.58	0.54	0.50	0.45	1.3	1.7*	98.3	0.0
19.589483	-34.724617	0.62	0.51	0.46	0.41	0.33	0.28	0.26	0.24	0.22	1.3	0.0	100.0	0.0
19.595700	-34.728683	0.40	0.34	0.31	0.28	0.23	0.19	0.18	0.17	0.16	1.3	0.0	100.0	0.0
19.596350	-34.730233	0.35	0.31	0.28	0.25	0.21	0.19	0.18	0.17	0.15	1.3	0.0	100.0	0.0
19.631883	-34.754417	0.35	0.31	0.27	0.24	0.20	0.17	0.16	0.15	0.14	1.3	0.0	100.0	0.0

Notes: *These samples contained shelly matter in the gravel

10.3 Sediment transport rates

10.3.1 Model setup

The MIKE 21 Coupled Flexible Mesh model (as described in Section 2.6) is used. The model simulates wave refraction, wave-driven currents, wind-driven currents and non-cohesive sediment transport over a two-dimensional domain. The model grid and bathymetry are similar to that used in the wave modelling (Figure 6.7) and the plume dispersion modelling (Figure 8.4). The grid is refined to less than 50 m in the nearshore areas.

10.3.2 Schematisation of wave and wind climate

The deepwater wave and wind hindcast data described in Section 6.2 is used to drive the model. The dataset used is the 10 year period from 1997 to 2006 at 6 hourly intervals. These data are binned into 147 conditions which are then simulated in the model.

The bin sizes used for the deepwater wave conditions are as follows: 2 m bins for H_{m0} , 25° bins for wave direction and 4 s bins for T_p. Only the longshore component of the wind is considered, since this component drives the longshore currents. The bin size for the longshore wind speed is 10 m/s.

To obtain one representative condition to model from all the conditions falling into one particular bin, H_{m0} and the wave direction are weighted by the wave energy flux $H_{m0}^2 T_p$ and the wind speed is weighted by the wind speed squared.

Each of the 147 conditions is modelled for 12 hours to achieve steady state current speeds under the imposed wave and wind forcing. The sediment transport rate and the rate of bed level change at the end of each 12 hour simulation are saved. The sediment transport rates are then weighted by the occurrence of each condition to obtain the annual sediment transport rates. Note that a fixed bed level is applied, i.e. no morphodynamic updating.

10.3.3 Model calibration

The model parameters used in the wave refraction model follow from the model calibration described in Section 6.4. The model parameters used in the hydrodynamic model follow from the model calibration described in Section 8.3.2.

The inputs to the sediment transport model include the grain size. Since this varies over the domain (Figure 10.1), separate simulations are performed using D_{50} grain sizes of 0.15, 0.2 and 0.3 mm throughout the domain. Based on a number of preliminary tests the additional parameter settings for the sediment transport model are selected as follows: critical Shields parameter = 0.05, ripples are included, bed slope effects are excluded, the deterministic formulation is used for the bed

concentration, streaming is excluded, density currents are excluded, helical flow is excluded, undertow is excluded, the wave theory is Stokes 1st order and the wave breaker index = 0.8.

The coupled wave, current and sediment transport model was first tested for a simplified case with a uniform 1:67 beach slope and a wave approaching 30° from normal. The results are seen to be qualitatively correct (Figures 10.2 and 10.3).

In the absence of sediment transport measurements at the Bantamsklip site, the model calibration procedure was to set up the model for the existing Koeberg layout and to compare the modelled net sediment transport entering the intake basin to the measured maintenance dredging volumes. The model includes the Koeberg cooling water intake pumps with an average flow rate of 86 m^3/s. The grain size is set to D_{50} = 0.2 mm, which is the typical grain size measured inside the basin (PRDW, 2002). The model gives a net sediment transport into the basin of 146 000 m^3/year (see Figure 10.4), which compares well to the average maintenance dredging volume of approximately 132 000 m^3/year (PRDW, 2002).

10.3.4 Results

The following layouts have been modelled (refer to Sections 9.2 and 9.3 for details of the layouts and the associated cooling water intake and outfall flow rates):

- Layout 1: Offshore tunnel intake and offshore tunnel outfall
- Layout 2: Basin intake and offshore tunnel outfall
- Layout 5: Offshore tunnel intake and nearshore channel outfall
- Layout 6: Basin intake and nearshore channel outfall

The offshore tunnel intakes and outfall structures will only have very localised impacts on the sediment transport field and these are too small to be resolved in this model. Layout 1 thus represents the pre-development sediment transport field.

The modelled net sediment transports for these layouts are shown in Figures 10.5 to 10.11. It is important to note that these are the potential sediment transport rates, assuming that the seabed is covered with sand. In rocky areas such as the reef offshore of the Nuclear Plant Corridor (see Figure 1.2) the actual sediment transport rates will be lower due to limited sediment availability.

These model results show the following:

- The net sediment transport field diverges at Sandy Point to the north-west of the Nuclear Plant Corridor and at Quoin Point to the south-east (see Figure 10.5), suggesting that these may approximate the boundaries of a semi-enclosed sediment cell.

- Directly in front of the Nuclear Plant Corridor is a point of low net transport indicted by the gray profile line in Figure 10.6.
- The intake basin used in Layouts 2 and 6 is positioned where the net sediment transport is low (see Figures 10.9 and 10.15), implying that a sand-bypassing scheme is unlikely to be required. This however needs to be confirmed as part of the detailed design studies.
- The modelled net sediment transport rate across the entrance of the intake basin can be used to estimate the maintenance dredging volumes for the basins. In Figures 10.7 and 10.9 the gray lines show where the transport has been calculated across the intake basin entrance. The results show an estimated 20 000 m^3/year maintenance dredging for both Layouts 2 and 6, which is significantly less than the average of 132 000 m^3/year for the existing Koeberg intake basin (PRDW, 2002). The reduction is due to the longer breakwaters and deeper entrance depths compared to Koeberg. These results do however assume that the basin entrance depth is maintained at 12 m and that there is no significant accretion of the beach on either side of the basin. This needs to be confirmed as part of the detailed design studies.
- The nearshore channel outfall is located in an area with a large net northerly sediment transport (see Figure 10.8). Although the actual transport will be significantly reduced by the rocky seabed and associated limited sediment availability, sediment accretion can be expected on the southerly updrift side of the channel and also on the northerly side due to current eddies and wave sheltering effects. Sediment will eventually bypass around the end of the channel, but there is little risk of blocking the outfall since the invert level at the offshore end of the channel is raised above the seabed (invert level -1 m CD compared to original seabed level of approximately -5 m CD) and the high-velocity discharge will scour away any localised accretion.
- The sensitivity of the model results to sediment grain sizes of 0.15 and 0.3 mm is illustrated in Figures 10.10 and 10.11. The sediment transport directions remain the same, but the smaller grain size increases the transport rate by a factor of between 2 and 4.

These model results suggest that wave-driven sediment transport will not create significant safety-related problems for the proposed new layouts. Further more detailed morphodynamic modelling will however need to be undertaken as part of the detailed design phase. An assessment of the coastline stability based on aerial photographs, beach profile measurements and cross-shore sediment transport modelling is presented in PRDW (2009a).

10.4 Suspended sediment concentrations

10.4.1 Background

For Layouts 1, 3 and 5 the proposed seawater intake is a tunnel extending to between 30 and 45 m water depth with the intake opening positioned 3 to 5 m above the seabed. One of the design parameters will be the volume of sand drawn into the intake which will have to be removed from the

proposed settling basin located on land in front of the cooling water pump house (Eskom, 2008c). Preliminary modelling is performed to estimate the volume of sand drawn into the intakes.

10.4.2 Measured suspended sediment concentrations

To date 78 water samples have been collected and analysed for Total Suspended Solids (TSS), which comprise both organic (e.g. algae) and inorganic (e.g. silt) particles suspended in the water column. The sampling positions are in the vicinity of Site A and Site B (see Figure 3.1). At Site A the total water depth is approximately 12 m and samples are taken at depths of 4 and 8 m below the water surface. At Site B the total water depth is approximately 30 m and samples are taken at depths of 4, 12, 20 and 28 m below the water surface. The results are tabulated below and plotted in Figure 10.16.

TABLE 10.2: MEASURED TOTAL SUSPENDED SOLIDS (TSS) AT BANTAMSKLIP SITE

Date	Longitude [deg]	Latitude [deg]	Total water depth [m CD]	Measurement depth below surface [m]	TSS [mg/L]
2008-06-18	19.5116	-34.7101	30	4	<5
	19.5116	-34.7101	30	12	<5
	19.5116	-34.7101	30	20	<5
	19.5116	-34.7101	30	28	<5
	19.5606	-34.7198	12	4	<5
	19.5606	-34.7198	12	8	<5
	19.5618	-34.7190	12	4	<5
	19.5603	-34.7176	12	4	<5
	19.5574	-34.7156	12	4	<5
	19.5548	-34.7150	12	4	<5
	19.5525	-34.7143	12	4	<5
2008-07-12	19.5116	-34.7101	30	4	<2
	19.5116	-34.7101	30	12	2
	19.5116	-34.7101	30	20	<2
	19.5116	-34.7101	30	28	<2
	19.5606	-34.7198	12	4	<2
	19.5606	-34.7198	12	8	6
	19.5618	-34.7190	12	4	3
	19.5603	-34.7176	12	4	<2
	19.5574	-34.7156	12	4	<2
	19.5548	-34.7150	12	4	5
	19.5525	-34.7143	12	4	<2
2008-08-05	19.5113	-34.7100	30	4	2
	19.5113	-34.7100	30	12	10
	19.5113	-34.7100	30	20	3
	19.5113	-34.7100	30	28	<2
	19.5606	-34.7198	12	2	<2
	19.5606	-34.7198	12	4	<2
	19.5606	-34.7198	12	6	<2
	19.5606	-34.7198	12	8	2
	19.5617	-34.7189	12	4	<2
	19.5589	-34.7175	12	4	2
	19.5572	-34.7156	12	4	3
	19.5547	-34.7150	12	4	2
	19.5525	-34.7142	12	4	<2
2008-11-01	19.5113	-34.7104	30	4	5
	19.5113	-34.7104	30	12	2
	19.5113	-34.7104	30	20	3
	19.5113	-34.7104	30	28	<2
	19.5602	-34.7198	12	4	<2

	19.5599	-34.7194	12	4	6
	19.5597	-34.7187	12	4	3
	19.5596	-34.7183	12	4	2
	19.5590	-34.7180	12	4	<2
	19.5566	-34.7191	12	4	5
2008-12-05	19.5113	-34.7104	30	4	5
	19.5113	-34.7104	30	12	5
	19.5113	-34.7104	30	20	4
	19.5113	-34.7104	30	28	10
	19.5602	-34.7198	12	4	3
	19.5599	-34.7194	12	8	4
	19.5602	-34.7198	12	4	6
	19.5599	-34.7194	12	4	7
	10.5597	-34.7187	12	4	4
	19.5596	-34.7183	12	4	2
	19.5590	-34.7180	12	4	<2
2009-03-07	19.5111	-34.7101	30	4	2
	19.5111	-34.7101	30	12	3
	19.5111	-34.7101	30	20	2
	19.5111	-34.7101	30	28	1
	19.5606	-34.7198	12	4	3
	19.5606	-34.7198	12	8	3
	19.5602	-34.7198	12	4	3
	19.5599	-34.7194	12	4	1
	10.5597	-34.7187	12	4	4
	19.5596	-34.7183	12	4	6
	19.5590	-34.7180	12	4	2
2009-04-04	19.5111	-34.7101	30	4	9
	19.5111	-34.7101	30	12	2
	19.5111	-34.7101	30	20	2
	19.5111	-34.7101	30	28	3
	19.5606	-34.7198	12	4	16
	19.5606	-34.7198	12	8	10
	19.5602	-34.7198	12	4	9
	19.5599	-34.7194	12	4	2
	10.5597	-34.7187	12	4	12
	19.5596	-34.7183	12	4	11
	19.5590	-34.7180	12	4	3

At Site A (total water depth = 12 m) the average TSS measured is 3.8 mg/L and the maximum is 16 mg/L. At the deeper Site B (total water depth = 30 m) the values are slightly lower, with an average TSS of 3.4 mg/L and a maximum of 10 mg/L. (For calculating the average values, TSS values of <5 mg/L and <2 mg/L have been set to 4 mg/L and 1 mg/L, respectively). The TSS concentration is relatively uniform over the water column (see Figure 10.12), implying that these are smaller cohesive sediment particles (D_{50} < 0.063 mm) rather than larger sand particles (which would show a significantly higher concentration near the seabed.

10.4.3 Model setup

The modelling is performed using the LITPACK model, as described in Section 2.7. The model inputs are the water depth, D_{50} grain size, the sediment grading defined by $(D_{84}/D_{16})^{0.5}$, the root-mean-square wave height $H_{rms} \approx H_{m0}/1.41$, the zero-crossing wave period $T_z \approx T_p/1.3$, wave direction, current speed, current direction and water temperature. The model output is the vertical profile of suspended sand concentration. The model only simulates non-cohesive sediments with grain sizes greater than 0.063 mm, i.e. sand particles.

Based on the settings established in the two-dimensional sediment transport modelling (Section 10.3.3) the parameter settings for the model are selected as follows: critical Shields parameter = 0.05, wave breaking dissipation factor beta = 0.15, ripples are included, bed slope effects are excluded, the deterministic formulation is used for the bed concentration, convective terms are included, density currents are excluded, the wave theory is Stokes 5th order and the wave breaker index = 0.8. A graded sand with 30 size fractions is modelled.

10.4.4 Conditions modelled

The conditions modelled are the same 147 binned wave/wind conditions used for the two-dimensional sediment transport simulations (Section 10.3.2). For each condition the two-dimensional model provides the waves and currents throughout the model domain. The wave and current parameters for each condition are extracted at the proposed intake positions in 30 m water depth (Layout 5, see Figure 9.5) and 45 m depth (Layouts 1 and 3, see Figures 9.1 and 9.3) for use in the suspended sediment model. The water temperature (which influences the particle settling velocity) is set to a conservatively high value of 16°C (see Figure 7.2).

The measured sediment grain sizes are presented in Table 10.1 and Figure 10.1. The seven available nearshore samples have a D_{50} ranging from 0.14 to 0.61 mm. For these simulations the most conservative D_{50} of 0.14 mm is used, along with a conservatively high sediment grading of 1.5.

10.4.5 Results

An example of the vertical profile of suspended sand concentration modelled for one input wave/current condition is shown in Figure 10.13. It is seen that the sand concentration decreases logarithmically with increasing distance from the seabed.

The proposed intake opening is positioned 3 to 5 m above the seabed (Eskom, 2008c), while the intake flow rate for a power output of 10 000 MWe is 456 m^3/s (see Table 9.1). For a particular wave/current condition, a preliminary estimate of the volume of sand drawn into the intake can be calculated as the suspended sand concentration at the vertical position of the intake opening multiplied by the intake flow rate. It is assumed that the intake structure itself does not influence the suspended sand profile and that the seabed is covered in sand, i.e. no rocks. The extent to which this assumption is true will depend on the detailed design of the intake structure: the intake geometry, the number of intake openings, the intake velocities, the extent of scour protection around the structure, etc. Since these details are not yet available, the results below should be viewed as preliminary.

The sand volume drawn into the intake is calculated for each of the 147 wave/current conditions. The annual sand volume is then calculated by adding the volumes for each condition, taking into account the percentage occurrence of each condition. The final volume is then adjusted from solid volume to

bulk volume assuming a sediment porosity of 0.4. In addition to the annual average sand volume, the maximum sand concentration and the maximum short-term sand volume are obtained from the 147 conditions. Results are presented for the proposed intake levels of 3 and 5 m above the seabed, as well as 1 m above seabed to account for the drawing in of sand from below the level of the intake, or for sand build-up around the intake.

TABLE 10.3: PRELIMINARY ESTIMATE OF SAND VOLUME DRAWN INTO COOLING WATER INTAKE

	Annual sand volume [m^3/year]	**Short-term maximum sand volume [m^3/day]**	**Maximum sand concentration [mg/L = ppm by mass]**
Depth = 30 m			
Intake 1 m above seabed	7 500	700	26
Intake 3 m above seabed	4 000	300	12
Intake 5 m above seabed	2 500	250	9
Depth = 45 m			
Intake 1 m above seabed	2 500	350	14
Intake 3 m above seabed	1 500	200	8
Intake 5 m above seabed	1 000	150	6

Note that the model only simulates non-cohesive sediments with grain sizes greater than 0.063 mm, i.e. sand particles. Finer mud and clay particles that may be present in the water column as a background concentration are not modelled. Assuming an average background concentration of 3.4 mg/L (Section 10.4.2) and a porosity of 0.4, the annual cohesive sediment volume drawn into the cooling water intake would be 31 000 m^3/year, which is significantly higher than the sand volumes given in Table 10.3. Whether these cohesive particles will have time to settle in the settling basin, or pass through the heat exchangers and be discharged back to sea, will depend on the design and geometry of the settling basin.

The sediment volumes estimated above are significantly lower than the average maintenance dredging at the present Koeberg intake basin of approximately 132 000 m^3/year (PRDW, 2002).

11. CONCLUSIONS AND RECOMMENDATIONS

Numerical models and data analysis frameworks have been set up to characterise the following parameters at the Bantamsklip site:

- Water levels
- Tsunami flooding
- Wave height, period and direction
- Seawater temperatures
- Currents
- Thermal plume dispersion and recirculation for typical intake and outfall configurations
- Sediment transport
- Suspended sediment concentrations.

The numerical models have been calibrated using measurements undertaken at the site as part of the ongoing measurement programme.

The results will be used in the Coastal Engineering Investigations Report (PRDW, 2009a), the SSR Chapter on Oceanography and Coastal Engineering, as well as other chapters in the SSR dealing with marine ecology and risk assessment. The results will also be used for the EIA study being conducted for Nuclear-1.

The oceanographic measurement programme is scheduled to run until August 2010 and it is strongly recommended that the programme continue as scheduled.

Additional research is required to better define the risk from local tsunamigenic sources. The Council for Geoscience report (CGS, 2008b) recommends the following approach:

- Further research including all available stratigraphic/sedimentological/geomorphological data should be undertaken to better define the risk from offshore slump generated tsunami.
- In depth research into the global frequency, locality and magnitude of meteotsunami should be undertaken to further quantify the risk. In particular, the atmospheric conditions along the west coast prior to the 1969 event should be compared with those of its 2008 counterpart
- Because of the relatively short history of tsunami records along the South African coast, the database should be extended by conducting an investigation of palaeotsunami in the stratigraphic record. No systematic work has yet been conducted along this coast. Areas of focus should be in the vicinity of planned nuclear facilities.

REFERENCES

1. Bayworld (2008) Bottom Temperature Studies along the South African Coast. A Bottom Temperature Project to Determine Temperature Ranges Needed for Nuclear Power Station Cooling Systems for ESKOM. Bayworld Centre for Research and Education, Progress Report #1, August 2008.
2. Bayworld (2009) Bottom Temperature Studies along the South African Coast. A Bottom Temperature Project to Determine Temperature Ranges Needed for Nuclear Power Station Cooling Systems for ESKOM. Bayworld Centre for Research and Education, Progress Report #2, February 2009.
3. Borrero J, Sieh K, Chlieh M and Synolakis C (2006). Tsunami Inundation Modeling for Western Sumatra. PNAS, 26 December 2006, vol. 103, no. 52.
4. CGS (2008a) A Probabilistic Tsunami Hazard Assessment for Coastal South Africa from Distant Tsunamogenic areas. By A. Kijko, V. Midzi, J. Ramperthap and M. Singh. Council for Geoscience Report No. 2008 - 0156, Revision 2.
5. CGS (2008b) Potential Sources of Tsunami Along the South African Coast. By D.L. Roberts. Council for Geoscience Report Number: 2008 - 0220 .
6. DHI (2008a) MIKE 21 SW, Spectral Waves FM Module, User Guide. Danish Hydraulics Software.
7. DHI (2008b) LITPACK, An Integrated Modelling System for Littoral Processes and Coastline Kinetics. User Guide, Danish Hydraulics Software.
8. DHI (2008c) MIKE 21 Flow Model, User Guide. Danish Hydraulics Software
9. DHI (2008d) MIKE 21/3 Coupled Model FM, User Guide. Danish Hydraulics Software.
10. DHI (2008e) MIKE 21 Flow Model FM, Sand Transport Model, User Guide. Danish Hydraulics Software.
11. DHI (2008f) EVA, Extreme Value Analysis, User Guide. Danish Hydraulics Software.
12. DHI (2008g) MIKE 21 Tidal Analysis and Prediction Module, Scientific Documentation. Danish Hydraulics Software.
13. DHI (2008h) MIKE C-MAP, Extraction of World Wide Bathymetry Data and Tidal Information, User Guide. Danish Hydraulics Software.
14. Dingle R (1977) The anatomy of a large submarine slump on a sheared continental margin (SE Africa). Journal of the Geological Society of London 134; 293-310.
15. Dingle R, Birch G, Bremner J, de Decker R, du Plessis A, Engelbrecht J, Fincham M, Fitton T, Flemming B, Gentle R, Goodlad S, Martin A, Mills E, Moir G, Parker R, Robson S, Rogers J, Salmon D, Siesser W, Simpson E, Summerhayes C, Westall C and Winter A (1987). Deep-sea sedimentary environments around southern Africa, South-East Atlantic and South-West Indian Oceans. Annals of the South African Museum 98, 1–27.
16. Doneker, RL, Jirka, GH and Hinton, SW (2007). CORMIX User Manual: A Hydrodynamic Mixing Zone Model and Decision Support System for Pollutant Discharges into Surface

Waters. Office of Science and Technology, U.S. Environmental Protection Agency, Washington, DC.

17. Eskom (1985) Koeberg meteorological data report, Spring 1985, Koeberg Weather Station.
18. Eskom (2006) Koeberg Site Safety Report, Chapter 8, Oceanography and Cooling Supply, Rev 3.
19. Eskom (2007) Areva, EPR Technical Description, Rev A. Received from Eskom, August 2007.
20. Eskom (2008a) Plant Parameter Envelope for 10 000 MWe for NSIP Site Safety Reports, Document provided by Israel Sekoko, Eskom, on 1 September 2008.
21. Eskom (2008b) Nuclear-1 consistent EIA data set (Rev. 2). Document (Excel spreadsheet) provided by Andre Nel, Eskom, on 2 October 2008.
22. Eskom (2008c) Cooling Water Intake and Outfall Works for the Eskom Nuclear-1 Sites, Conceptual Arrangements. Nuclear Programmes Department Nuclear-1, Document No. 300-9, September 2008.
23. Eskom (2008d) Draft Environmental Impact Assessment Report, Environmental Impact Assessment for a 400 MW(t) Pebble Bed Modular Reactor Demonstration Power Plant. DEAT Reference No: 12/12/20/745, Arcus Gibb, September 2008.
24. Eskom (2009) 1010 Nuclear Sites - Re: Draft_P-3257-P.pdf, Email from I Saayman, Eskom, dated 13 August 2009.
25. Grilli S and Watts P (2005) Tsunami Generation by Submarine Mass Failure, 1: Modelling, Experimental Validation and Sensitivity Analysis. Journal of Waterway, Port, Coastal and Ocean Engineering, November/December 2005.
26. Grilli S, Ioualalen M, Asavanant J, Shi F, Kirby J and Watts P (2007). Source Constraints and Model Simulation of the December 26, 2005, Indian Ocean Tsunami. Journal of Waterway, Port, Coastal, and Ocean Engineering, Vol. 133, No. 6, November, 2007.
27. Hartnady C and Okal E (2007). Mentawai tsunami effect at Port Elizabeth, South Africa on 12-14 September 2007, South Afr. J. Sci., submitted, 2007.
28. IAEA (2003) Flood Hazard for Nuclear Power Plants on Coastal and River Sites, Safety Guide No. NS-G-3.5. International Atomic Energy Agency.
29. Okada Y (1985) Surface Deformation to Shear and Tensile Faults in a Half-Space. Bull. Seism. Soc. Am., 75, [4], 1135-1154.
30. PBMR (2009) Transmittal of PBMR Information on Thermal Output and Cooling Water Requirements, Letter from PBMR Client Office dated 2009-07-31 with reference P-3257-P (NRR).
31. PRDW (2002) Eskom, Koeberg Nuclear Power Station, Cooling Water Intake Basin, Dredging Strategy, Updated Strategy – May 2002. PRDW Report 201/2/01, May 2002.

32. PRDW (2008) Eskom, Nuclear1 EIA: Modelling of Construction Stage Brine Discharge. Report No. 1010/5/001, October 2008.

33. PRDW (2009a) Eskom Site Safety Reports, Coastal Engineering Investigations Report, Bantamsklip. Prestedge Retief Dresner Wijnberg (Pty) Ltd, Report 1010/3/102 Rev 03, September 2009.

34. PRDW (2009b) Eskom Site Safety Reports, Numerical Modelling of Coastal Processes, Duynefontein. Prestedge Retief Dresner Wijnberg (Pty) Ltd, Report 1010/4/101 Rev 03, September 2009.

35. Rabinovich A and Thomson R (2007). The 26 December 2004 Sumatra Tsunami: Analysis of Tide Gauge Data from the World Ocean Part 1. Indian Ocean and South Africa. Pure and Applied Geophysics, 164 (2007), 261–308.

36. Rattey, D and Potgieter J (1987). Koeberg Nuclear Power Station, Warm Water Plume Report, August 1987.

37. South African Tide Tables (2008) SAN HO-2. Published by the Hydrographer, South African Navy, ISBN 0-9584817-3-3.

38. Watts P, Grilli S, Kirby J, Fryer G and Tappin D (2003). Landslide Tsunami Case Studies Using a Boussinesq Model and a Fully Nonlinear Tsunami Generation Model. Natural Hazards and Earth System Sciences, Vol. 3, 2003, pp. 391-402.

FIGURES

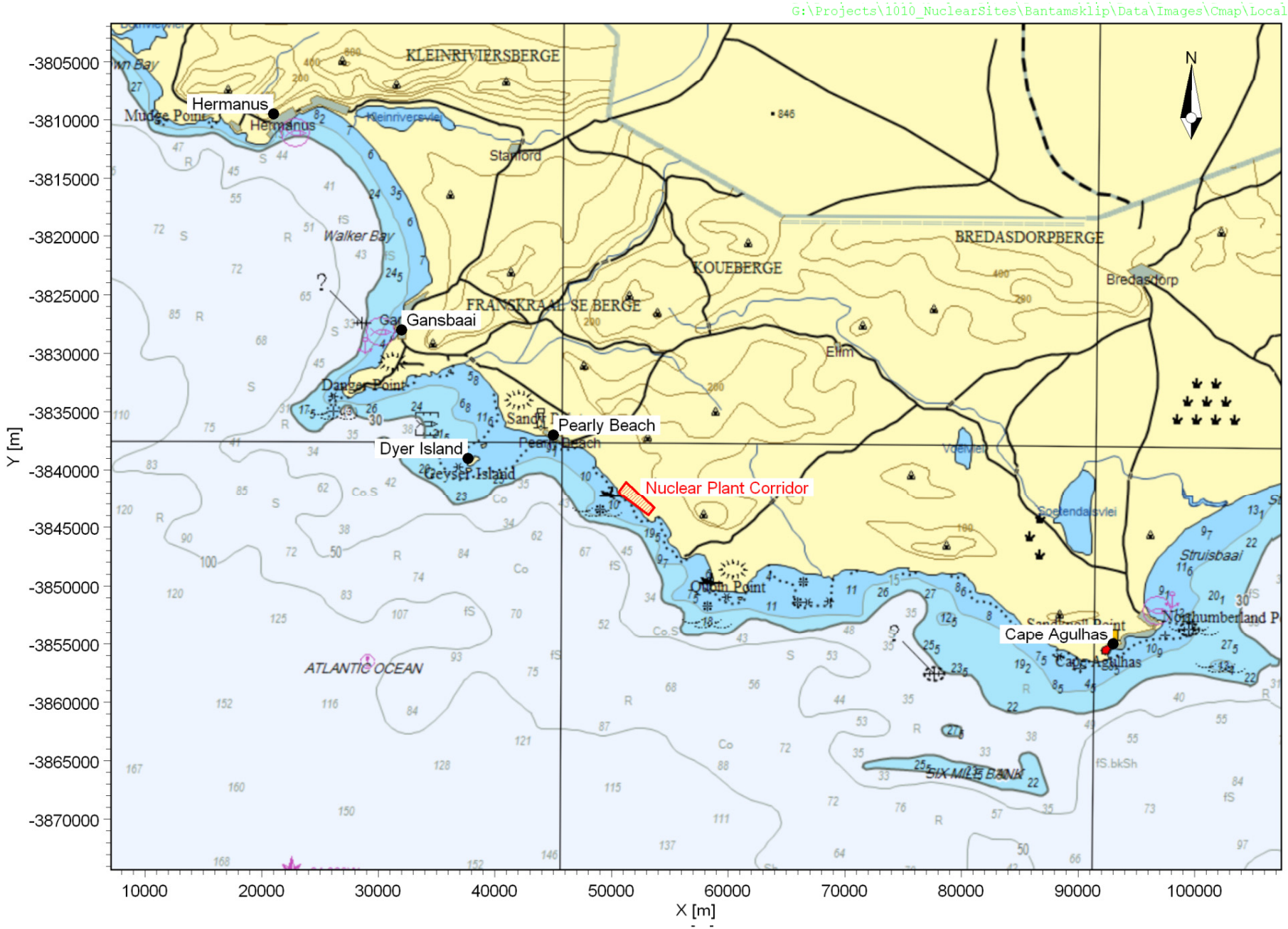

Title:

Locality map for Bantamsklip site.

Figure No.

1.1

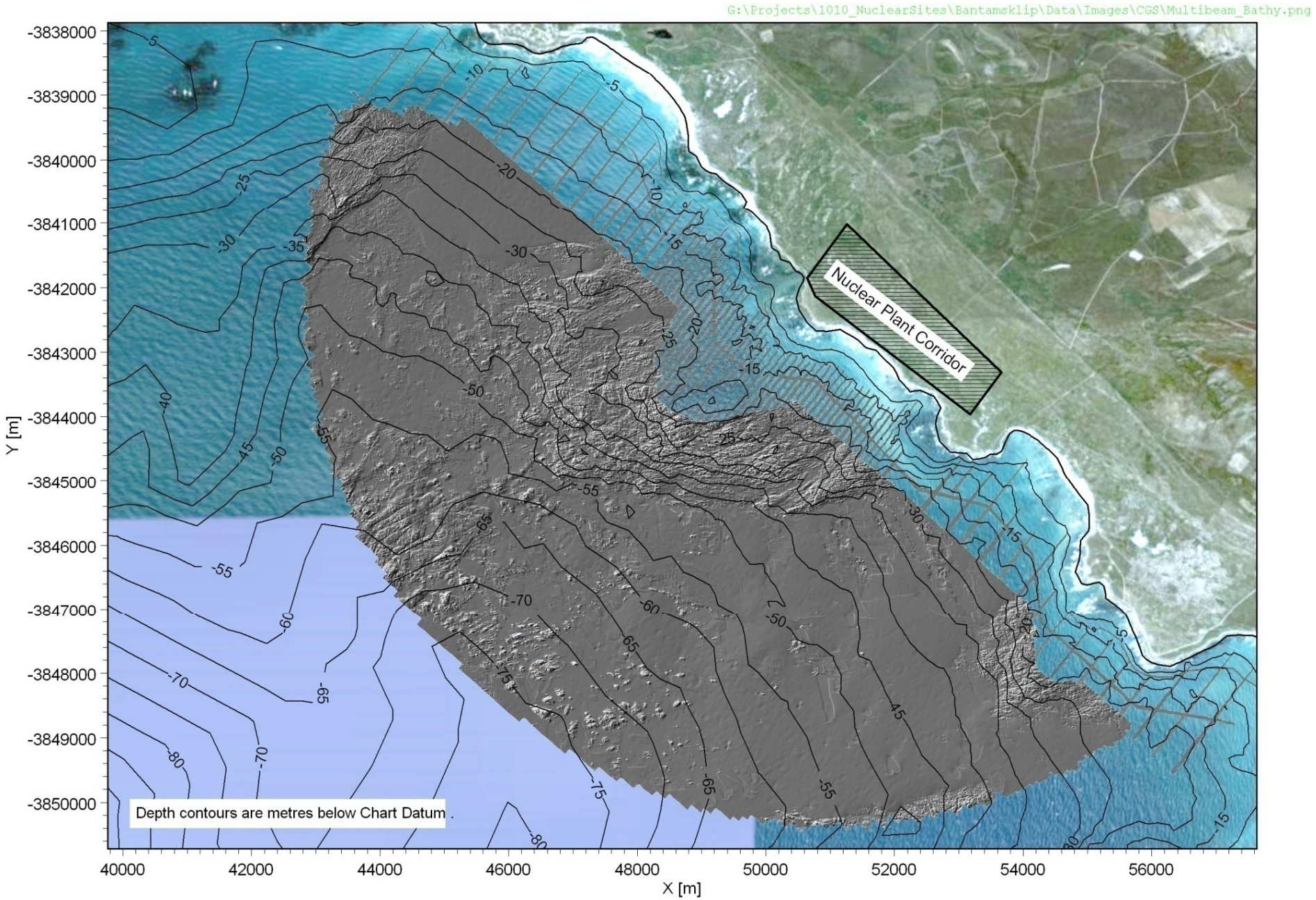

Title:

Multi-beam bathymetric survey showing seabed features.

Figure No.

1.2

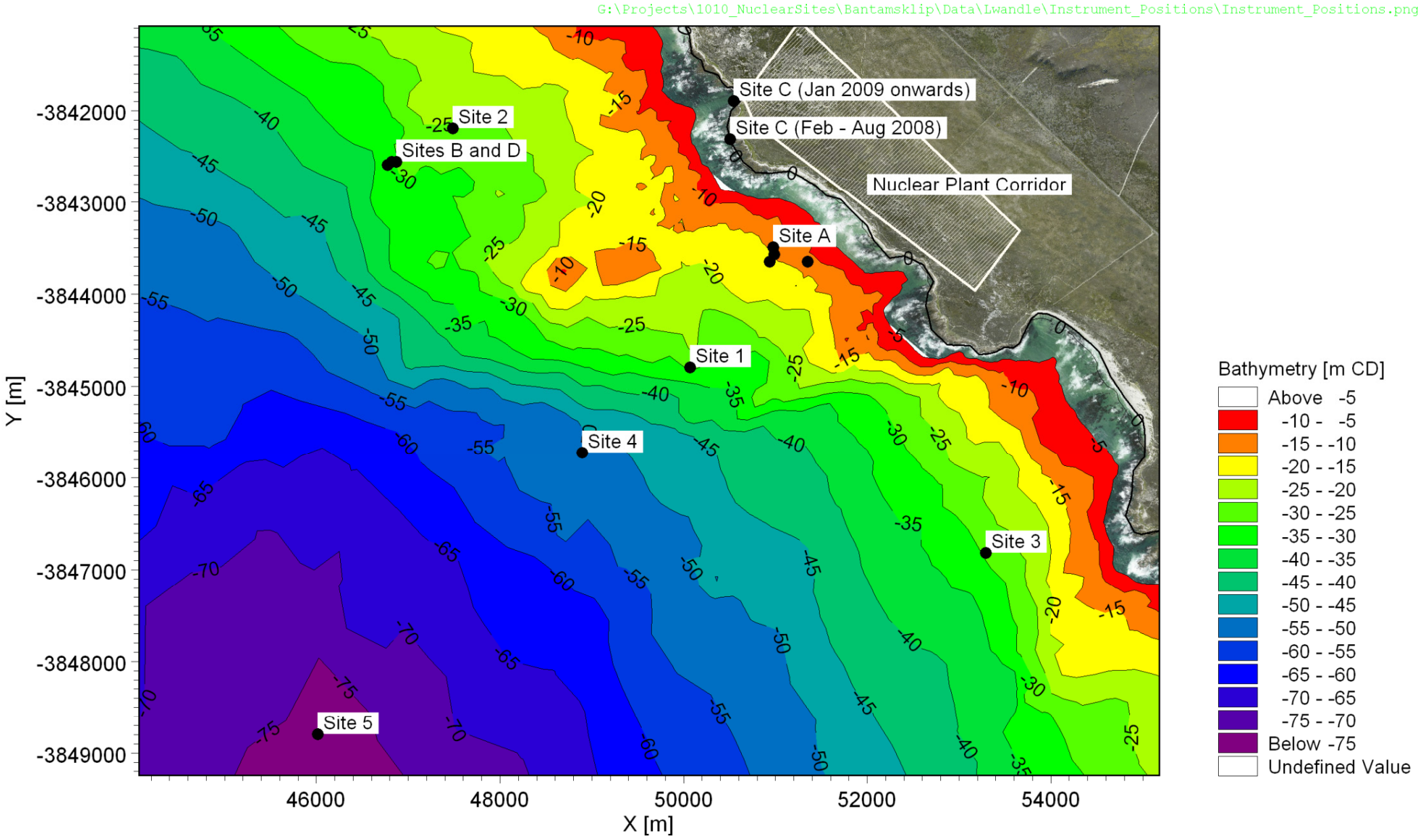

Title:

Bathymetry and location of instruments deployed at Bantamsklip.

Figure No.

3.1

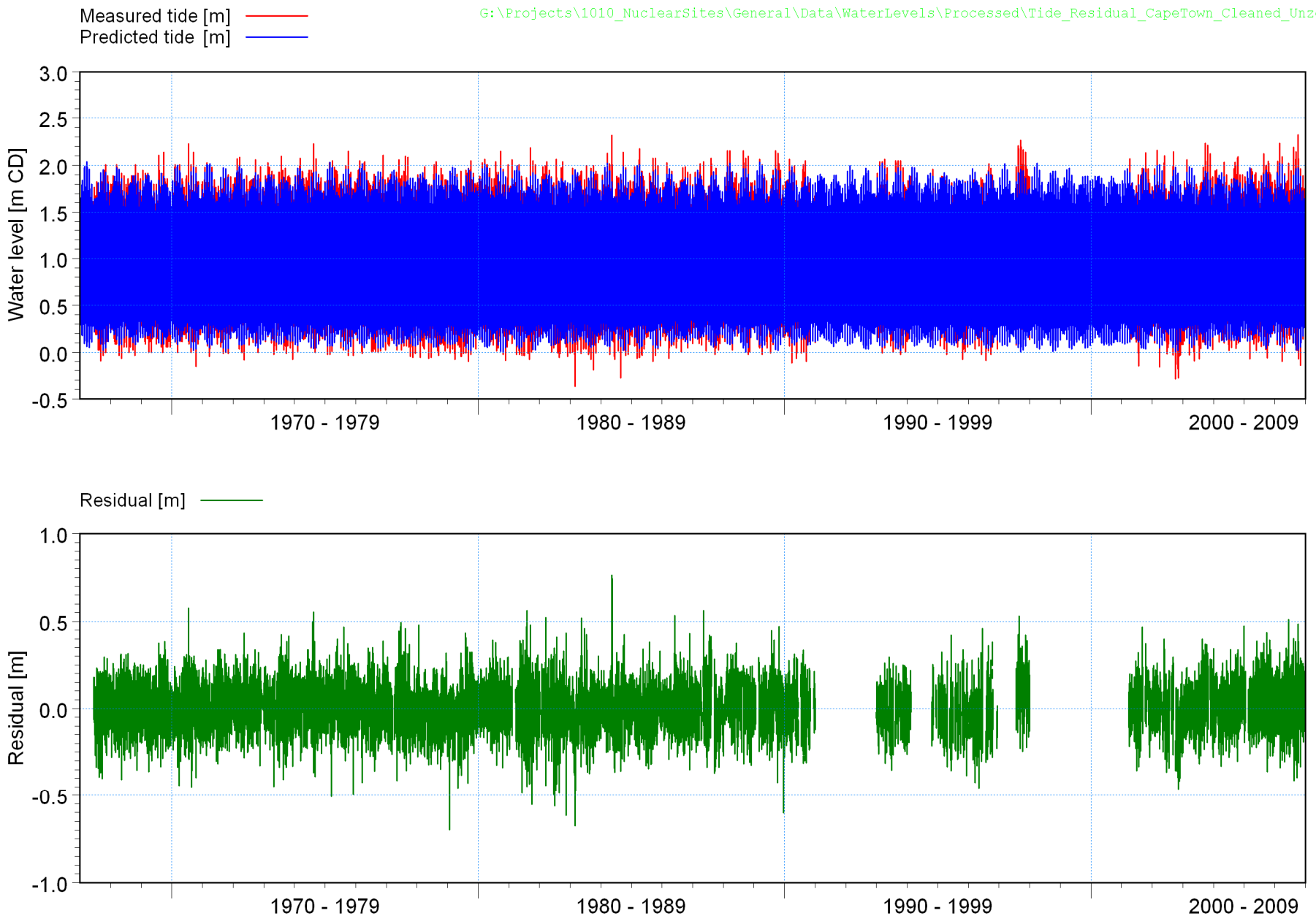

Title:

Analysis of storm surge: Measured tide, predicted tide and residual at Cape Town. Full 40 year dataset.

Figure No.

4.1

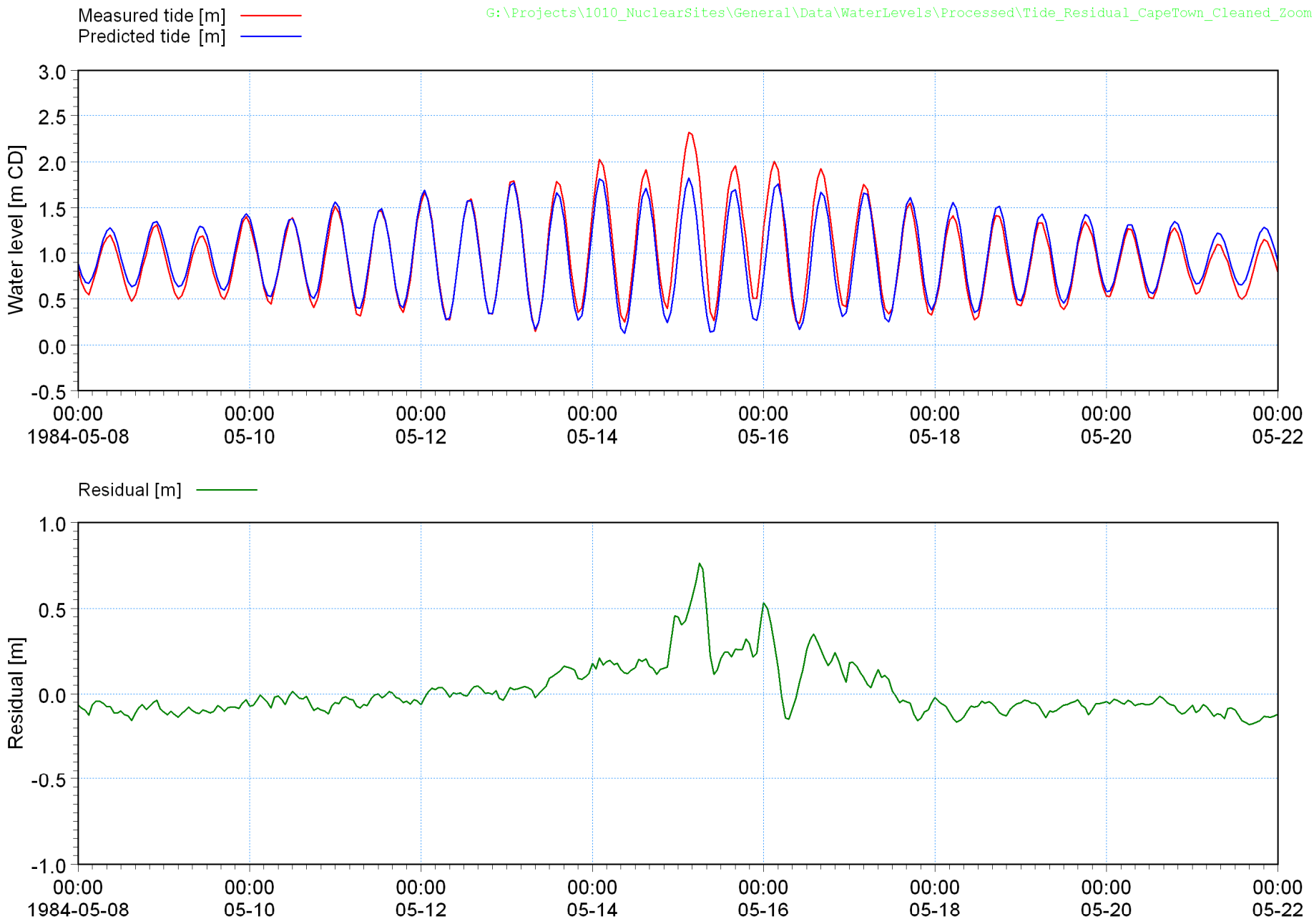

Title:

Analysis of storm surge: Measured tide, predicted tide and residual at Cape Town. Fourteen days including the May 1984 storm event.

Figure No.

4.2

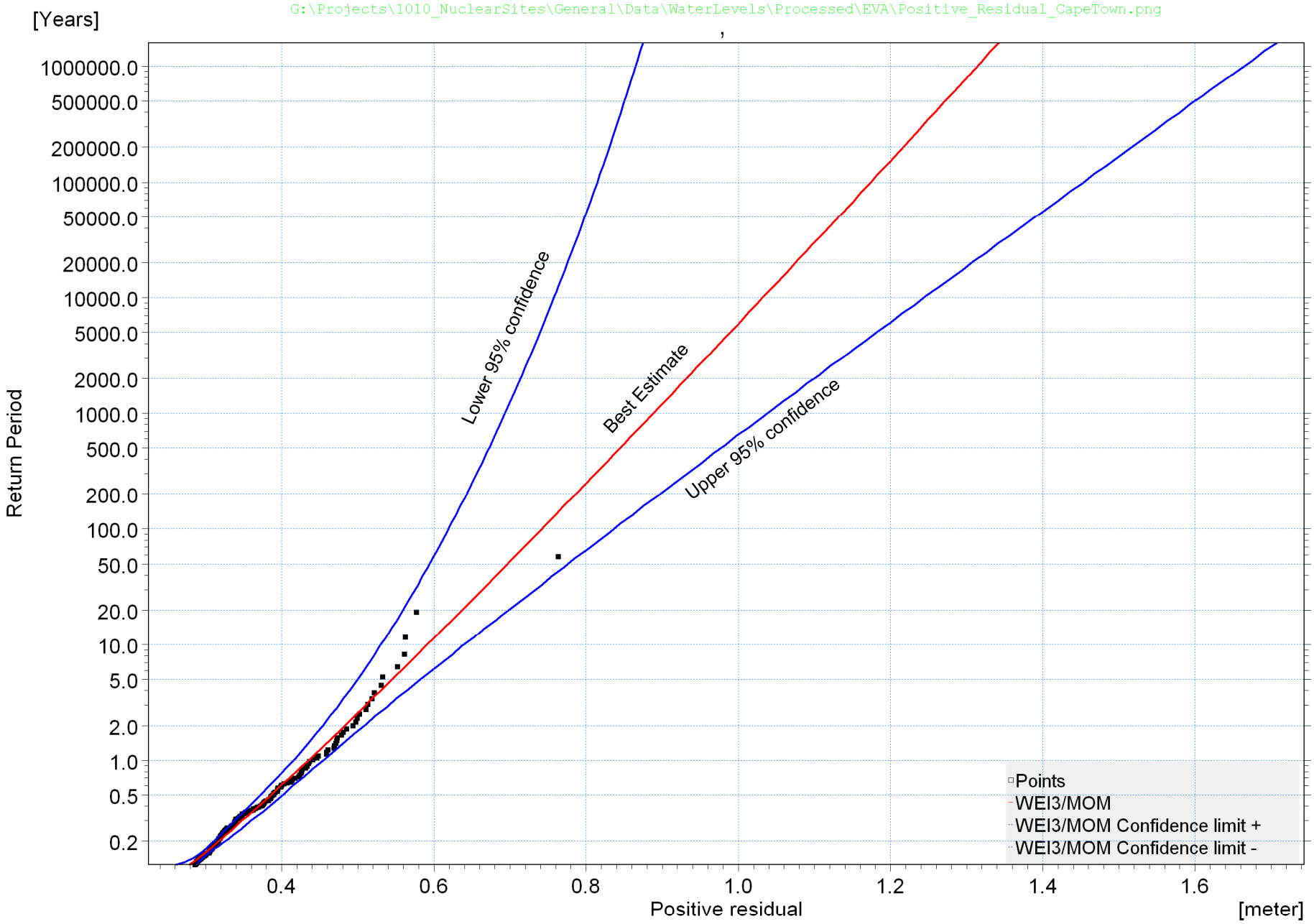

Title:

Extreme value analysis of positive storm surge at Cape Town.

Figure No.

4.3

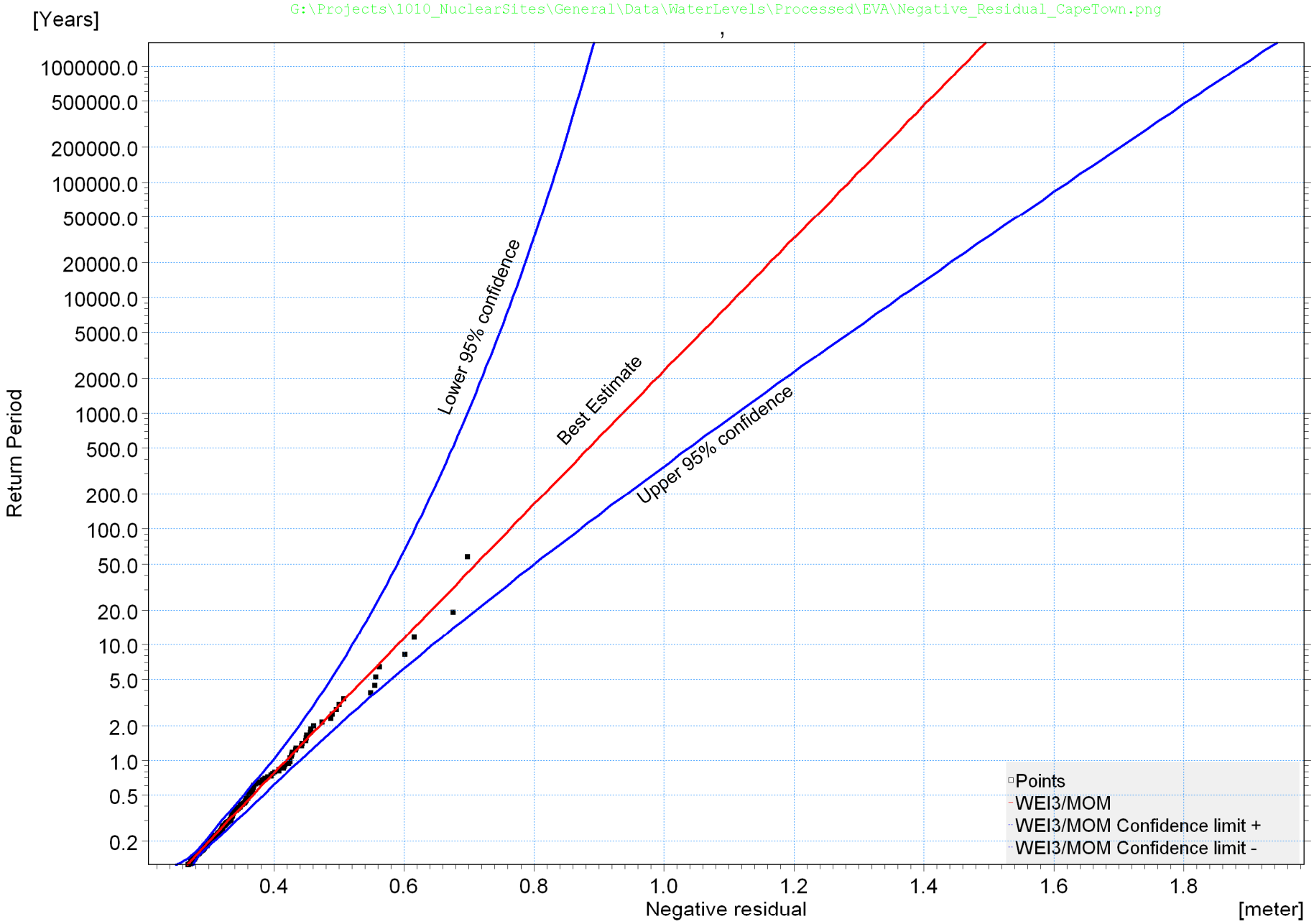

Title:

Extreme value analysis of negative storm surge at Cape Town.

Figure No.

4.4

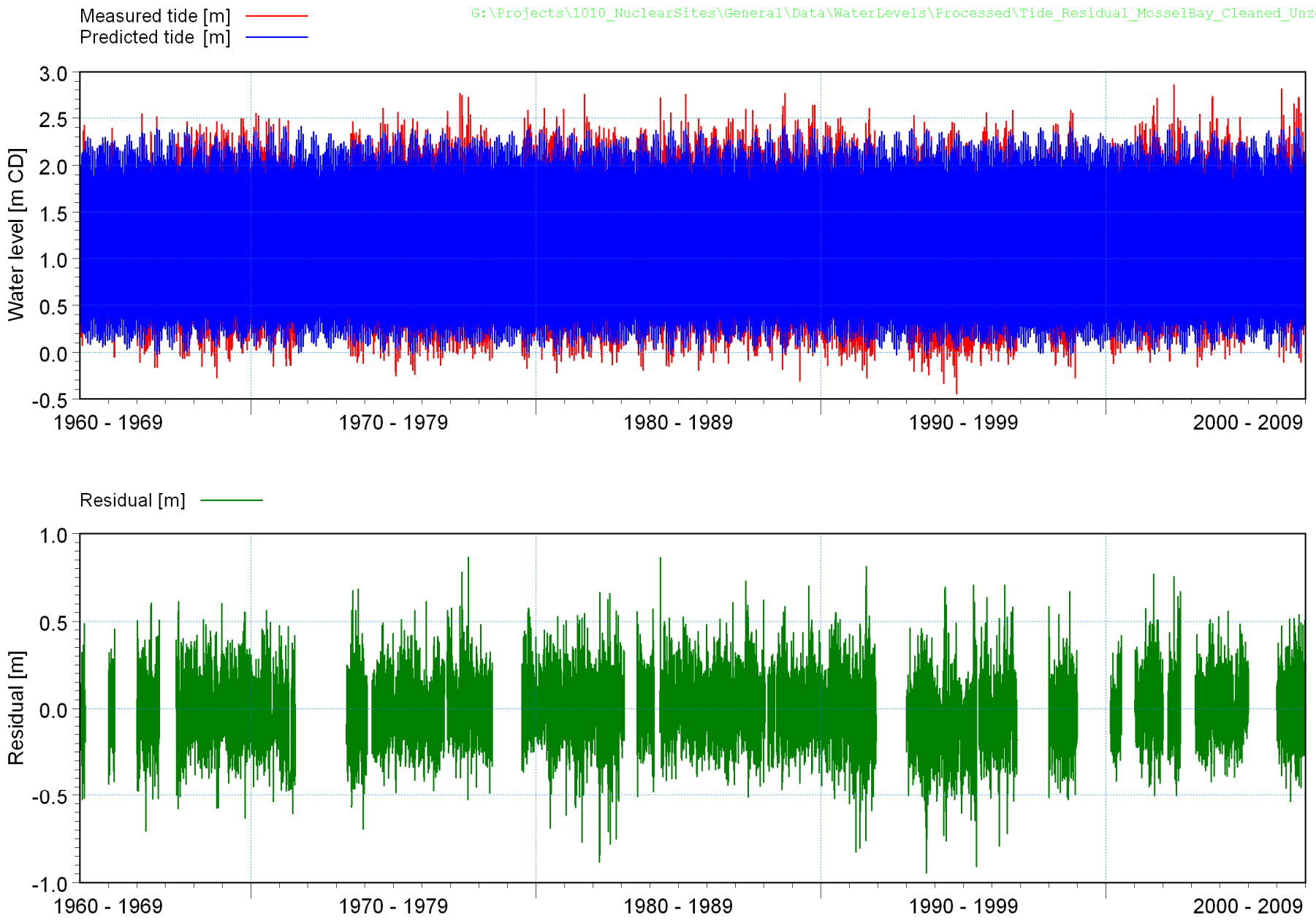

Title:

Analysis of storm surge: Measured tide, predicted tide and residual at Mossel Bay. Full 43 year dataset.

Figure No.

4.5

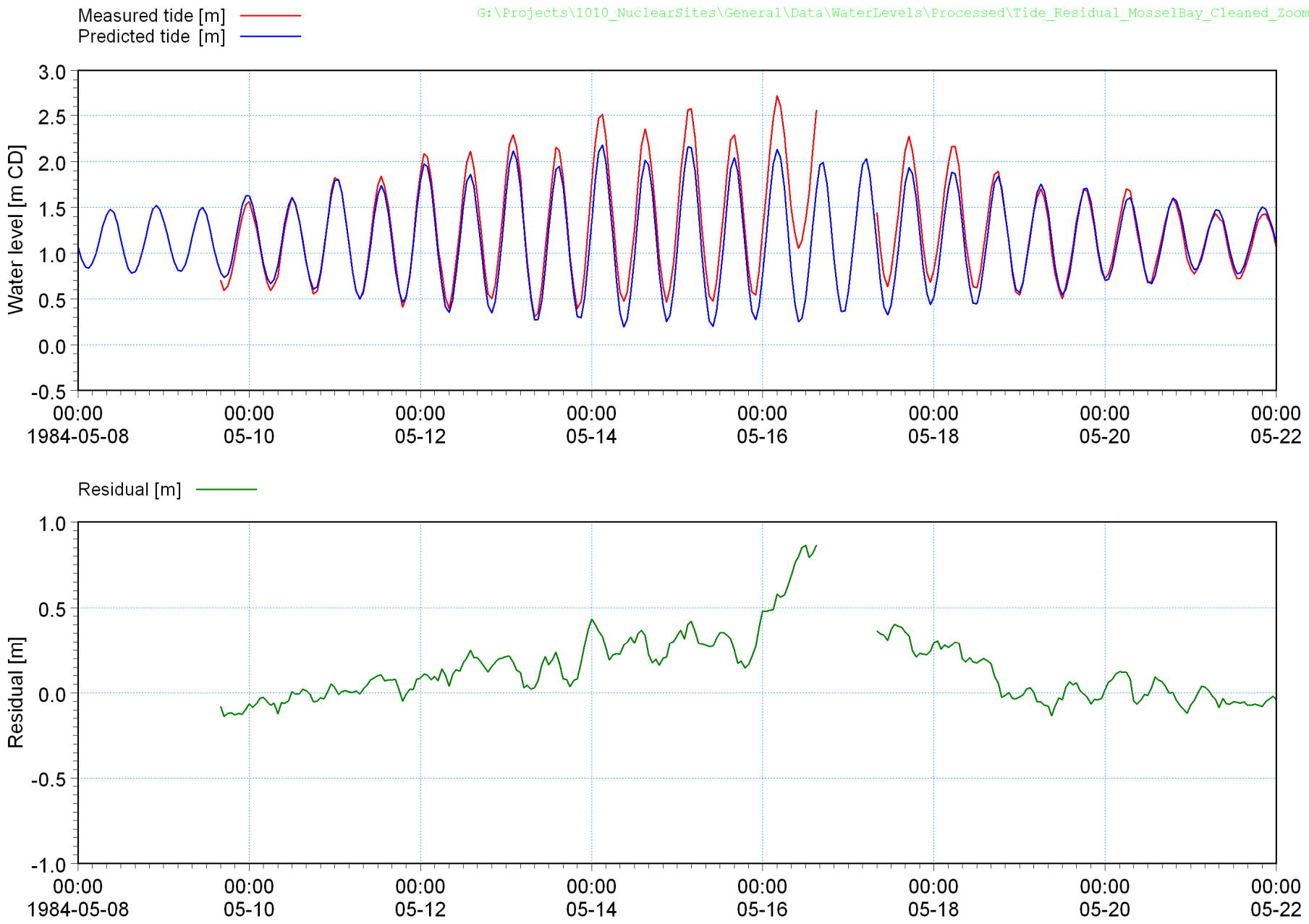

Title:

Analysis of storm surge: Measured tide, predicted tide and residual at Mossel Bay. Fourteen days including the May 1984 storm event.

Figure No.

4.6

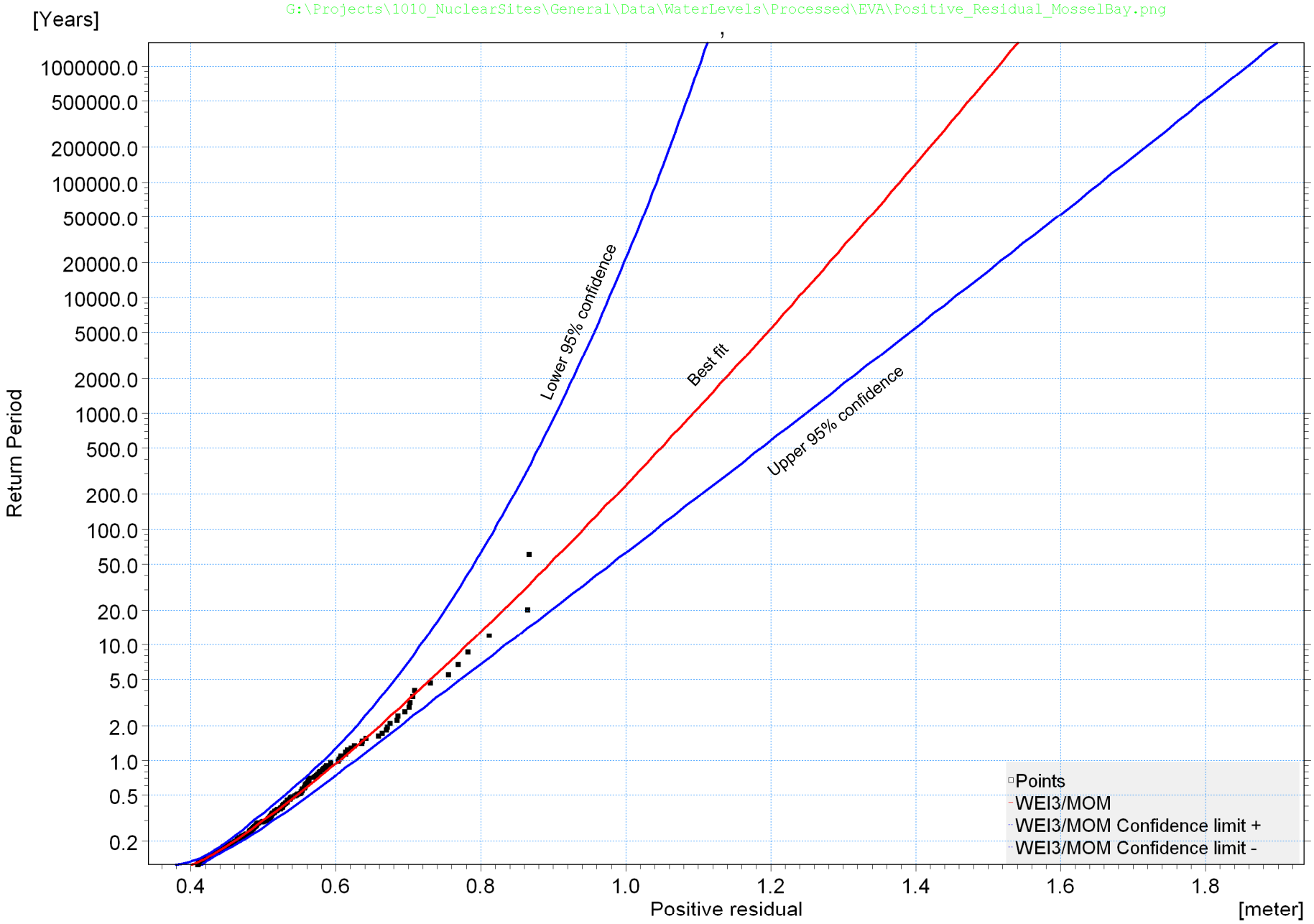

Title:

Extreme value analysis of positive storm surge at Mossel Bay.

Figure No.

4.7

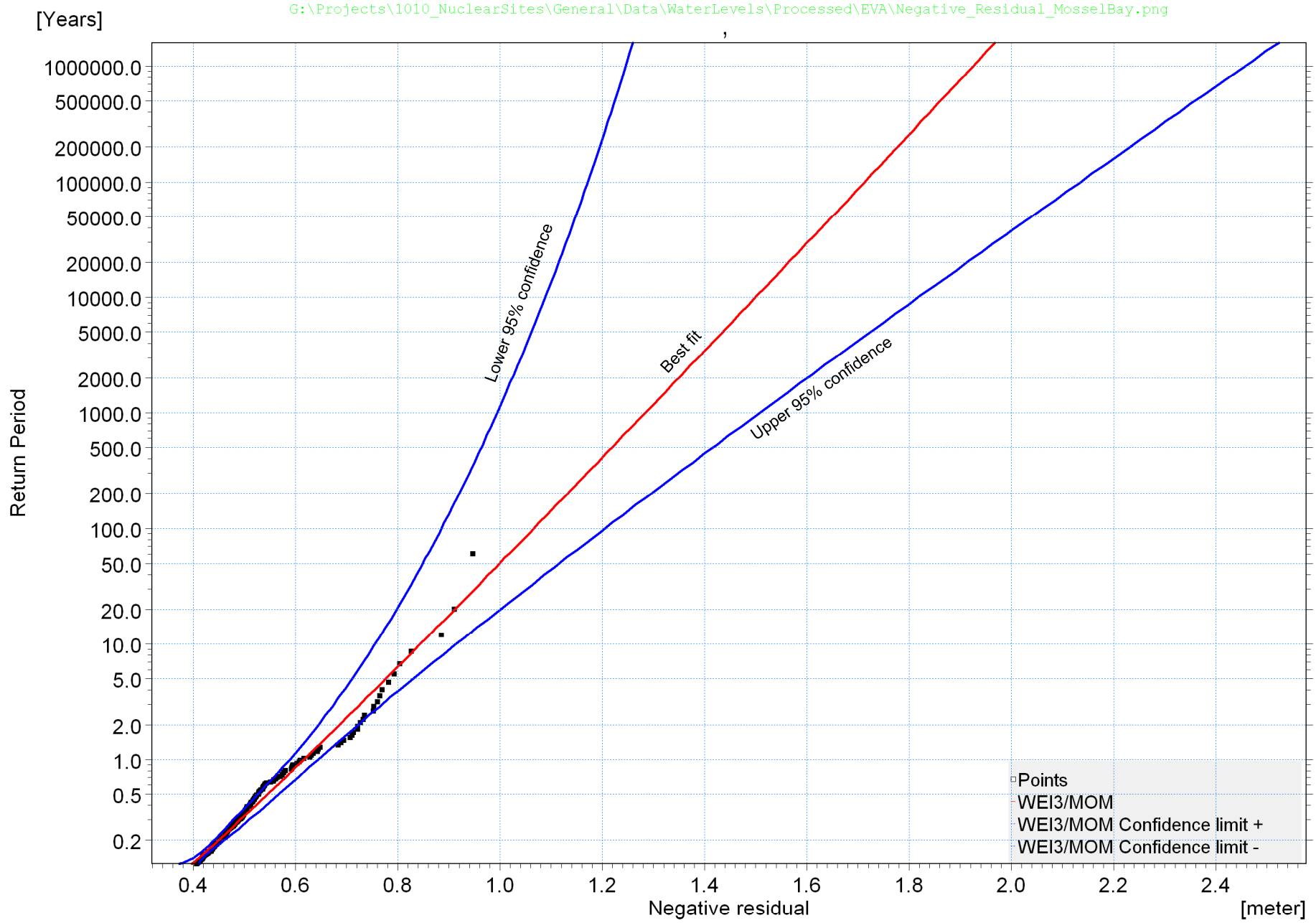

Title:

Extreme value analysis of negative storm surge at Mossel Bay.

Figure No.

4.8

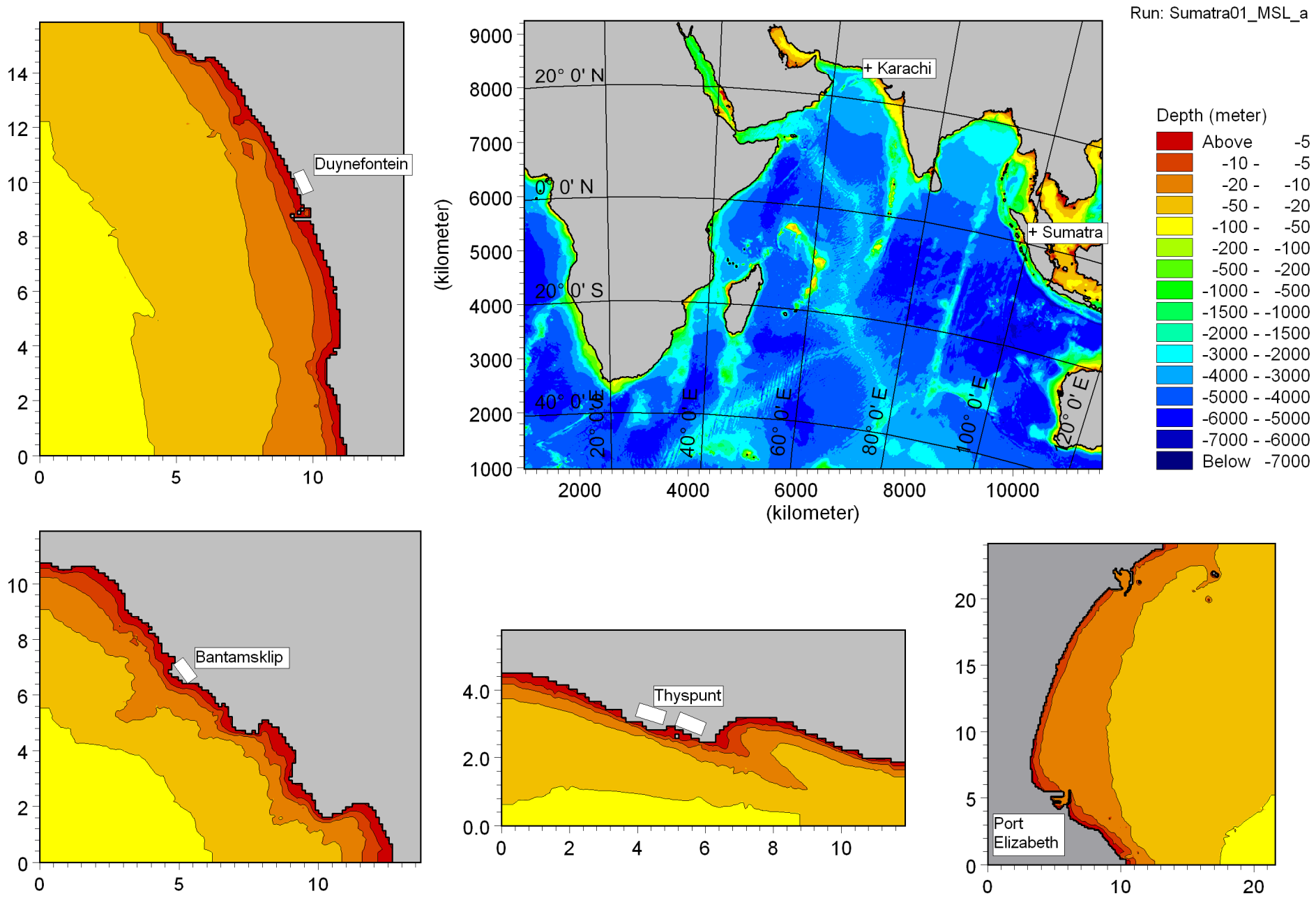

Title:

Model bathymetry used for tsunami modelling of Sumatra and Karachi earthquake events.

Figure No.

5.1

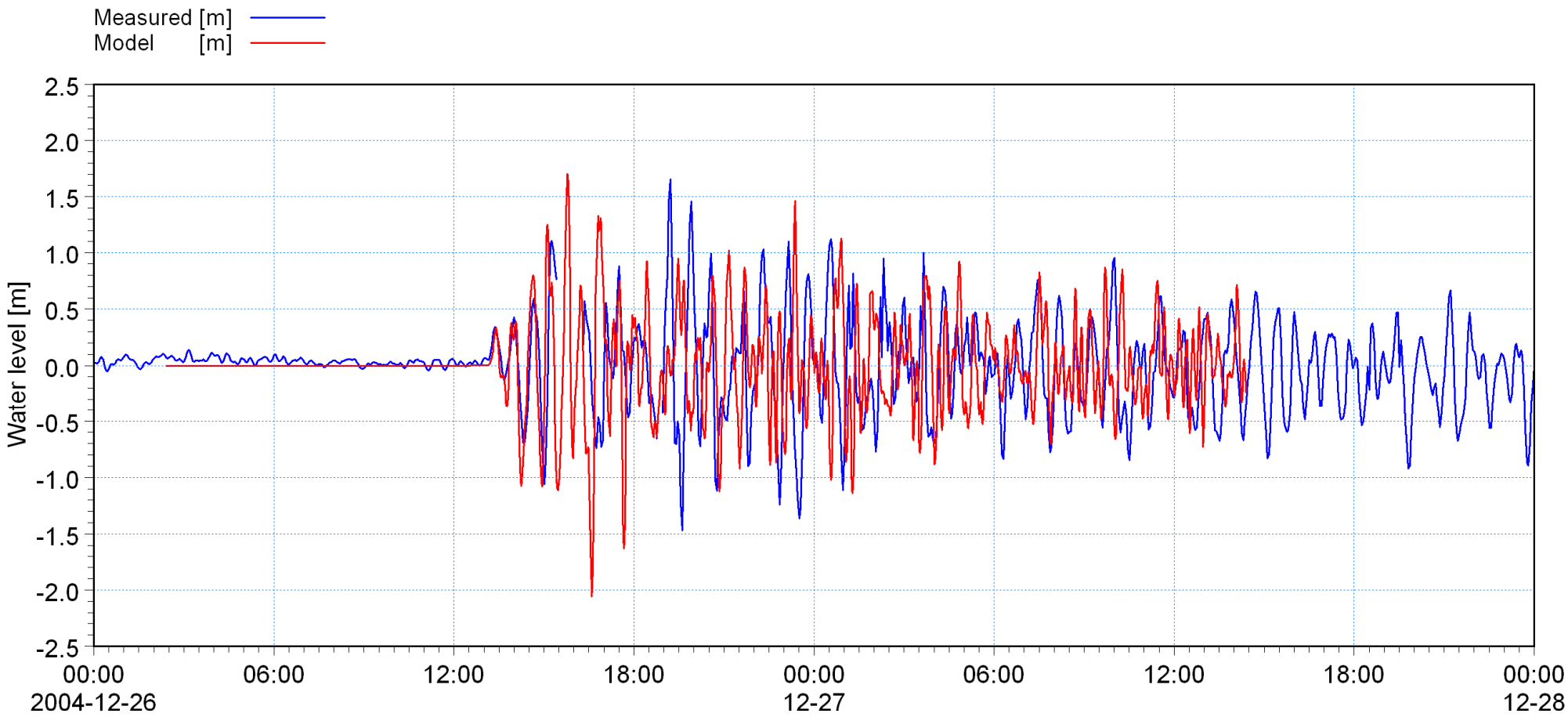

Title:

Calibration of tsunami model: Measured and modelled water levels due to the tsunami in the Port of Port Elizabeth for the 26 December 2004 Sumatra event.

Figure No.

5.2

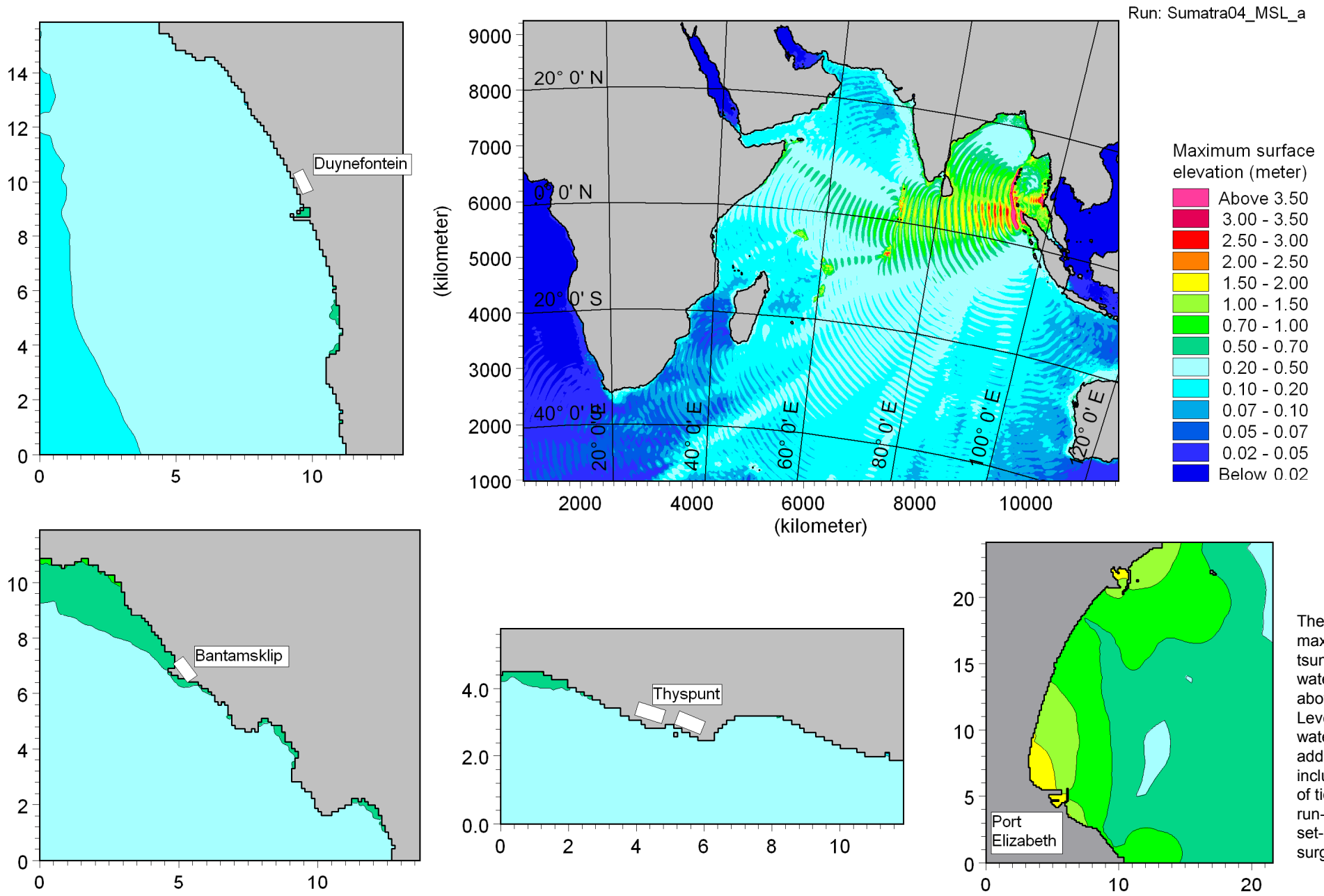

These are the maximum tsunami-induced water levels above Still Water Level. The total water level will additionally include the effect of tide, wave run-up, wave set-up and storm surge.

Title:

Maximum water levels predicted during tsunami event.
Source is Sumatra A: 26 December 2004 earthquake, Mw = 9.2.

Figure No.

5.3

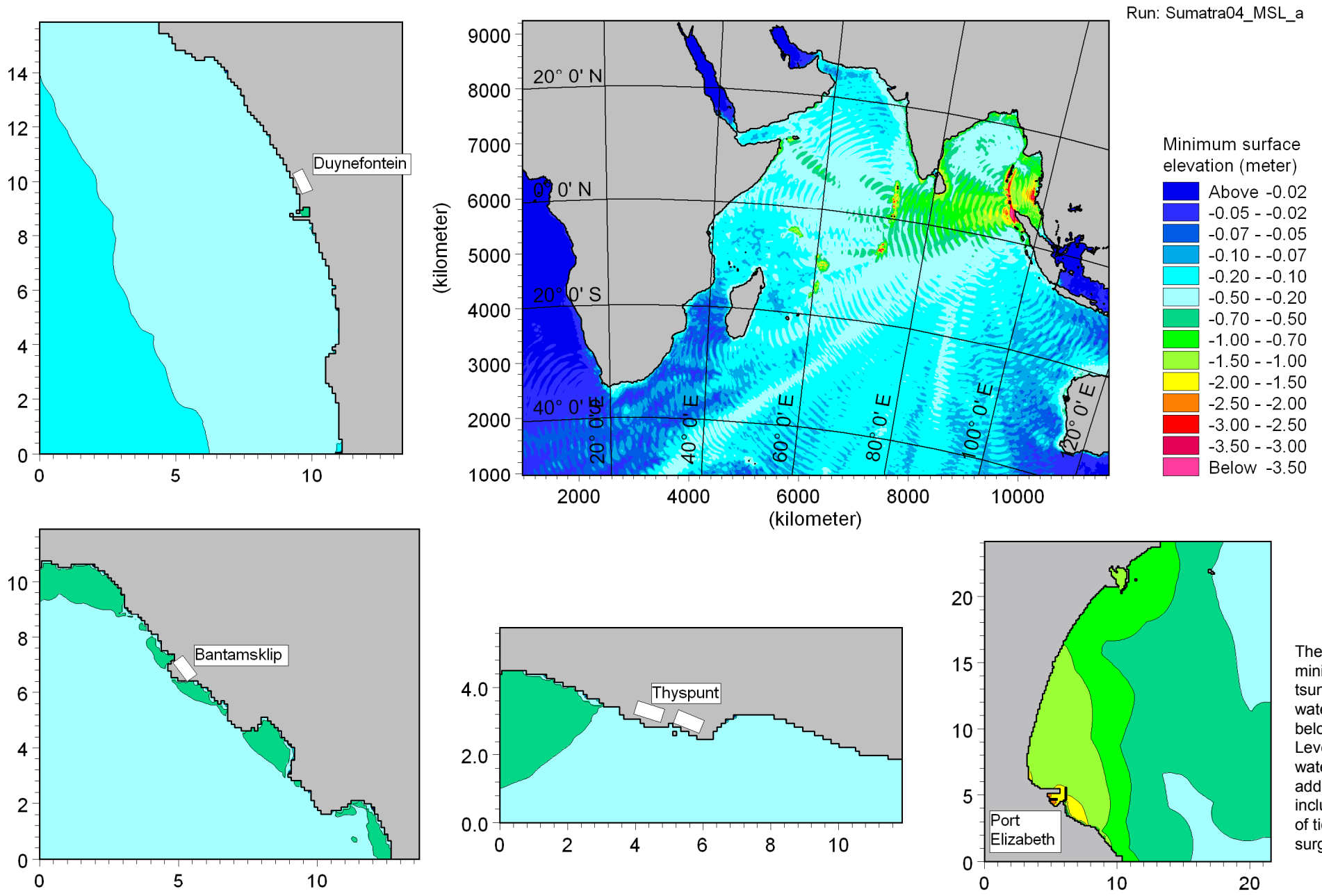

These are the minimum tsunami-induced water levels below Still Water Level. The total water level will additionally include the effect of tide and storm surge.

Title:

Minimum water levels predicted during tsunami event.
Source is Sumatra A: 26 December 2004 earthquake, Mw = 9.2.

Figure No.

5.4

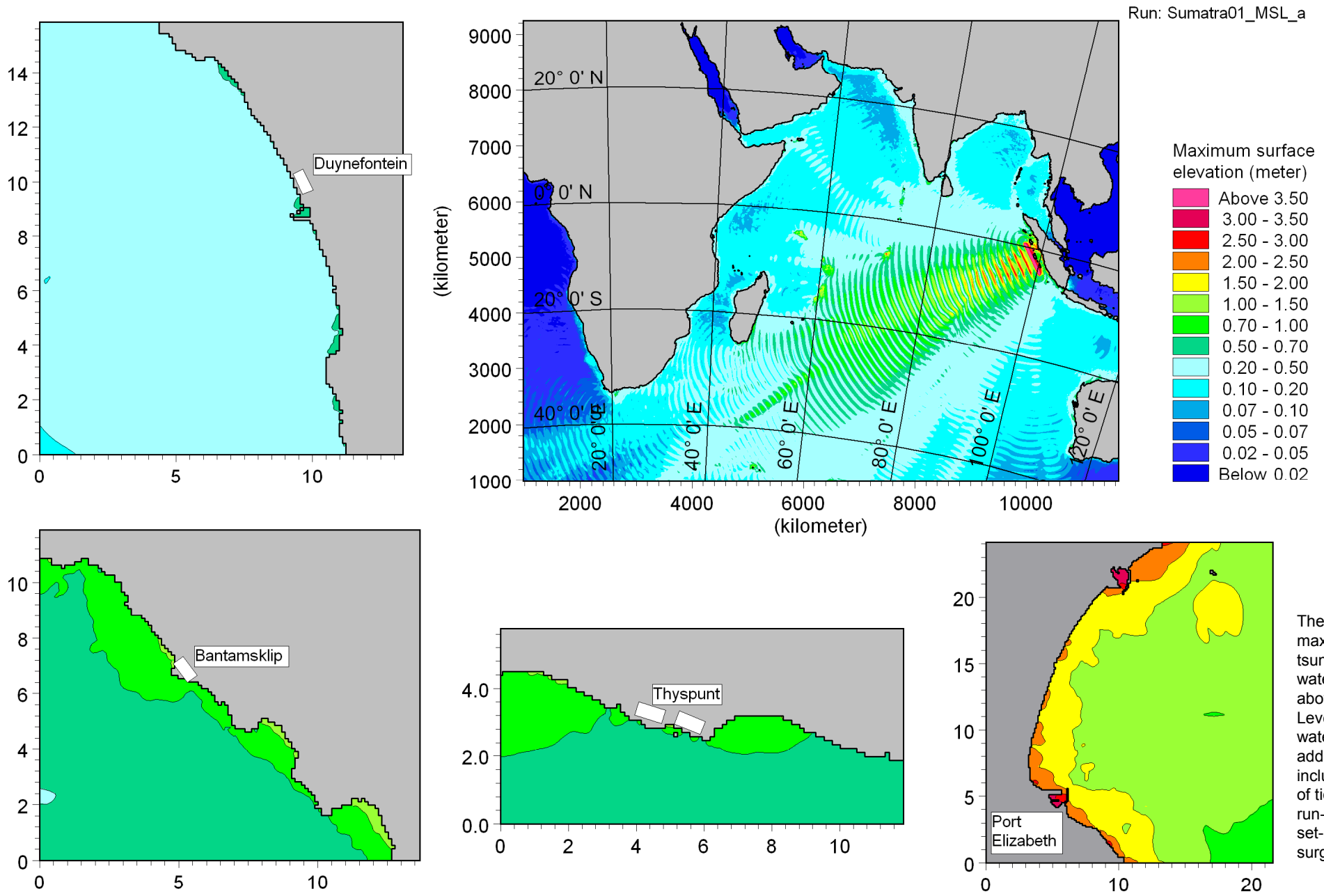

These are the maximum tsunami-induced water levels above Still Water Level. The total water level will additionally include the effect of tide, wave run-up, wave set-up and storm surge.

Title: **Maximum water levels predicted during tsunami event. Source is Sumatra B: maximum credible earthquake determined by the Council for Geoscience, Mw = 9.2.**

Figure No. **5.5**

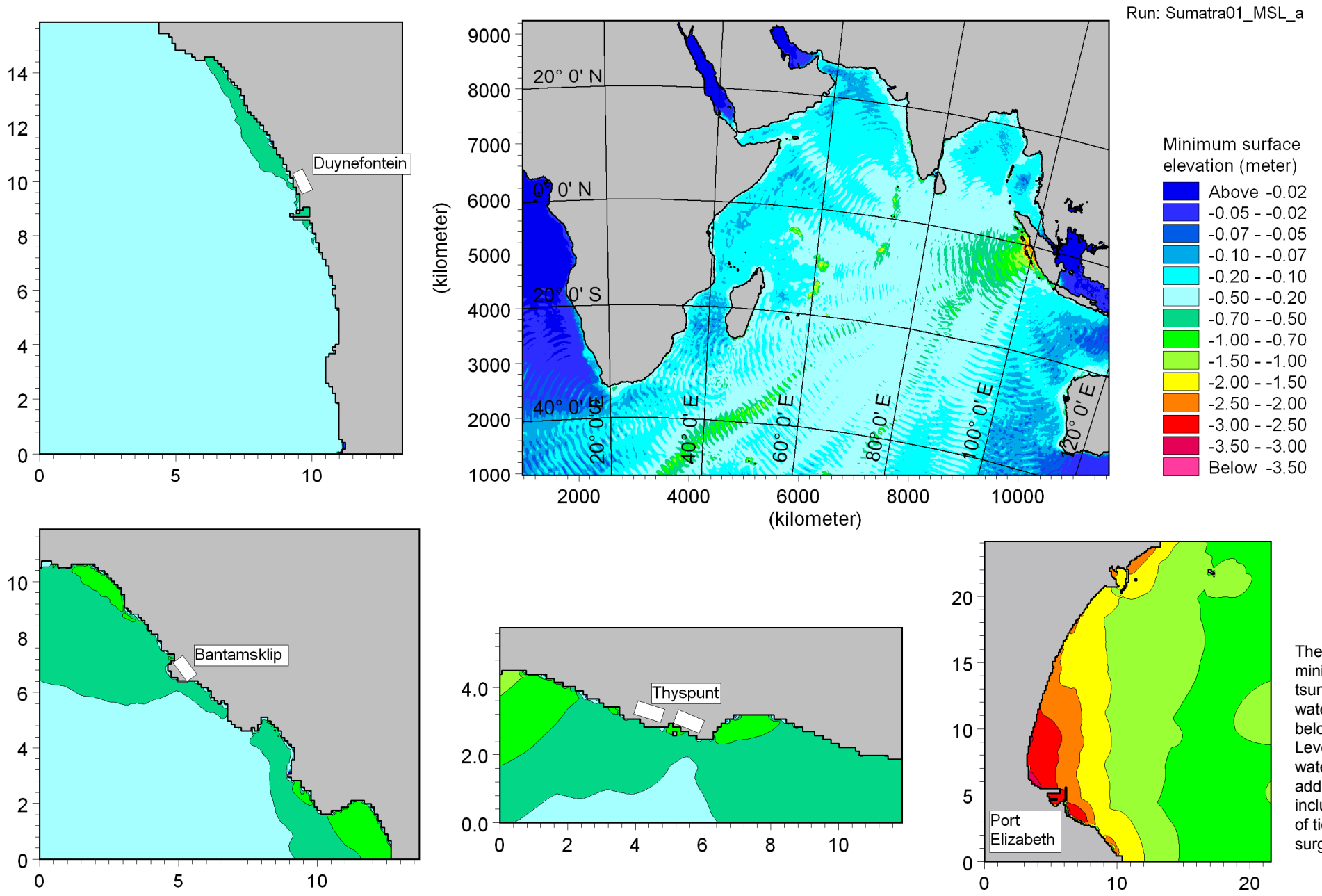

These are the minimum tsunami-induced water levels below Still Water Level. The total water level will additionally include the effect of tide and storm surge.

Title: **Minimum water levels predicted during tsunami event. Source is Sumatra B: maximum credible earthquake determined by the Council for Geoscience, Mw = 9.2.**

Figure No. **5.6**

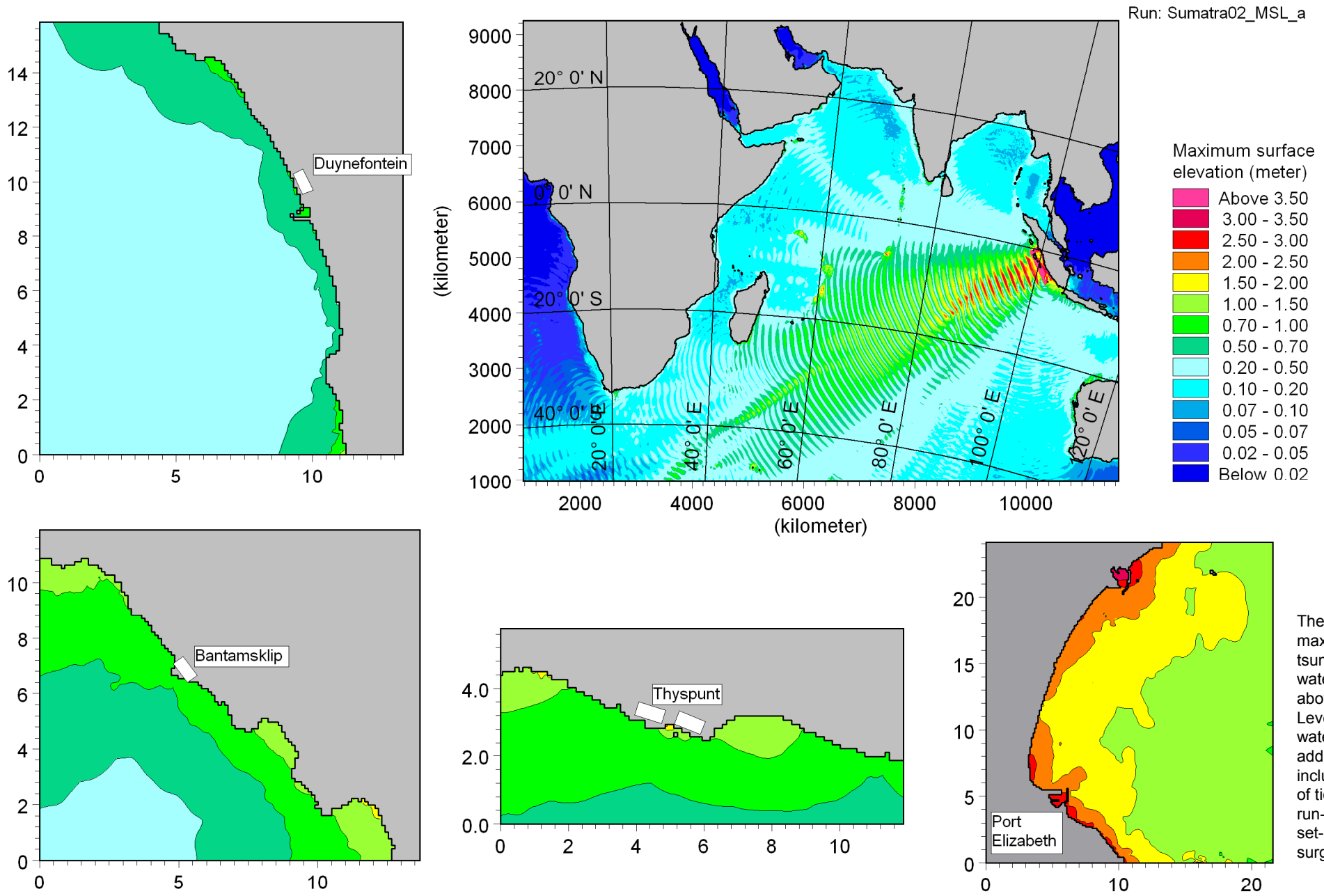

These are the maximum tsunami-induced water levels above Still Water Level. The total water level will additionally include the effect of tide, wave run-up, wave set-up and storm surge.

Title:

Maximum water levels predicted during tsunami event.
Source is a Sumatra C: maximum plausible event from Borrero *et al* (2006), Mw = 9.3.

Figure No.

5.7

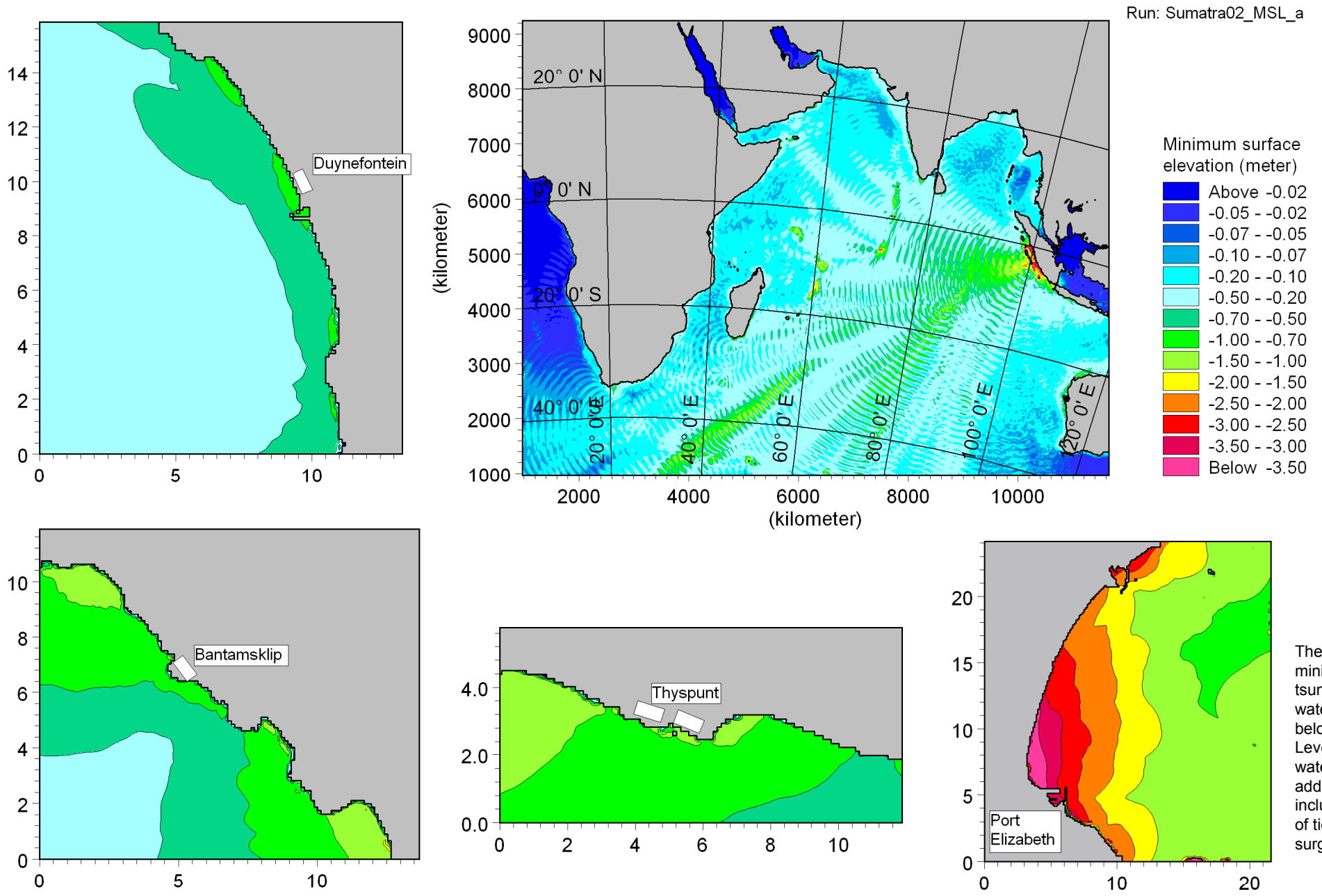

These are the minimum tsunami-induced water levels below Still Water Level. The total water level will additionally include the effect of tide and storm surge.

Title:

Minimum water levels predicted during tsunami event.
Source is a Sumatra C: maximum plausible event from Borrero *et al* (2006), Mw = 9.3.

Figure No.

5.8

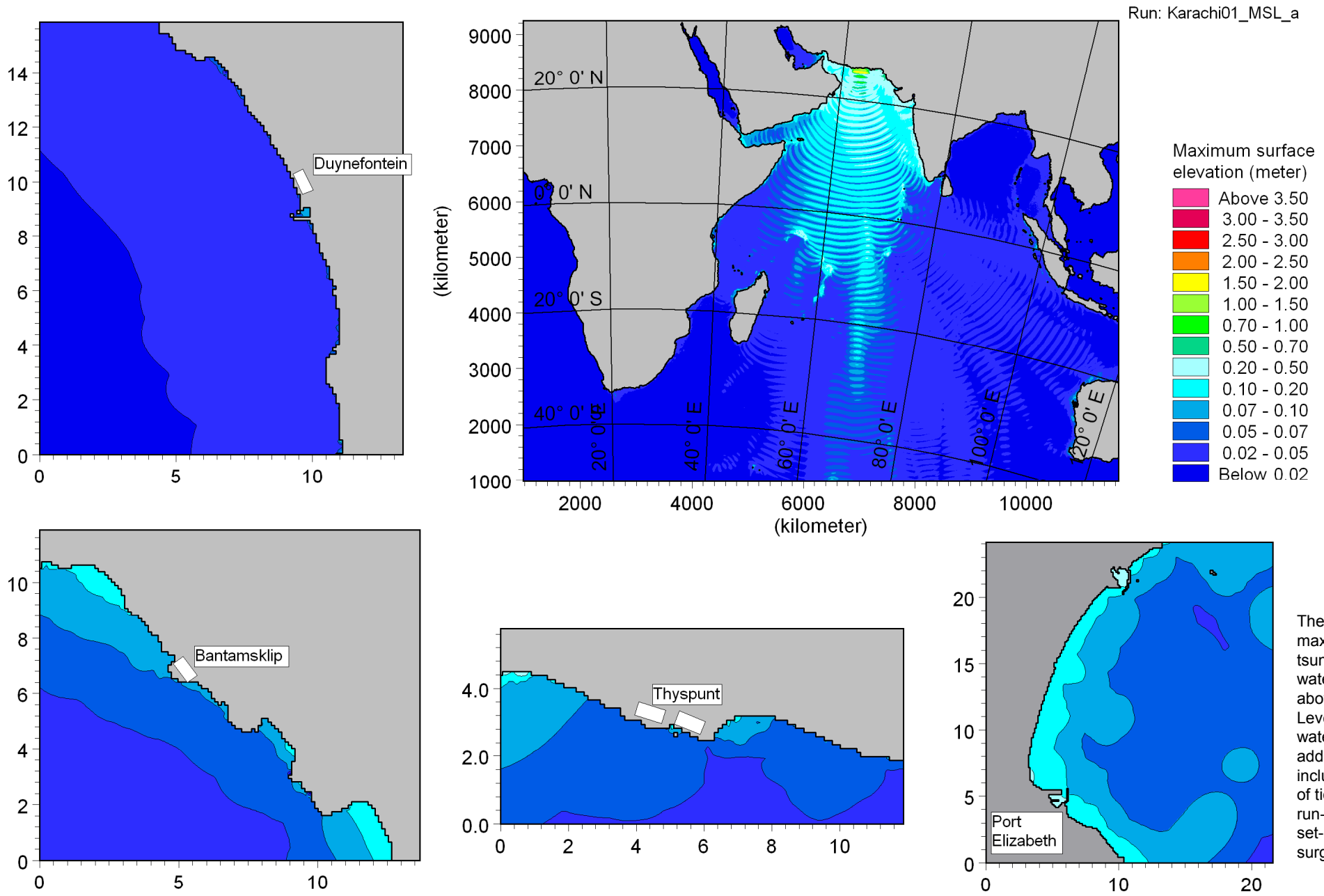

These are the maximum tsunami-induced water levels above Still Water Level. The total water level will additionally include the effect of tide, wave run-up, wave set-up and storm surge.

Title: **Maximum water levels predicted during tsunami event. Source is Karachi A: maximum credible earthquake determined by the Council for Geoscience, Mw =8.4.**

Figure No. **5.9**

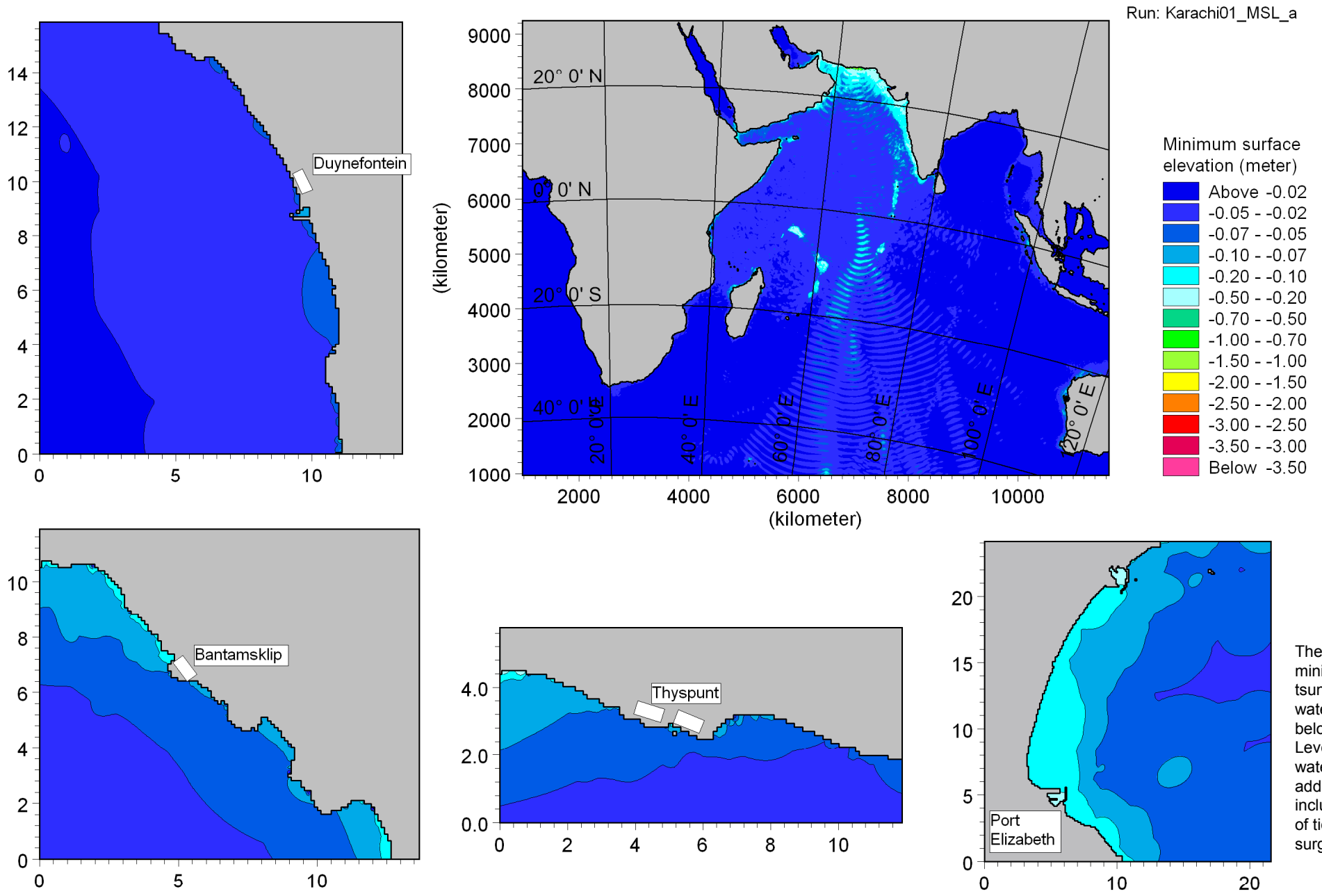

These are the minimum tsunami-induced water levels below Still Water Level. The total water level will additionally include the effect of tide and storm surge.

Title: **Minimum water levels predicted during tsunami event. Source is Karachi A: maximum credible earthquake determined by the Council for Geoscience, Mw =8.4.**

Figure No. **5.10**

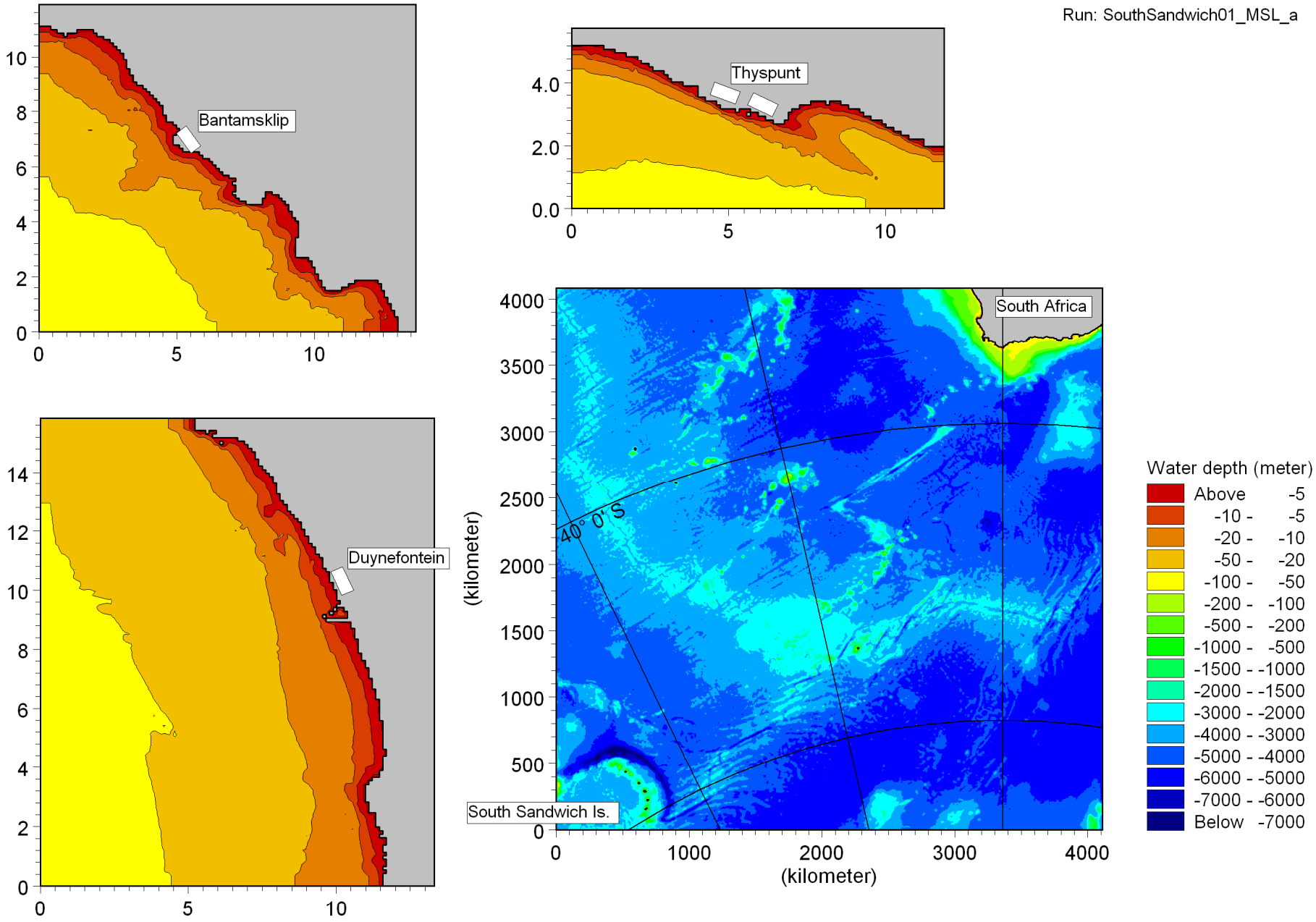

Title:

Model bathymetry used for tsunami modelling of the South Sandwich Islands earthquake events.

Figure No.

5.11

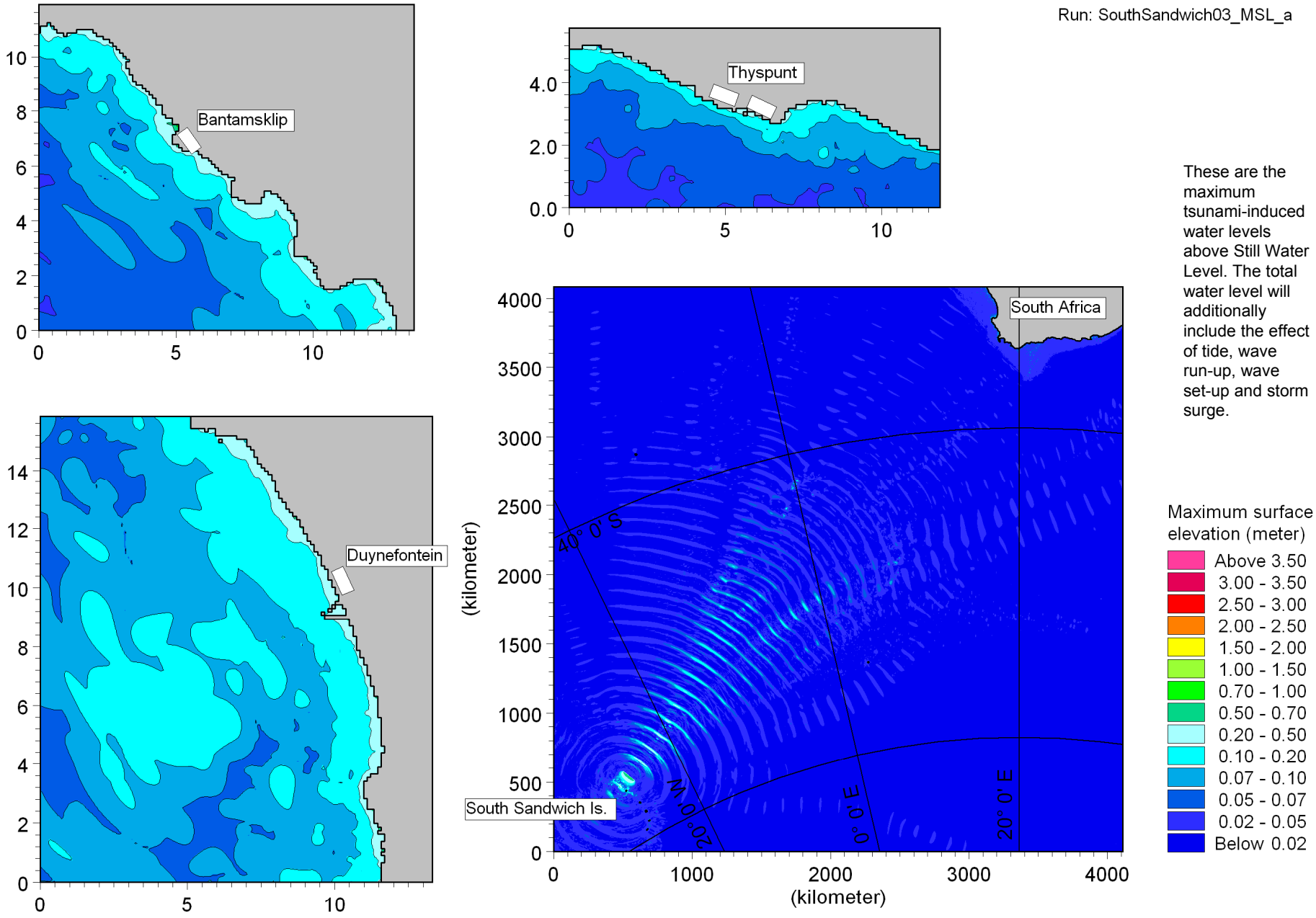

Title: **Maximum water levels predicted during tsunami event.**
Source is South Sandwich Islands A: maximum credible earthquake determined by the Council for Geoscience, Mw = 7.6.

Figure No.
5.12

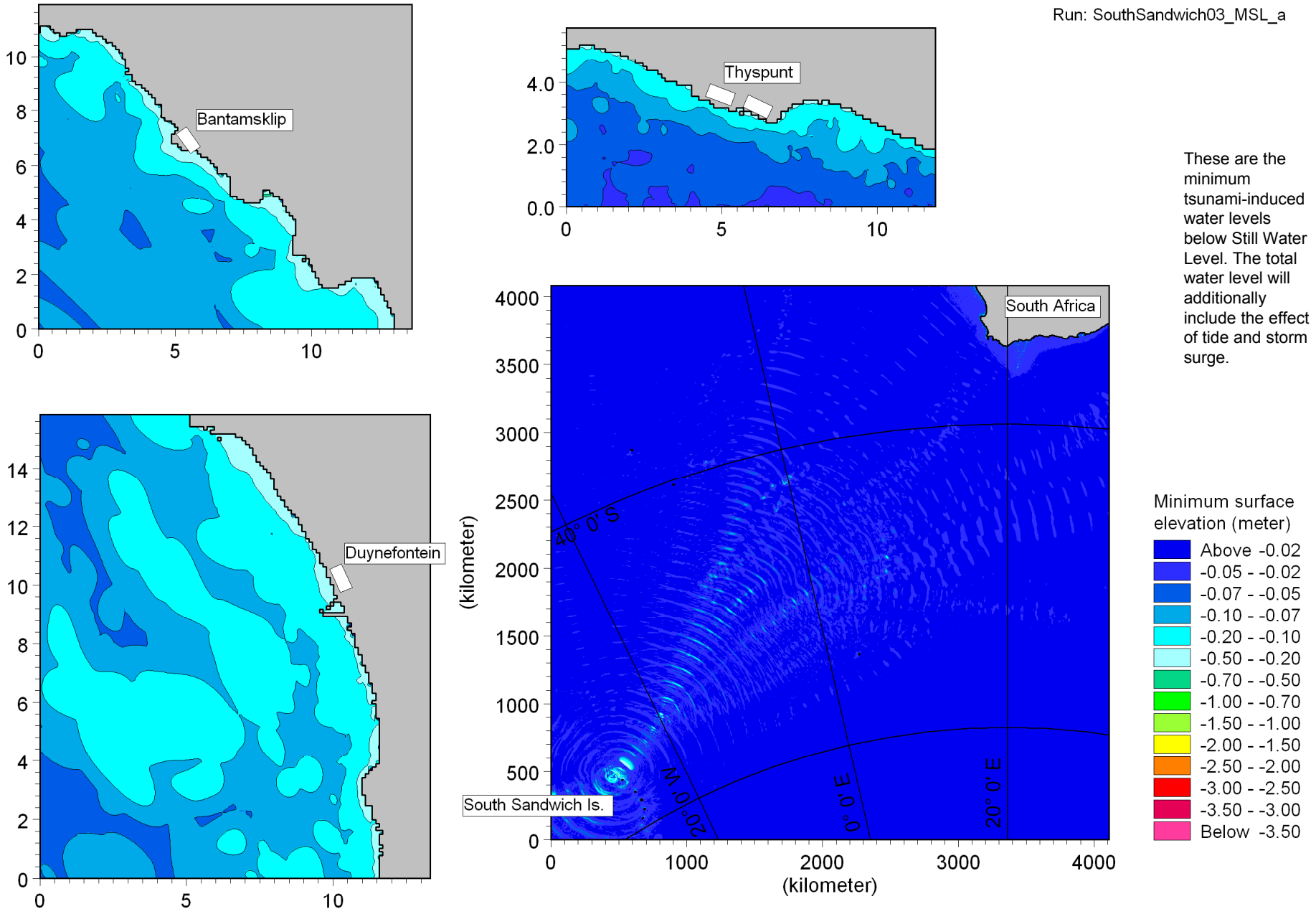

Title: **Minimum water levels predicted during tsunami event.**
Source is South Sandwich Islands A: maximum credible earthquake determined by the Council for Geoscience, Mw = 7.6.

Figure No.
5.13

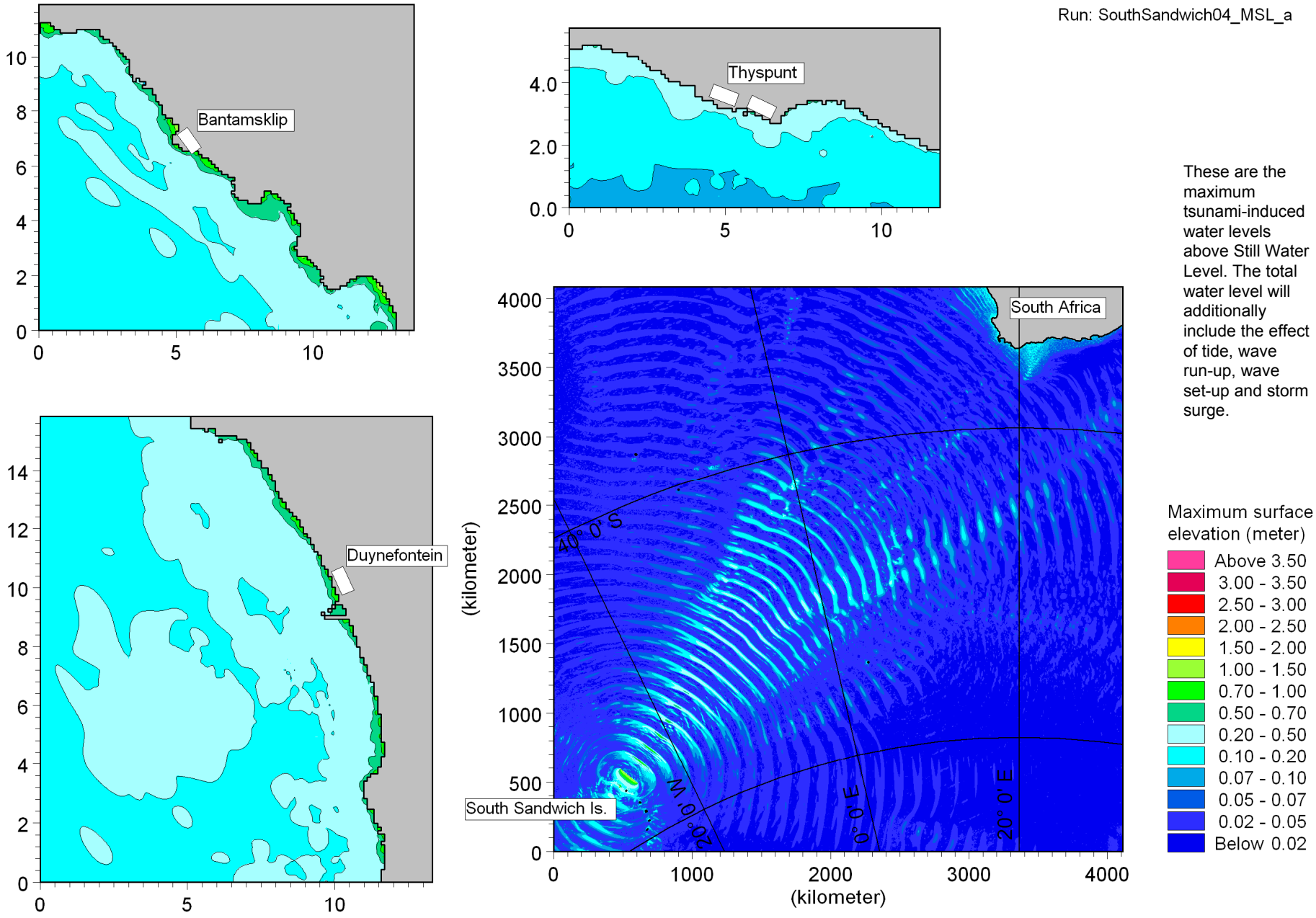

Title:

Maximum water levels predicted during tsunami event.
Source is South Sandwich Islands B: magnitude increased to Mw = 8.0.

Figure No.
5.14

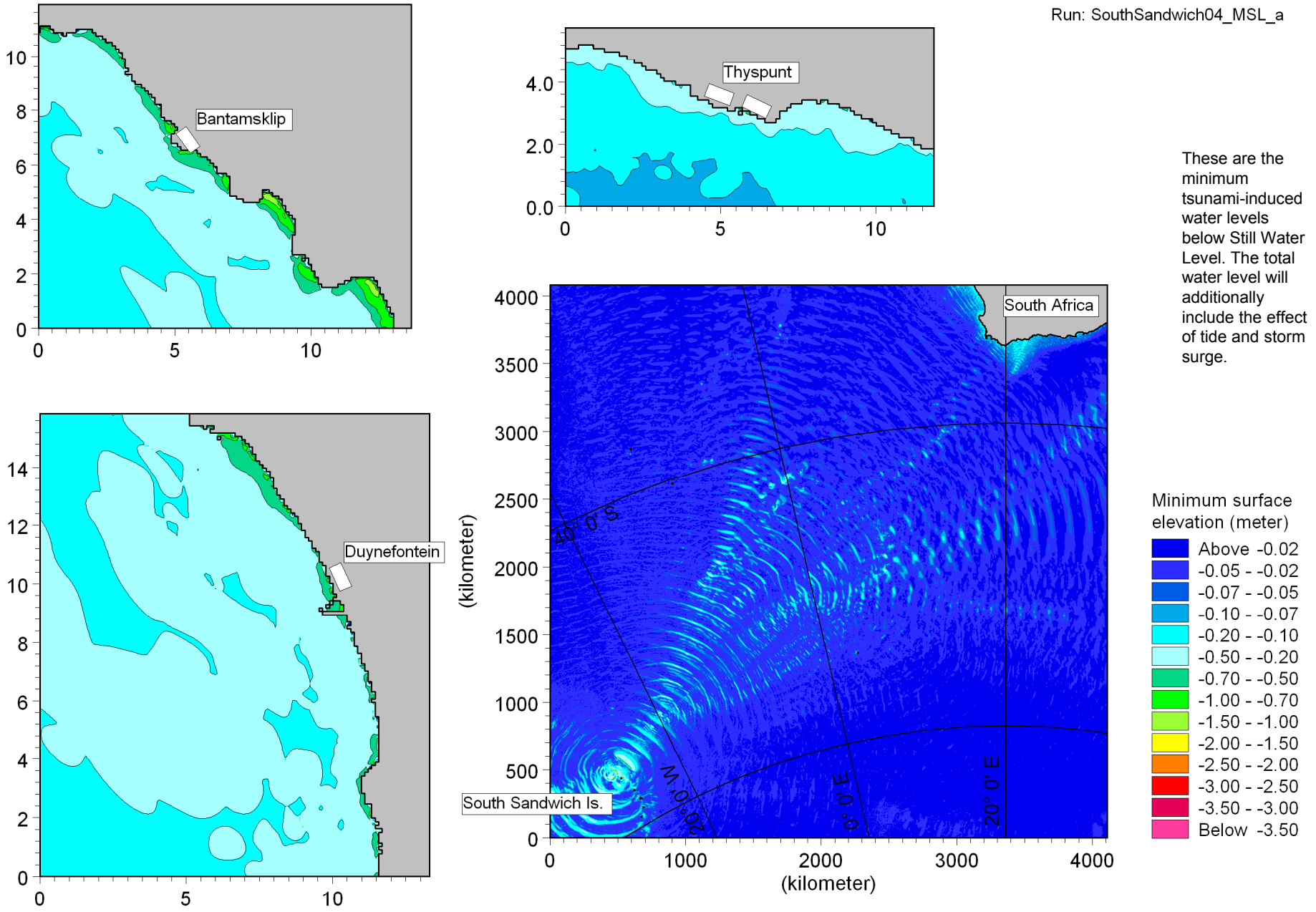

Title:

Minimum water levels predicted during tsunami event.
Source is South Sandwich Islands B: magnitude increased to Mw = 8.0.

Figure No.
5.15

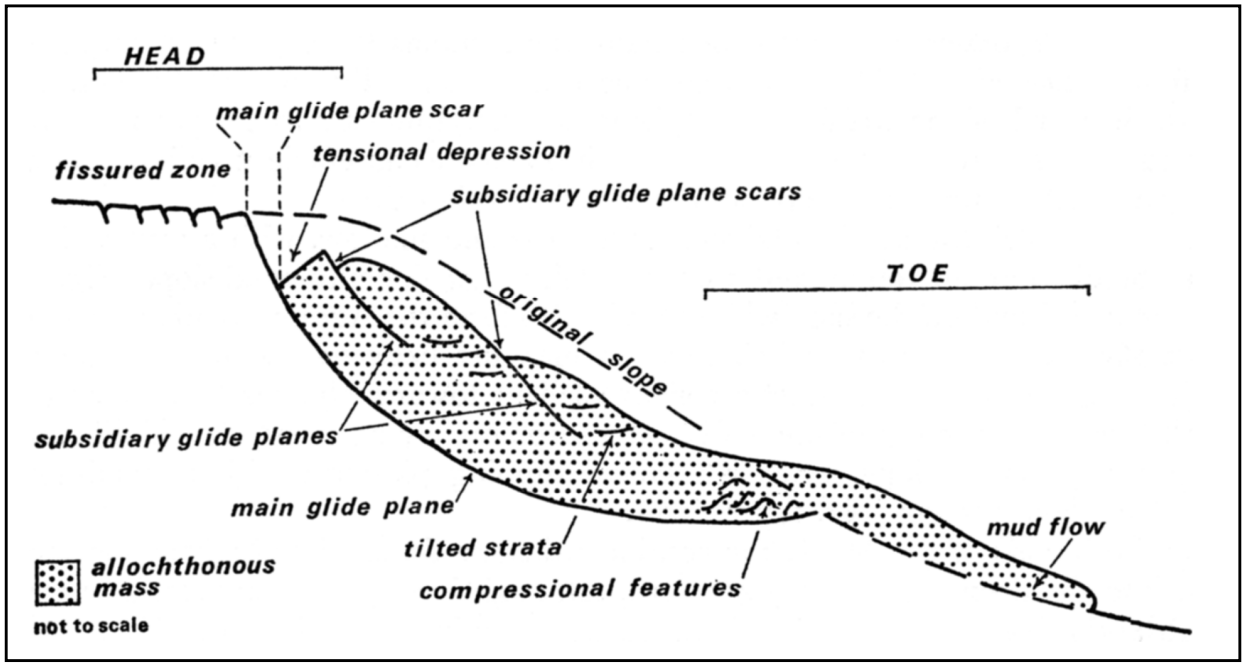

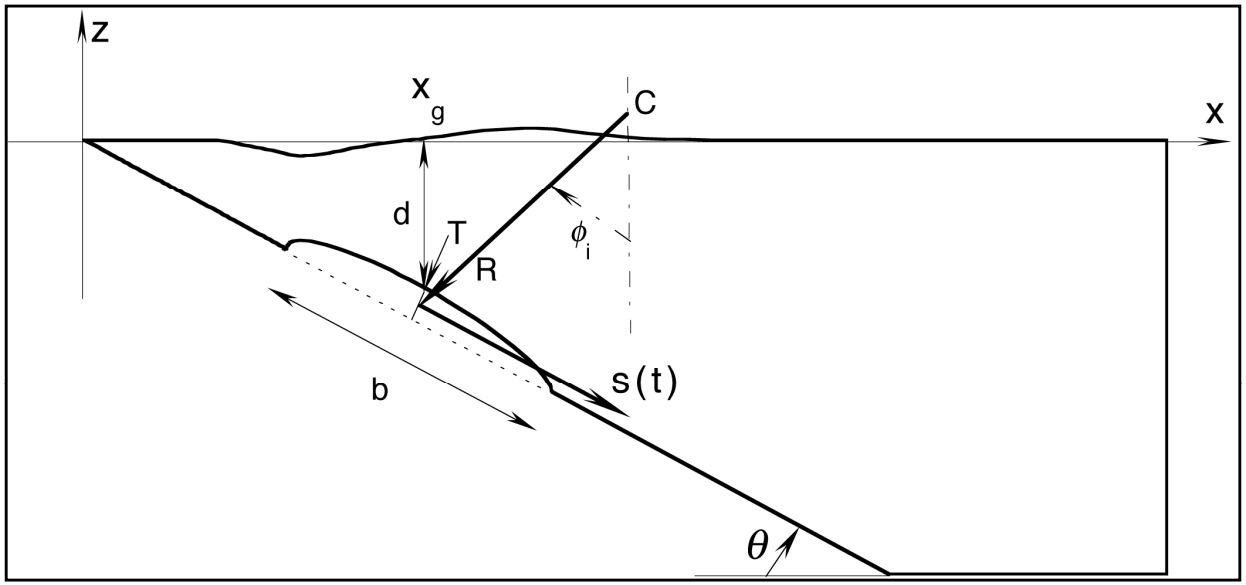

	Title: **Top: Main morphological and structural features of submarine slumps (Dingle, 1977). Bottom: Parameters defining slump model (Watts *et al,* 2003).**	**Figure No.** **5.16**

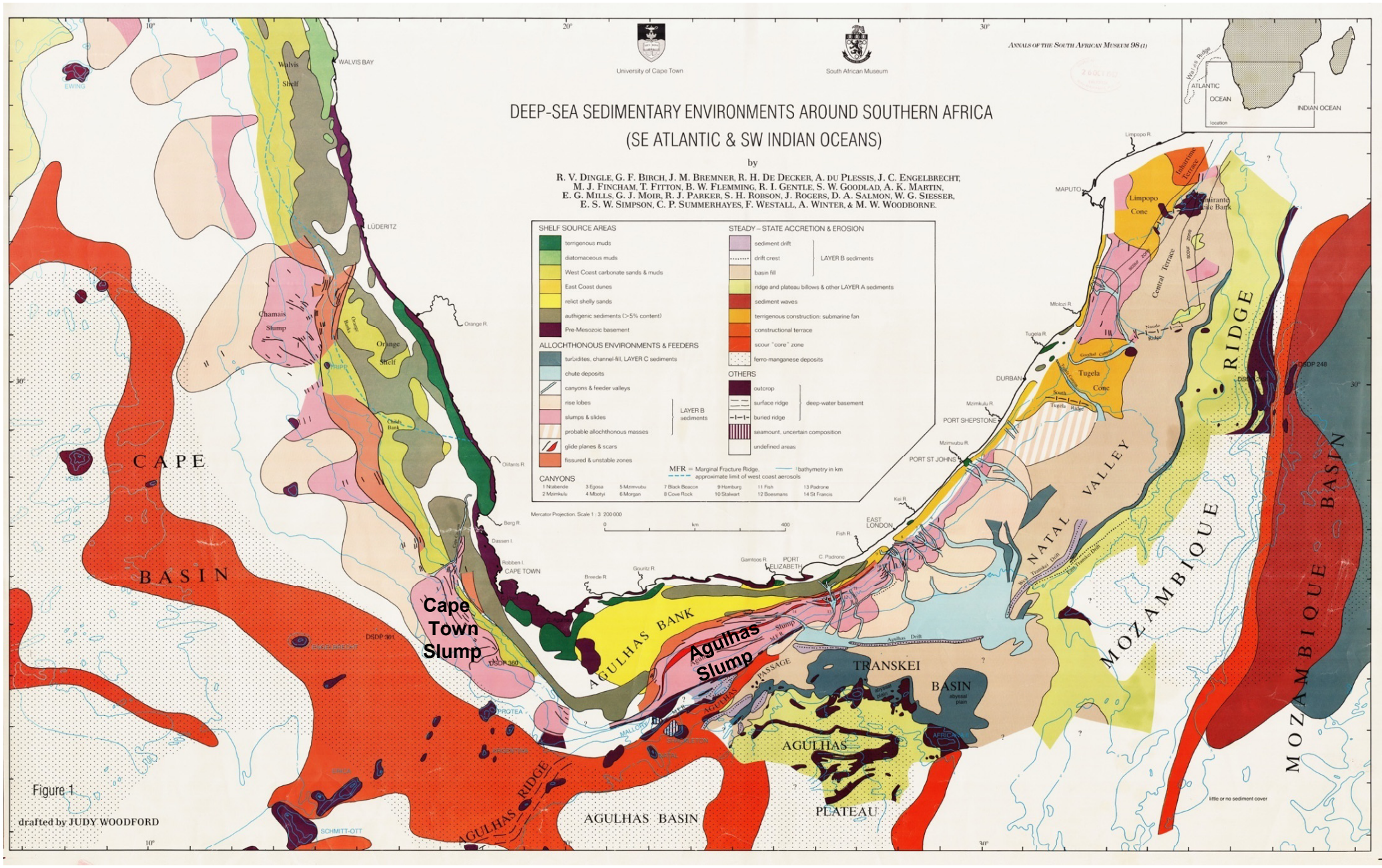

Title:

Location of slump zones around Southern Africa shown in pink (Dingle *et al*, 1987).

Figure No.

5.17

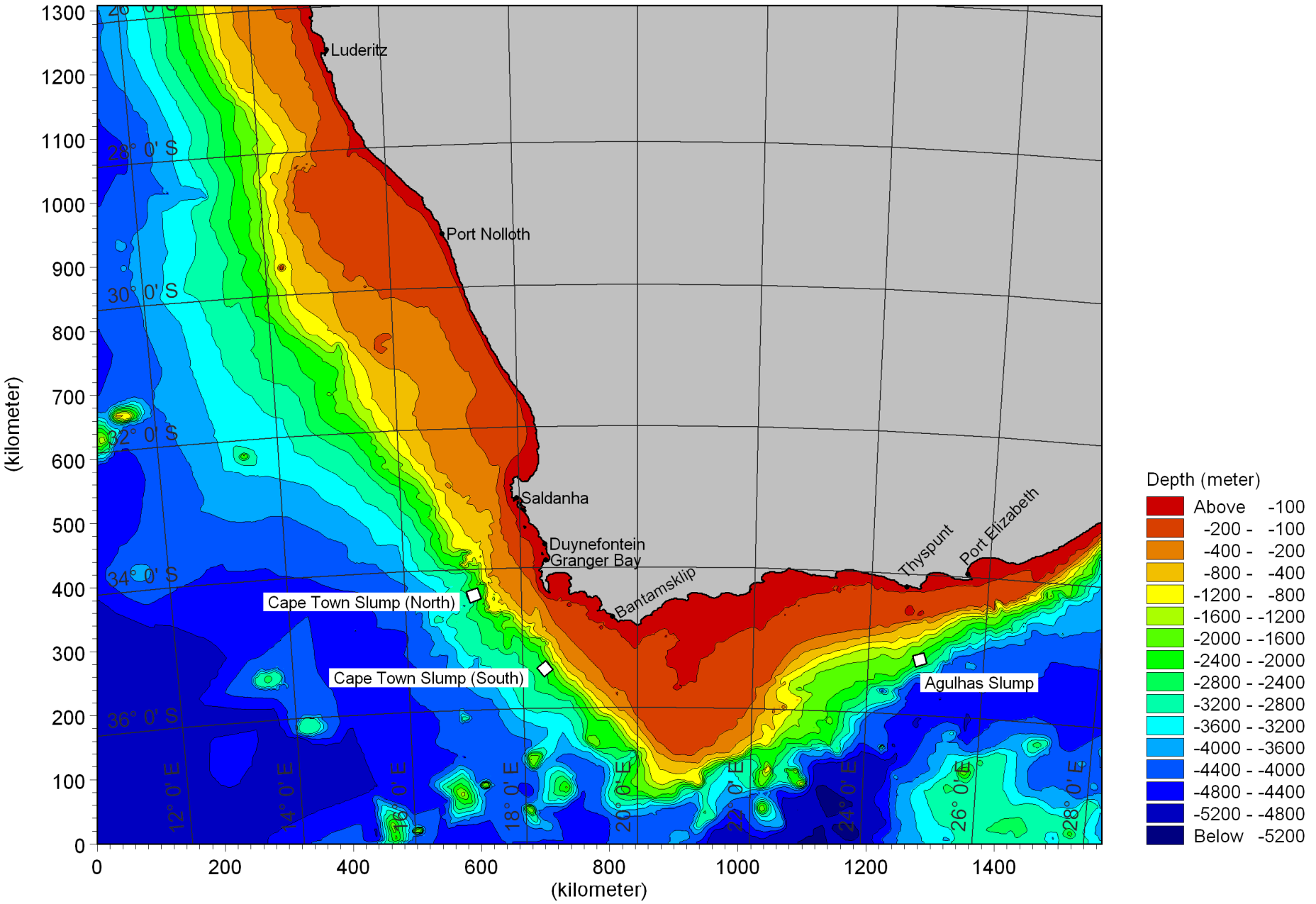

Title:

Model bathymetry used for tsunami modelling due to slumps on the South African shelf margin. Locations of the three slumps modelled are indicated.

Figure No.

5.18

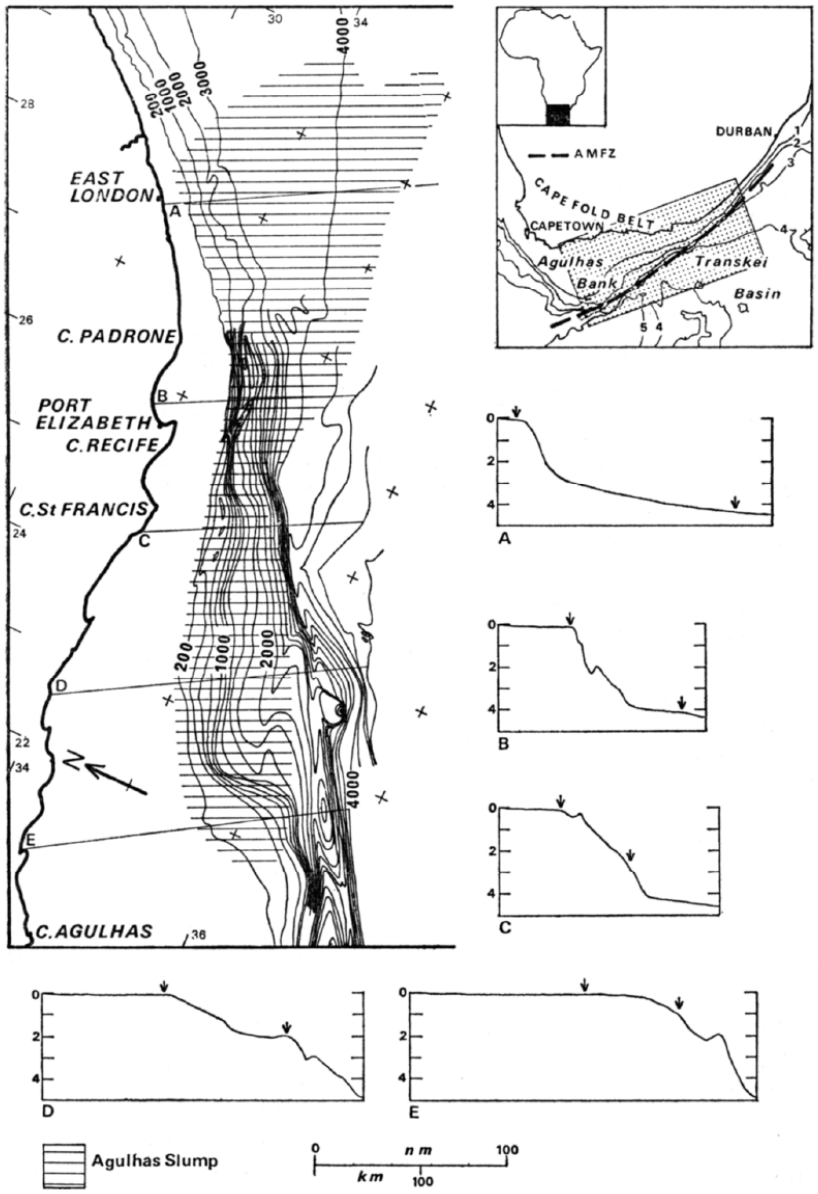

FIG. 1. Bathymetry (in metres) and bathymetric profiles (in kilometres) on the SE Agulhas Bank. Insert shows location of area; AMFZ, Agulhas marginal fracture zone. Arrows on profiles show limits of slump.

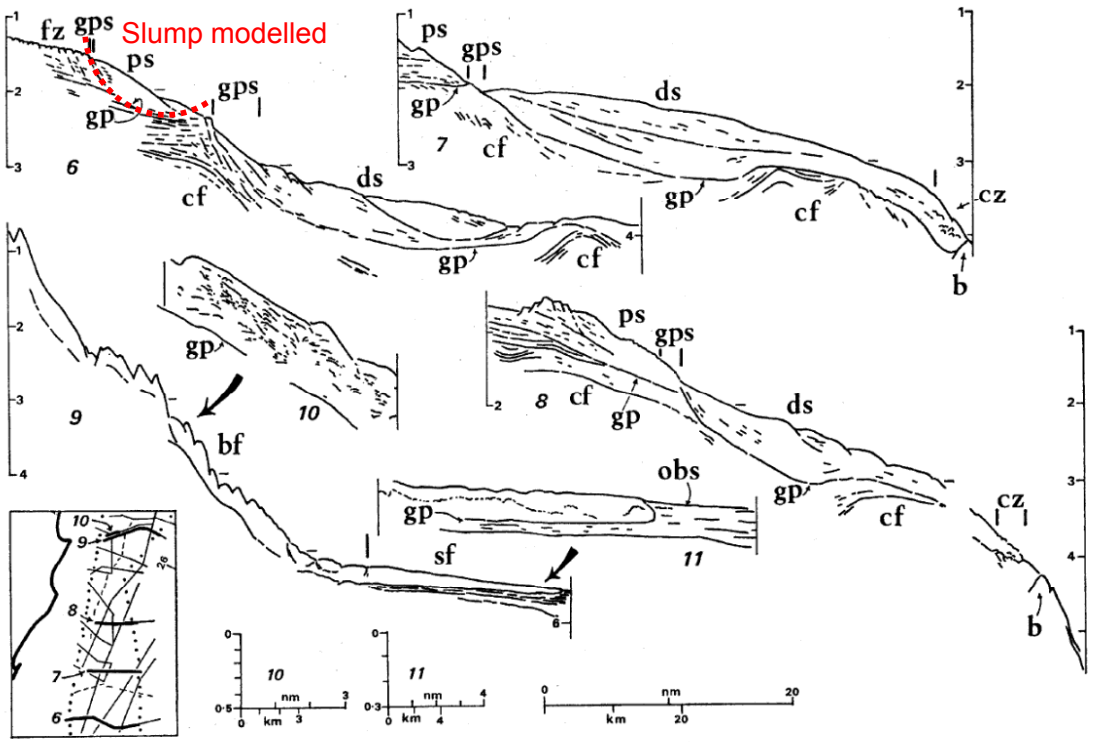

FIG. 6. Replotted (6–9) and traced (10 & 11) seismic profiles across the distal part of the Agulhas Slump. Vertical scales in seconds DT. For abbreviations see explanation to Fig. 4. For location of profile 11 see Fig. 3.

	Title: **Details of the Agulhas Slump (Dingle, 1977).**	**Figure No.** **5.19**

Run: Agulhas01b

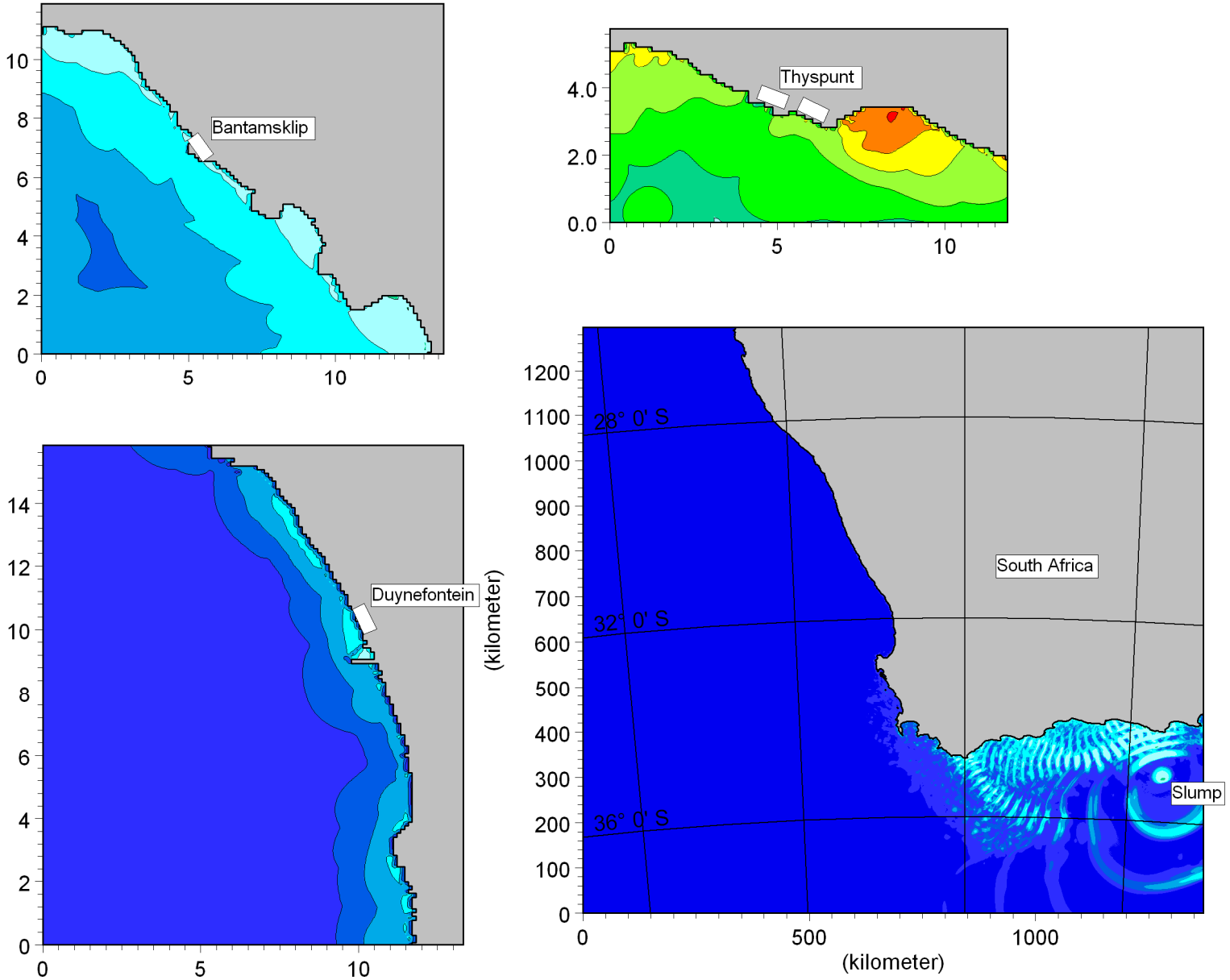

Title:

Maximum water levels predicted during tsunami event.
Source is theoretical Agulhas Slump with volume of slumped sediment = 80 km³.

Figure No.
5.20

Run: Agulhas01b

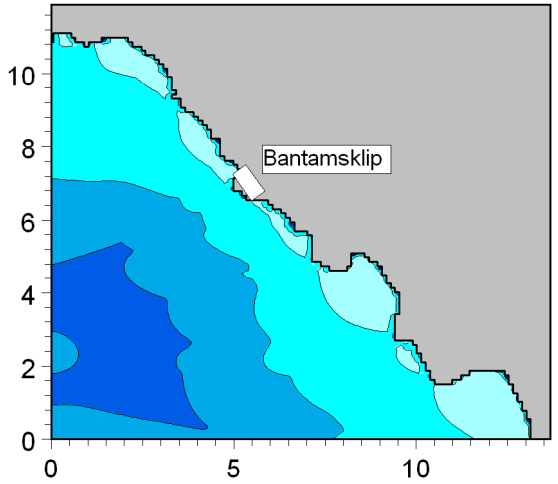

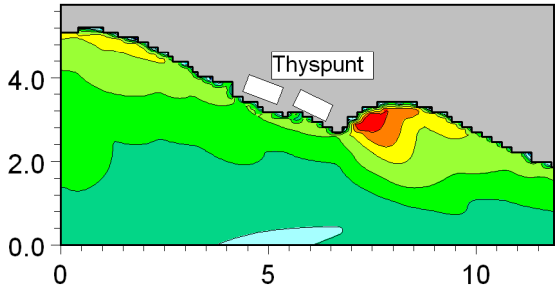

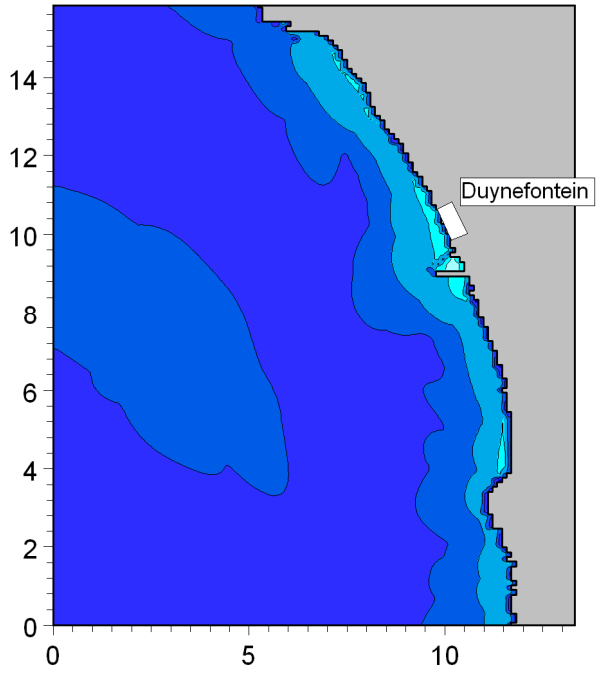

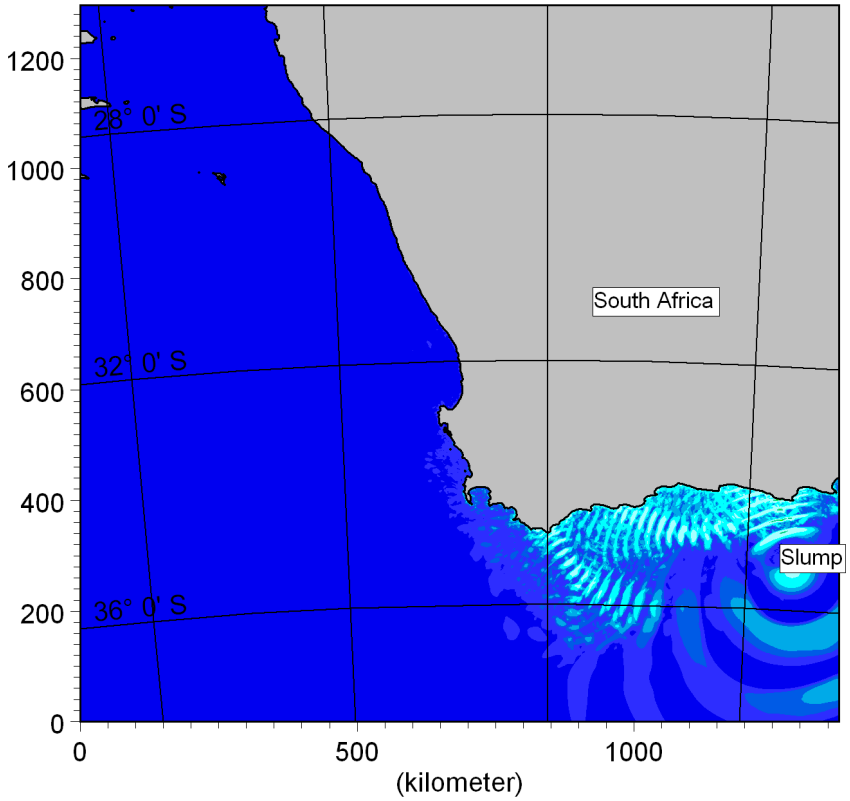

Minimum surface elevation (meter)

- Above -0.02
- -0.05 - -0.02
- -0.07 - -0.05
- -0.10 - -0.07
- -0.20 - -0.10
- -0.50 - -0.20
- -0.70 - -0.50
- -1.00 - -0.70
- -1.50 - -1.00
- -2.00 - -1.50
- -2.50 - -2.00
- -3.00 - -2.50
- -3.50 - -3.00
- Below -3.50

Title:

Minimum water levels predicted during tsunami event.
Source is theoretical Agulhas Slump with volume of slumped sediment = 80 km³.

Figure No.
5.21

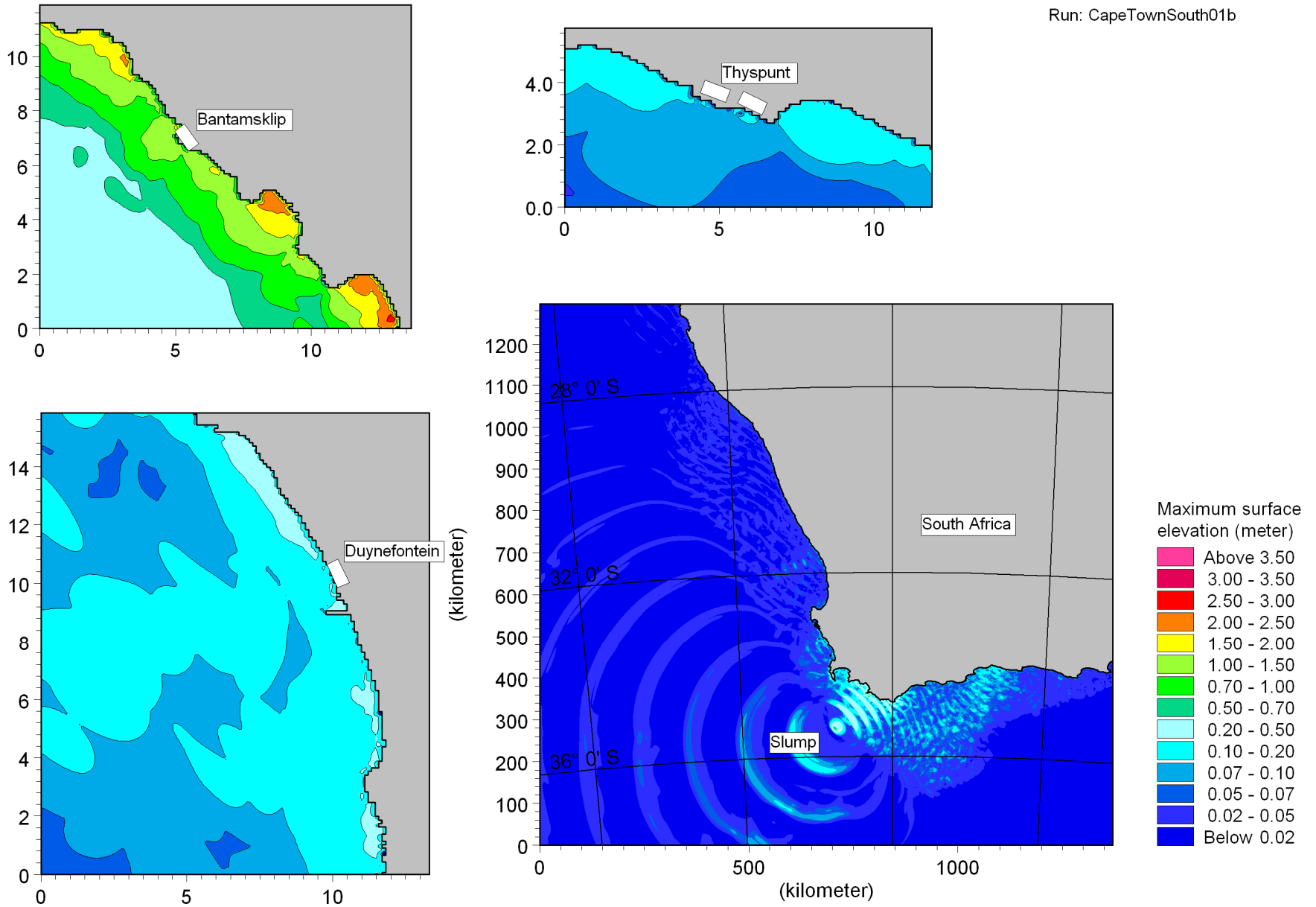

Title:

Maximum water levels predicted during tsunami event.
Source is theoretical Cape Town Slump (South) with volume of slumped sediment = 80 km³.

Figure No.
5.22

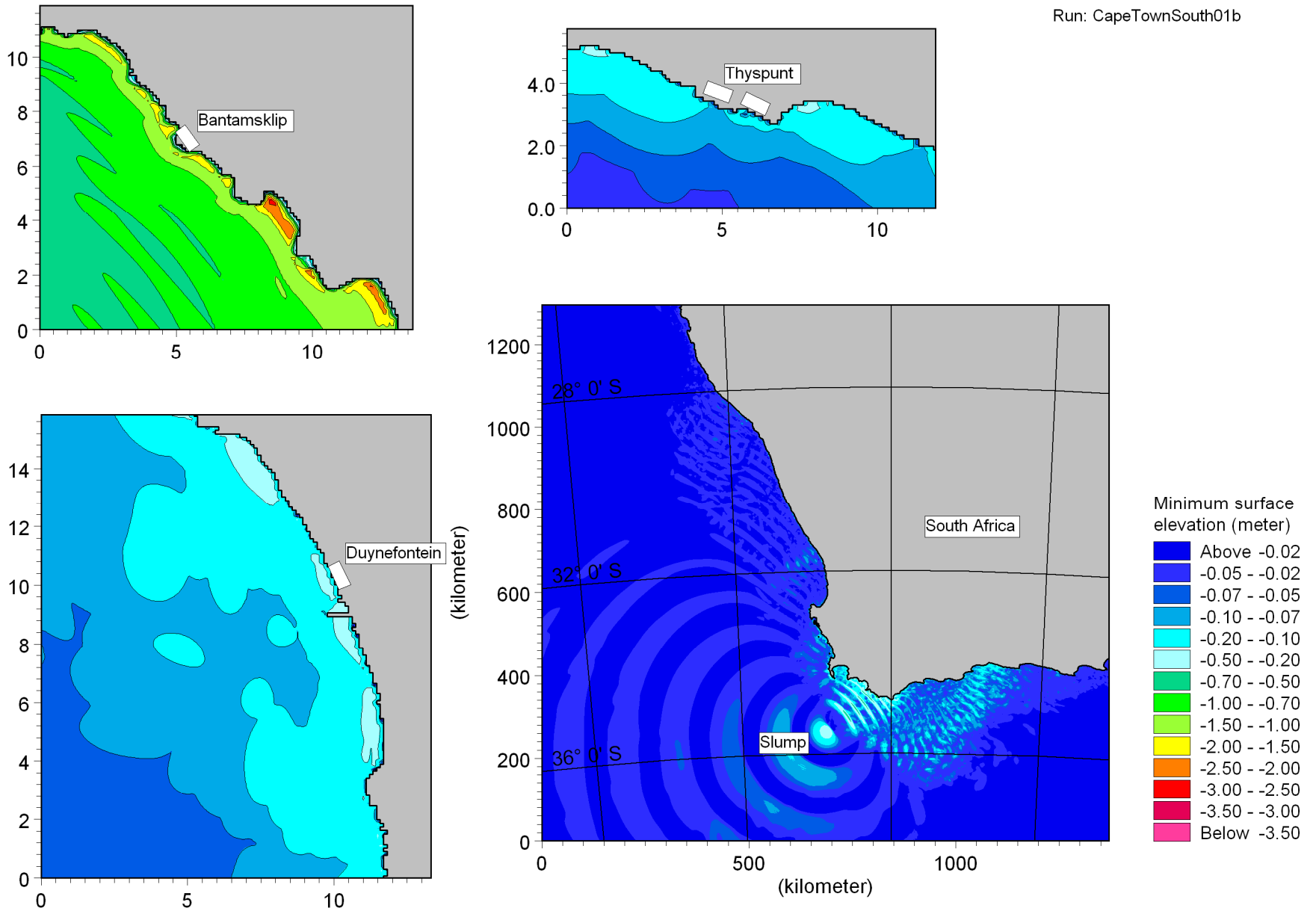

Title:

Minimum water levels predicted during tsunami event.
Source is theoretical Cape Town Slump (South) with volume of slumped sediment = 80 km³.

Figure No.
5.23

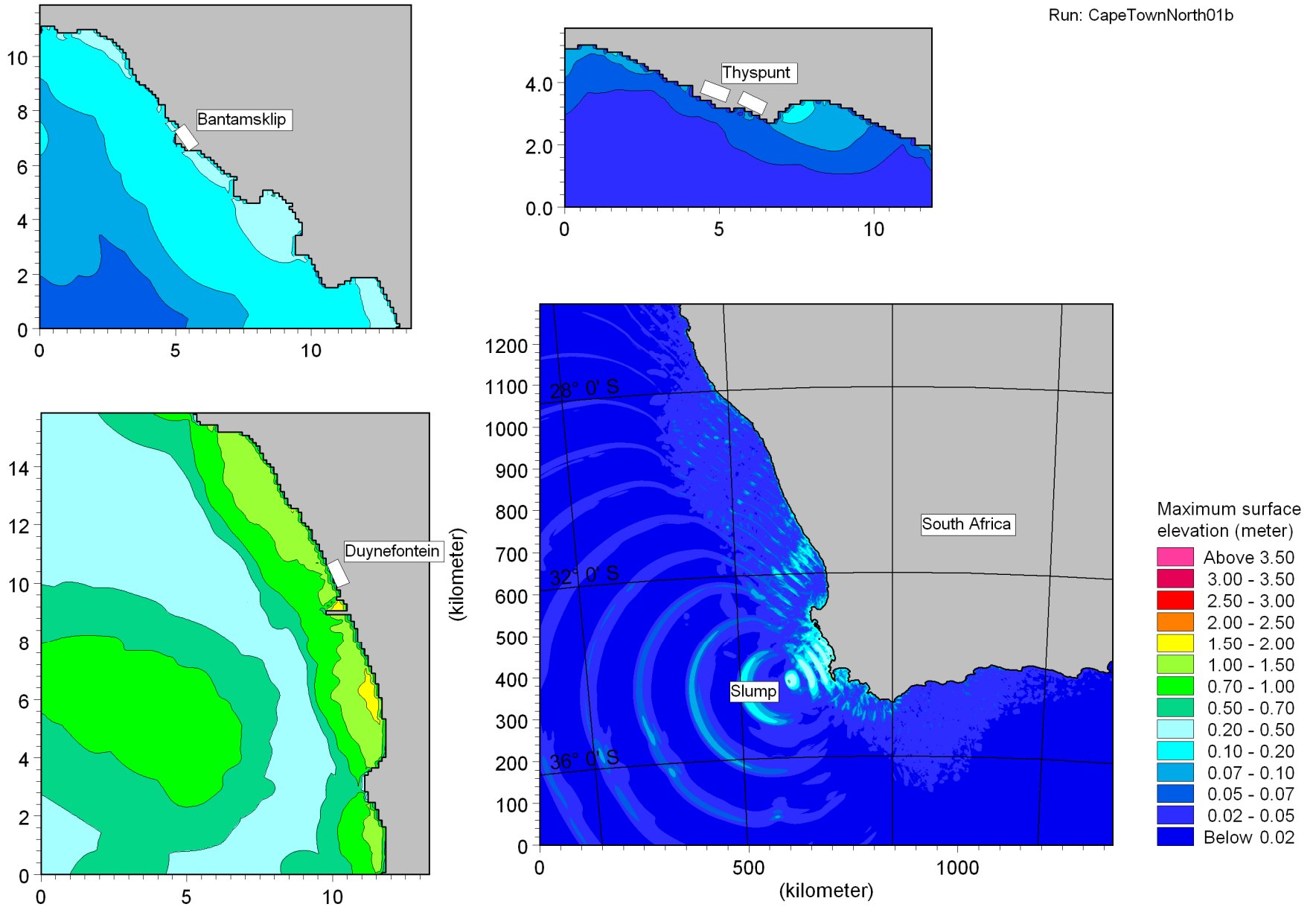

Title:

Maximum water levels predicted during tsunami event.
Source is theoretical Cape Town Slump (North) with volume of slumped sediment = 80 km³.

Figure No.
5.24

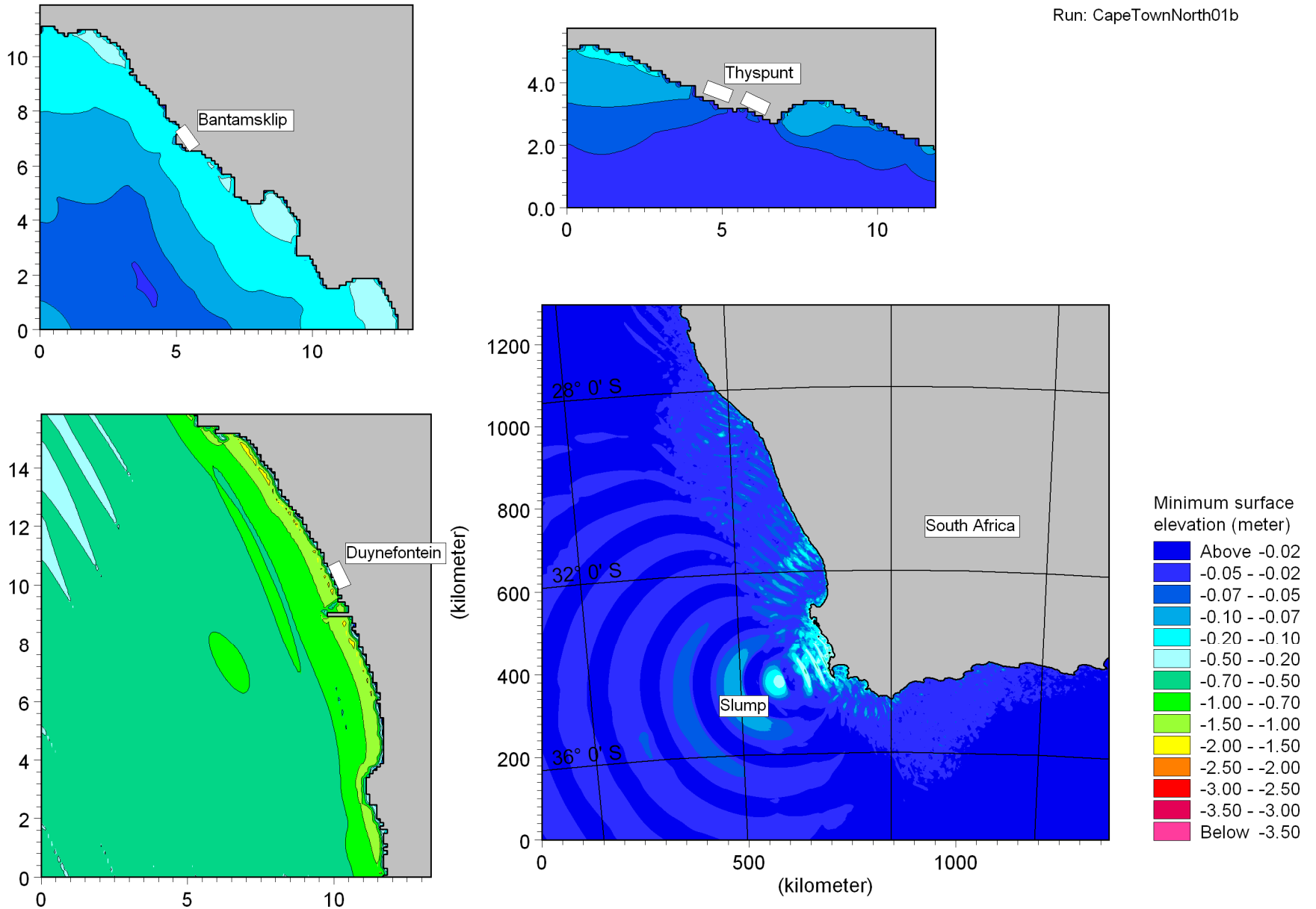

Title:

Minimum water levels predicted during tsunami event.
Source is theoretical Cape Town Slump (North) with volume of slumped sediment = 80 km³.

Figure No.
5.25

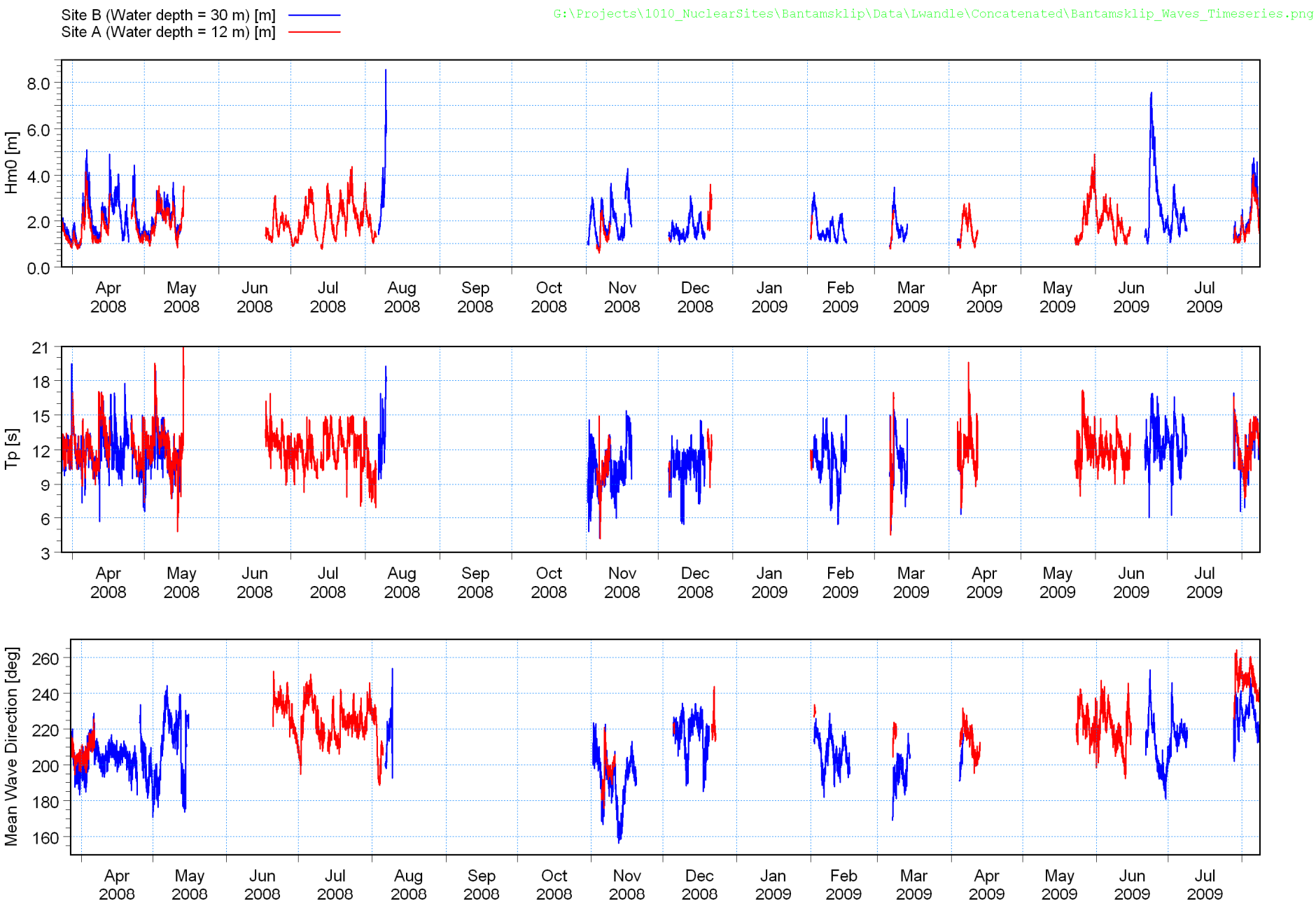

Title:

Wave measurements at Bantamsklip Sites A and B.
Time-series of wave parameters (refer to Figure 3.1 for instrument positions).

Figure No.

6.1

G:\Projects\1010_NuclearSites\Bantamsklip\Data\Lwandle\Concatenated\Bantamsklip_Waves_Timeseries_Storms.png

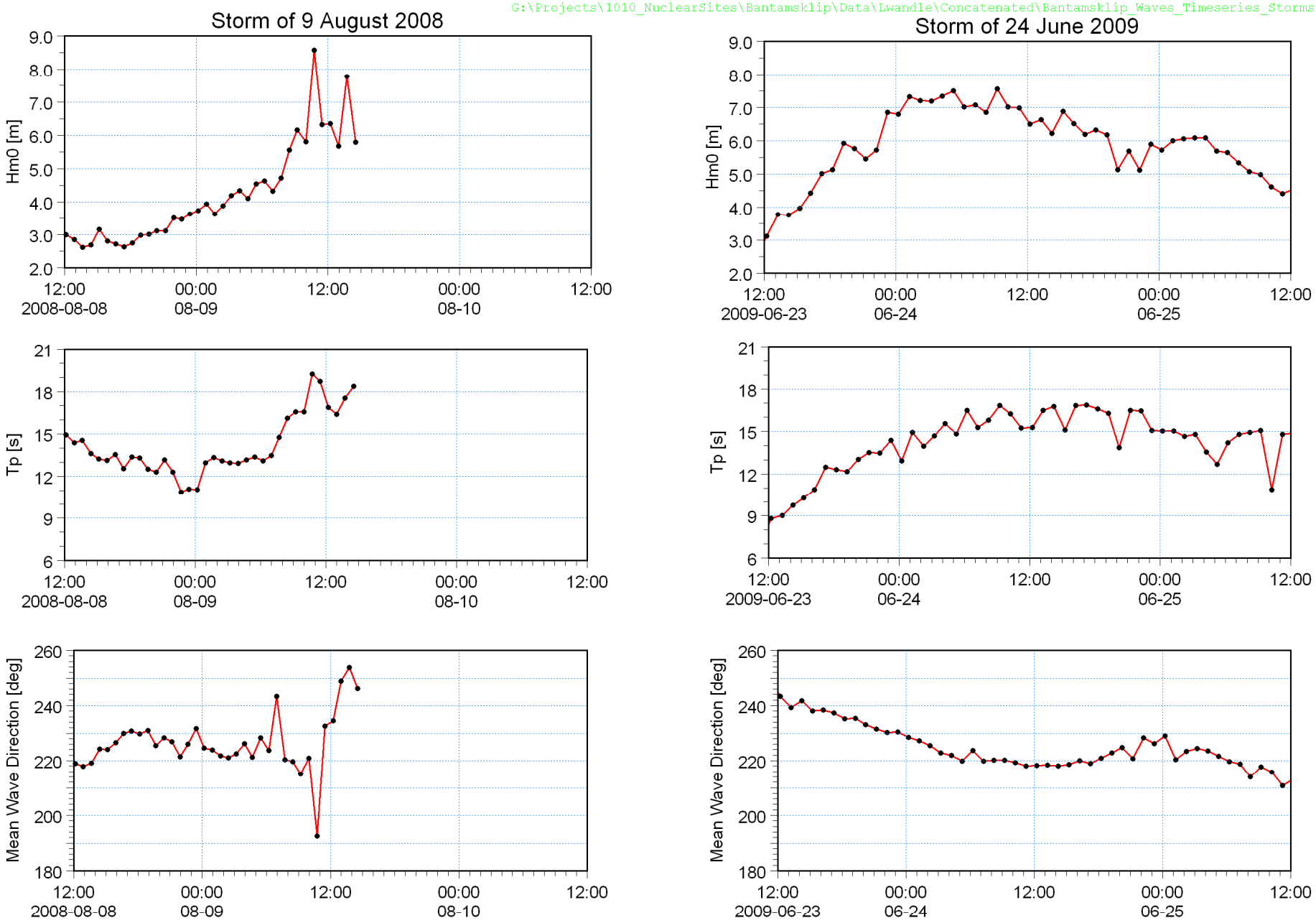

Title:

Wave measurements at Bantamsklip Site B during two storm events.
Time-series of wave parameters (refer to Figure 3.1 for instrument positions).

Figure No.

6.2

Wave Rose

G:\Projects\1010_NuclearSites\Bantamsklip\Data\Lwandle\Concatenated\Bantamsklip_Waves_A_Rose.png

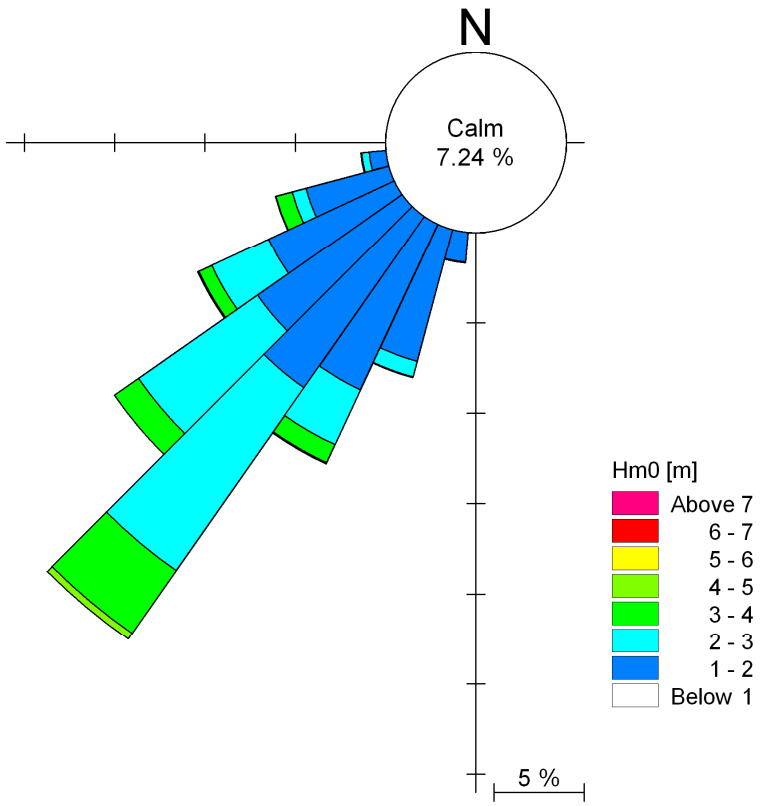

Wave Height Histogram

000.0%: 0.59953
025.0%: 1.27571
050.0%: 1.75703
080.0%: 2.44395
095.0%: 3.25093
099.0%: 3.78779
100.0%: 4.89736

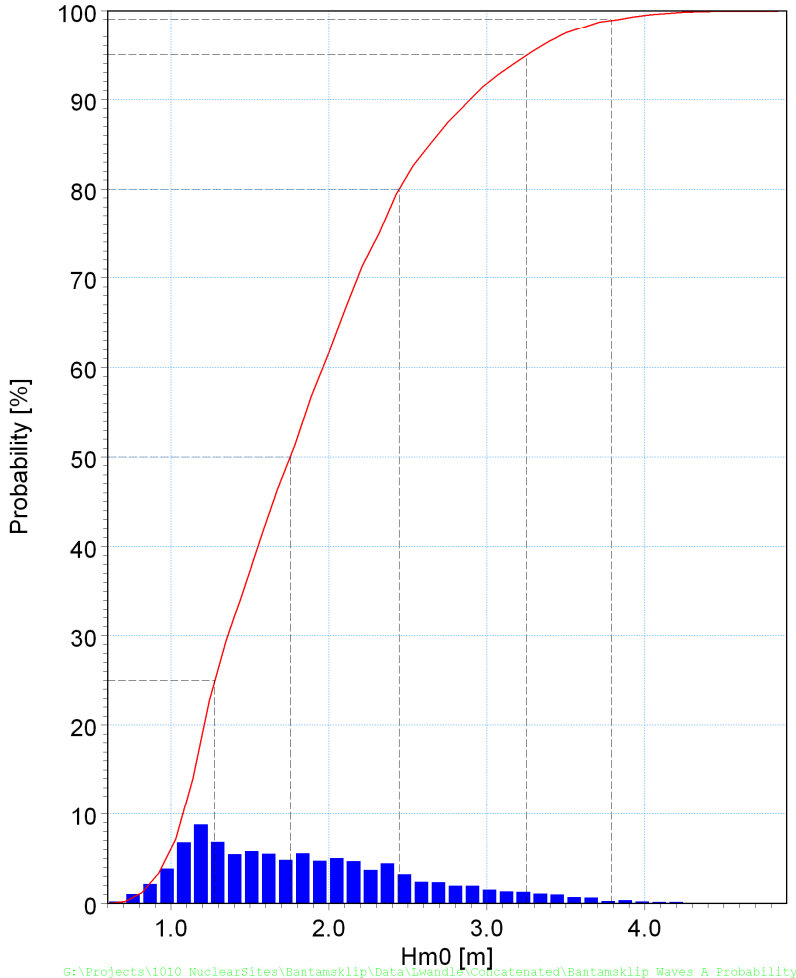

G:\Projects\1010_NuclearSites\Bantamsklip\Data\Lwandle\Concatenated\Bantamsklip_Waves_A_Probability.png

Title:

Wave measurements at Bantamsklip Site A (refer to Figure 3.1 for instrument position). Wave rose and histogram of wave heights.

Figure No.

6.3

Wave Rose

G:\Projects\1010_NuclearSites\Bantamsklip\Data\Lwandle\Concatenated\Bantamsklip_Waves_B_Rose.png

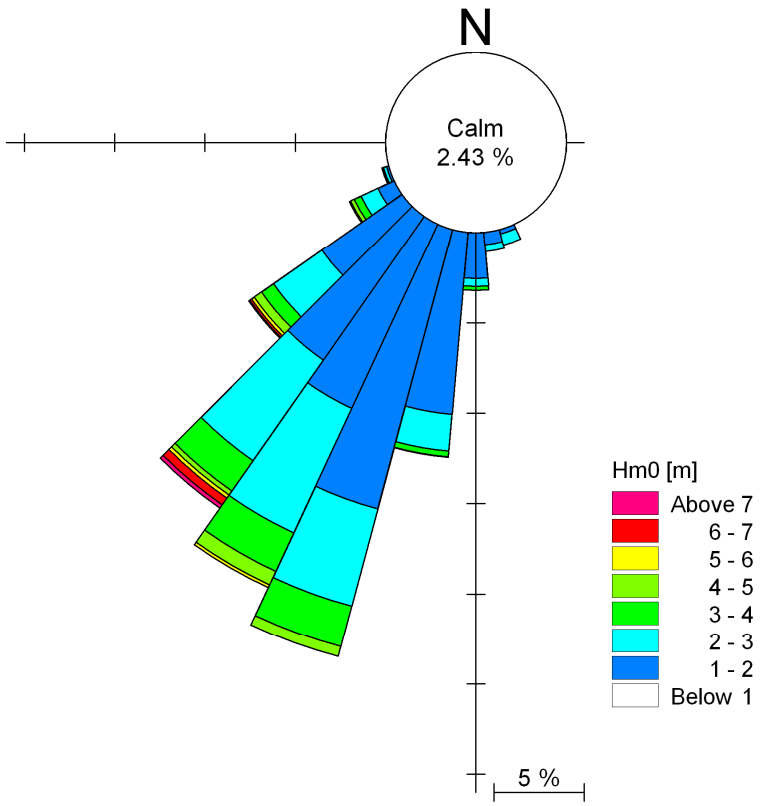

Wave Height Histogram

000.0%: 0.74274
025.0%: 1.39220
050.0%: 1.77773
080.0%: 2.64680
095.0%: 3.80255
099.0%: 5.81015
100.0%: 8.57920

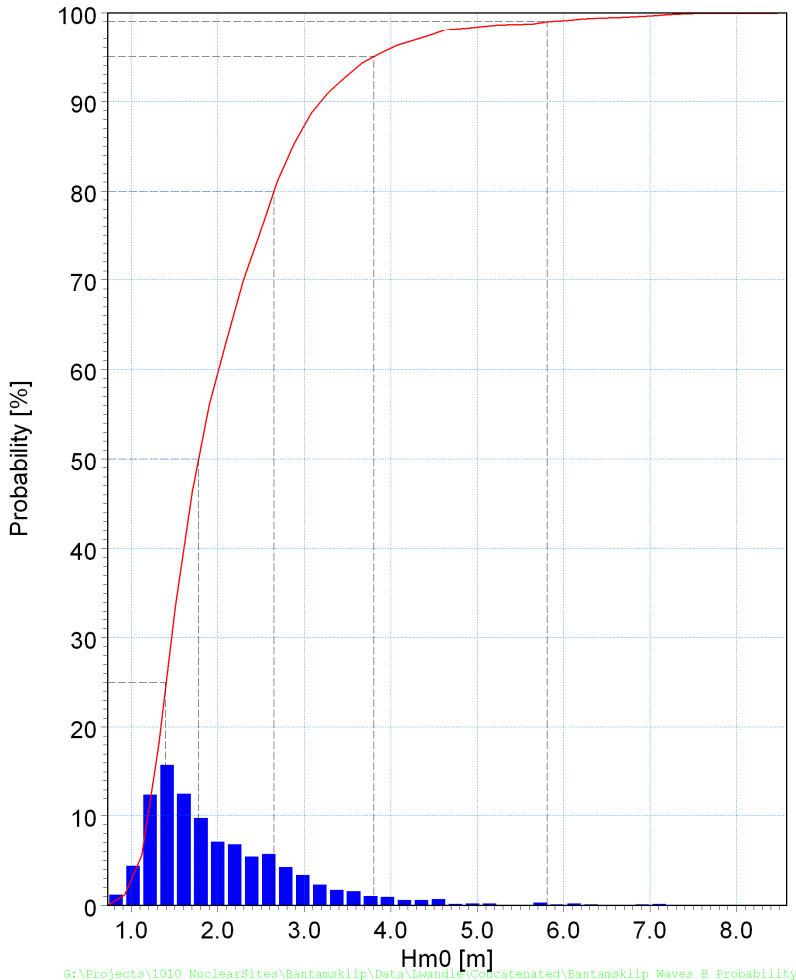

G:\Projects\1010_NuclearSites\Bantamsklip\Data\Lwandle\Concatenated\Bantamsklip_Waves_B_Probability.png

Title:

Wave measurements at Bantamsklip Site B (refer to Figure 3.1 for instrument position). Wave rose and histogram of wave heights.

Figure No.

6.4

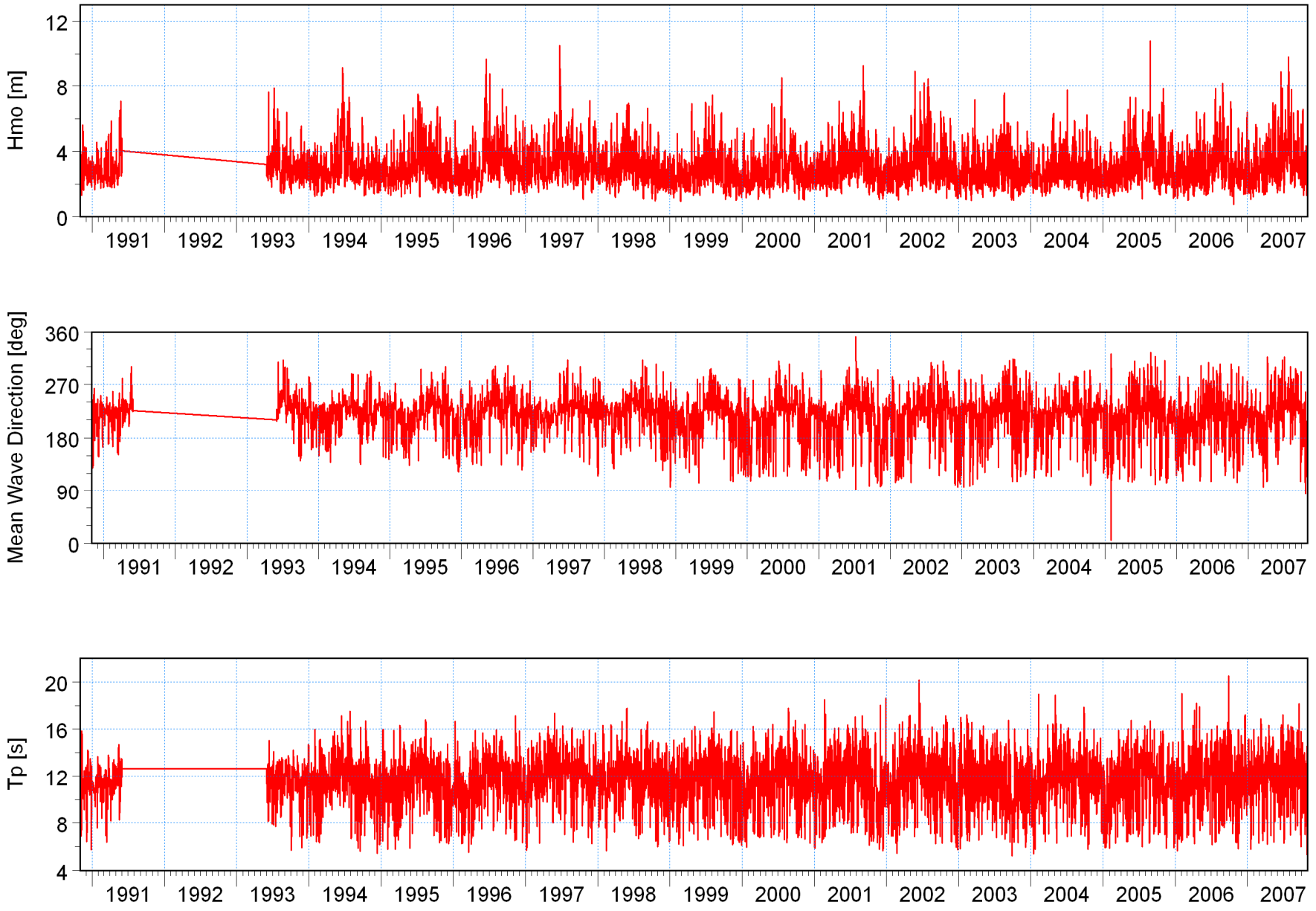

G:\Projects\1010_NuclearSites\Bantamsklip\Data\Waves\Processed\Wave_Parameters_Oceanor_e190_s350_Timeseries.png

Title: **Time-series of offshore wave hindcast parameters. Position is 60 km south-west of Bantamsklip in 180 m depth at position E 19.0°, S 35.0° (refer to Figure 6.7).**

Figure No. **6.5**

Wave Rose

G:\Projects\1010_NuclearSites\Bantamsklip\Data\Waves\Processed\Wave_Rose_e190_s350.png

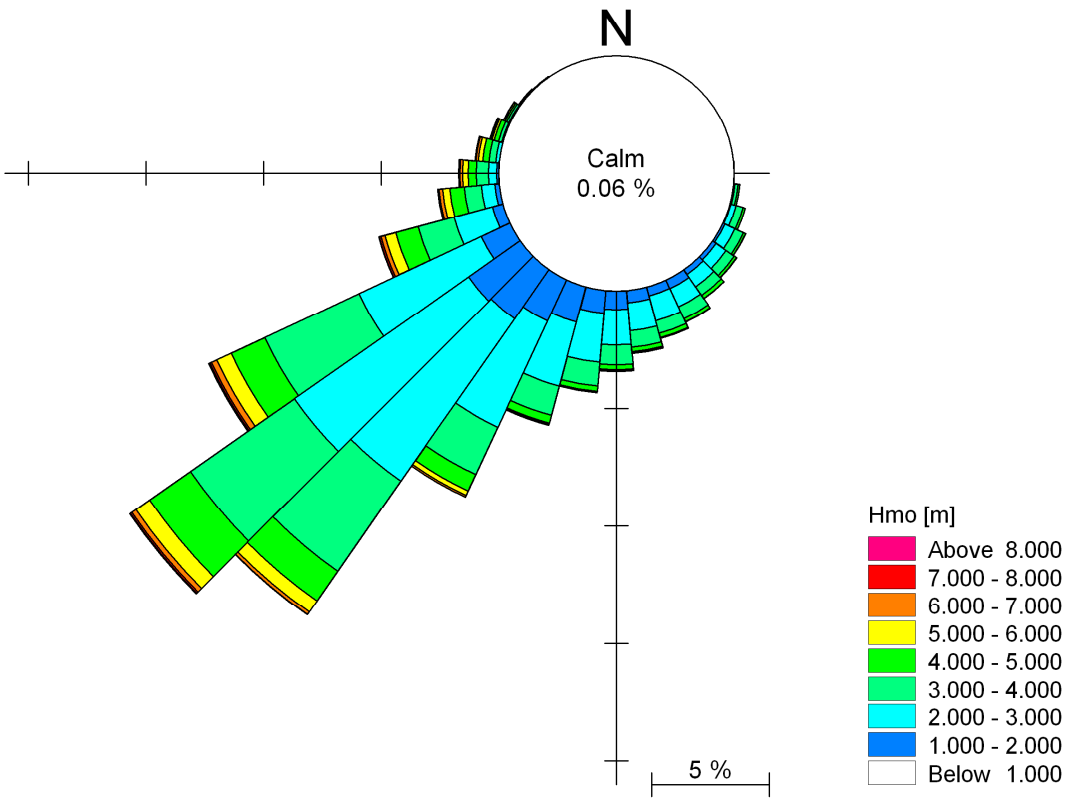

Wave Height Histogram

000.0%: 0.76000
025.0%: 2.27000
050.0%: 2.83000
075.0%: 3.57000
100.0%: 10.80000

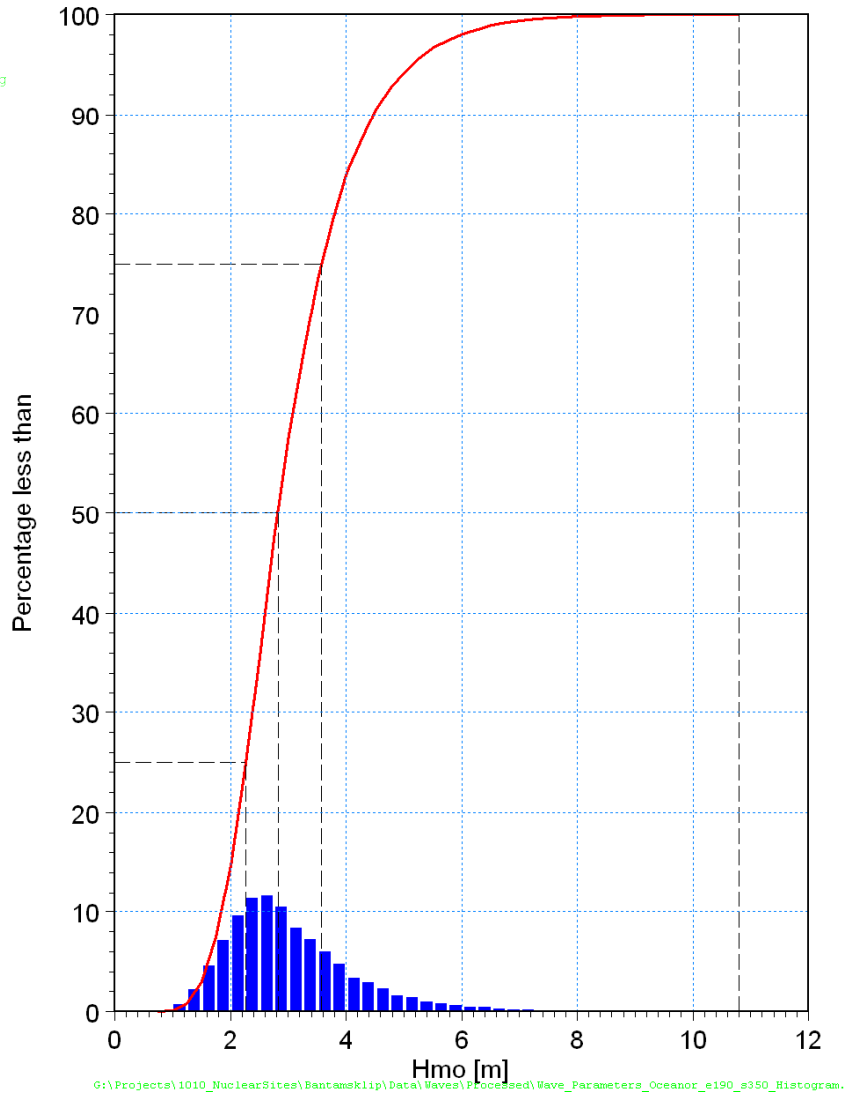

G:\Projects\1010_NuclearSites\Bantamsklip\Data\Waves\Processed\Wave_Parameters_Oceanor_e190_s350_Histogram.

Title: **Rose and histogram of offshore wave hindcast data. Position is 60 km south-west of Bantamsklip in 180 m depth at position E 19.0°, S 35.0° (refer to Figure 6.7).**

Figure No. **6.6**

G:\Projects\1010_NuclearSites\Bantamsklip\Models\Waves\c\SW_Mesh.png

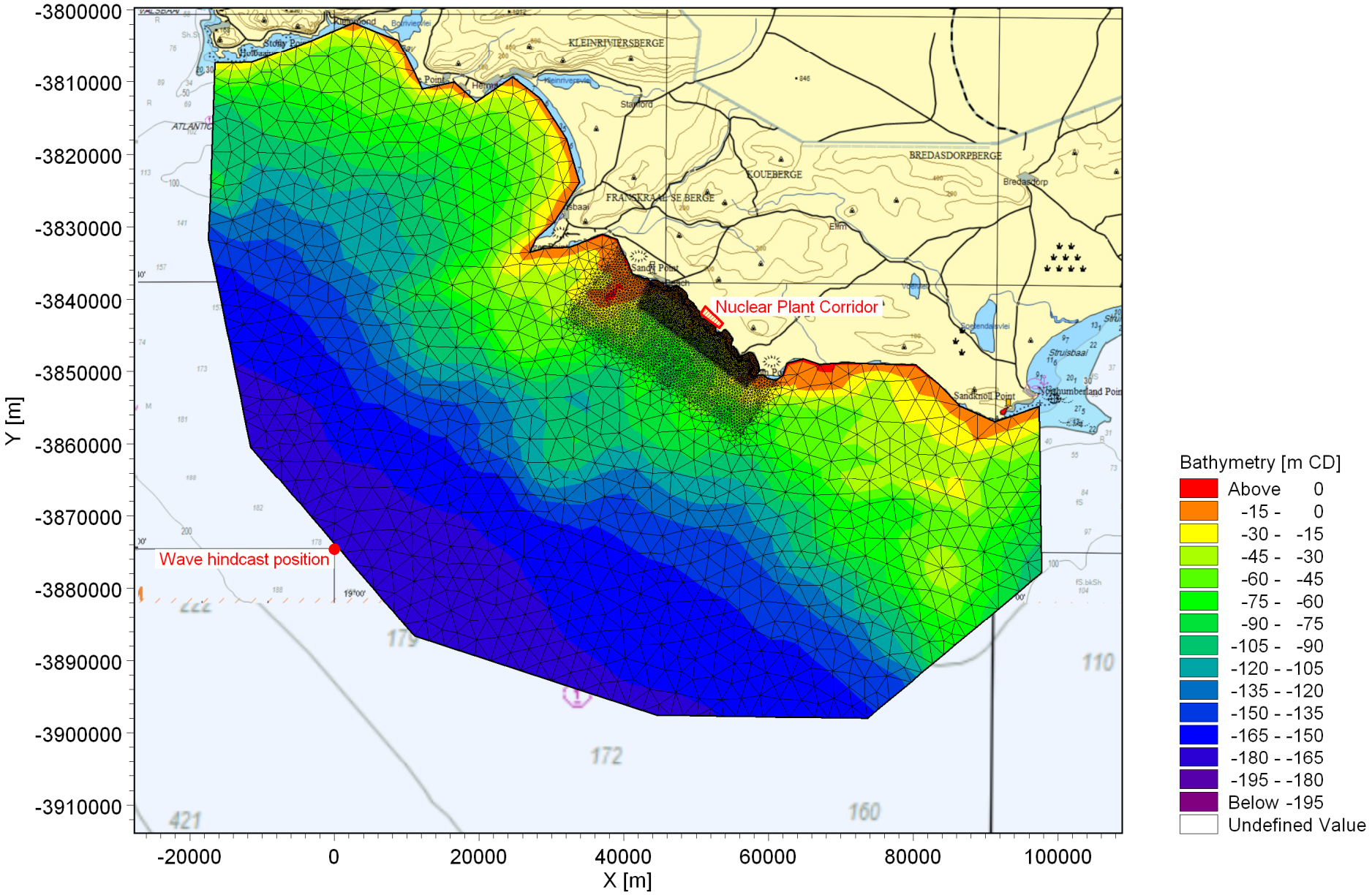

Title:

Numerical mesh used for wave refraction modelling.

Figure No.

6.7

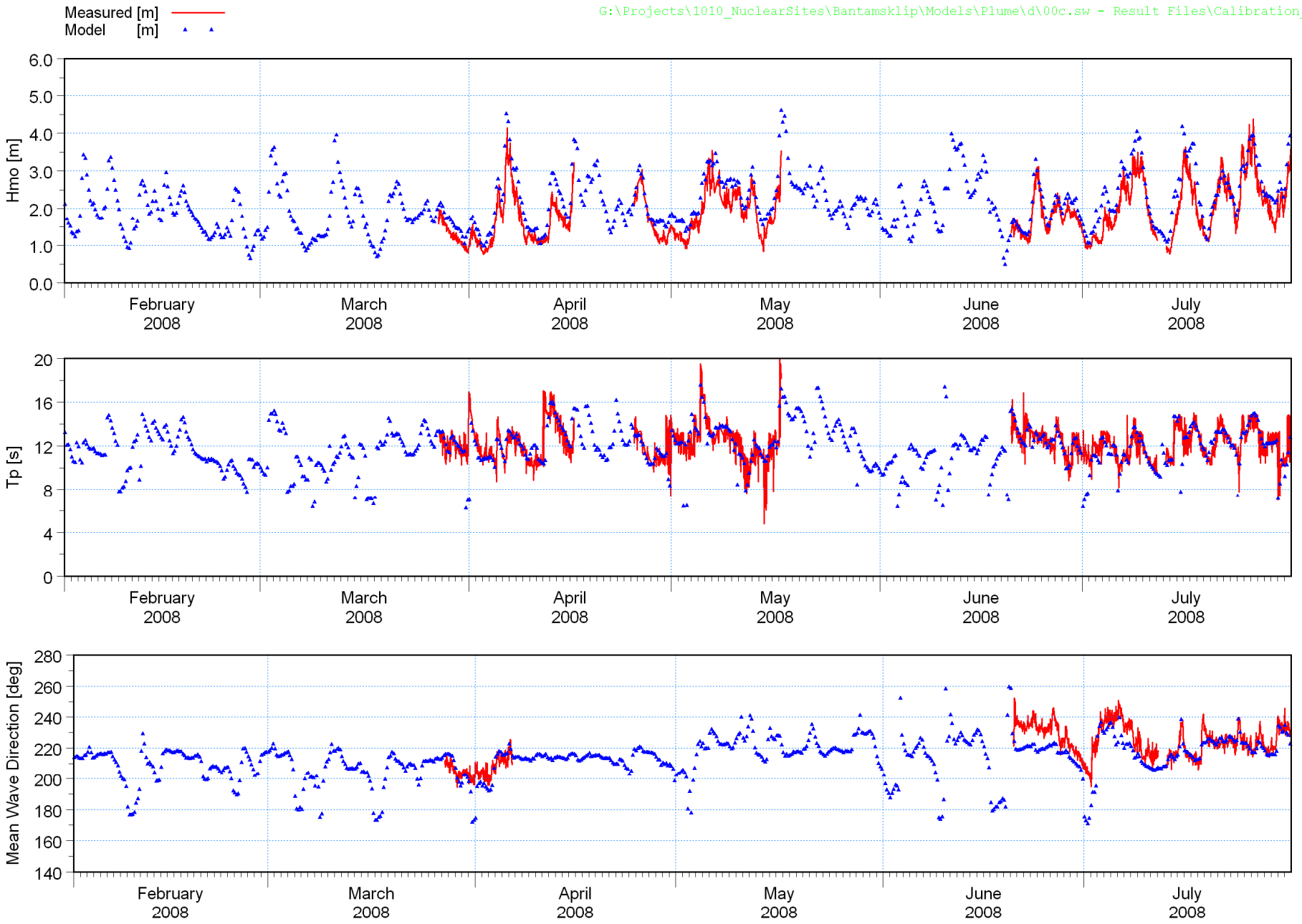

Title:

Calibration of wave model.
Measured and modelled time-series of wave parameters at Site A (refer to Figure 3.1 for location).

Figure No.
6.8

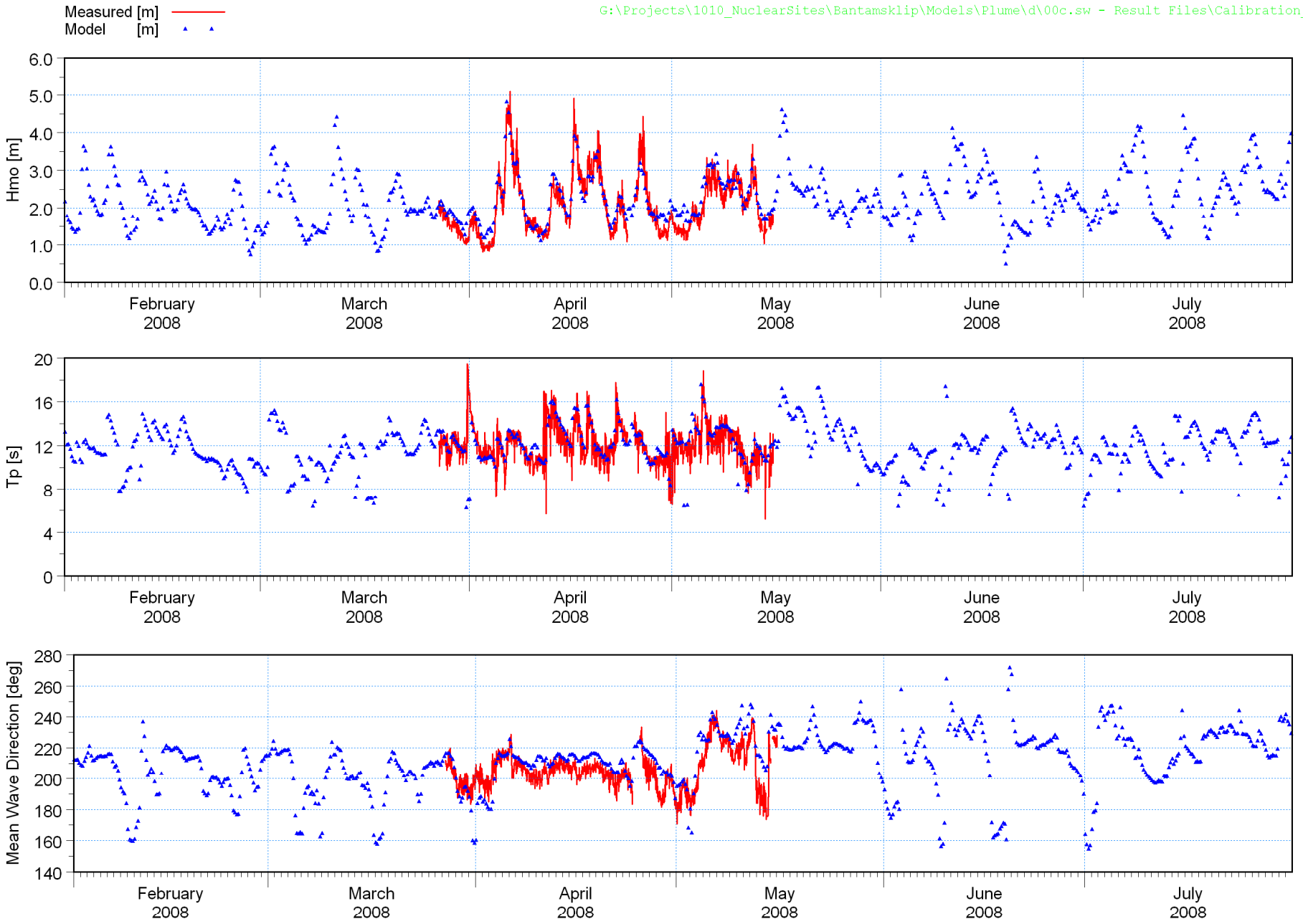

Title:

Calibration of wave model.
Measured and modelled time-series of wave parameters at Site B (refer to Figure 3.1 for location).

Figure No.
6.9

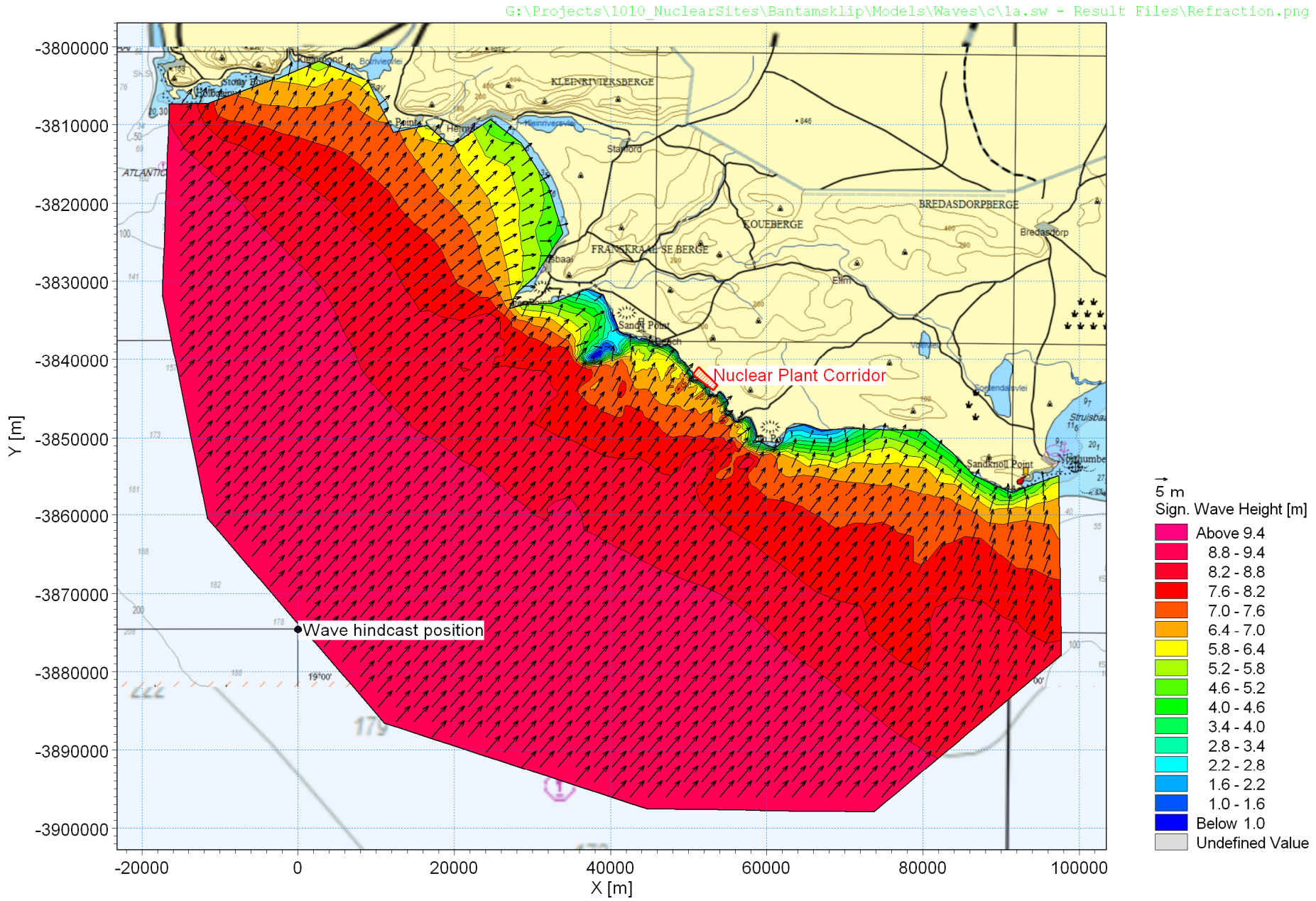

Time Step 1733 of 2108.

Title:

Example of wave refraction from offshore to Bantamsklip site.
Deepwater wave condition: H_{m0} = 9.2 m, T_p = 16.4 s, Mean direction = 221°.

Figure No.

6.10

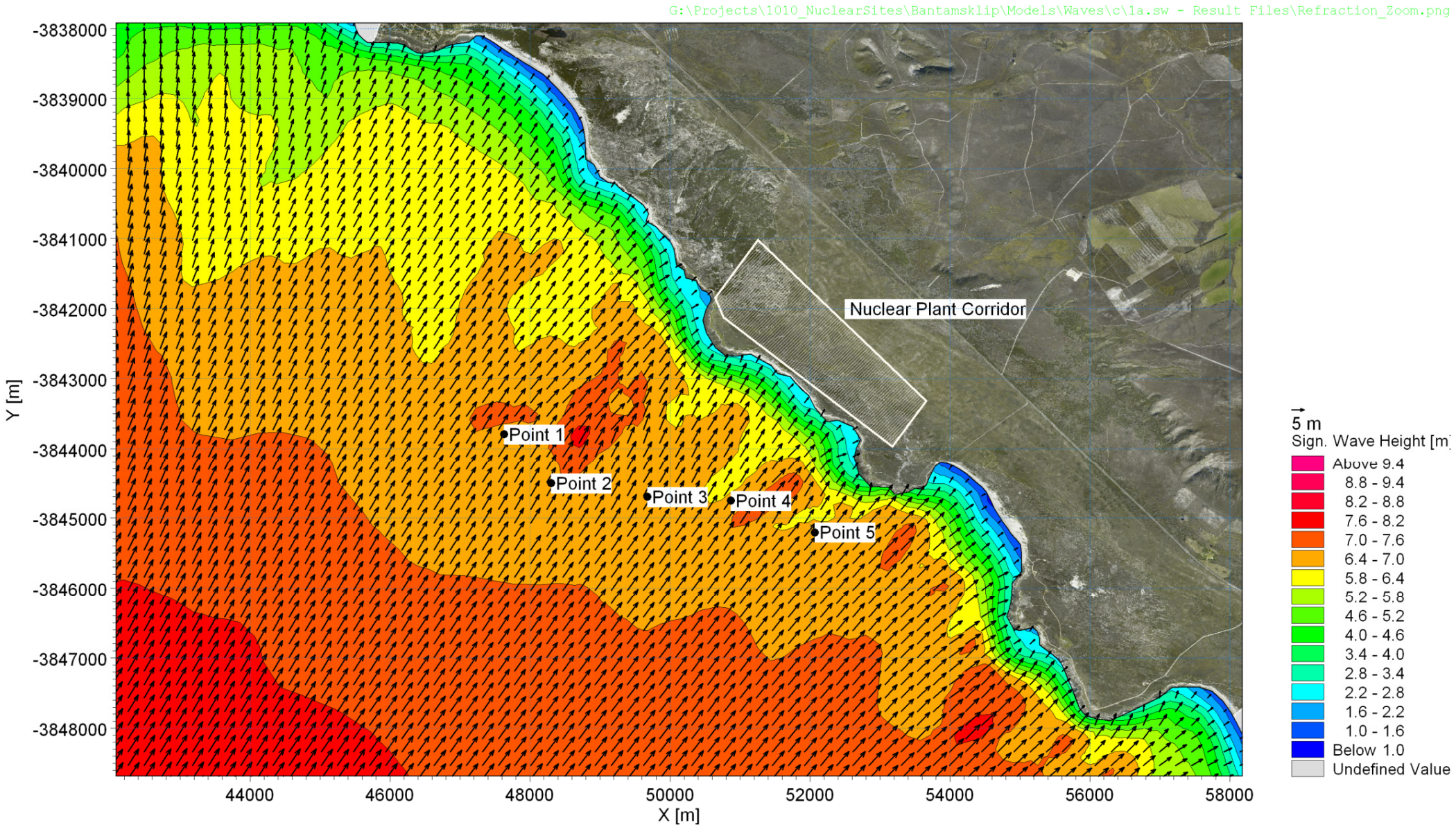

Title: **Example of wave refraction from offshore to Bantamsklip site. Deepwater wave condition: H_{m0} = 9.2 m, T_p = 16.4 s, Mean direction = 221°. Model output points along -30 m CD contour are indicated.**

Figure No. **6.11**

Wave Rose

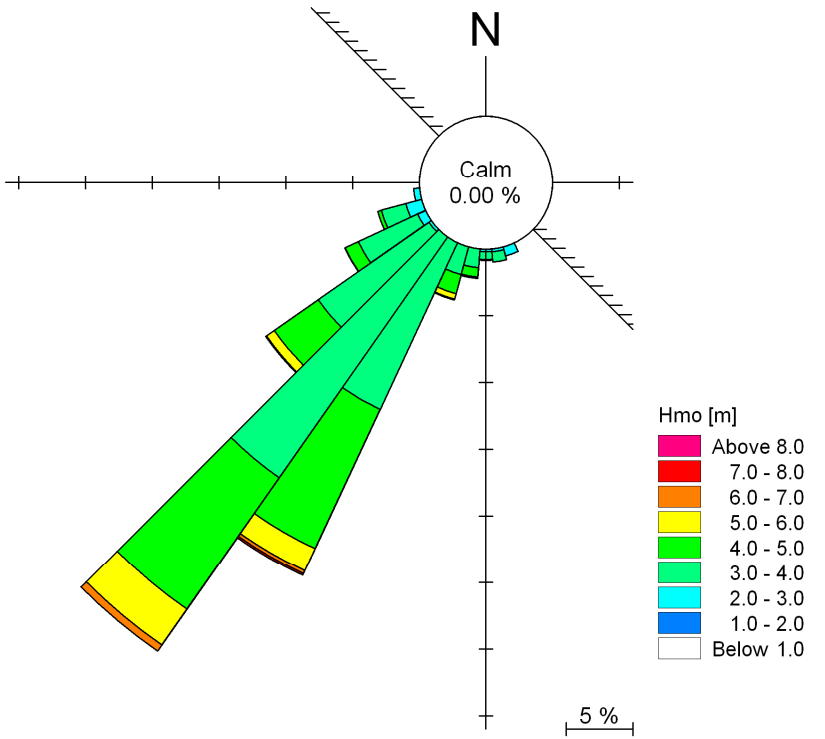

G:\Projects\1010_NuclearSites\Bantamsklip\Models\Waves\c\la.sw - Result Files\Parameters_Point_Post_Point1_Rose.png

Wave Height – Period Relationship

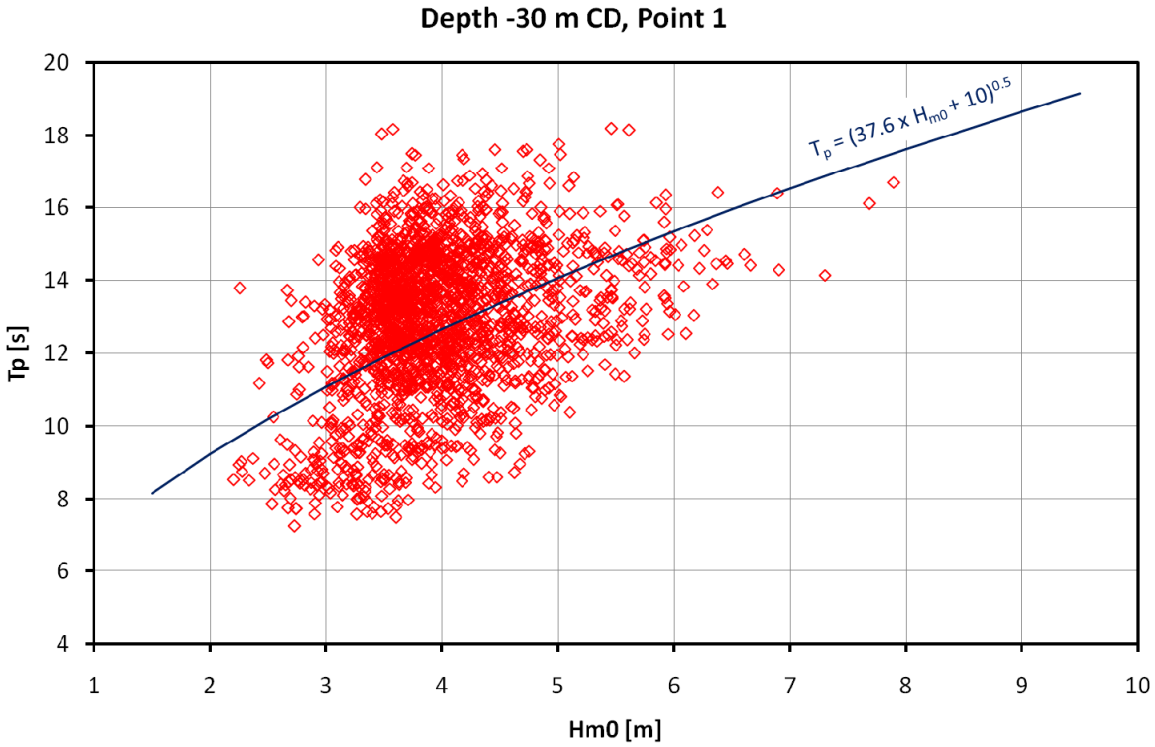

Title:

Characterisation of storm waves refracted to -30 m CD depth contour at Bantamsklip site. Position is Point 1 (see Fig 6.11). Includes only storms where the offshore H_{m0} > 4.5 m.

Figure No.

6.12

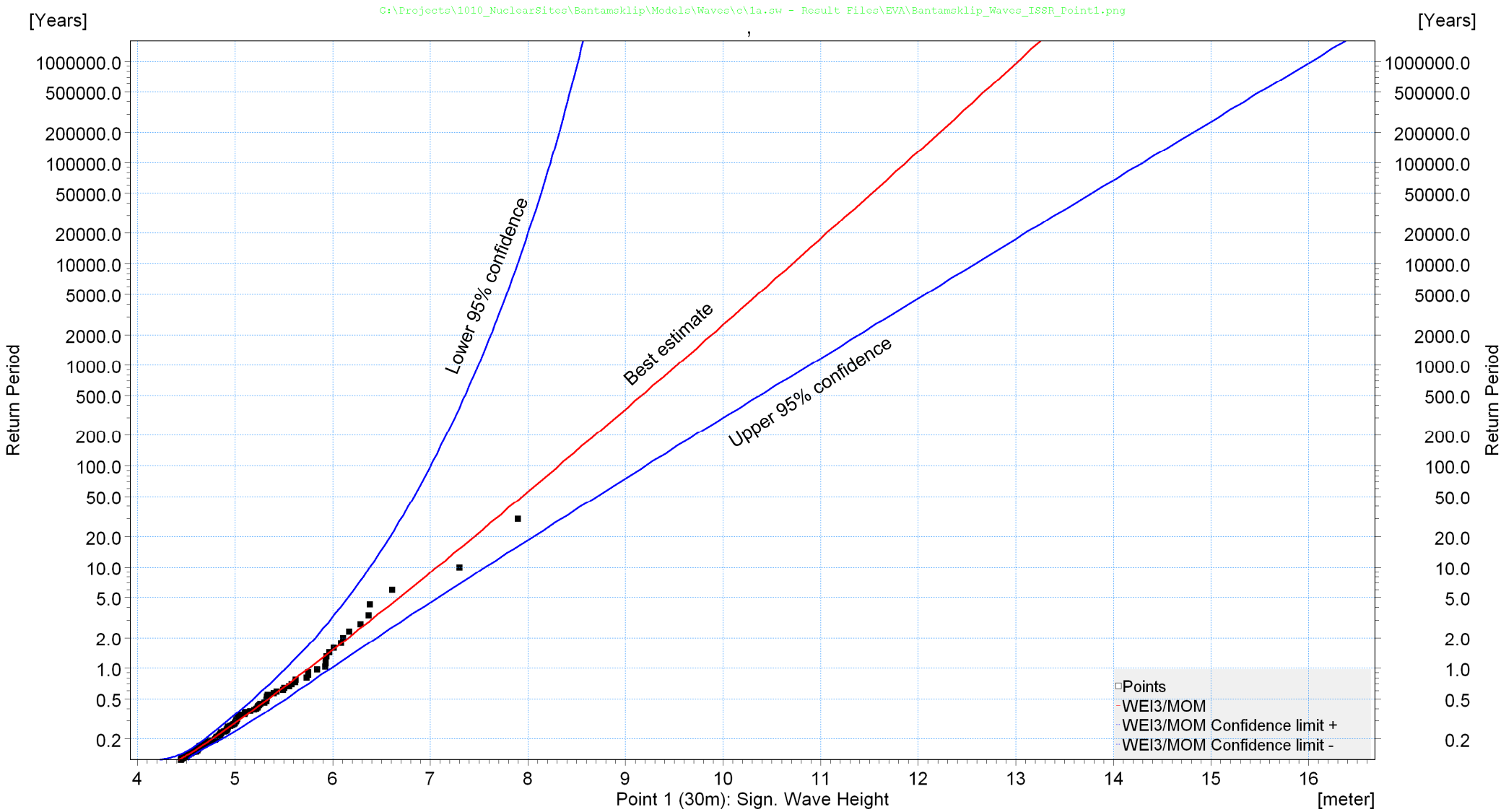

Title:

Extreme value analysis of waves at -30 m CD depth at Bantamsklip. Position is Point 1 (see Fig 6.11).

Figure No.

6.13

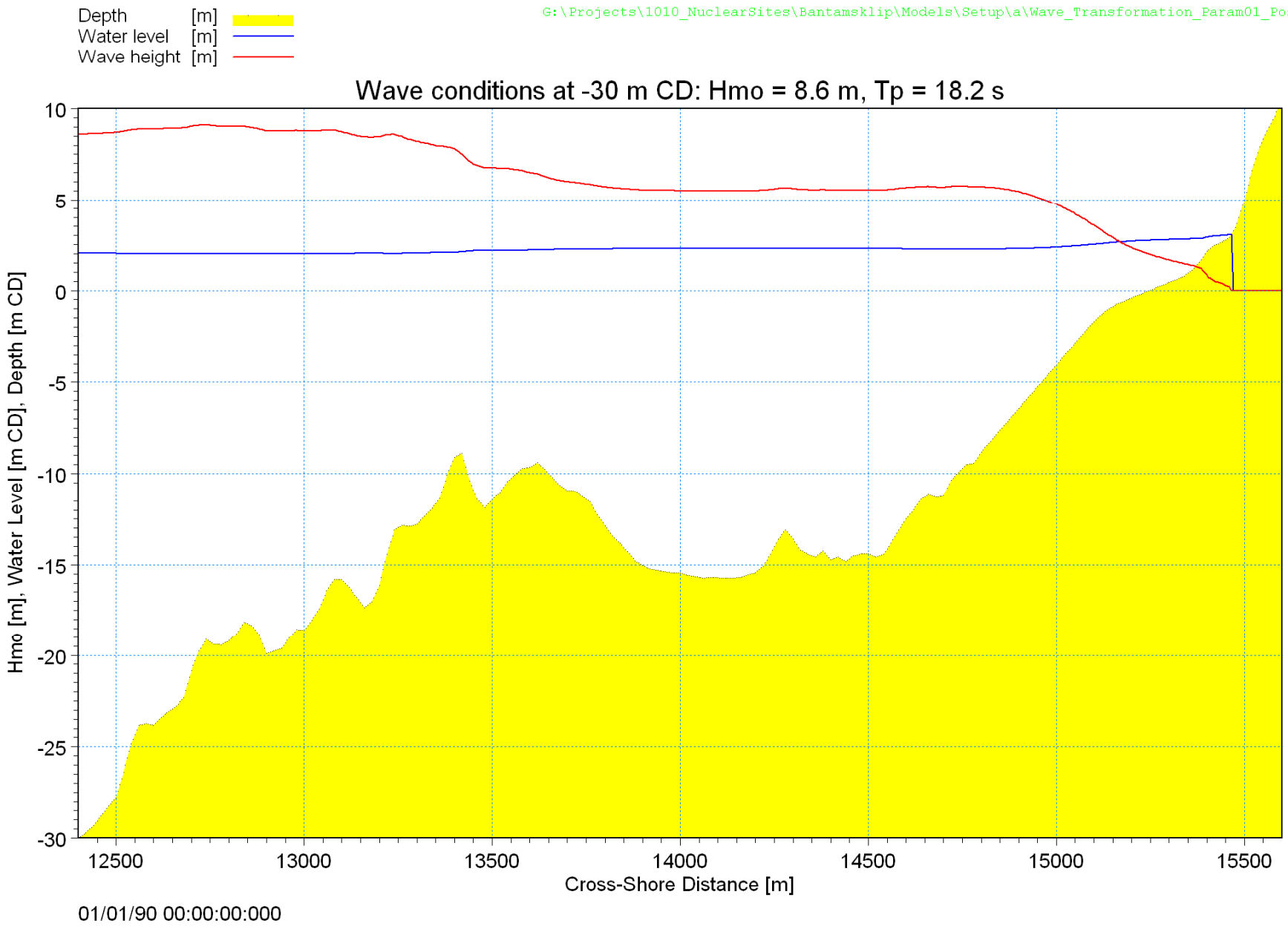

Title:

Example of cross-shore wave transformation modelling from -30 m CD depth to shoreline.

Figure No.

6.14

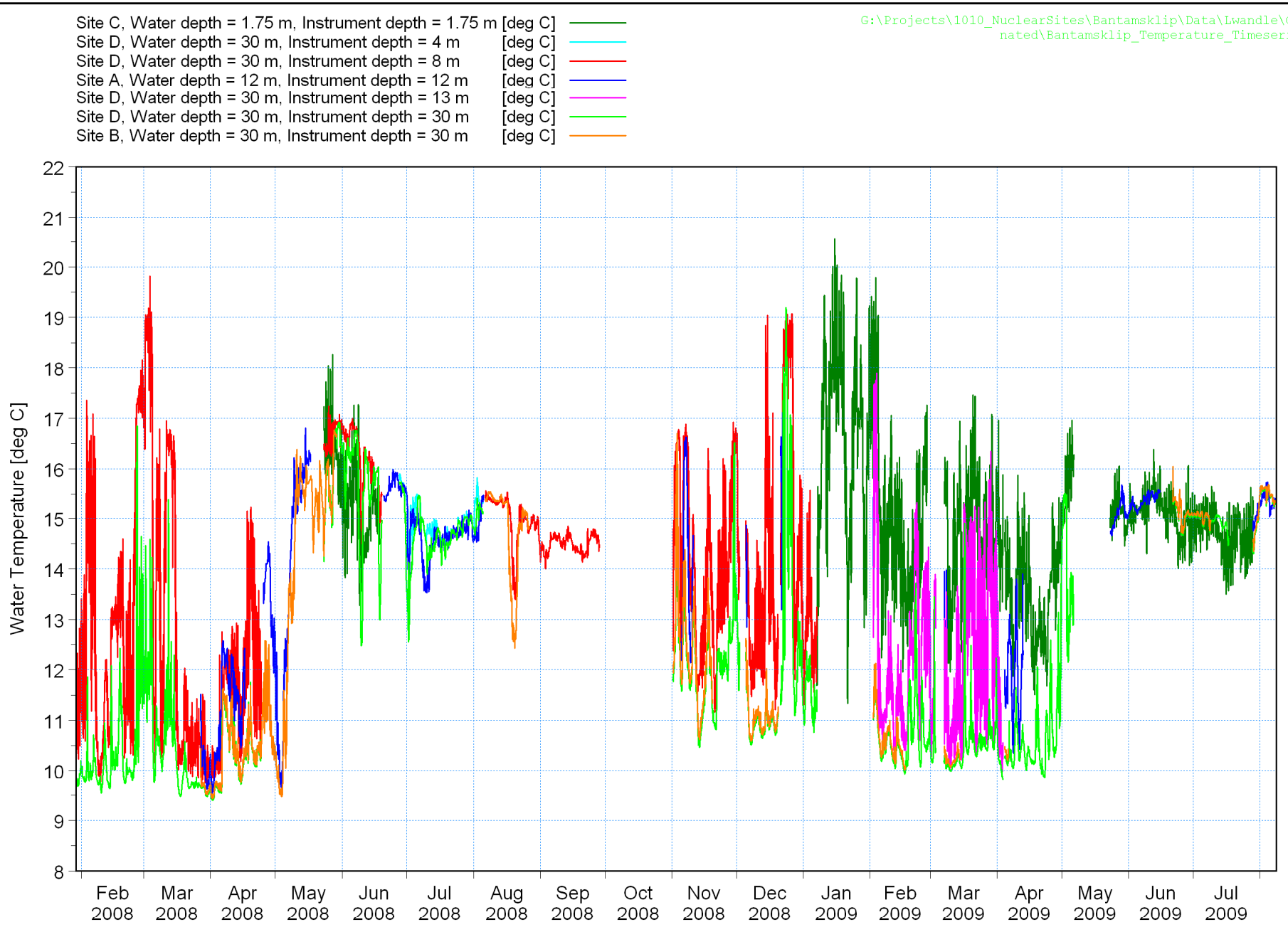

Title:

Seawater temperatures measured at Bantamsklip for SSR.
(Refer to Figure 3.1 for instrument positions).

Figure No.

7.1

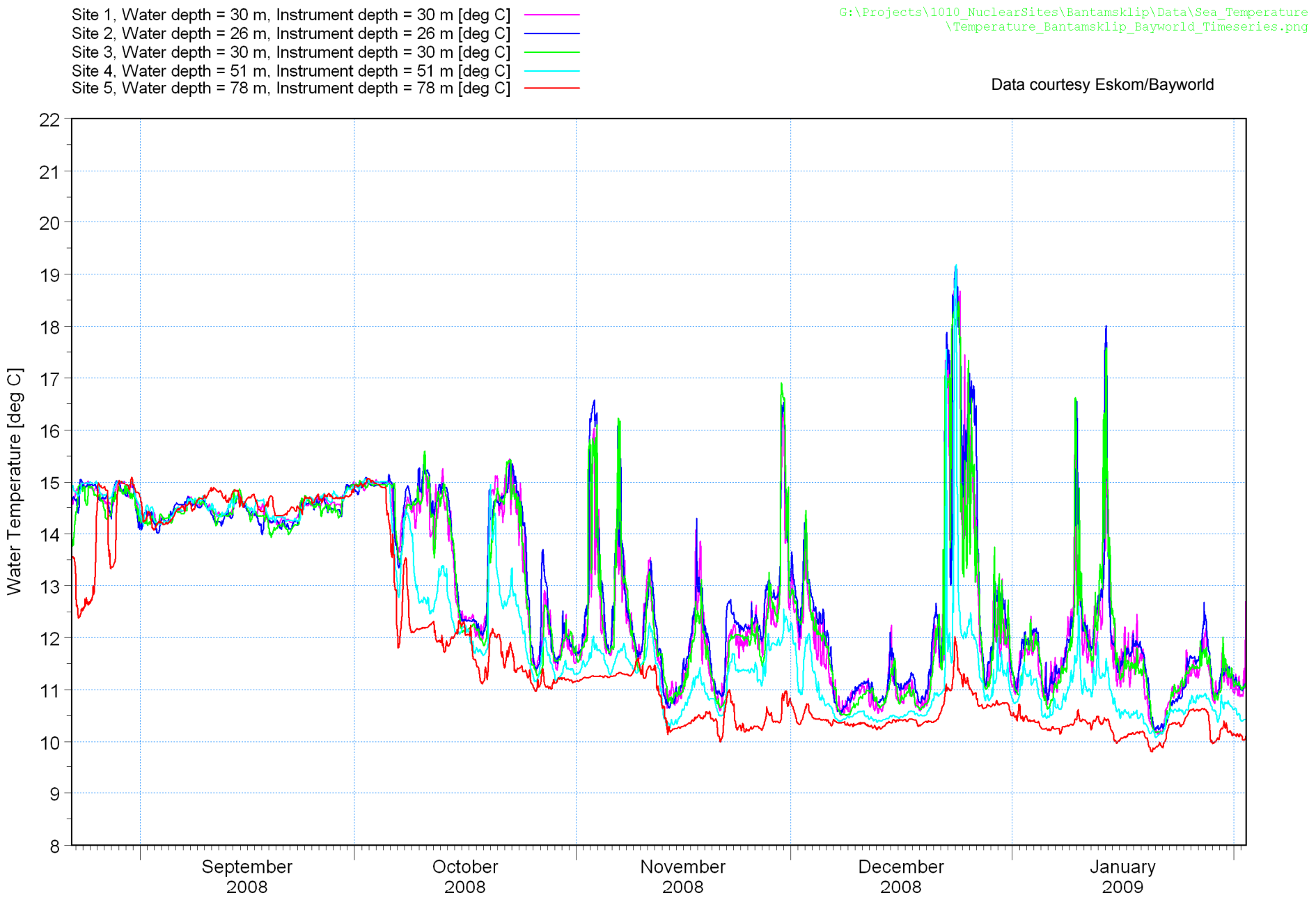

Title:

Seawater temperatures measured at Bantamsklip by Bayworld (2008, 2009).
(Refer to Figure 3.1 for instrument positions).

Figure No.

7.2

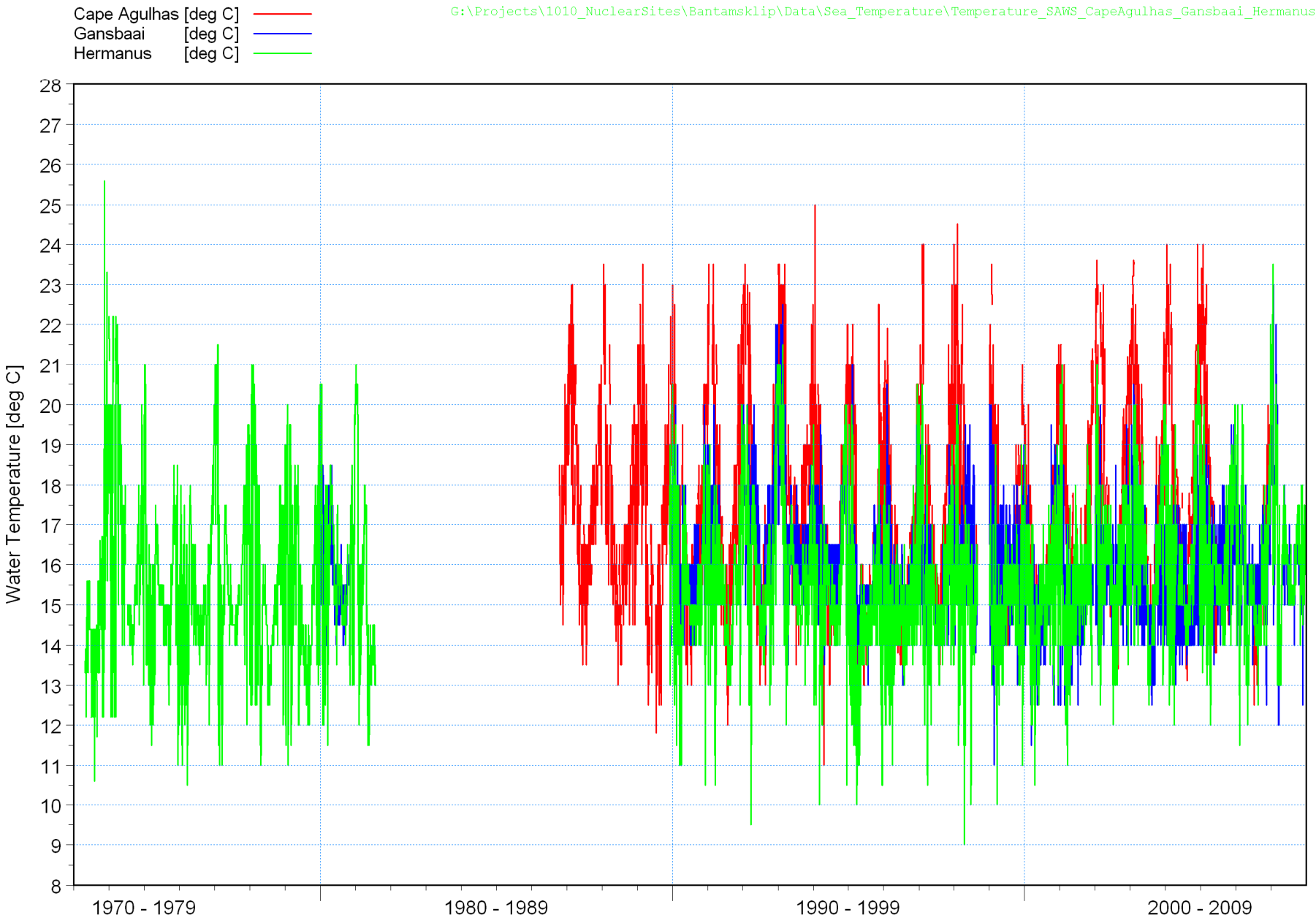

Title:

Seawater temperatures measured in surf-zone at Cape Agulhas, Gansbaai and Hermanus (refer to Figure 1.1 for locations).

Figure No.

7.3

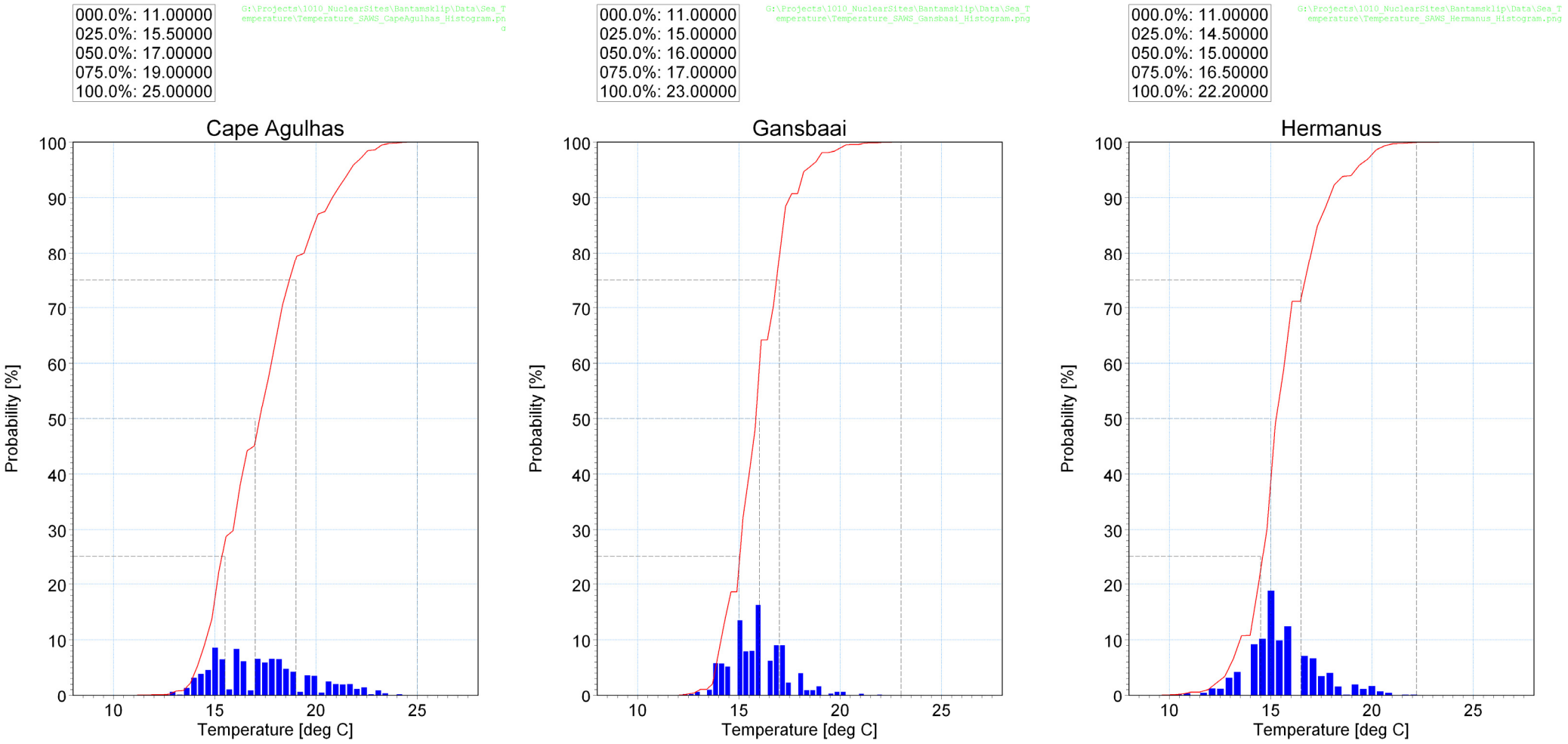

Title:

Histograms of measured seawater temperatures in surf-zone at Cape Agulhas, Gansbaai and Hermanus (refer to Figure 1.1 for locations).

Figure No.

7.4

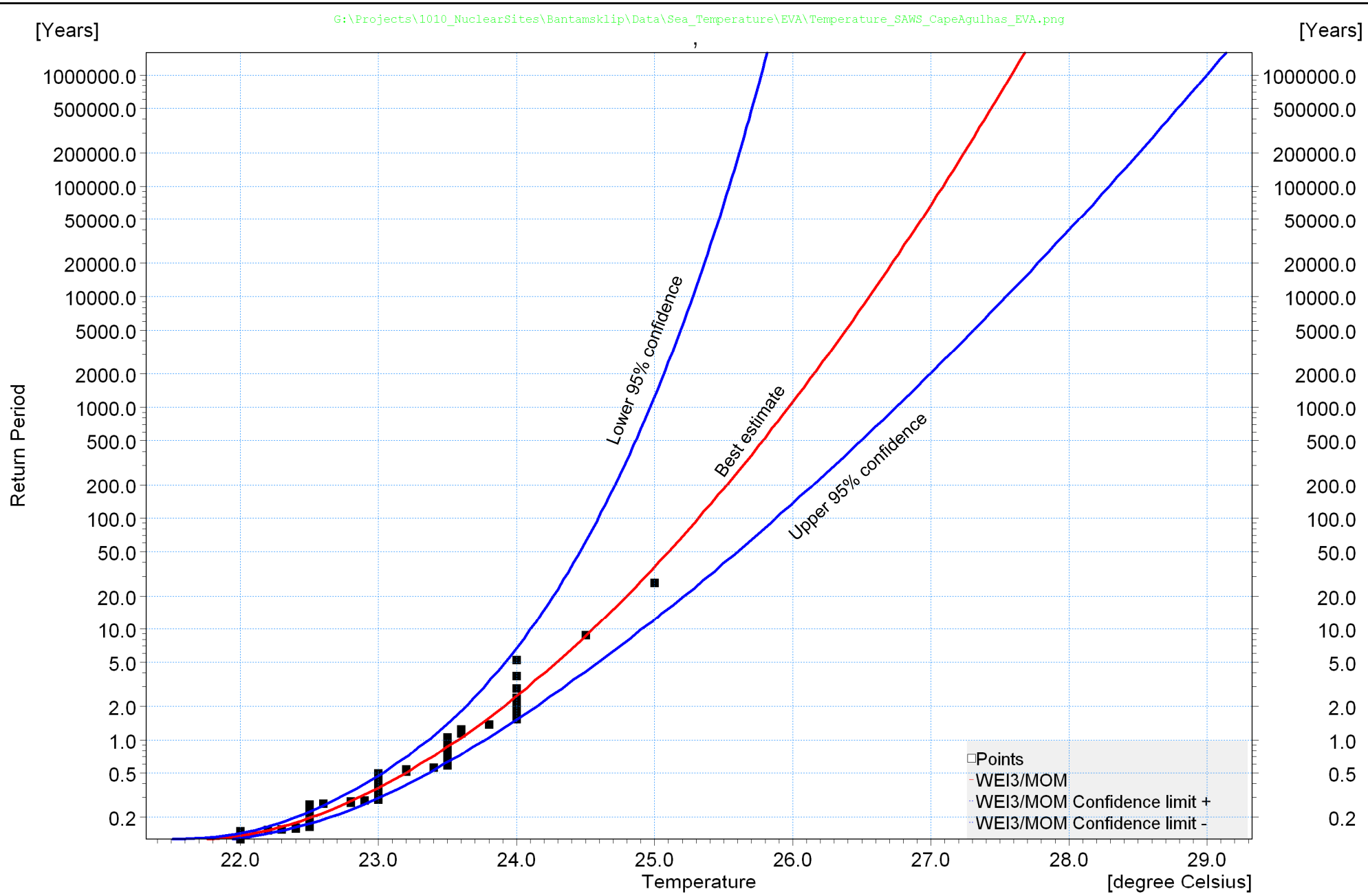

Title:

Extreme Value Analysis of measured seawater temperatures in surf-zone at Cape Agulhas.

Figure No.

7.5

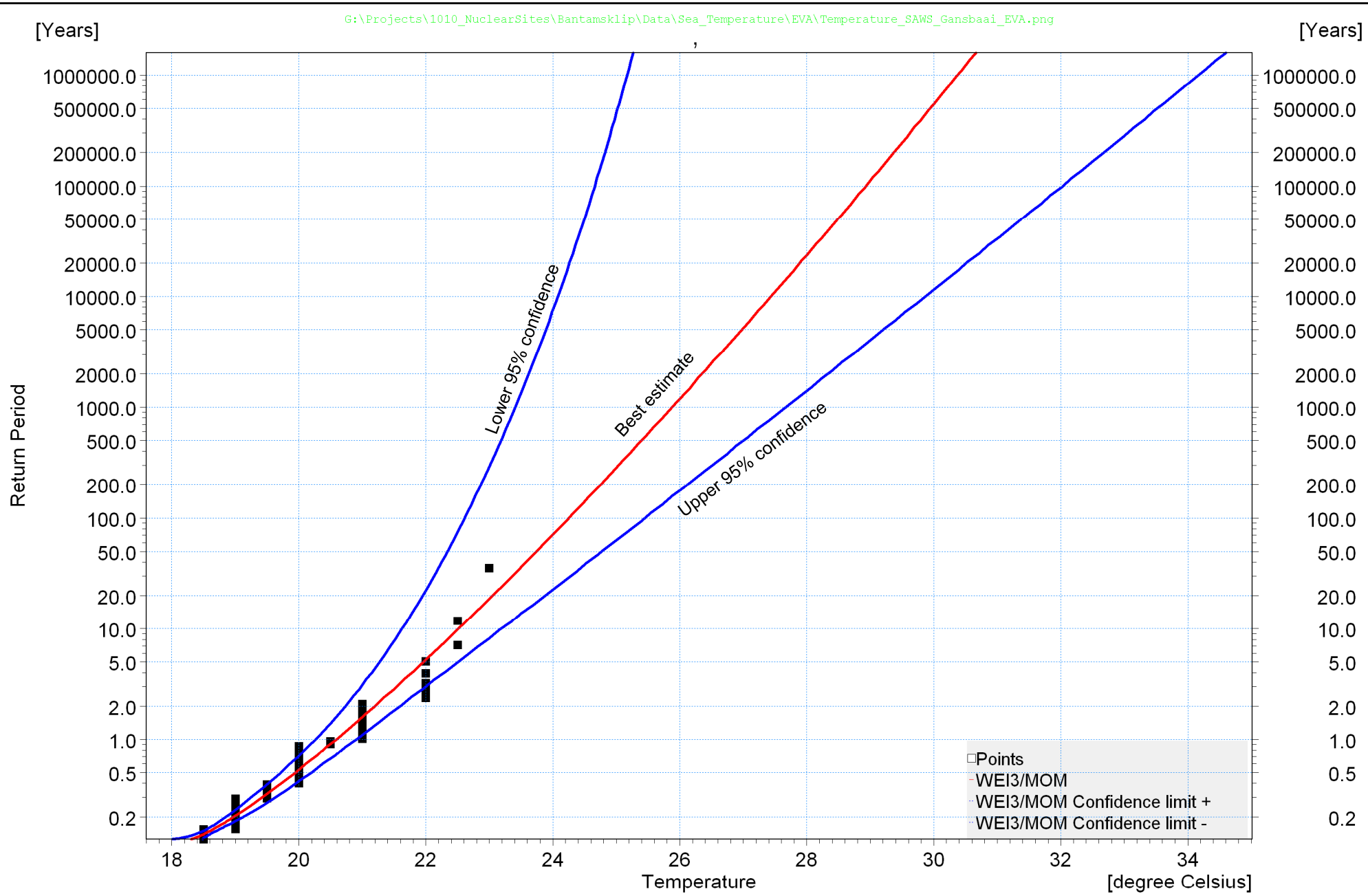

Title:

Extreme Value Analysis of measured seawater temperatures in surf-zone at Gansbaai.

Figure No.

7.6

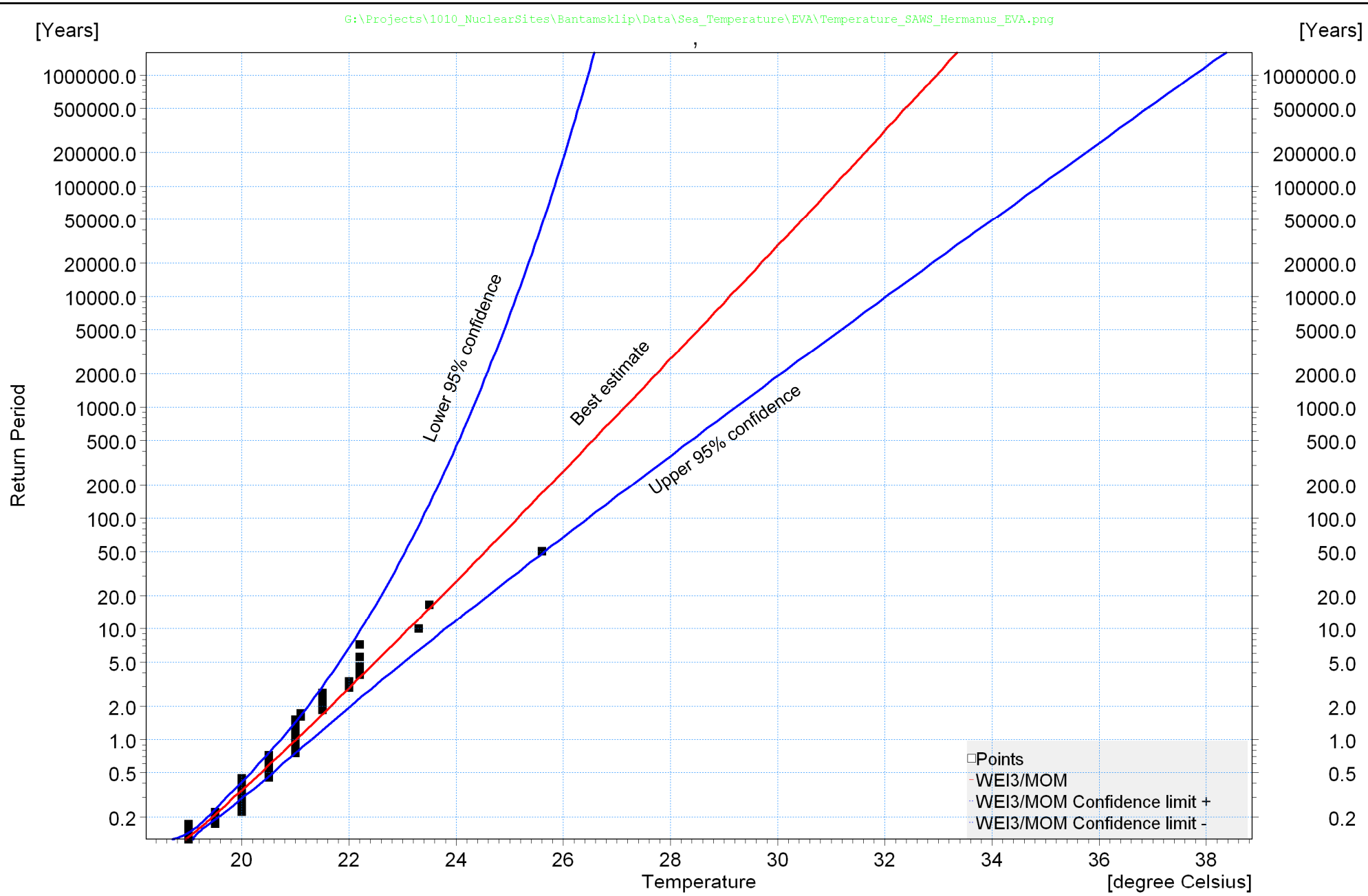

Title:

Extreme Value Analysis of measured seawater temperatures in surf-zone at Hermanus.

Figure No.

7.7

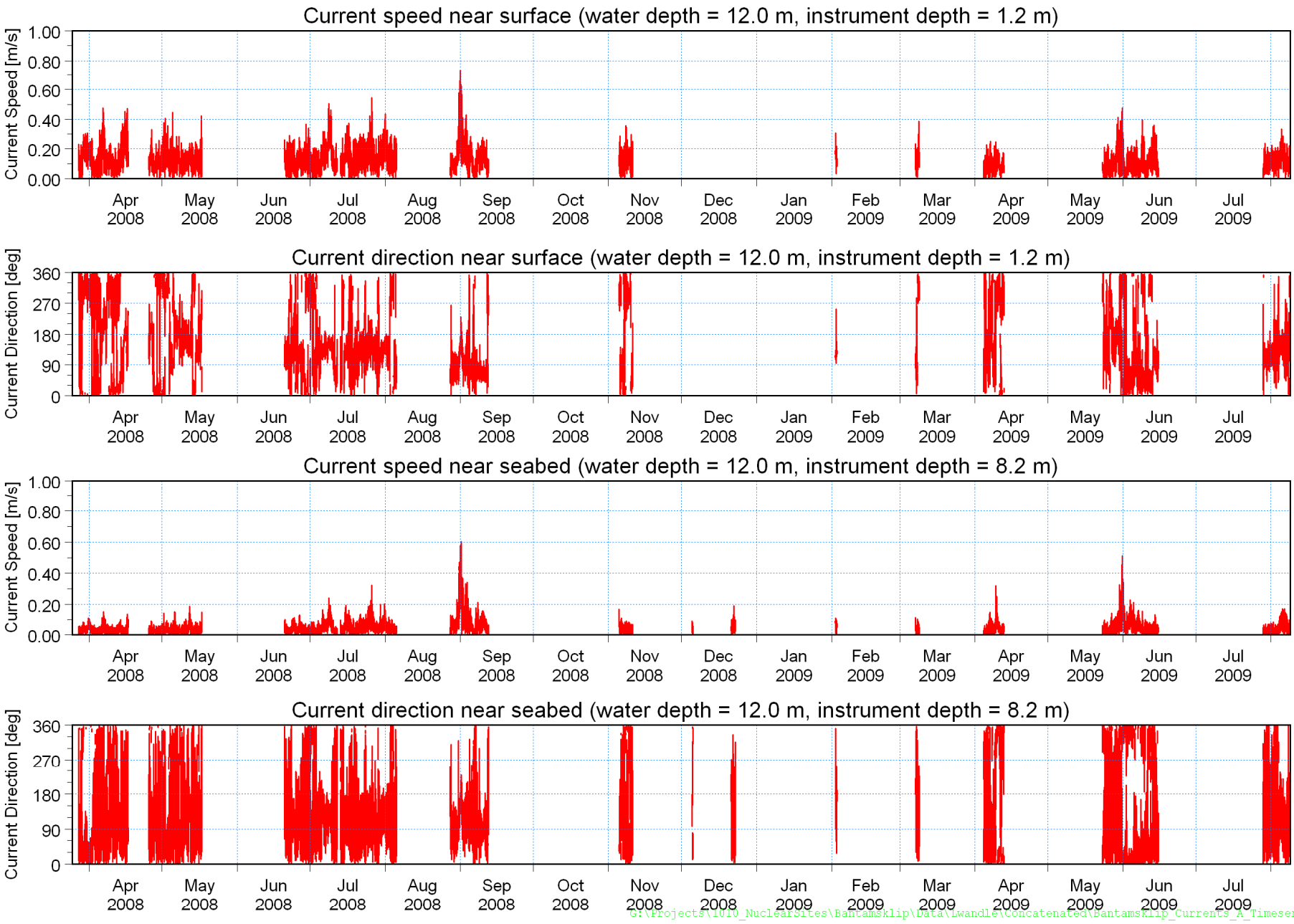

Title:

Current measurements at Site A (refer to Figure 3.1 for position).
Time-series of near surface and near bottom currents.

Figure No.

8.1

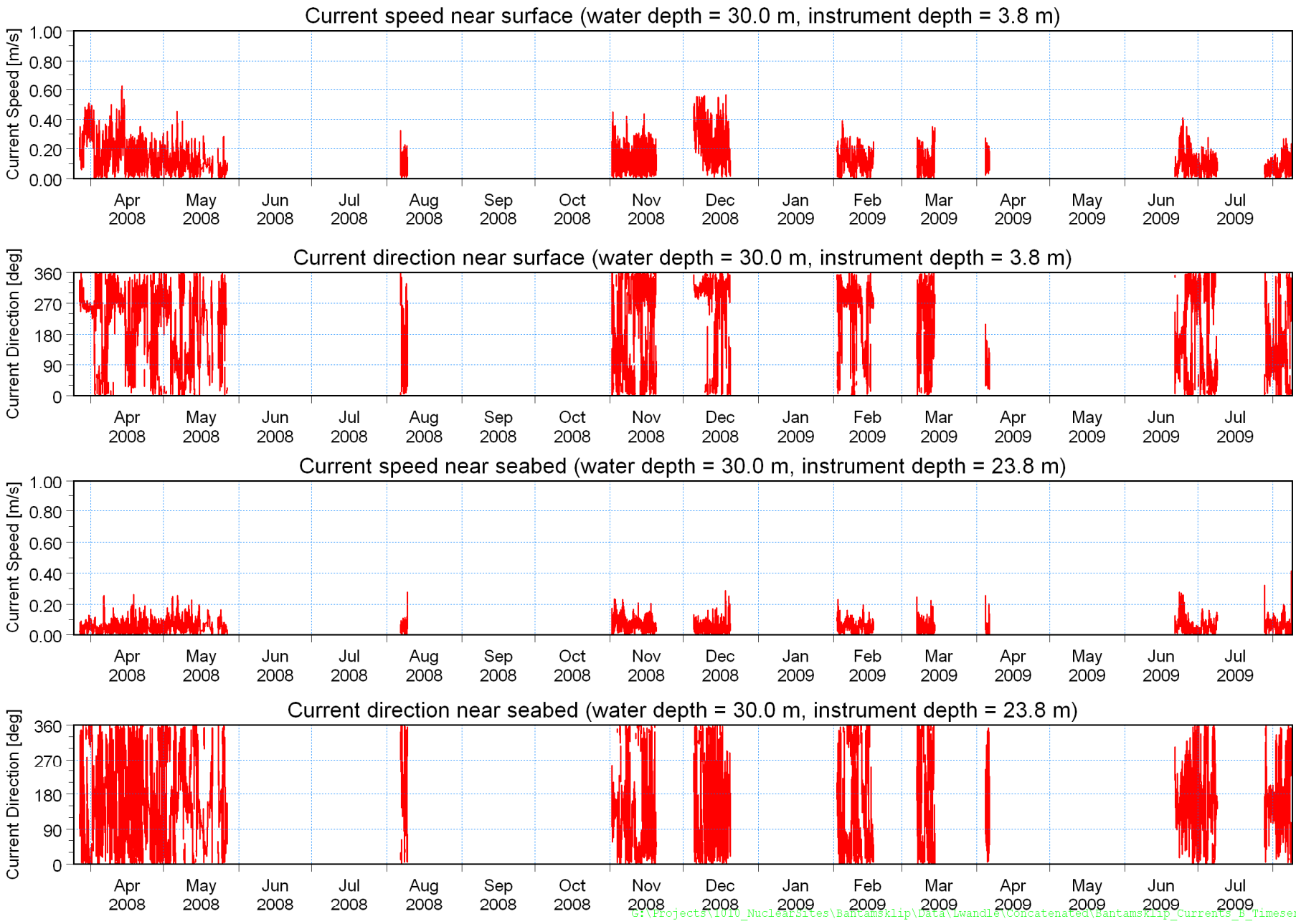

Title:

Current measurements at Site B (refer to Figure 3.1 for position).
Time-series of near surface and near bottom currents.

Figure No.

8.2

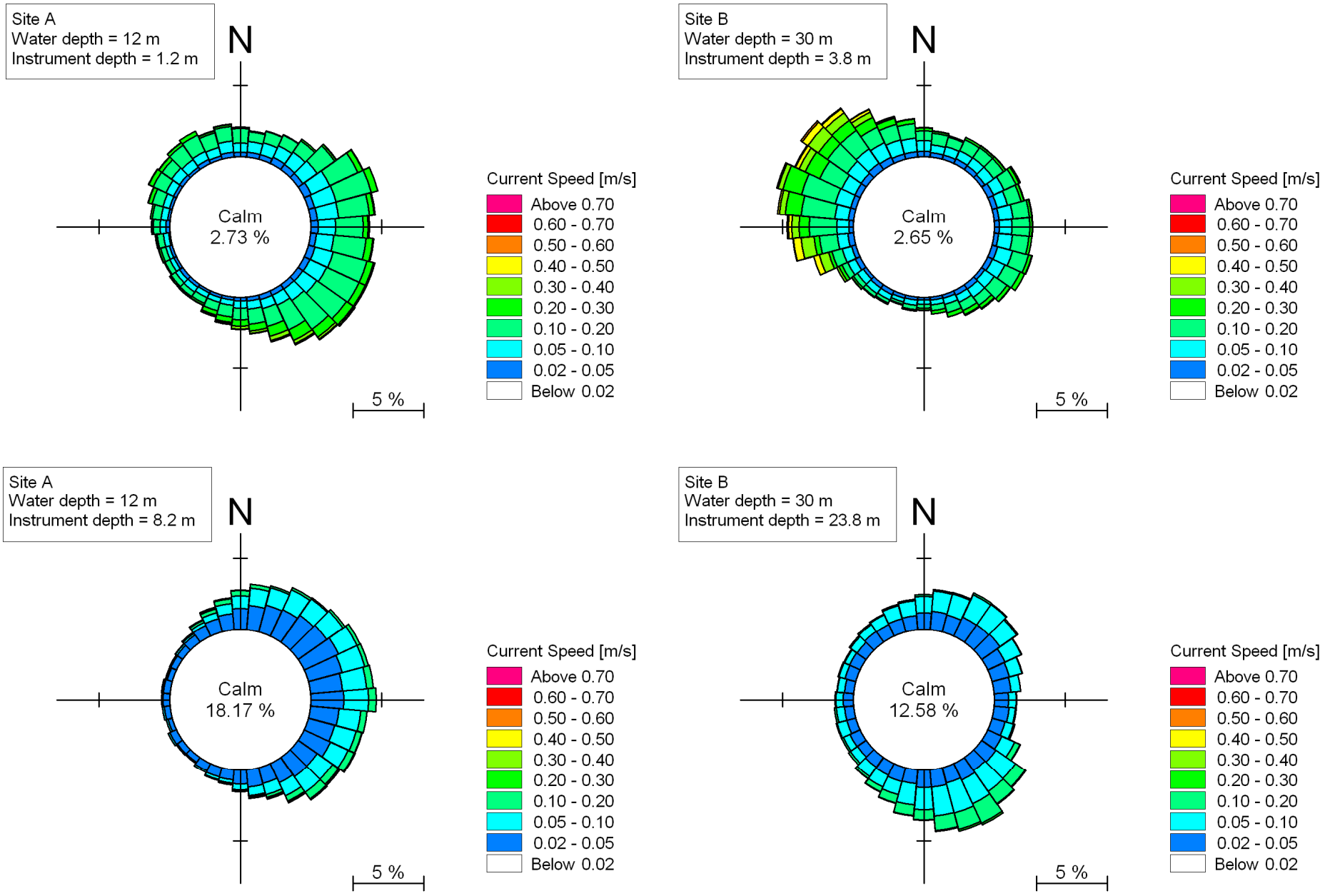

Title:

Current measurements at Sites A and B (refer to Figure 3.1 for locations). Near surface and near seabed current rose plots.

Figure No.

8.3

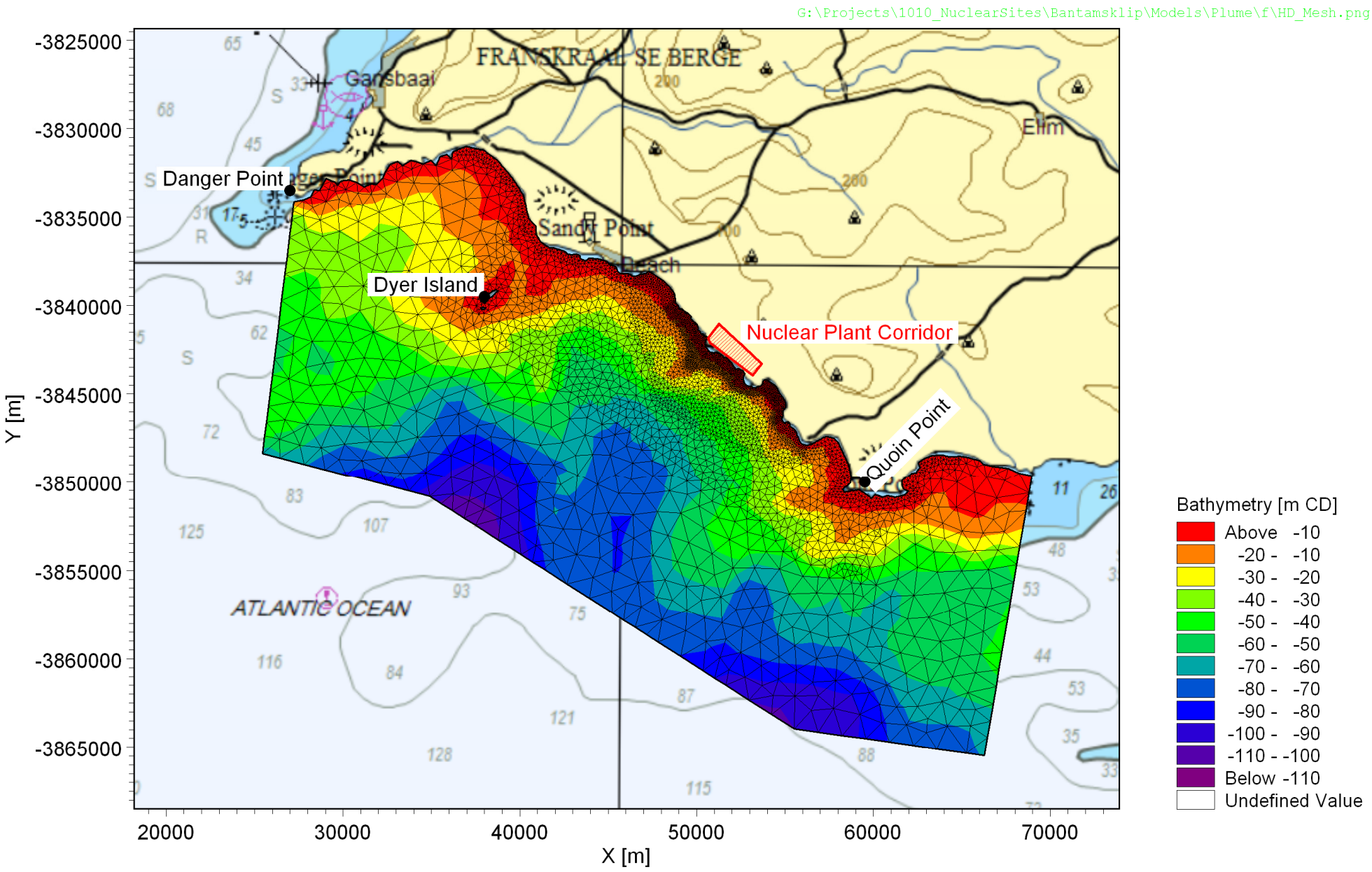

Title:

Numerical mesh and bathymetry used for hydrodynamic modelling.

Figure No.

8.4

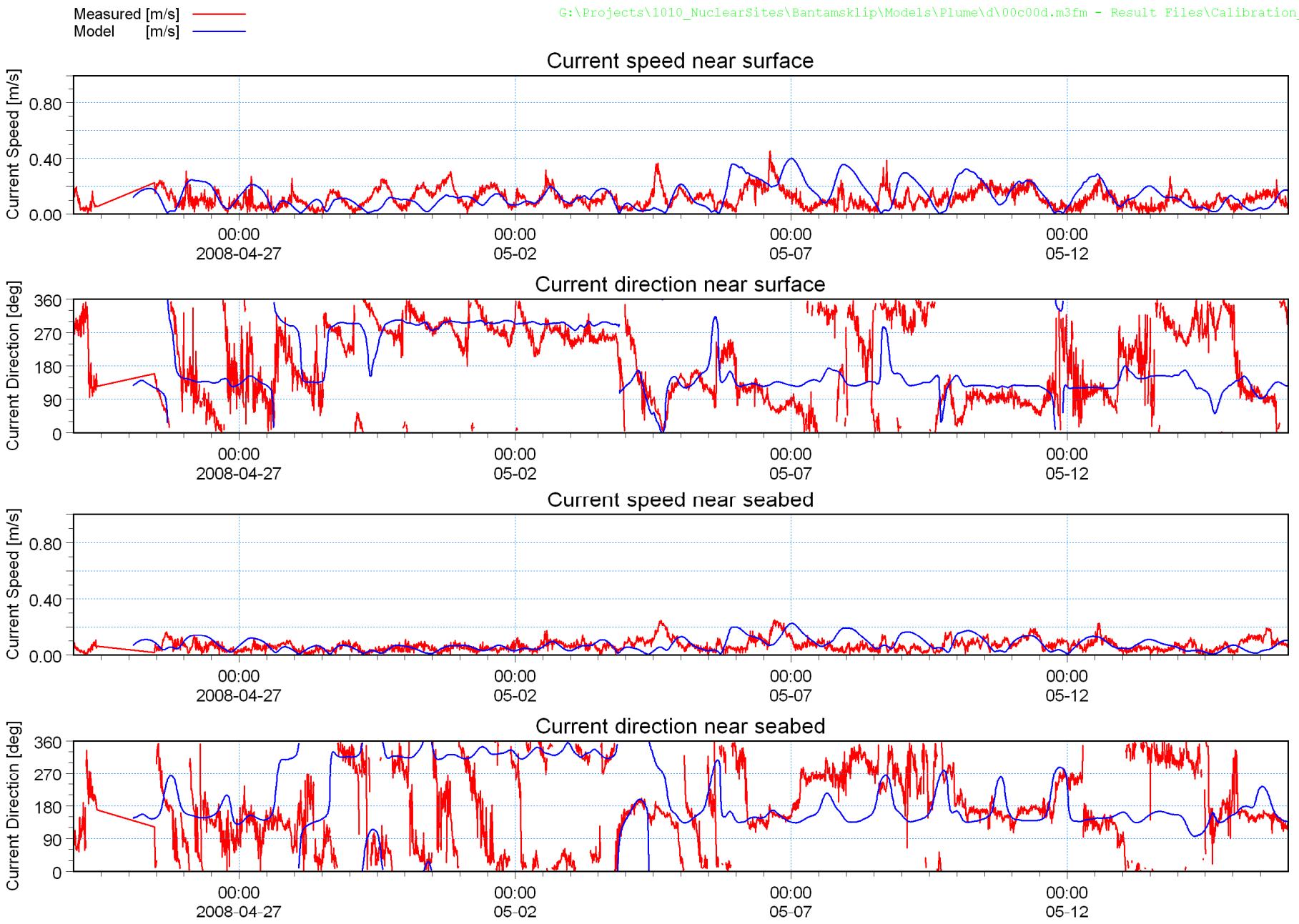

Title: **Calibration of hydrodynamic model: current speed and direction. Measured and modelled time-series of currents at Bantamsklip Site B for period April and May 2008. (refer to Figure 3.1 for location).**

Figure No.

8.5

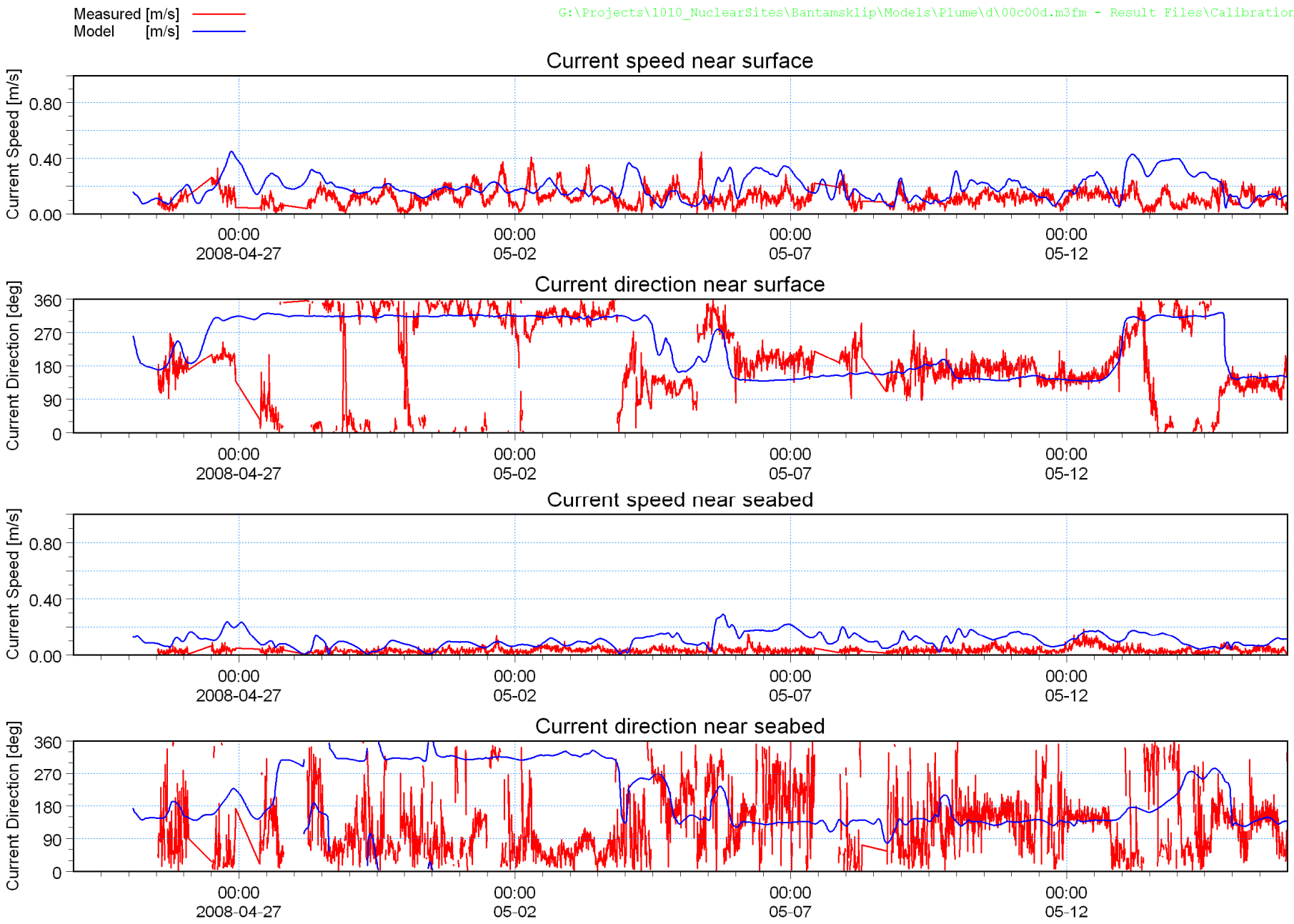

Title: **Calibration of hydrodynamic model: current speed and direction. Measured and modelled time-series of currents at Bantamsklip Site A for period April and May 2008. (refer to Figure 3.1 for location).**

Figure No. **8.6**

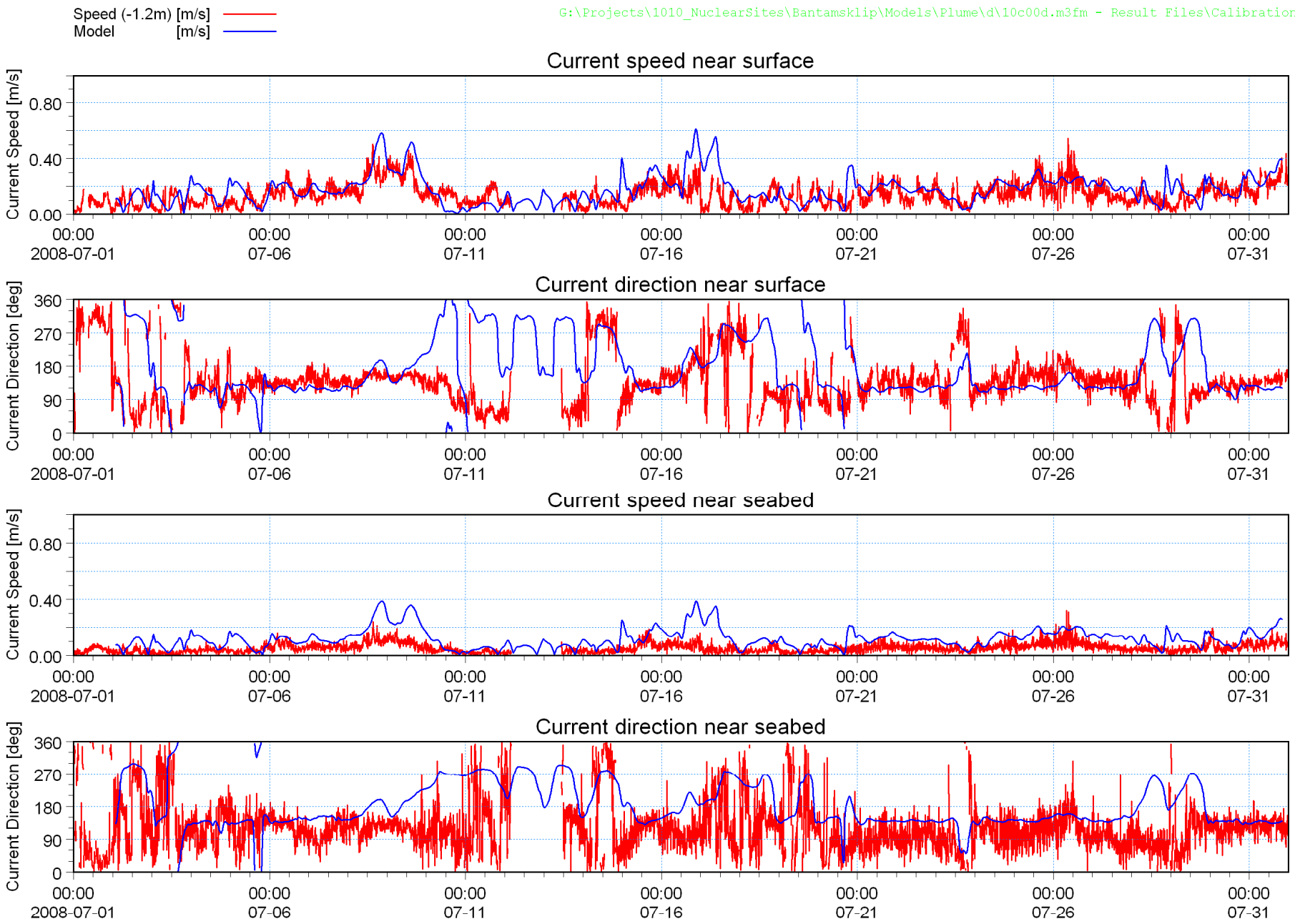

Title: **Calibration of hydrodynamic model: current speed and direction. Measured and modelled time-series of currents at Bantamsklip Site A for period July 2008. (refer to Figure 3.1 for location).**

Figure No. **8.7**

G:\Projects\1010_NuclearSites\Koeberg\Models\Plume\f\21b04c.m3fm - Result Files\Calibration_14October1985.png

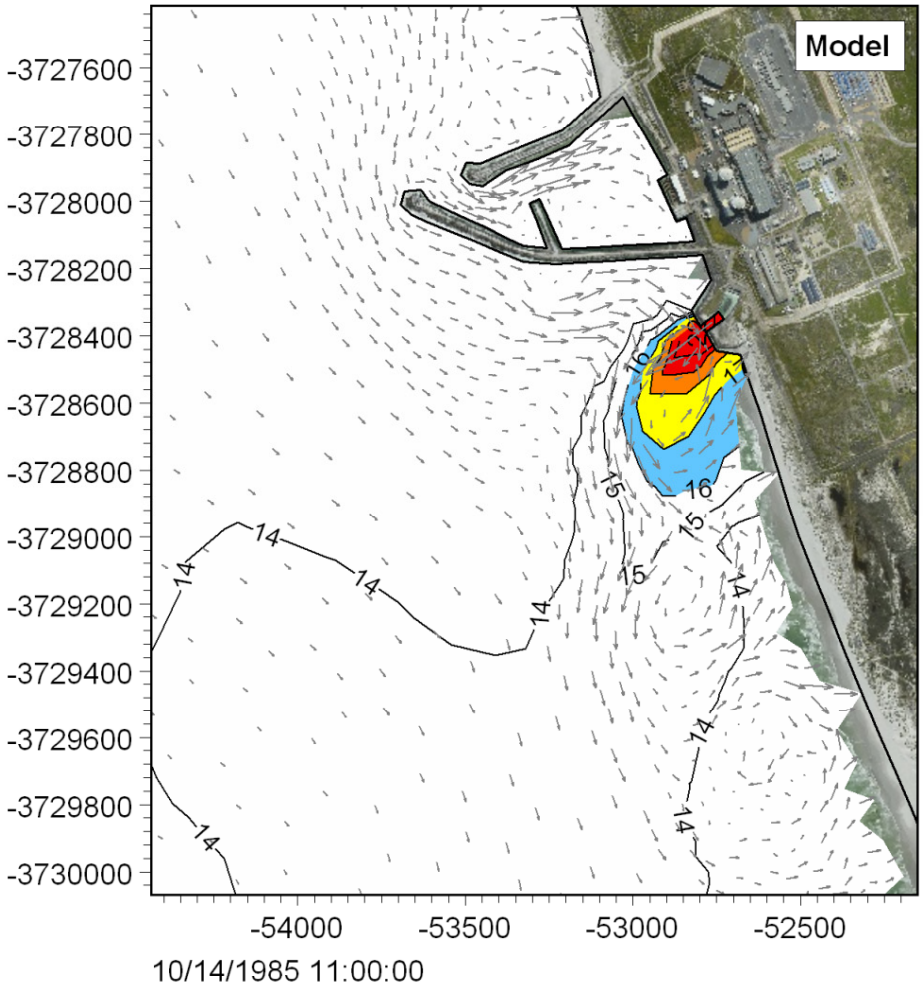

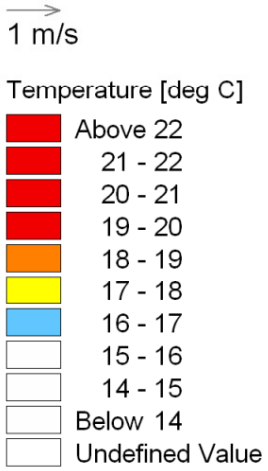

Title: **Calibration of hydrodynamic model: thermal plume dispersion at Koeberg. Modelled surface temperatures at 11:00 and measured surface temperatures between 11:20 and 11:50 on 14 October 1985. Vectors show modelled currents.**

Figure No. **8.8**

G:\Projects\1010_NuclearSites\Koeberg\Models\Plume\f\21b04c.m3fm - Result Files\Calibration_16October1985.png

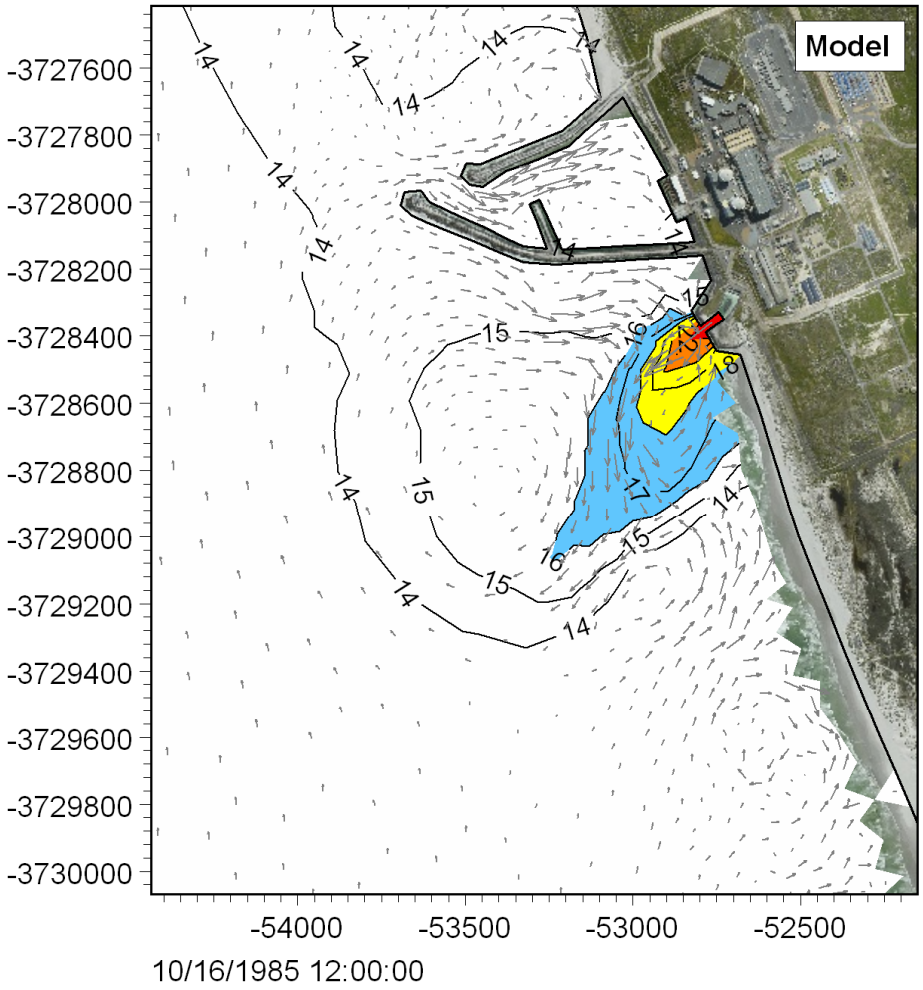

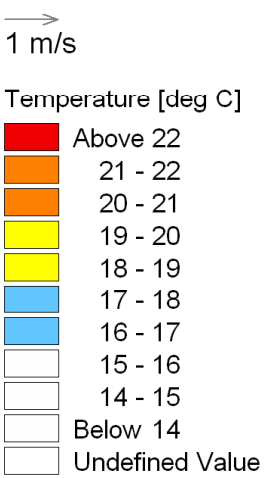

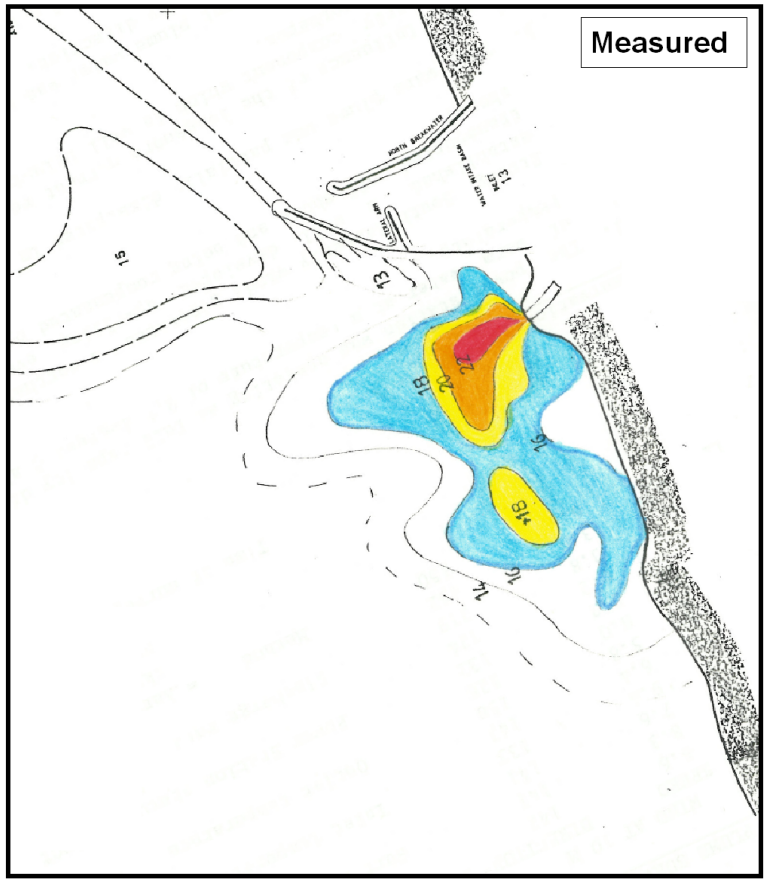

Title: **Calibration of hydrodynamic model: thermal plume dispersion at Koeberg. Modelled surface temperatures at 12:00 and measured surface temperatures between 11:30 and 12:15 on 16 October 1985. Vectors show modelled currents.**

Figure No. **8.9**

G:\Projects\1010_NuclearSites\Koeberg\Models\Plume\f\21b04c.m3fm - Result Files\Calibration_18October1985.png

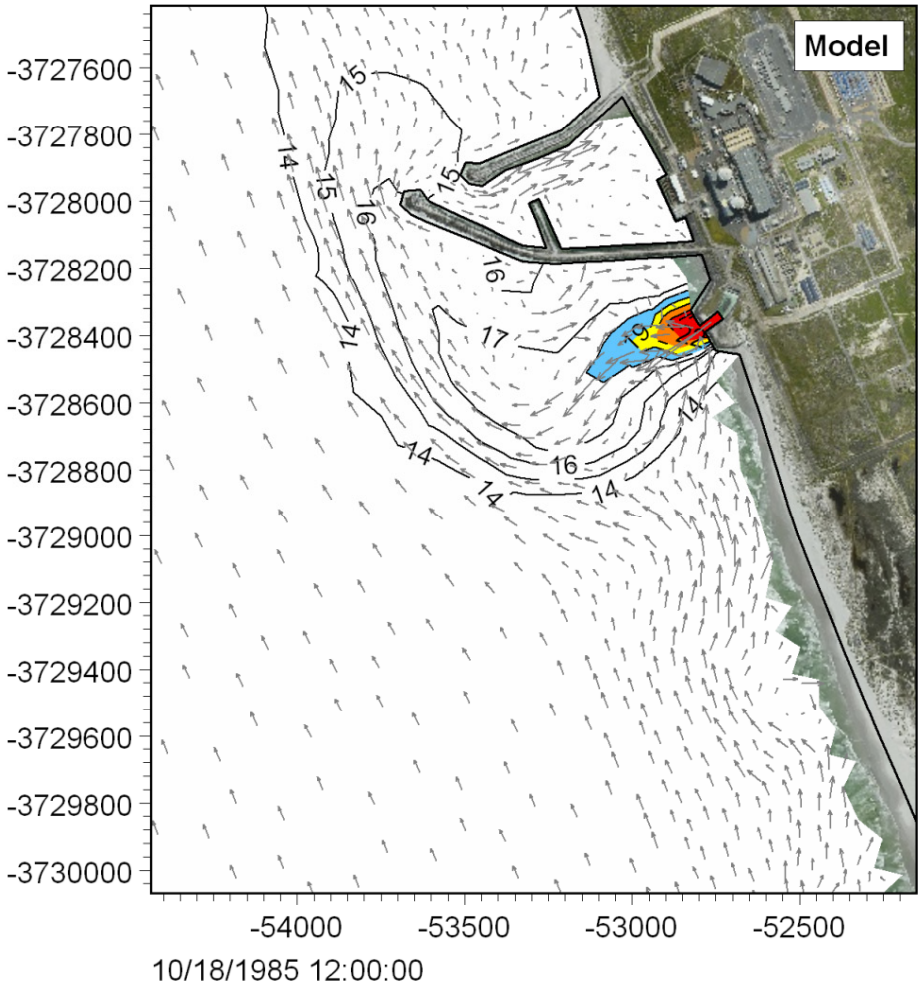

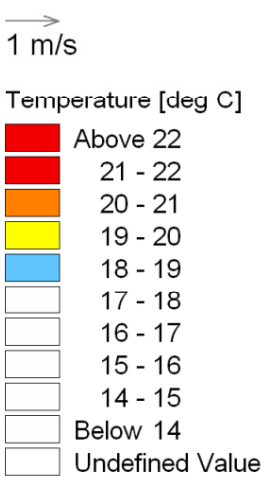

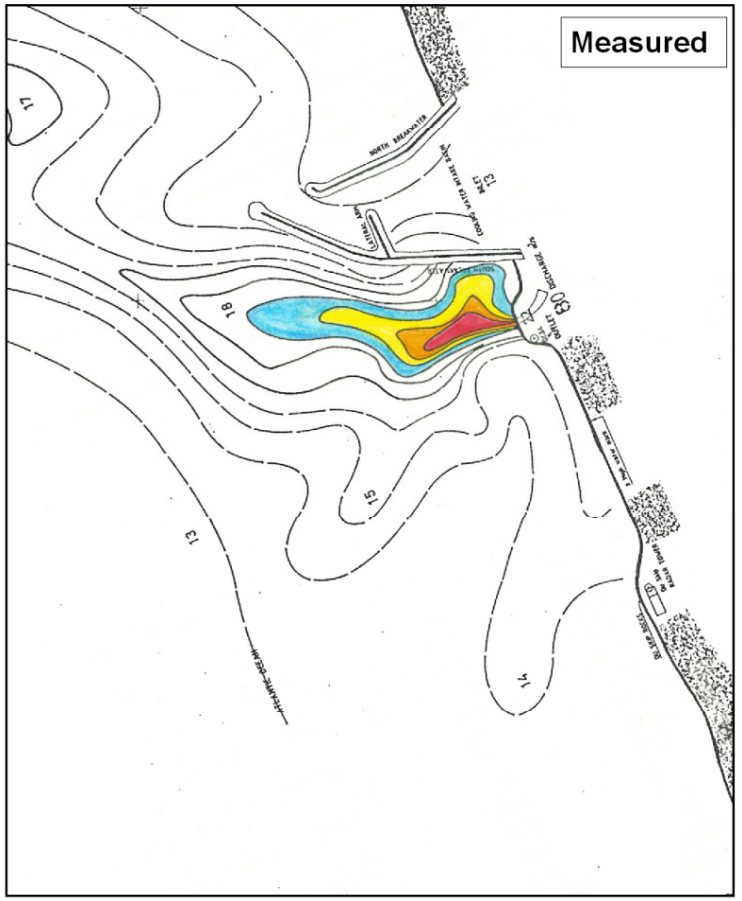

Title: Calibration of hydrodynamic model: thermal plume dispersion at Koeberg. Modelled surface temperatures at 12:00 and measured surface temperatures between 11:18 and 12:10 on 18 October 1985. Vectors show modelled currents.

Figure No. 8.10

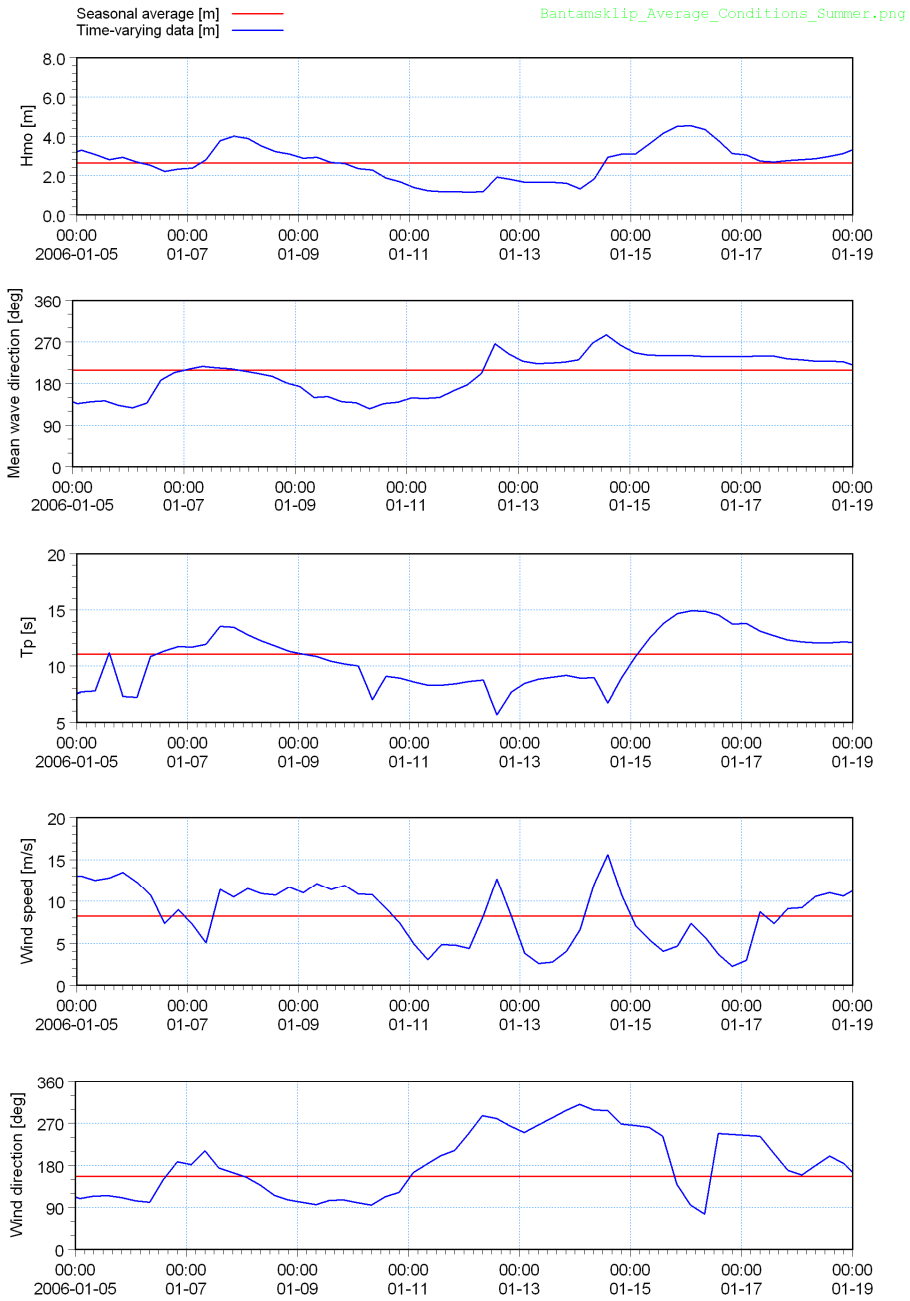

Title:

Wave and wind time-series used in hydrodynamic and plume modelling.
14 day summer simulation period.

Figure No.

8.11

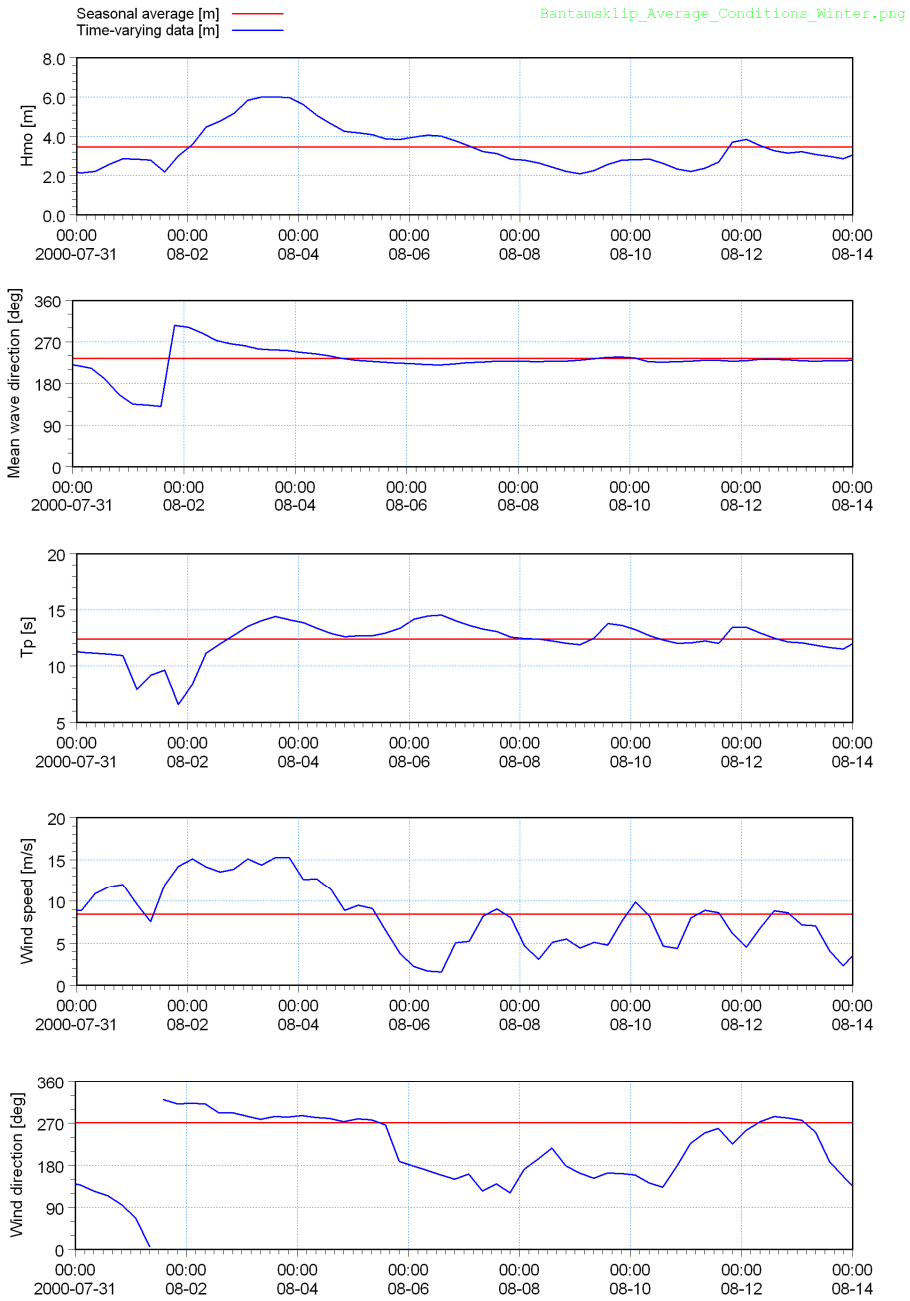

Title:

Wave and wind time-series used in hydrodynamic and plume modelling.
14 day winter simulation period.

Figure No.

8.12

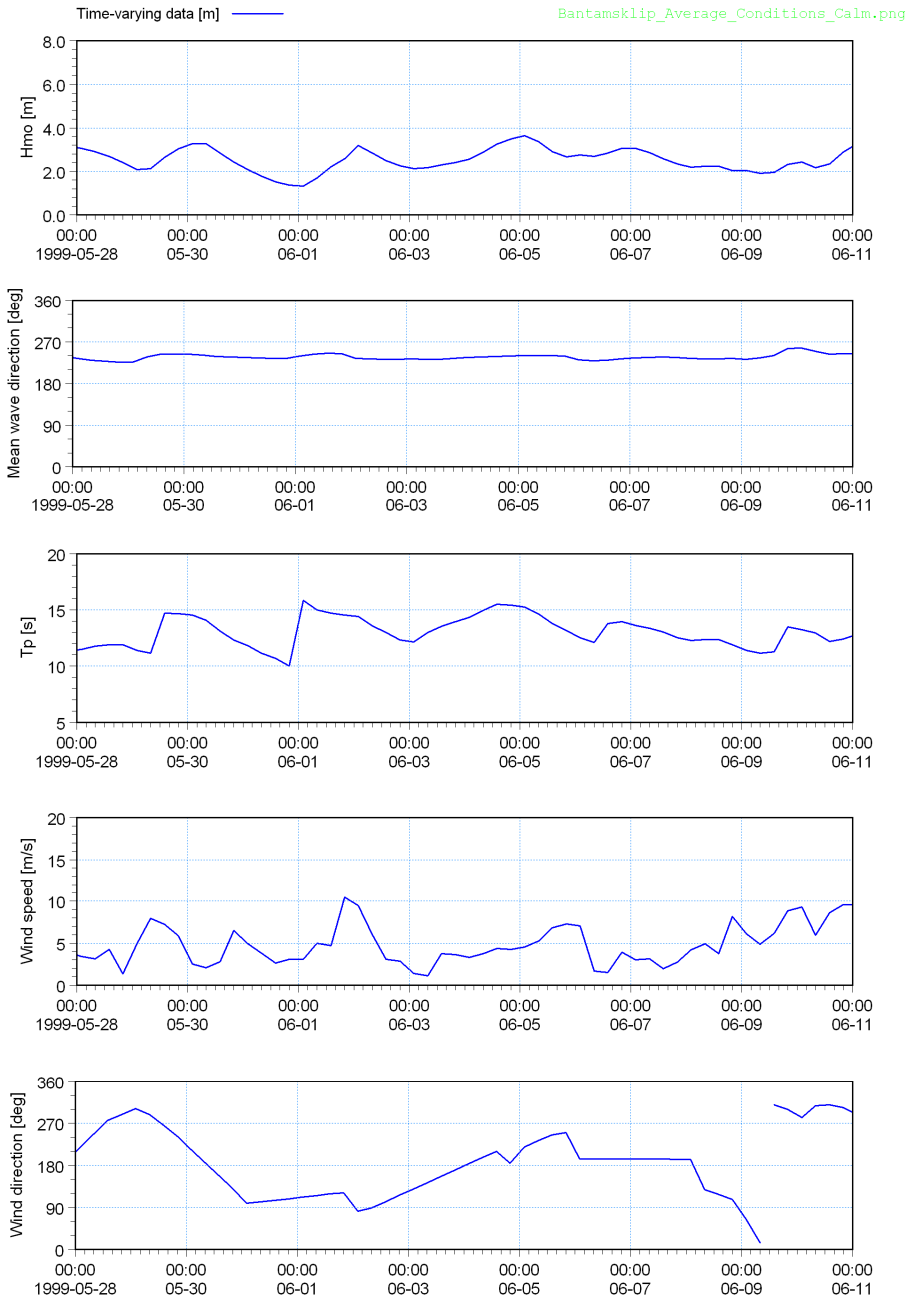

Title:

Wave and wind time-series used in hydrodynamic and plume modelling.
14 day calm simulation period.

Figure No.
8.13

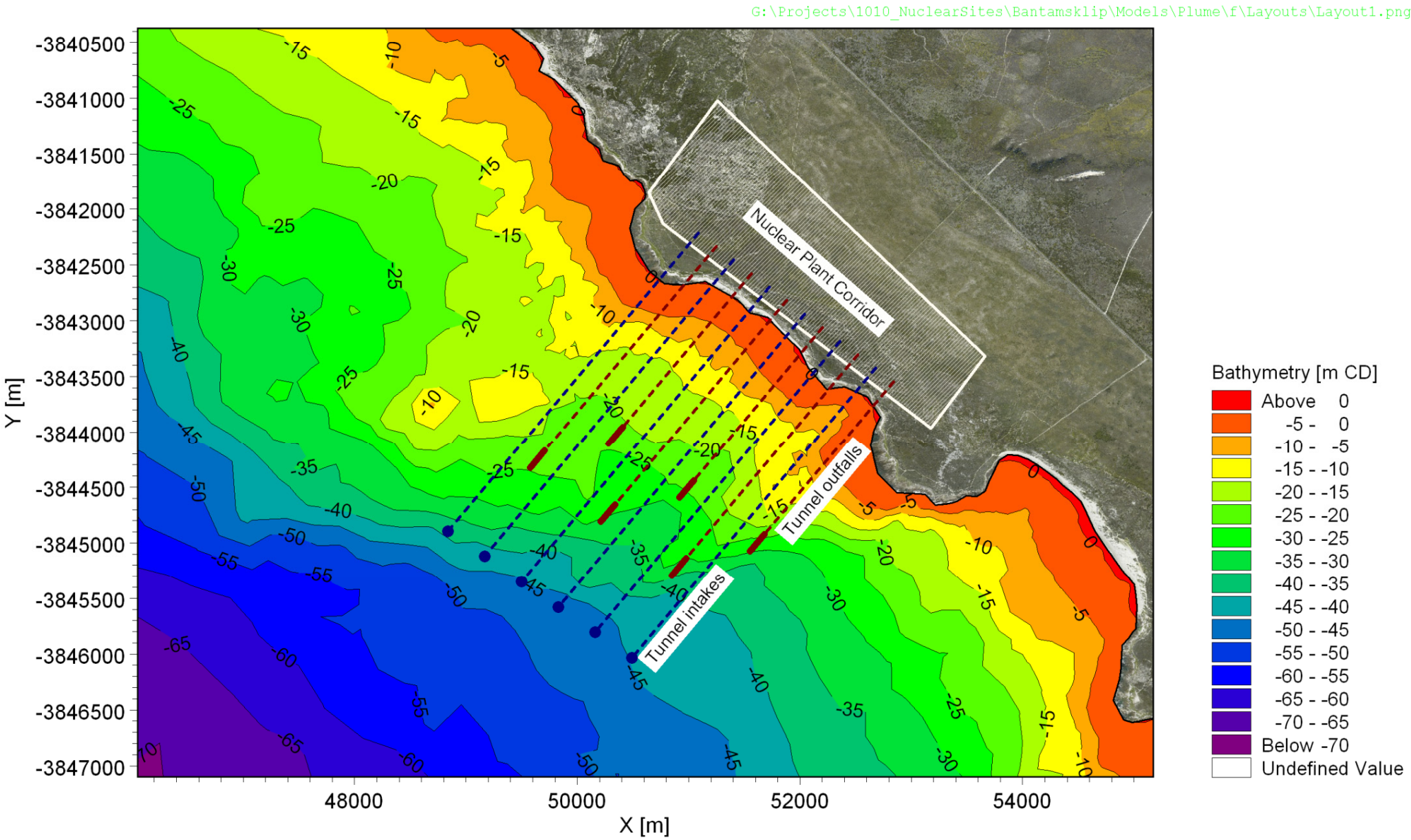

Title:

Layout 1: Offshore tunnel intake (45 m depth) and offshore tunnel outfall (25 m depth).

Figure No.

9.1

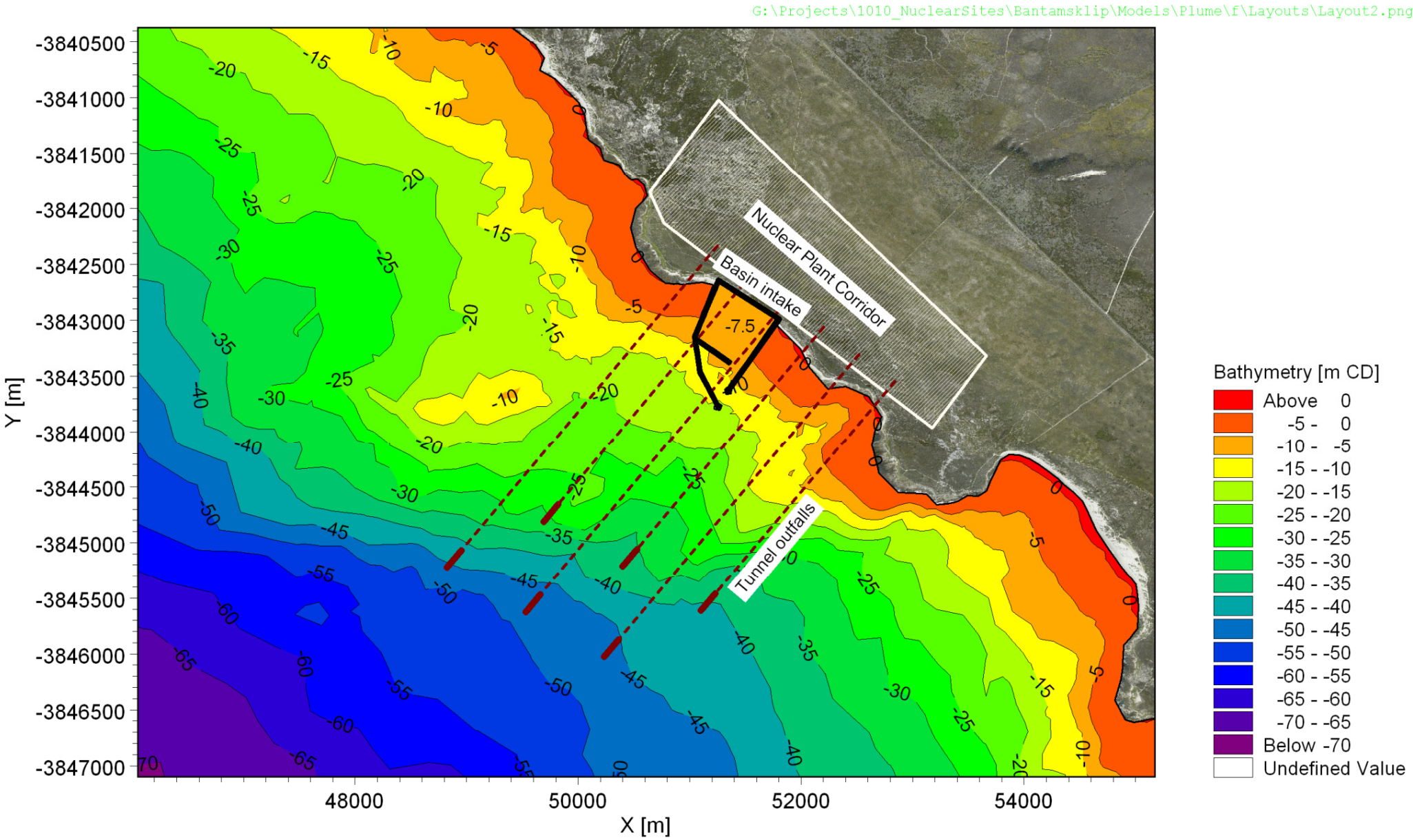

Title:

Layout 2: Basin intake and offshore tunnel outfall (40 m depth).

Figure No.

9.2

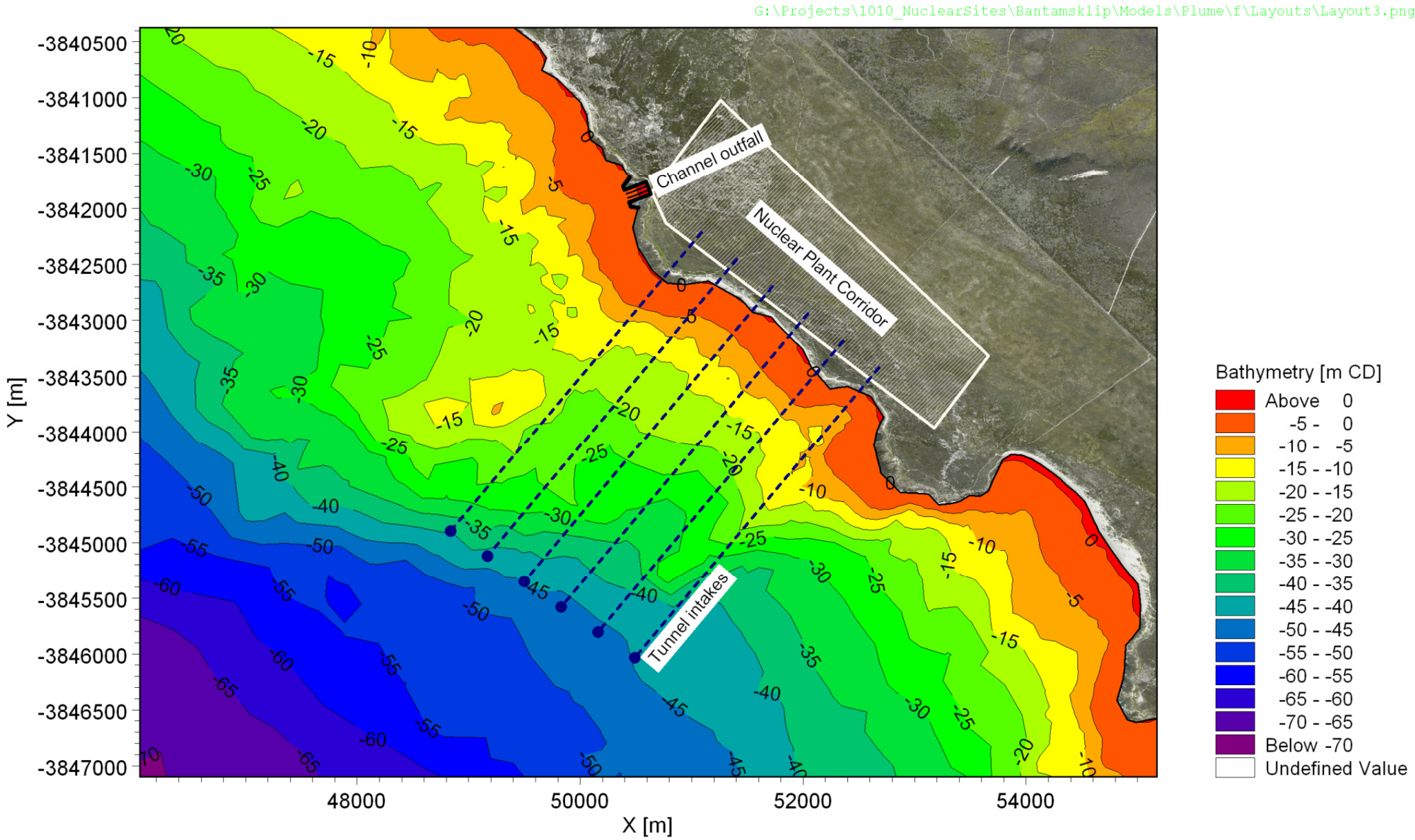

Title:

Layout 3: Offshore tunnel intake (45 m depth) and nearshore channel outfall (2 m depth).

Figure No.

9.3

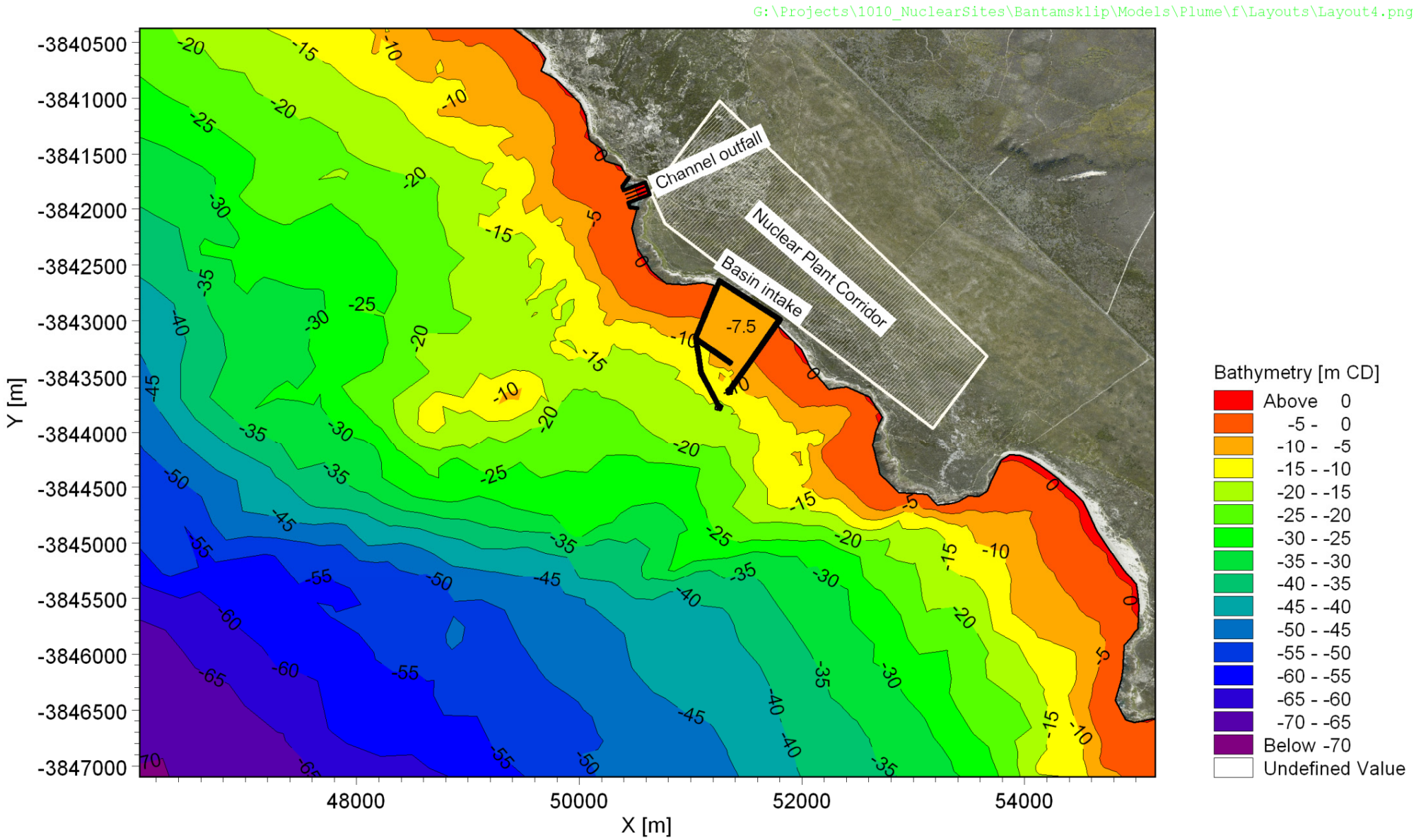

Title:

Layout 4: Basin intake and nearshore channel outfall (2 m depth).

Figure No.

9.4

G:\Projects\1010_NuclearSites\Bantamsklip\Models\Plume\f\Layouts\Layout5.png

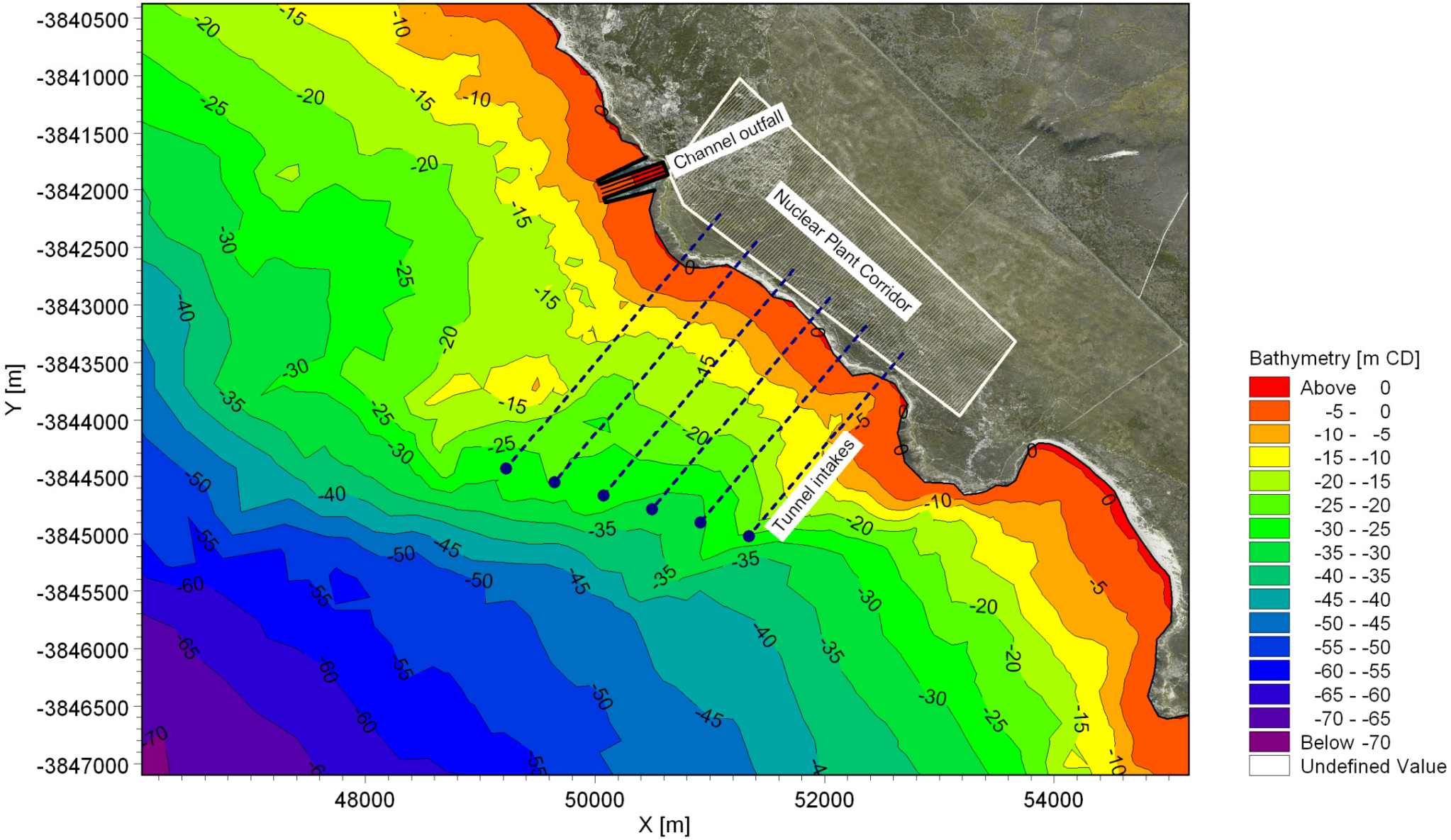

Title:

Layout 5: Offshore tunnel intake (30 m depth) and nearshore channel outfall (5 m depth).

Figure No.

9.5

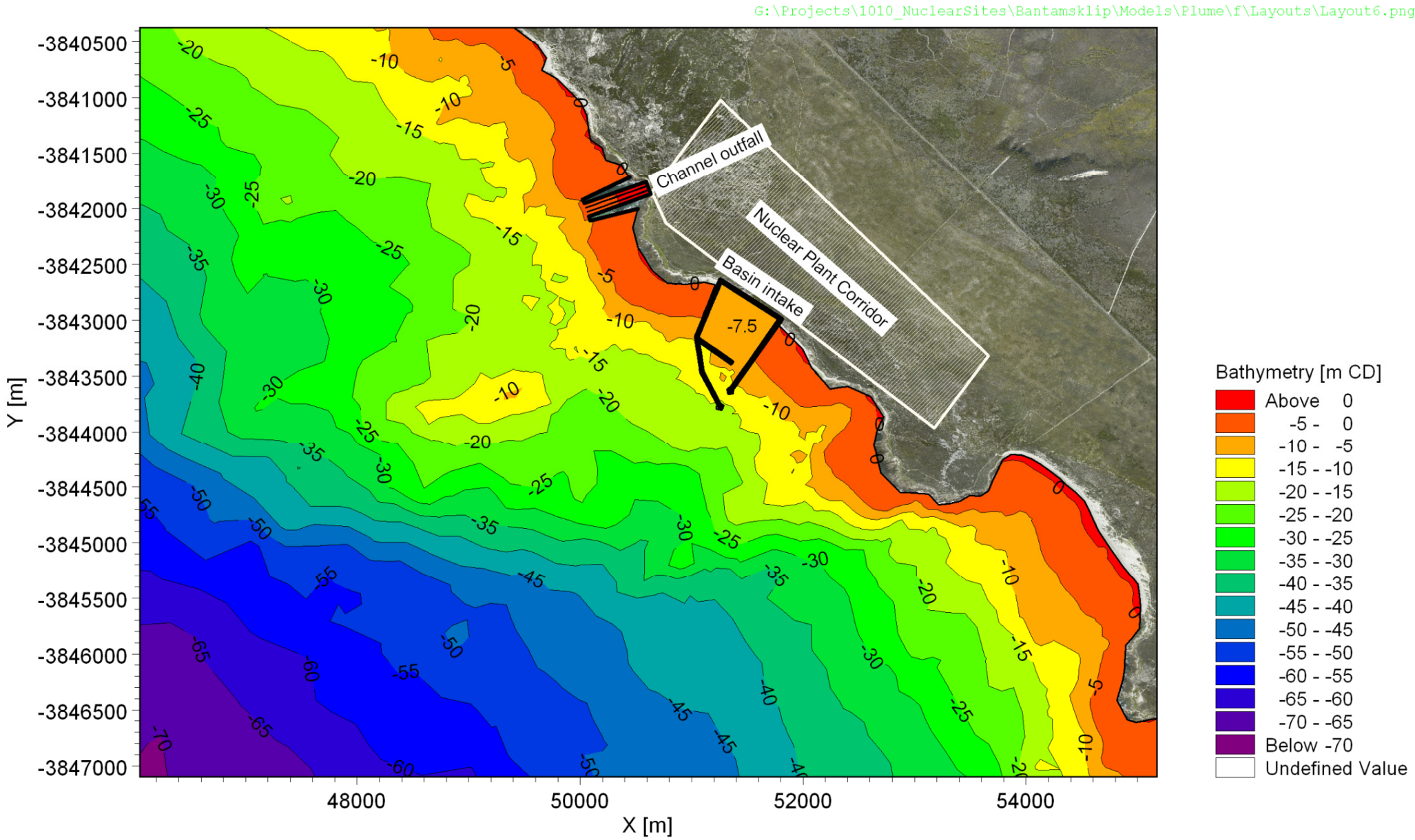

Title:

Layout 6: Basin intake and nearshore channel outfall (5 m depth).

Figure No.

9.6

End of near-field (Stratified Ambient)
End of near-field (Unstratified Ambient)
After 500 m (Stratified Ambient)
After 500 m (Unstratified Ambient)
After 1000 m (Stratified Ambient)
After 1000 m (Unstratified Ambient)
Far-field model approximation

G:\Projects\1010_NuclearSites\General\Data\Discharges\Cormix_Bantamsklip_Layout1.png

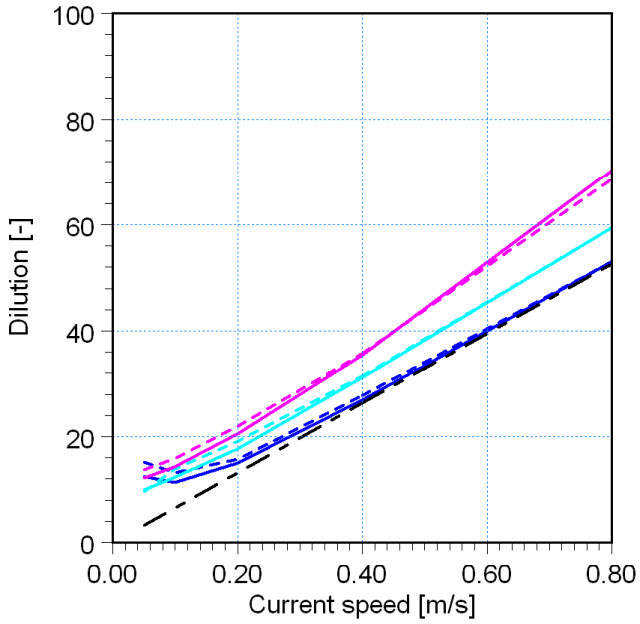

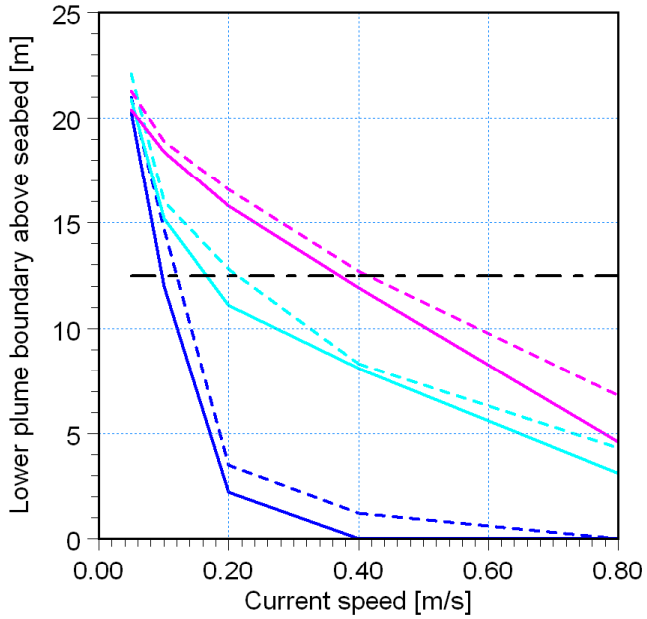

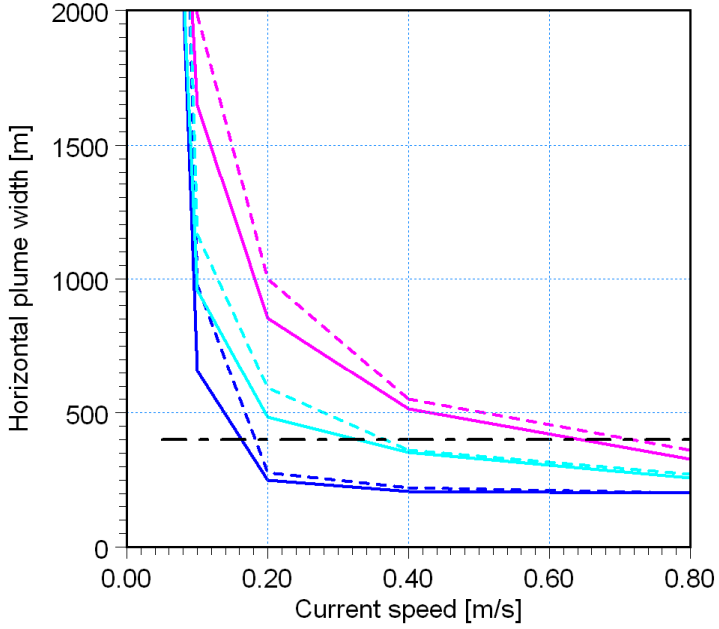

Title:

Near-field dilution modelling results.
Layout 1: Offshore tunnel outfall in 25 m depth.

Figure No.
9.7

End of near-field (Stratified Ambient)
End of near-field (Unstratified Ambient)
After 500 m (Stratified Ambient)
After 500 m (Unstratified Ambient)
After 1000 m (Stratified Ambient)
After 1000 m (Unstratified Ambient)
Far-field model approximation

G:\Projects\1010_NuclearSites\General\Data\Discharges\Cormix_Bantamsklip_Layout2.png

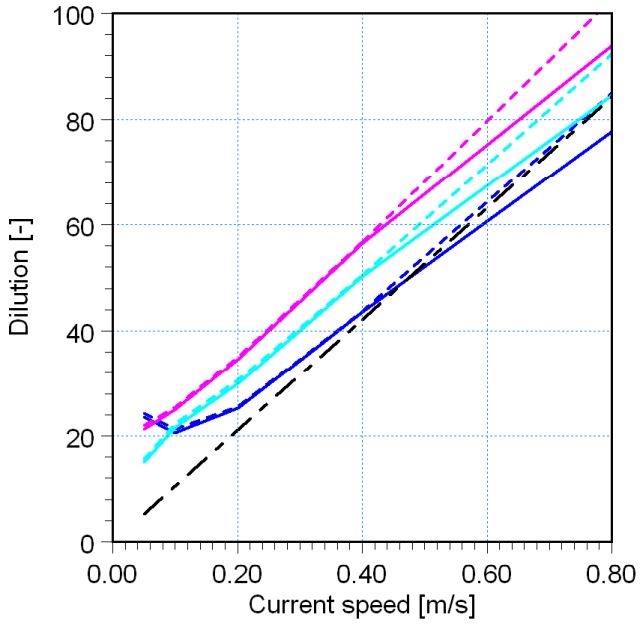

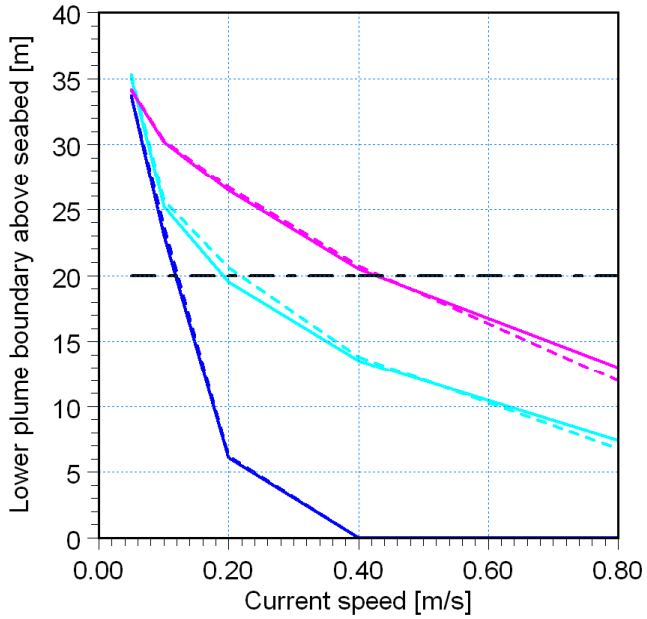

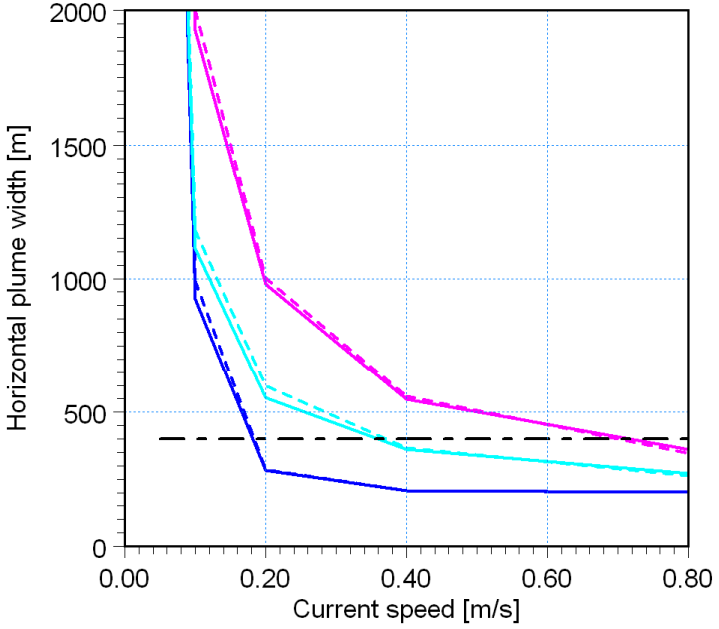

Title:

Near-field dilution modelling results.
Layout 2: Offshore tunnel outfall in 40 m depth.

Figure No.
9.8

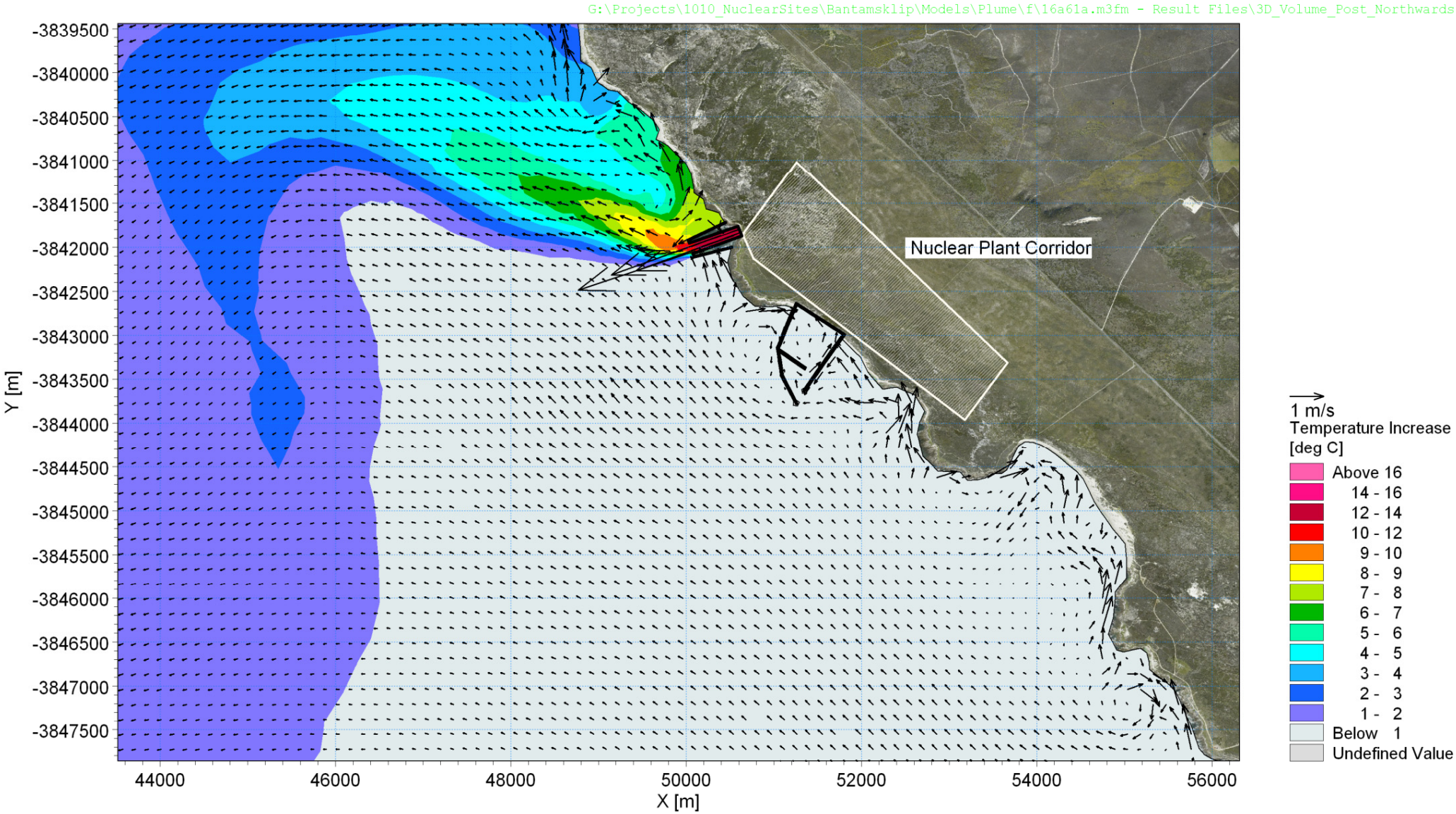

Title:

Example of modelled currents and thermal plume near water surface at a time when the currents are northward. Layout 6: Basin intake and nearshore channel outfall (5 m depth).

Figure No.

9.9

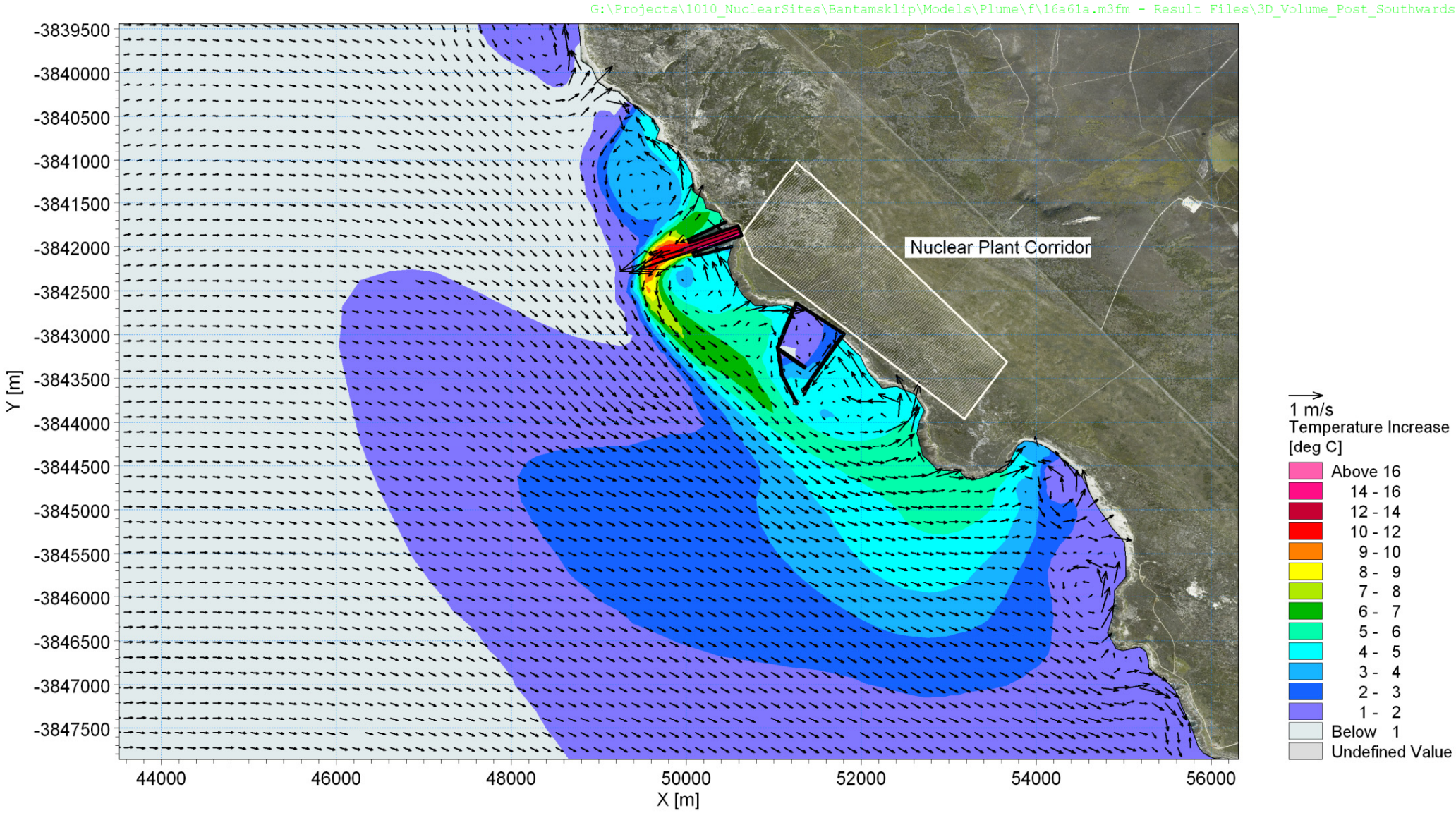

Title:

Example of modelled currents and thermal plume near water surface at a time when the currents are southward. Layout 6: Basin intake and nearshore channel outfall (5 m depth).

Figure No.

9.10

Mean Increase in Temperature Near Water Surface

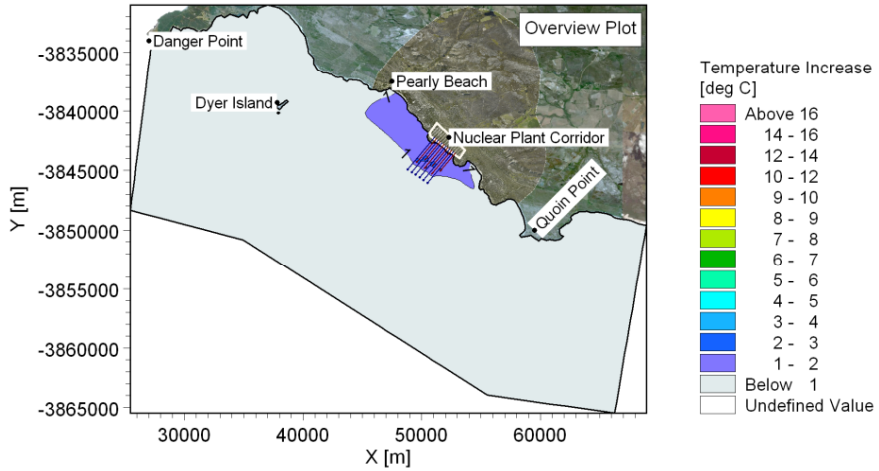

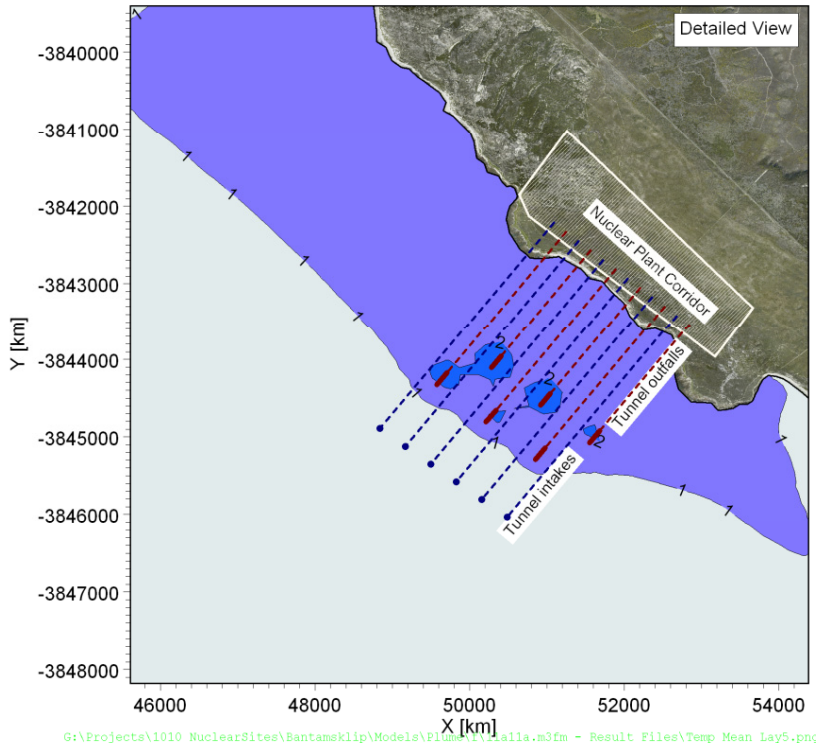

G:\Projects\1010_NuclearSites\Bantamsklip\Models\Plume\Ba11a.m3fm - Result Files\Temp_Mean_Lay5.png

Mean Increase in Temperature Near Seabed

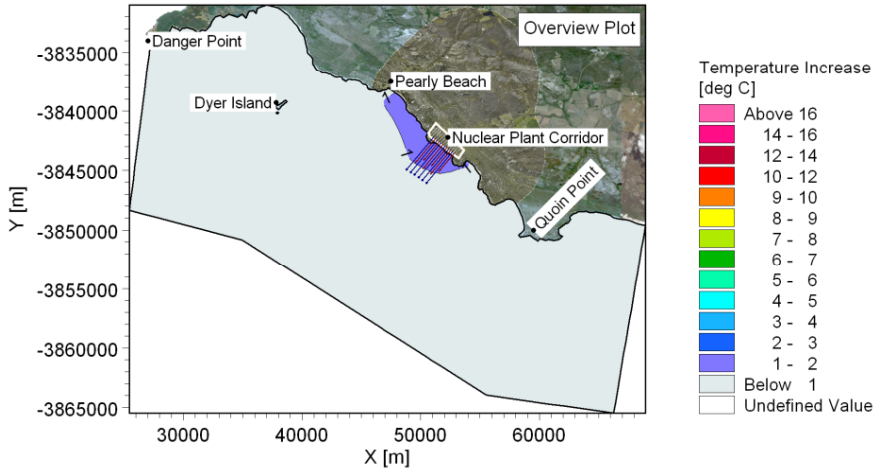

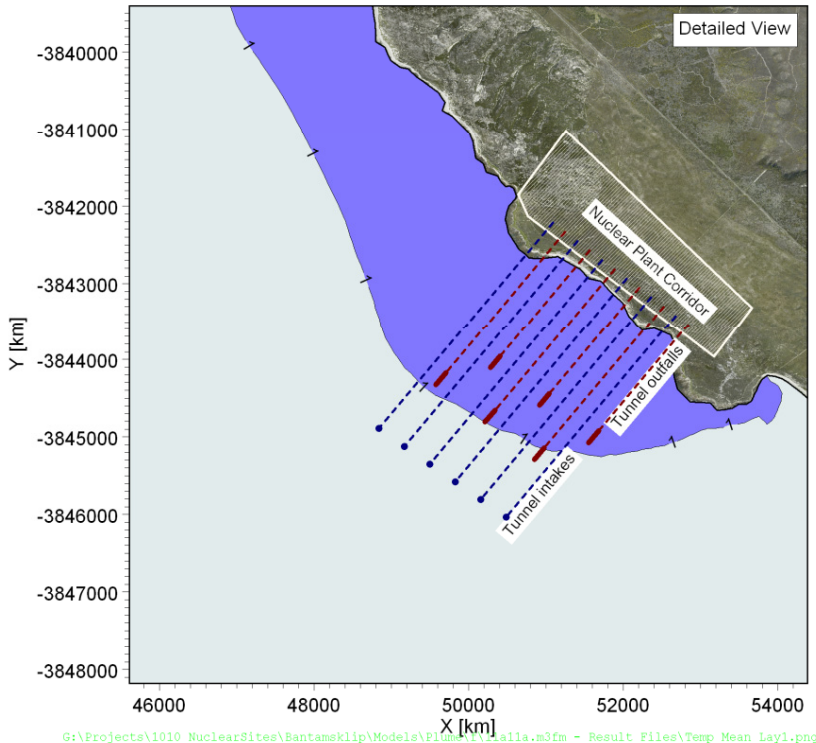

G:\Projects\1010_NuclearSites\Bantamsklip\Models\Plume\Ba11a.m3fm - Result Files\Temp_Mean_Lay1.png

Title: **Thermal plume modelling: Mean increase in temperature due to power station. Layout 1: Offshore tunnel intake (45 m depth) and offshore tunnel outfall (25 m depth). Power output: 10 000 MWe.**

Figure No. **9.11**

Maximum Increase in Temperature Near Water Surface

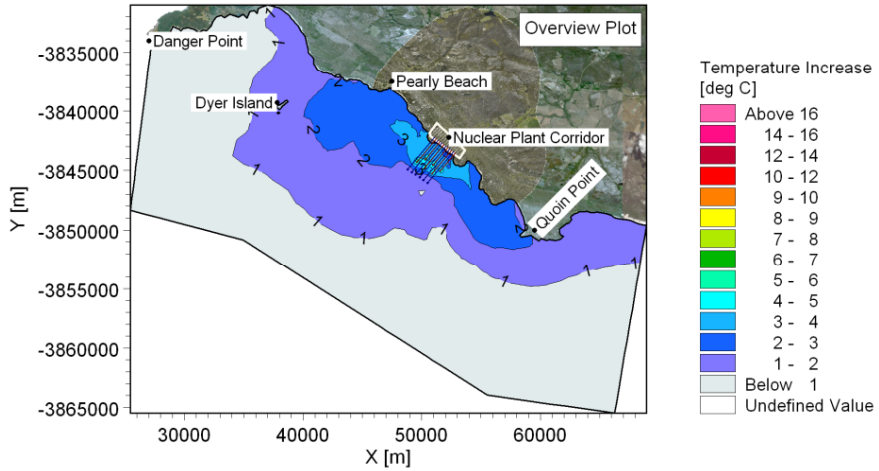

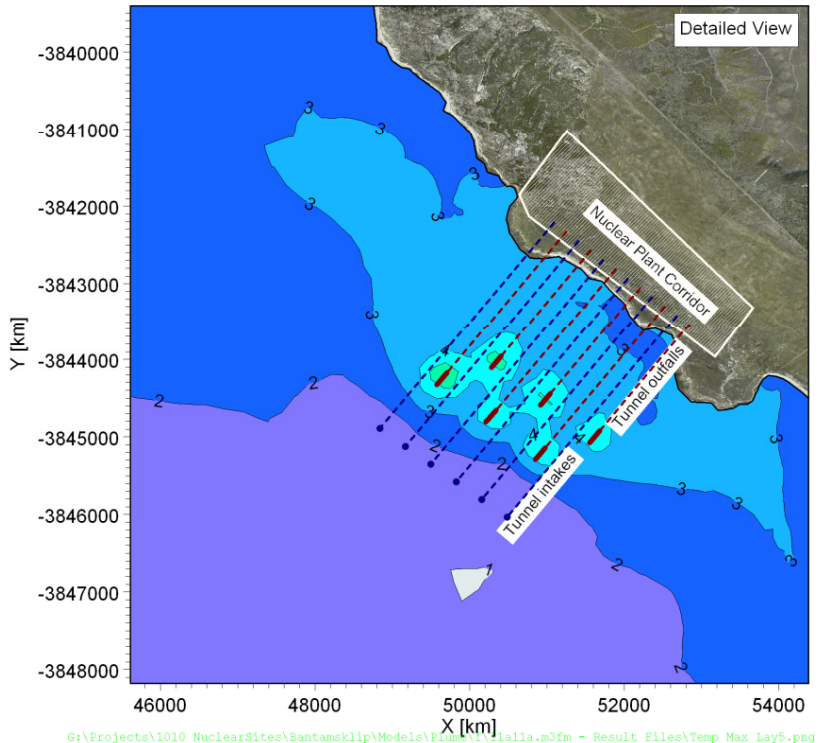

G:\Projects\1010_NuclearSites\Bantamsklip\Models\Plume\Plume11a11a.m3fm - Result Files\Temp_Max_Lay5.png

Maximum Increase in Temperature Near Seabed

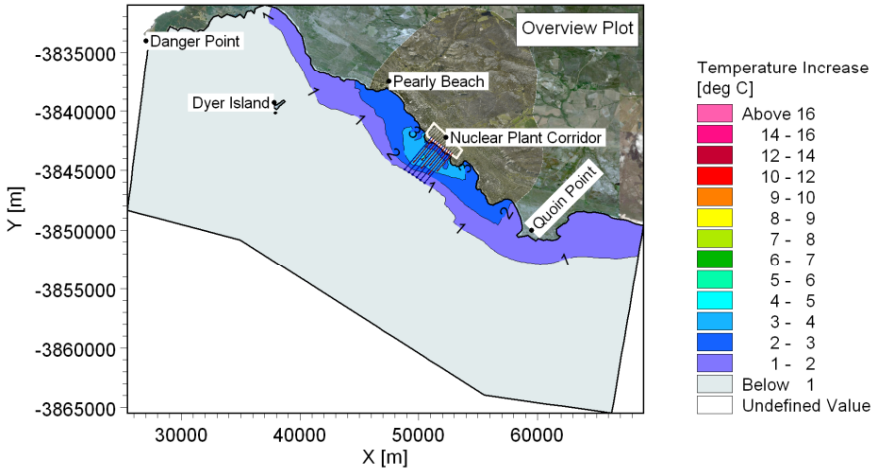

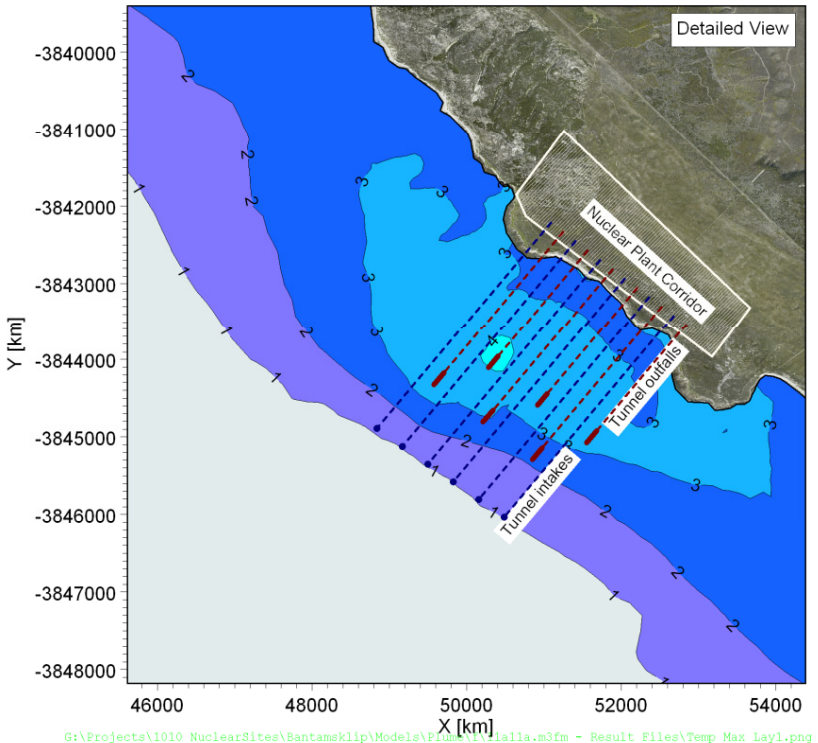

G:\Projects\1010_NuclearSites\Bantamsklip\Models\Plume\Plume11a11a.m3fm - Result Files\Temp_Max_Lay1.png

Title: **Thermal plume modelling: Maximum increase in temperature due to power station. Layout 1: Offshore tunnel intake (45 m depth) and offshore tunnel outfall (25 m depth). Power output: 10 000 MWe.**

Figure No. **9.12**

Mean Increase in Temperature Near Water Surface

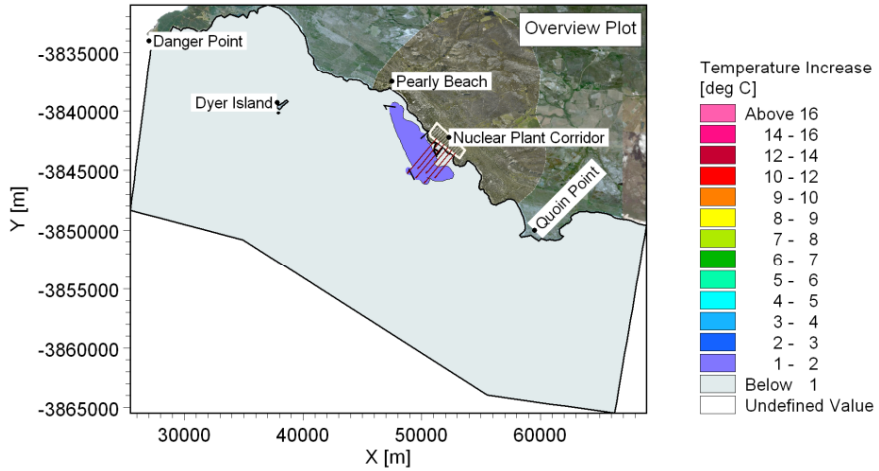

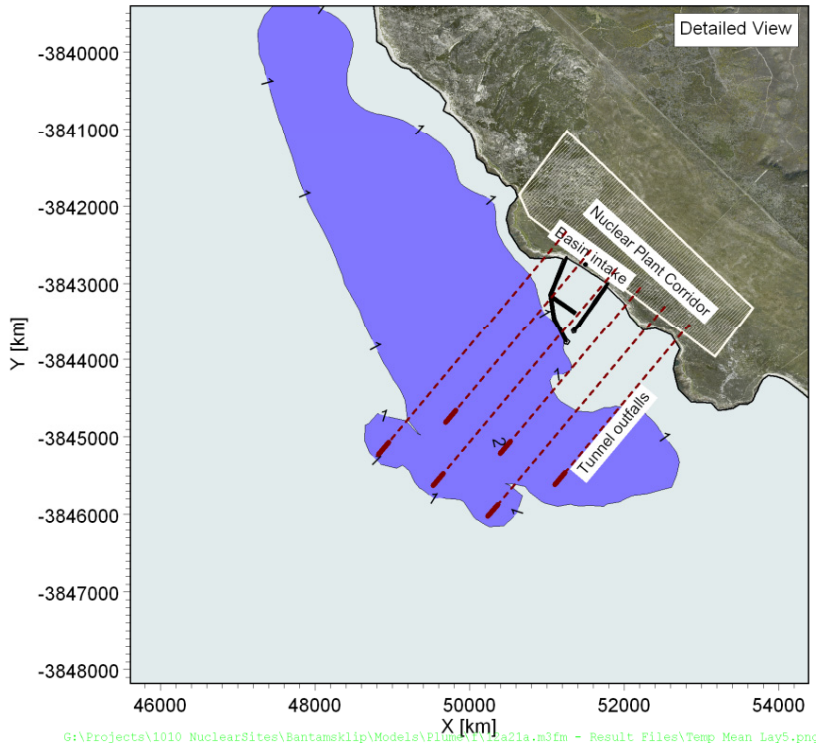

G:\Projects\1010_NuclearSites\Bantamsklip\Models\Plume\1_La21a.m3fm - Result Files\Temp_Mean_Lay5.png

Mean Increase in Temperature Near Seabed

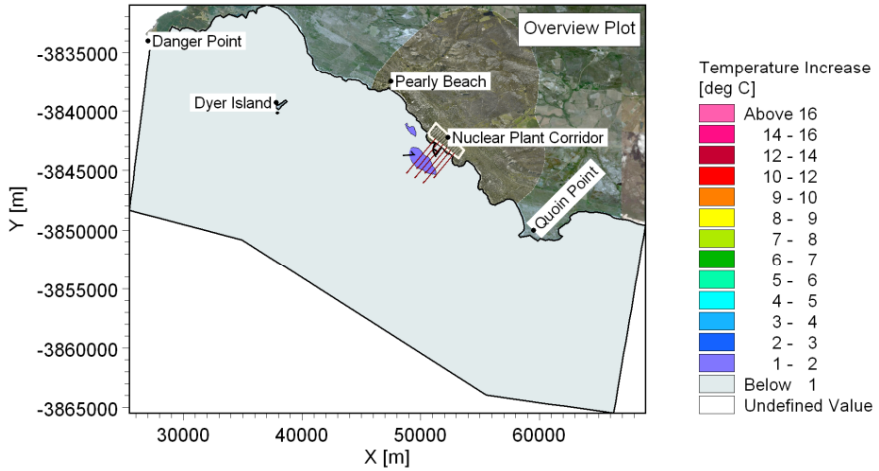

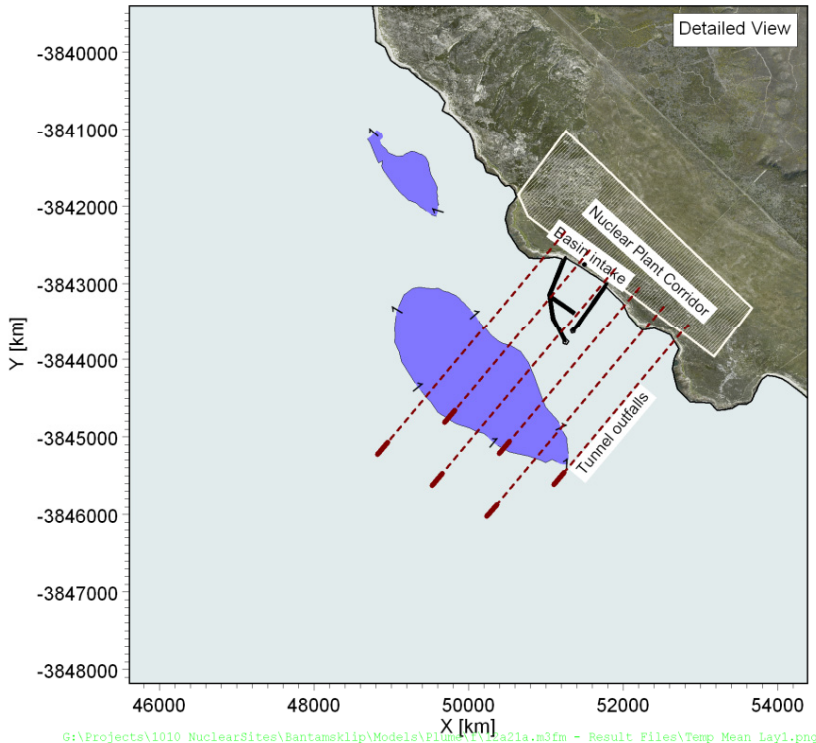

G:\Projects\1010_NuclearSites\Bantamsklip\Models\Plume\1_La21a.m3fm - Result Files\Temp_Mean_Lay1.png

Title: **Thermal plume modelling: Mean increase in temperature due to power station. Layout 2: Basin intake and offshore tunnel outfall (40 m depth). Power output: 10 000 MWe.**

Figure No. **9.13**

Maximum Increase in Temperature Near Water Surface

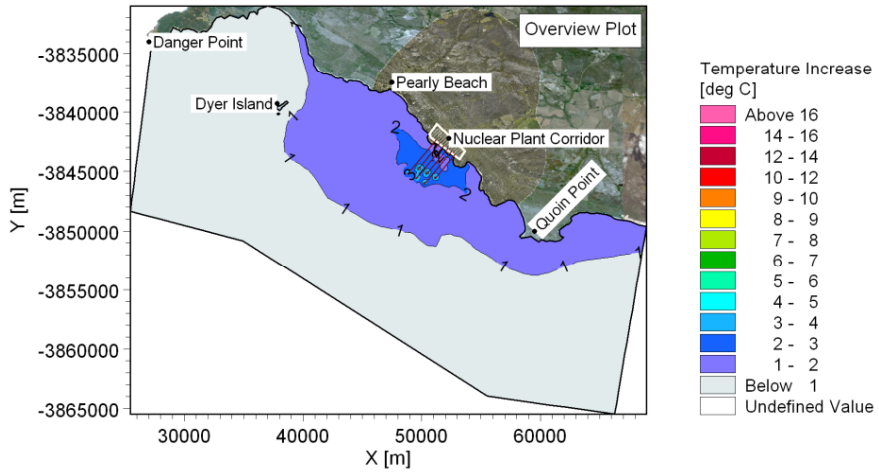

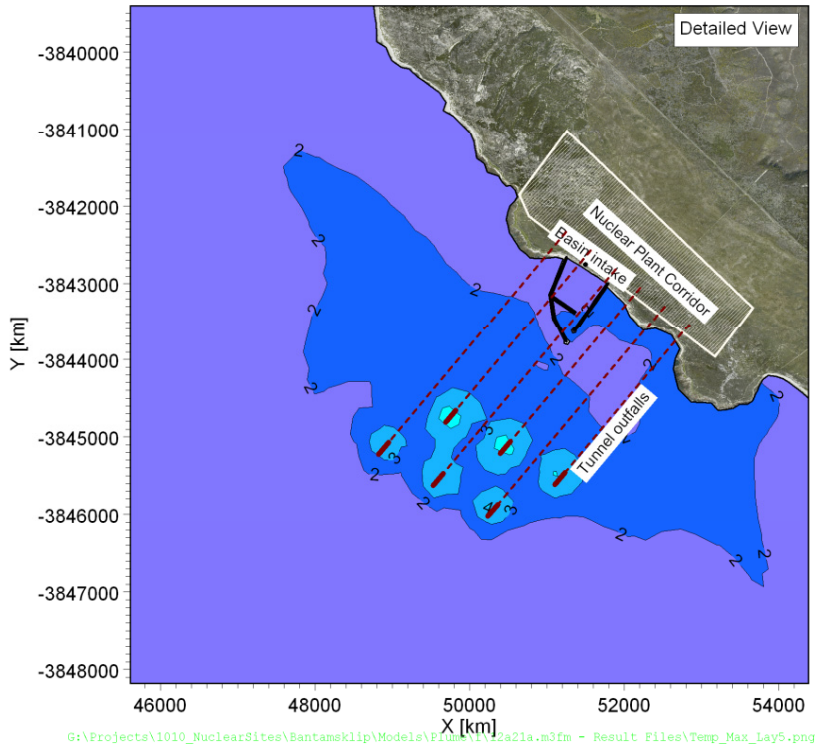

G:\Projects\1010_NuclearSites\Bantamsklip\Models\Plume\T12a21a.m3fm - Result Files\Temp_Max_Lay5.png

Maximum Increase in Temperature Near Seabed

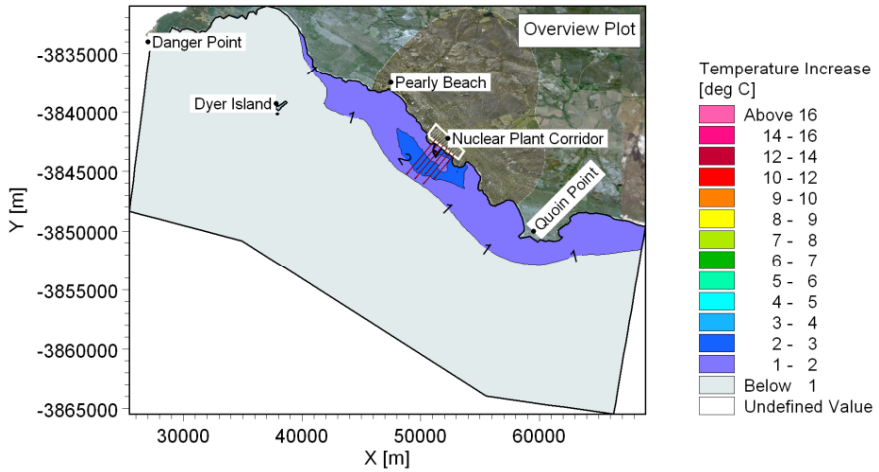

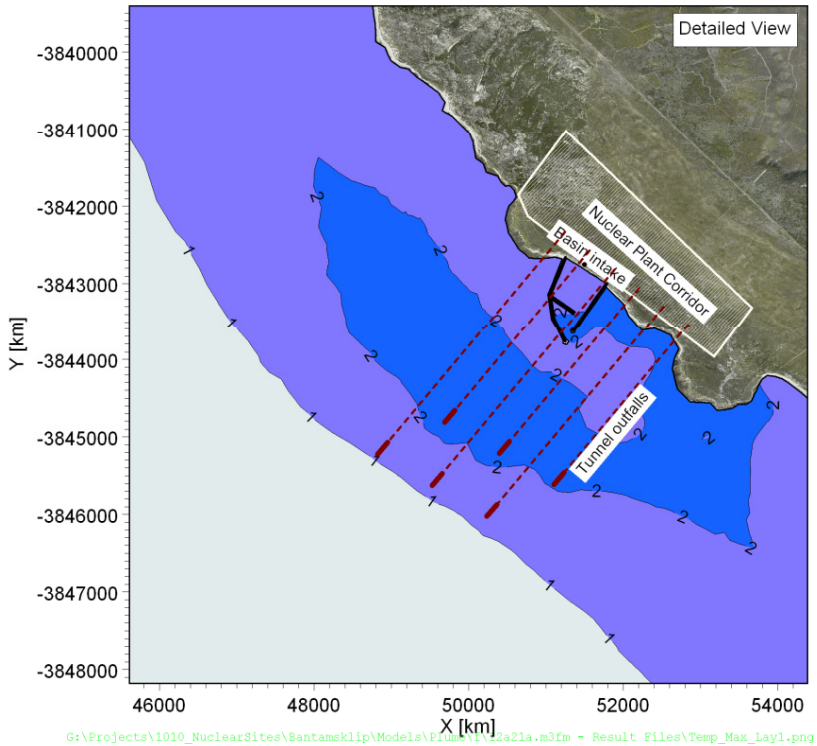

G:\Projects\1010_NuclearSites\Bantamsklip\Models\Plume\T12a21a.m3fm - Result Files\Temp_Max_Lay1.png

Title: **Thermal plume modelling: Maximum increase in temperature due to power station. Layout 2: Basin intake and offshore tunnel outfall (40 m depth). Power output: 10 000 MWe.**

Figure No. **9.14**

Mean Increase in Temperature Near Water Surface

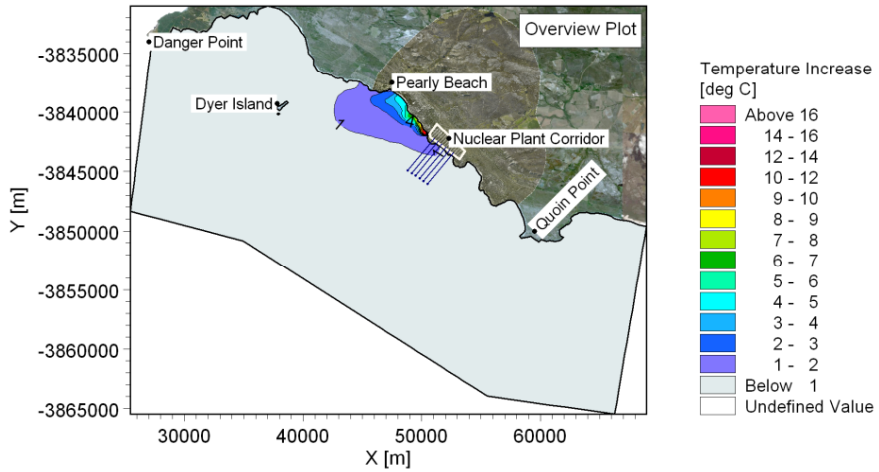

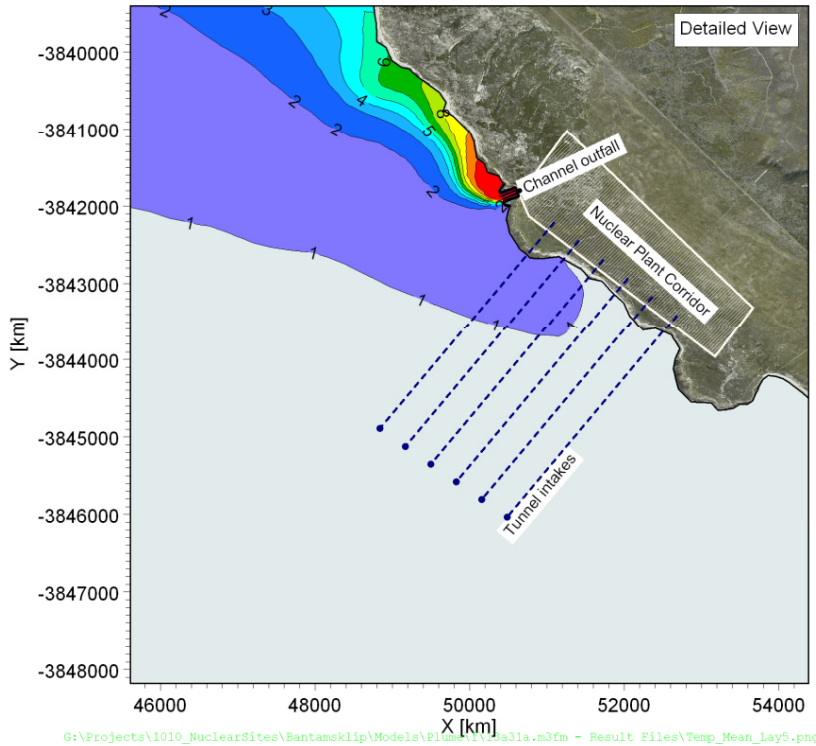

G:\Projects\1010_NuclearSites\Bantamsklip\Models\Plume\1_1a31a.m3fm - Result Files\Temp_Mean_Lay5.png

Mean Increase in Temperature Near Seabed

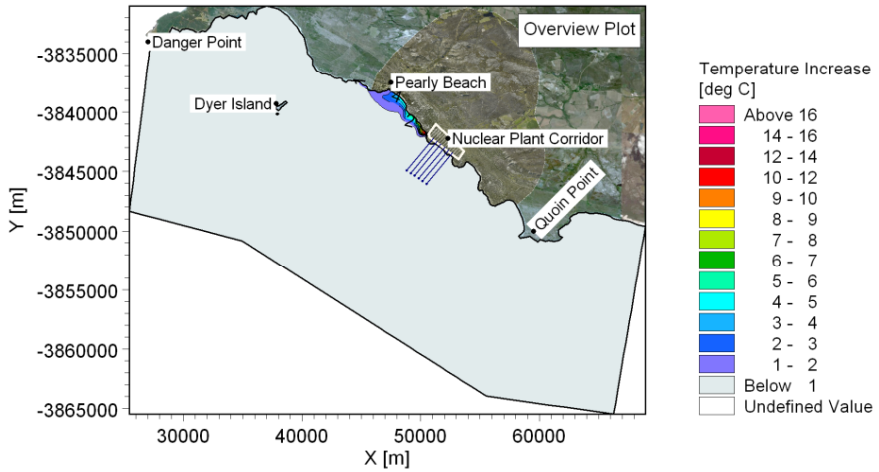

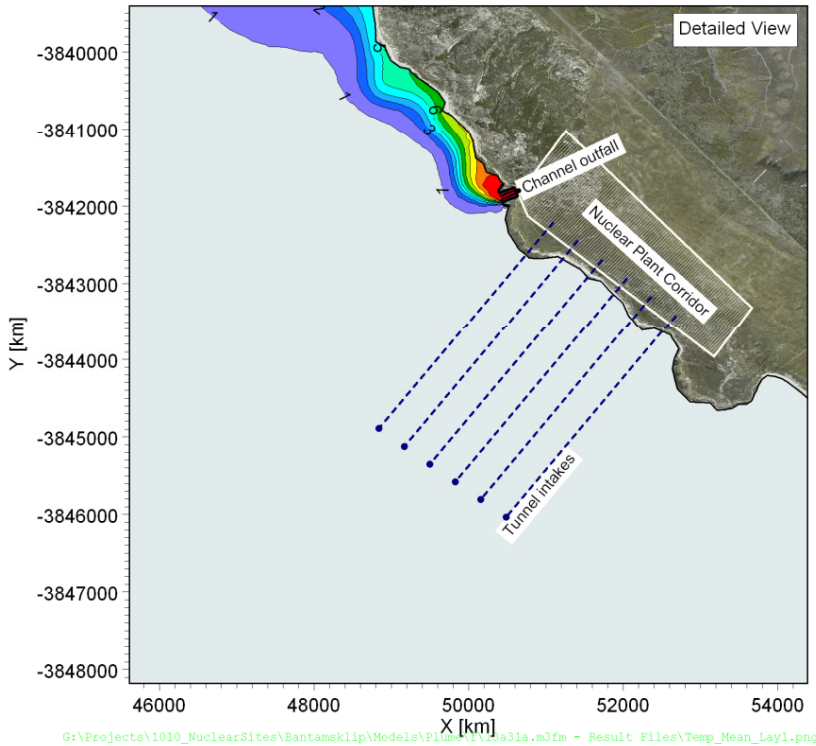

G:\Projects\1010_NuclearSites\Bantamsklip\Models\Plume\1_1a31a.m3fm - Result Files\Temp_Mean_Lay1.png

Title: **Thermal plume modelling: Mean increase in temperature due to power station. Layout 3: Offshore tunnel intake (45 m depth) and nearshore channel outfall (2 m depth). Power output: 10 000 MWe.**

Figure No. **9.15**

Maximum Increase in Temperature Near Water Surface

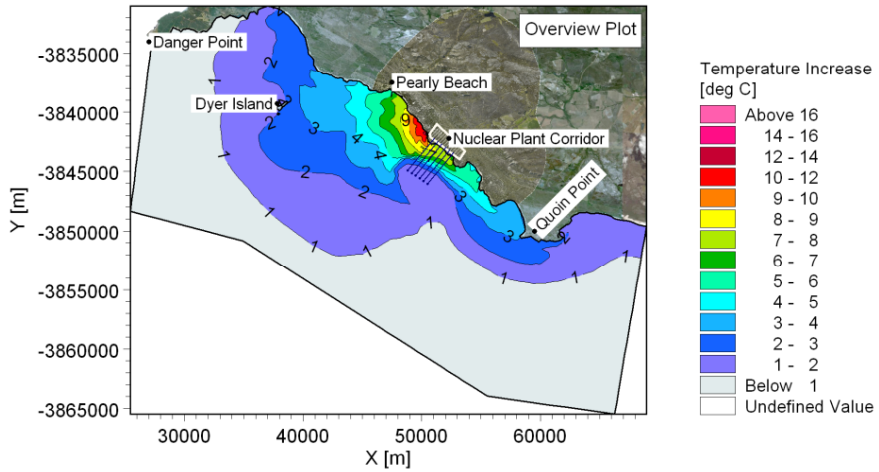

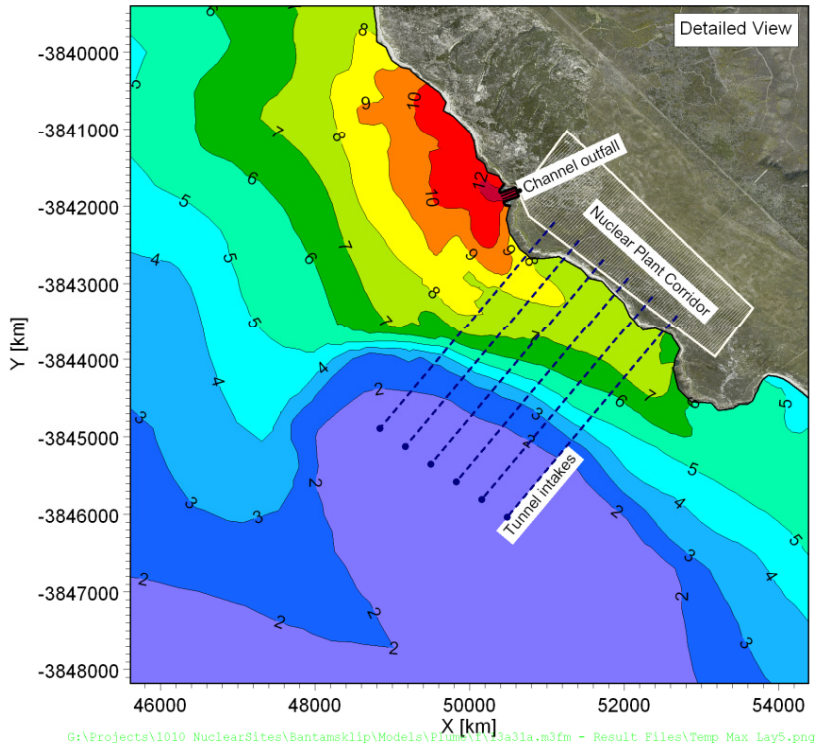

G:\Projects\1010_NuclearSites\Bantamsklip\Models\Plume\1_13a31a.m3fm - Result Files\Temp_Max_Lay5.png

Maximum Increase in Temperature Near Seabed

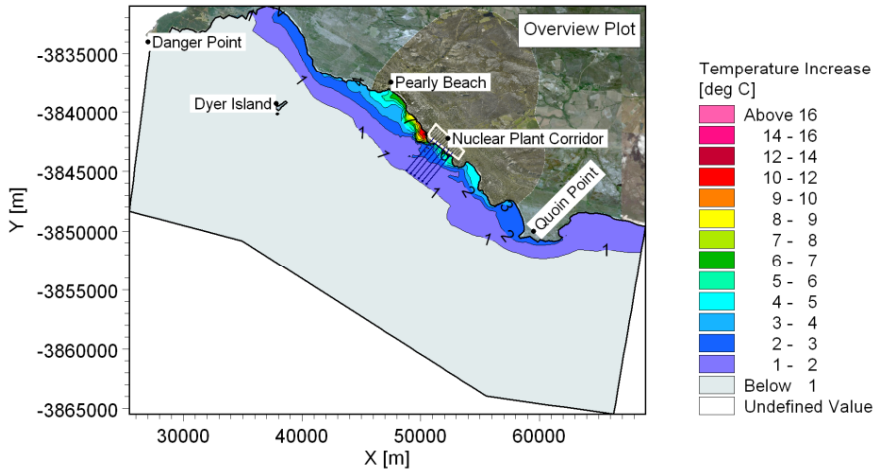

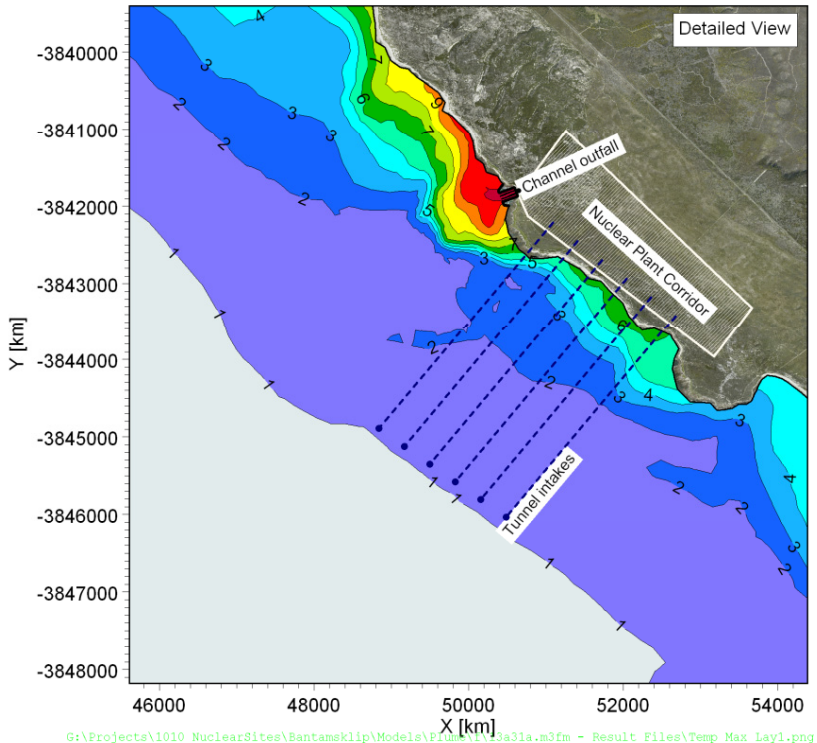

G:\Projects\1010_NuclearSites\Bantamsklip\Models\Plume\1_13a31a.m3fm - Result Files\Temp_Max_Lay1.png

Title: **Thermal plume modelling: Maximum increase in temperature due to power station. Layout 3: Offshore tunnel intake (45 m depth) and nearshore channel outfall (2 m depth). Power output: 10 000 MWe.**

Figure No. **9.16**

Mean Increase in Temperature Near Water Surface

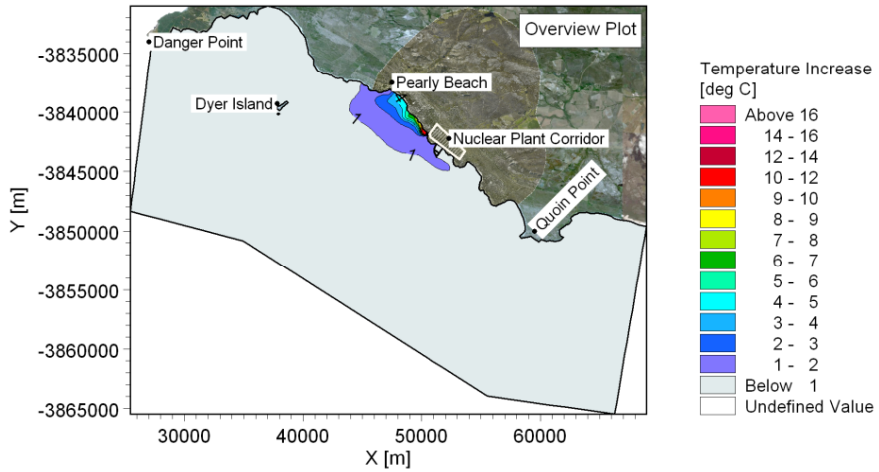

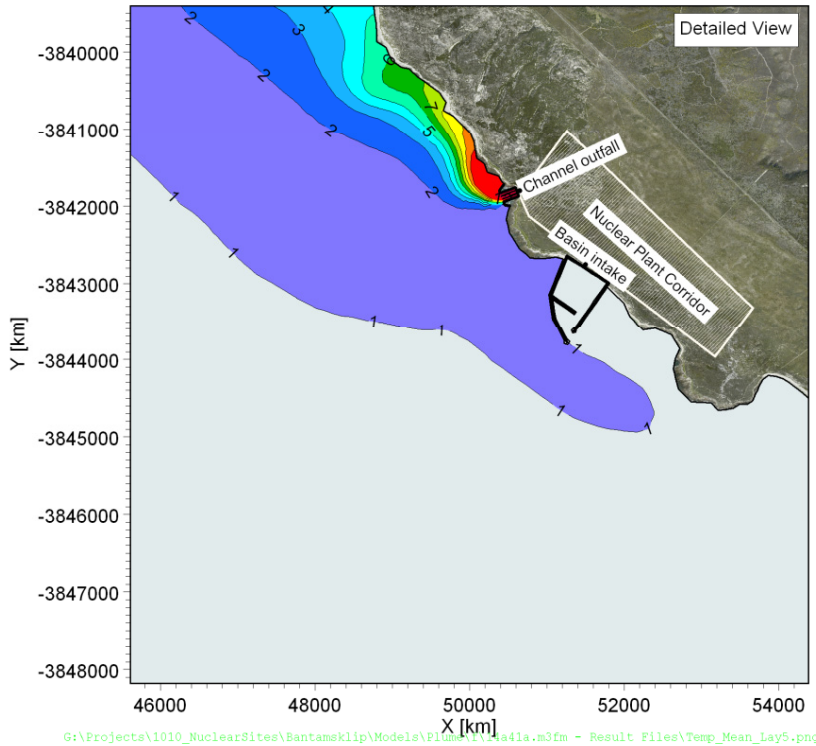

G:\Projects\1010_NuclearSites\Bantamsklip\Models\Plume\1_1a41a.m3fm - Result Files\Temp_Mean_Lay5.png

Mean Increase in Temperature Near Seabed

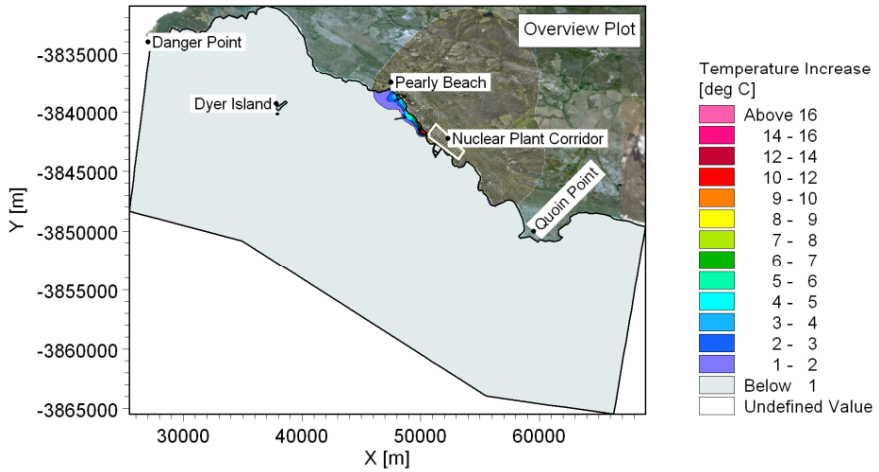

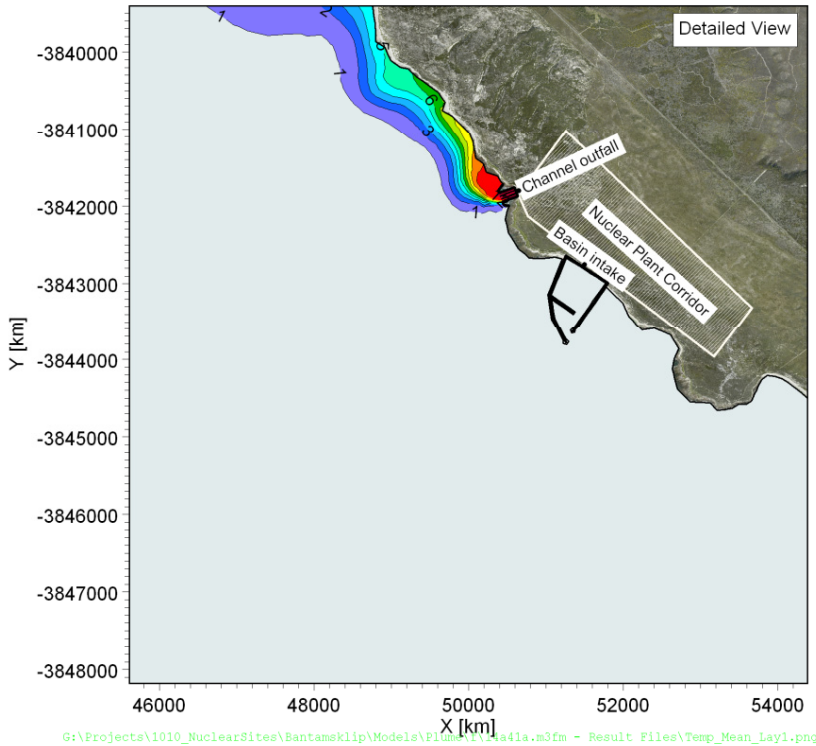

G:\Projects\1010_NuclearSites\Bantamsklip\Models\Plume\1_1a41a.m3fm - Result Files\Temp_Mean_Lay1.png

Title: **Thermal plume modelling: Mean increase in temperature due to power station. Layout 4: Basin intake and nearshore channel outfall (2 m depth). Power output: 10 000 MWe.**

Figure No. **9.17**

Maximum Increase in Temperature Near Water Surface

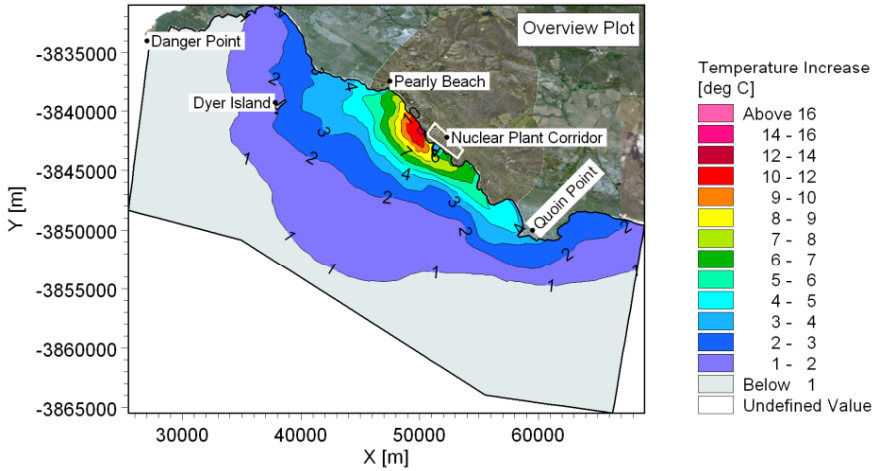

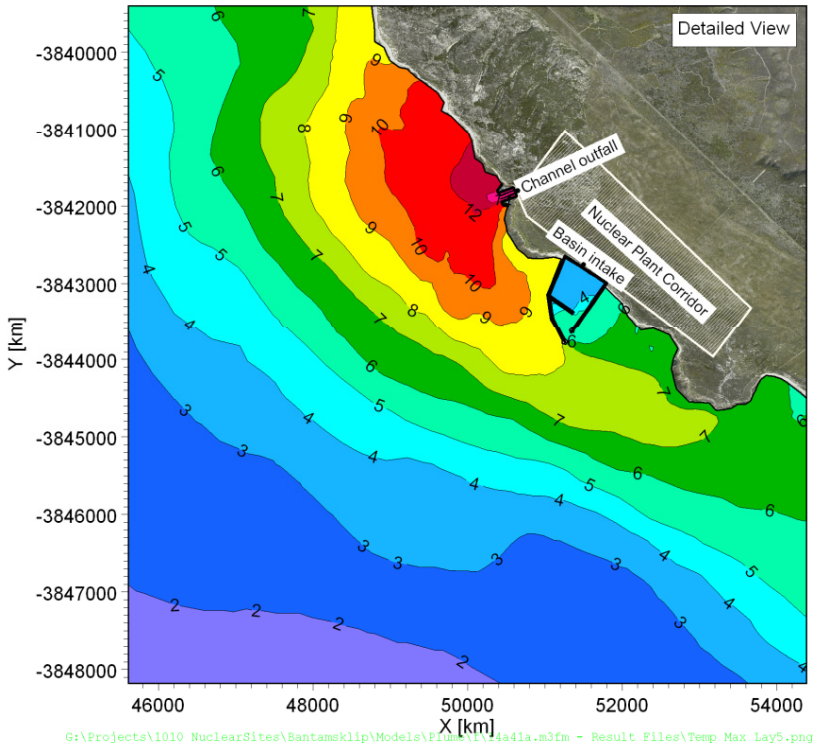

G:\Projects\1010_NuclearSites\Bantamsklip\Models\Plume\T14a41a.m3fm - Result Files\Temp_Max_Lay5.png

Maximum Increase in Temperature Near Seabed

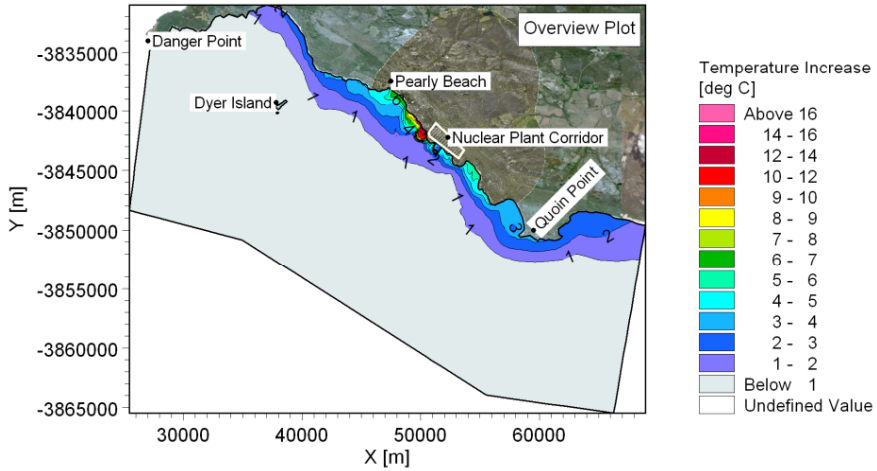

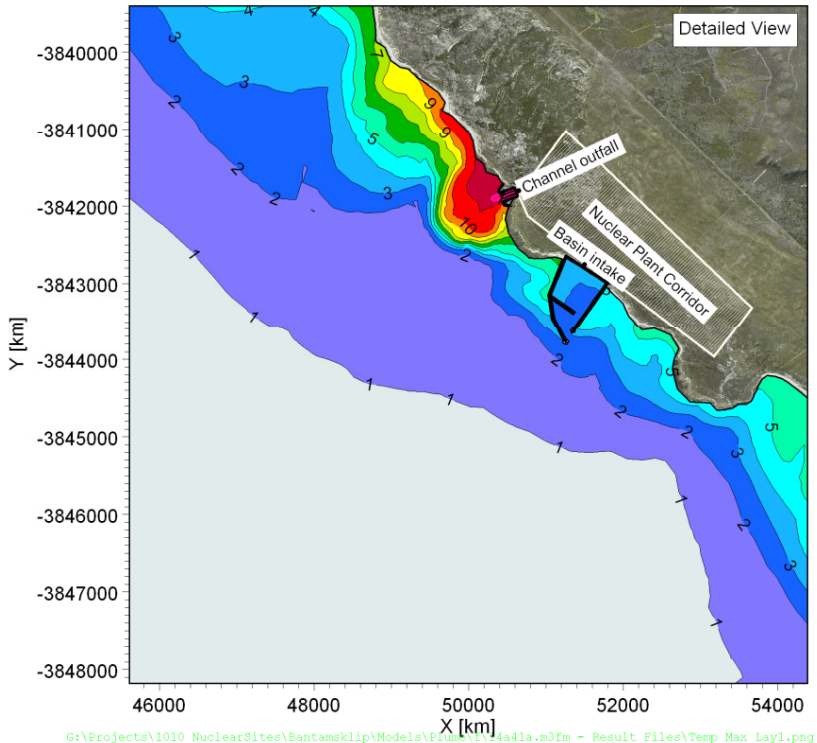

G:\Projects\1010_NuclearSites\Bantamsklip\Models\Plume\T14a41a.m3fm - Result Files\Temp_Max_Lay1.png

Title: **Thermal plume modelling: Maximum increase in temperature due to power station. Layout 4: Basin intake and nearshore channel outfall (2 m depth). Power output: 10 000 MWe.**

Figure No. **9.18**

Mean Increase in Temperature Near Water Surface

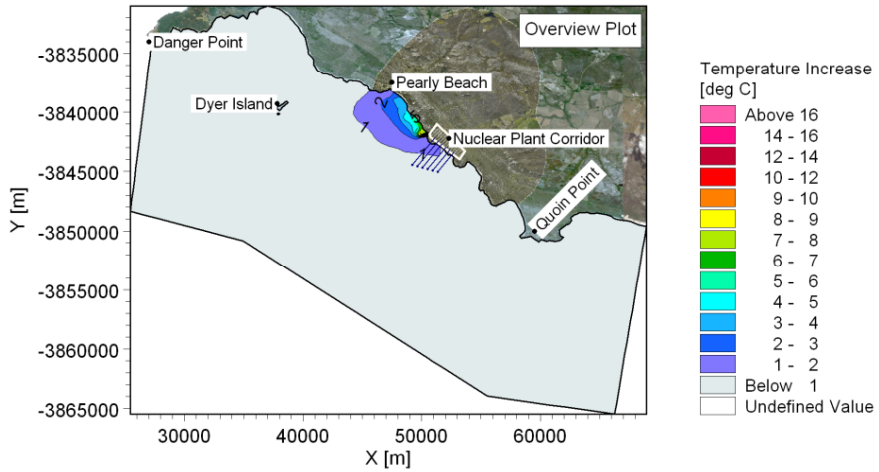

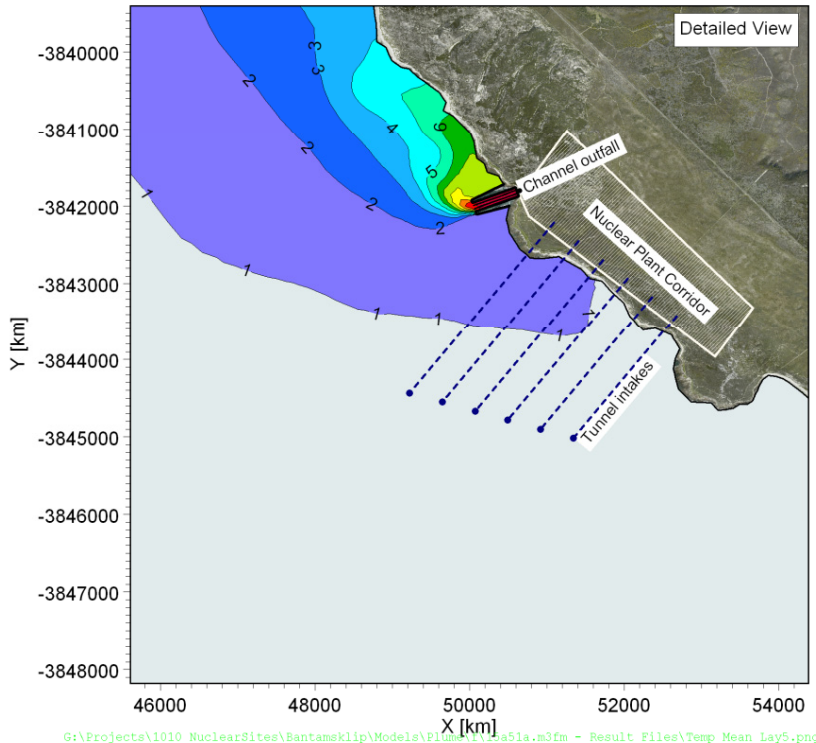

G:\Projects\1010_NuclearSites\Bantamsklip\Models\Plume\1_5a51a.m3fm - Result Files\Temp_Mean_Lay5.png

Mean Increase in Temperature Near Seabed

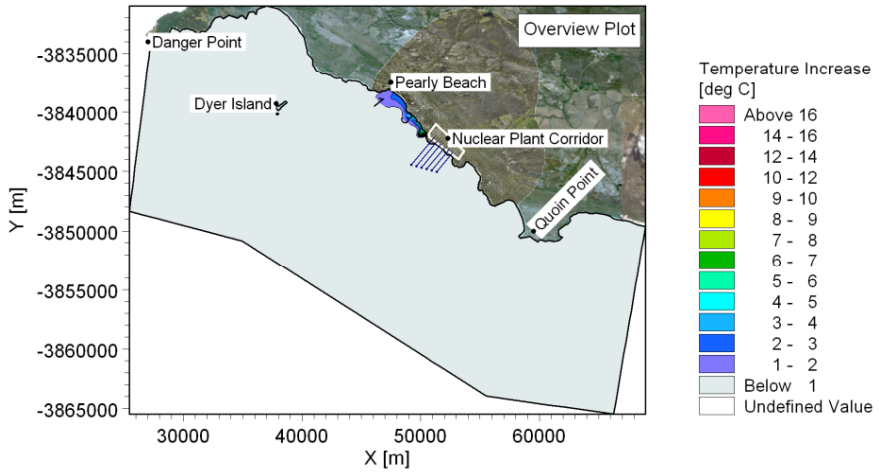

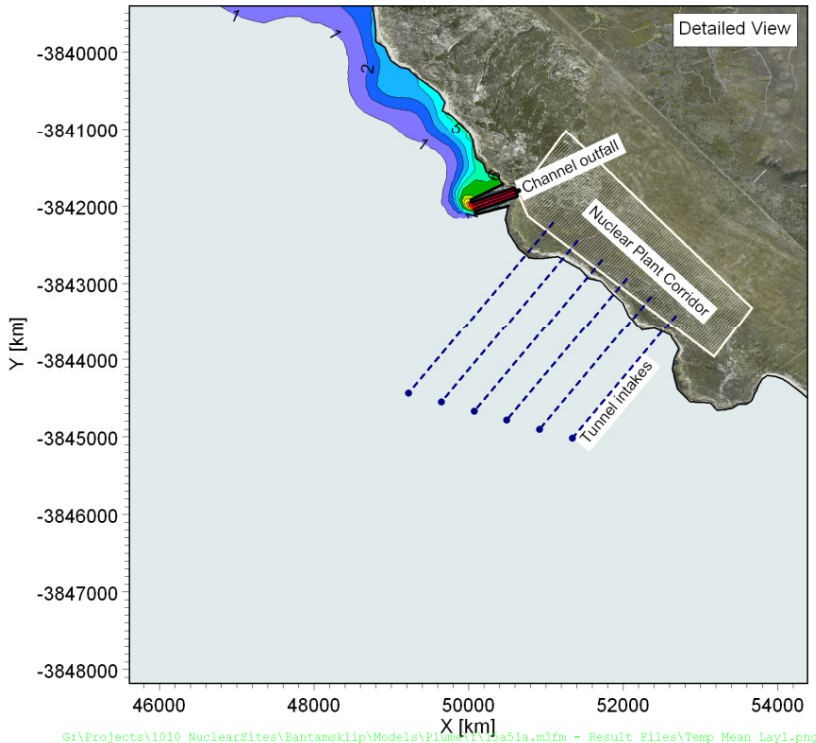

G:\Projects\1010_NuclearSites\Bantamsklip\Models\Plume\1_5a51a.m3fm - Result Files\Temp_Mean_Lay1.png

Title: **Thermal plume modelling: Mean increase in temperature due to power station. Layout 5: Offshore tunnel intake (30 m depth) and nearshore channel outfall (5 m depth). Power output: 10 000 MWe.**

Figure No. **9.19**

Maximum Increase in Temperature Near Water Surface

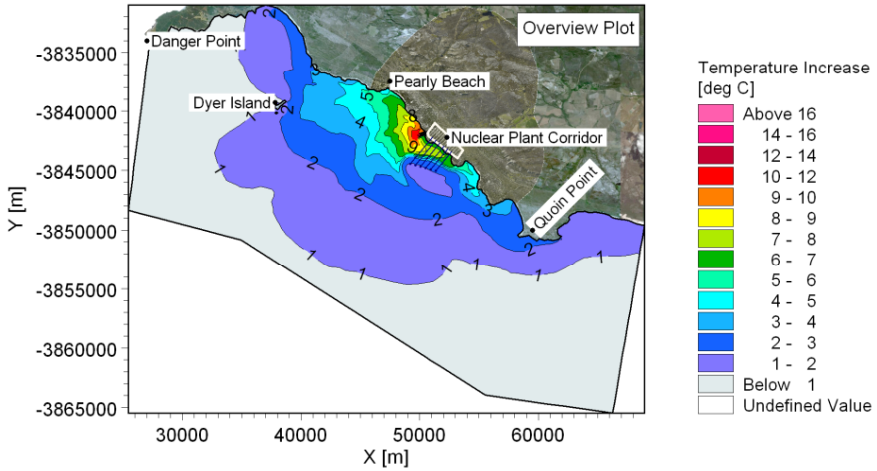

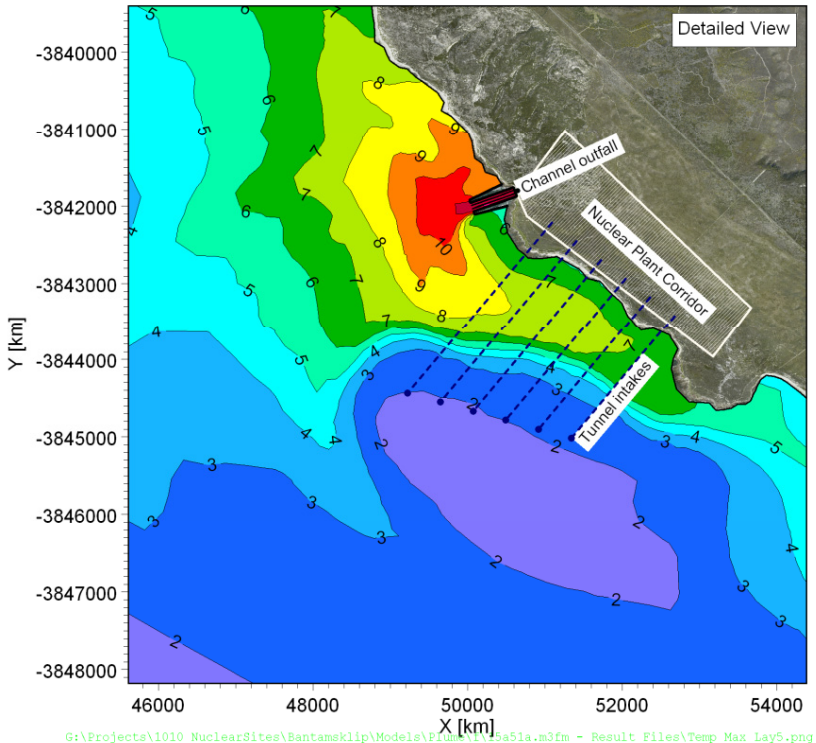

G:\Projects\1010_NuclearSites\Bantamsklip\Models\Plume\T15a51a.m3fm - Result Files\Temp_Max_Lay5.png

Maximum Increase in Temperature Near Seabed

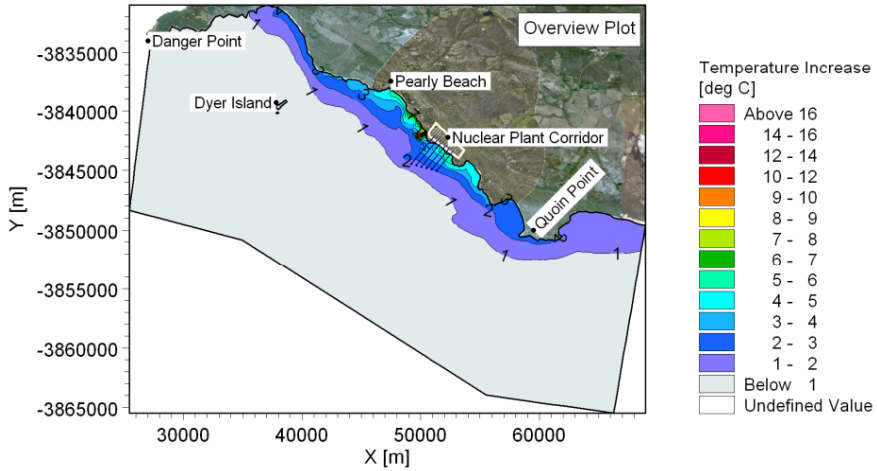

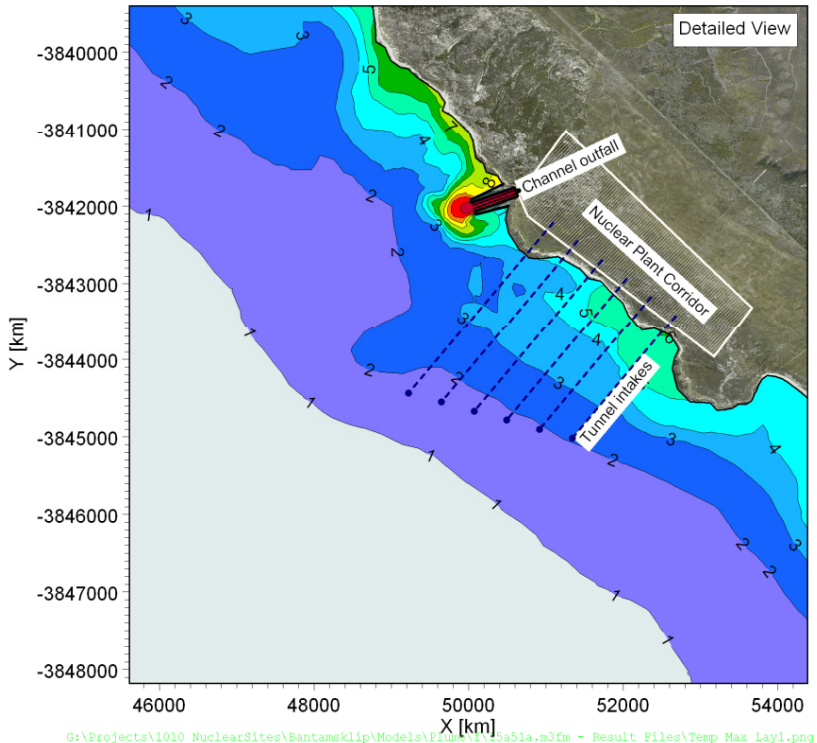

G:\Projects\1010_NuclearSites\Bantamsklip\Models\Plume\T15a51a.m3fm - Result Files\Temp_Max_Lay1.png

Title: **Thermal plume modelling: Maximum increase in temperature due to power station. Layout 5: Offshore tunnel intake (30 m depth) and nearshore channel outfall (5 m depth). Power output: 10 000 MWe.**

Figure No. **9.20**

Mean Increase in Temperature Near Water Surface

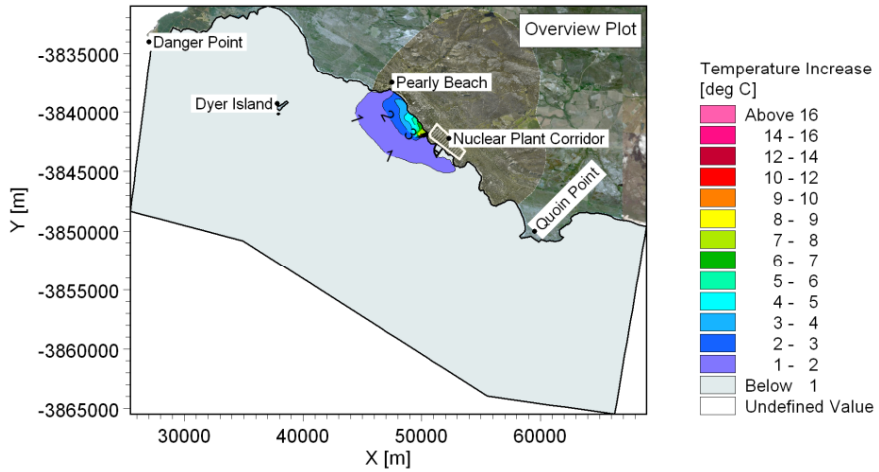

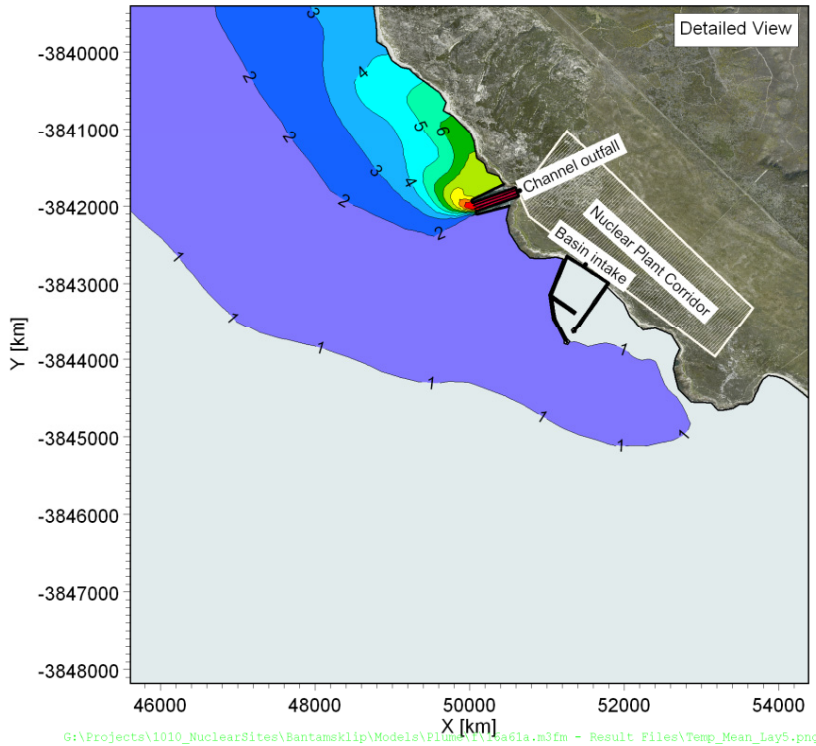

G:\Projects\1010_NuclearSites\Bantamsklip\Models\Plume\1_2a61a.m3fm - Result Files\Temp_Mean_Lay5.png

Mean Increase in Temperature Near Seabed

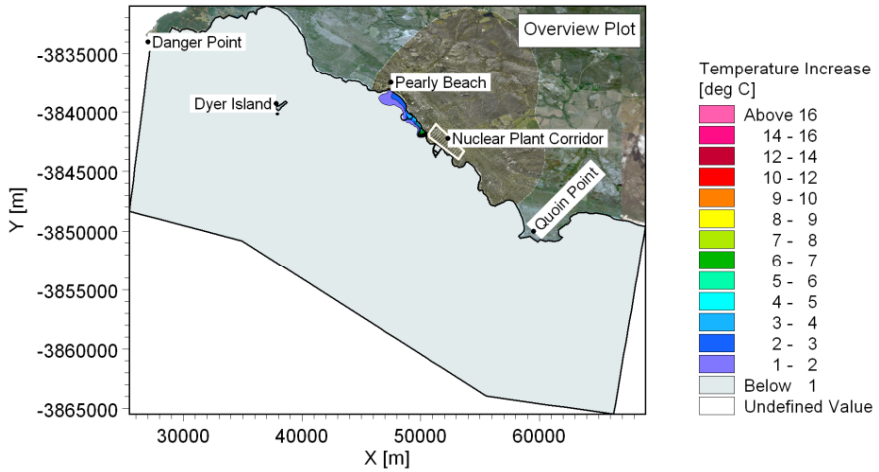

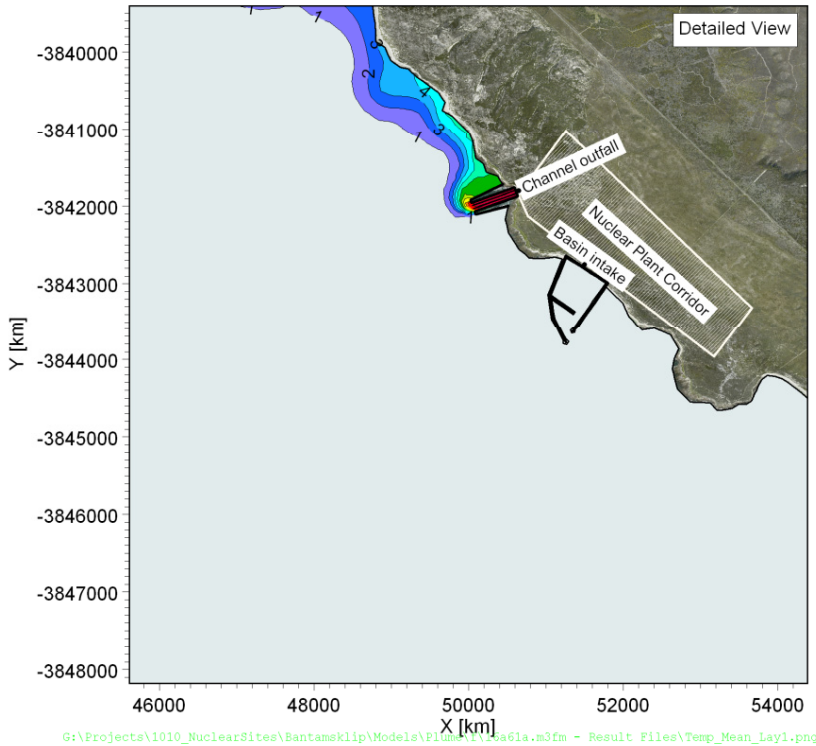

G:\Projects\1010_NuclearSites\Bantamsklip\Models\Plume\1_2a61a.m3fm - Result Files\Temp_Mean_Lay1.png

Title: **Thermal plume modelling: Mean increase in temperature due to power station. Layout 6: Basin intake and nearshore channel outfall (5 m depth). Power output: 10 000 MWe.**

Figure No. **9.21**

Maximum Increase in Temperature Near Water Surface

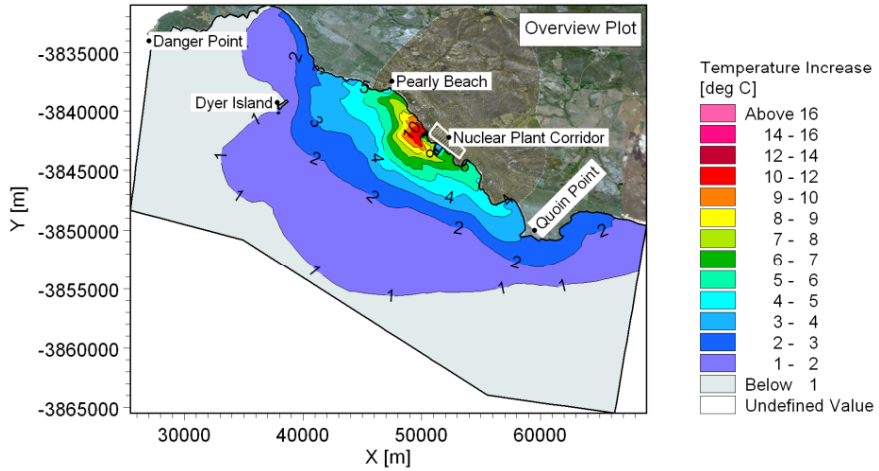

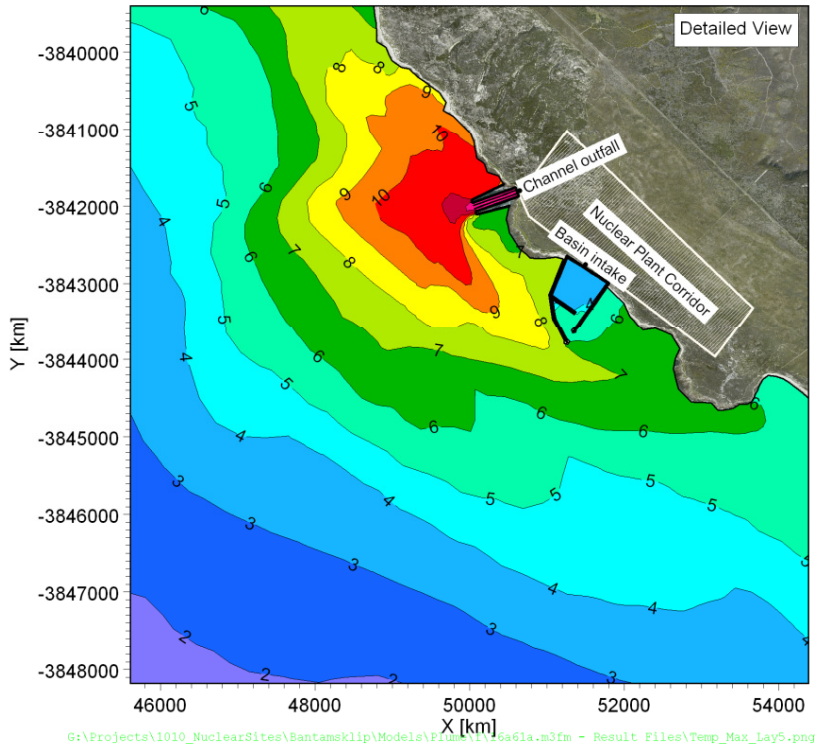

G:\Projects\1010_NuclearSites\Bantamsklip\Models\Plume\T16a61a.m3fm - Result Files\Temp_Max_Lay5.png

Maximum Increase in Temperature Near Seabed

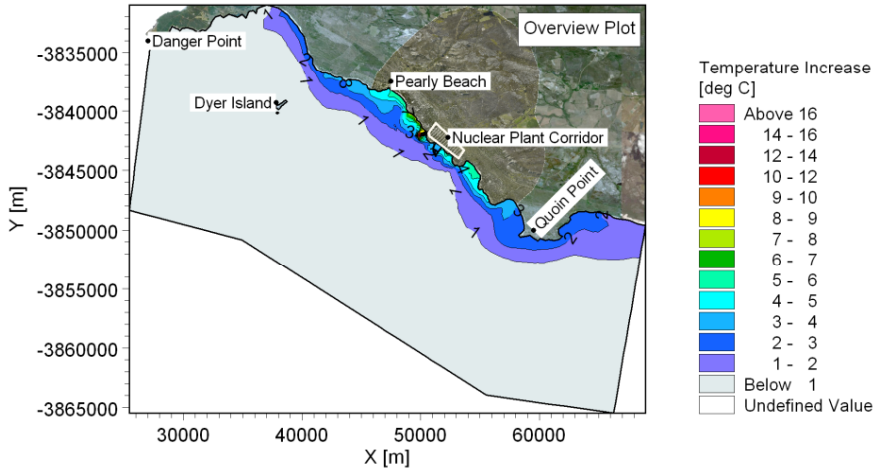

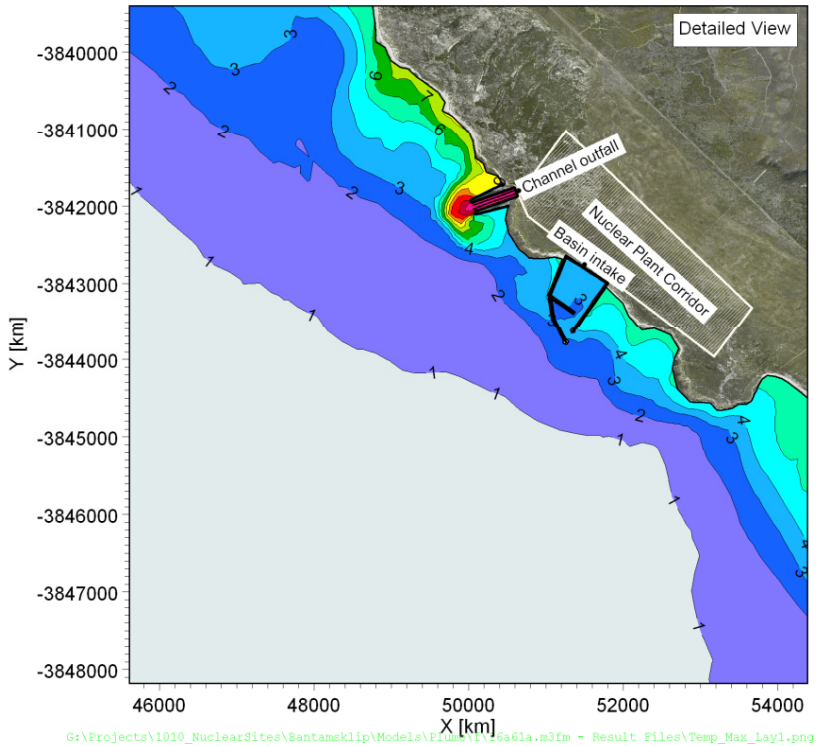

G:\Projects\1010_NuclearSites\Bantamsklip\Models\Plume\T16a61a.m3fm - Result Files\Temp_Max_Lay1.png

Title: **Thermal plume modelling: Maximum increase in temperature due to power station. Layout 6: Basin intake and nearshore channel outfall (5 m depth). Power output: 10 000 MWe.**

Figure No. **9.22**

Mean Increase in Temperature Near Water Surface

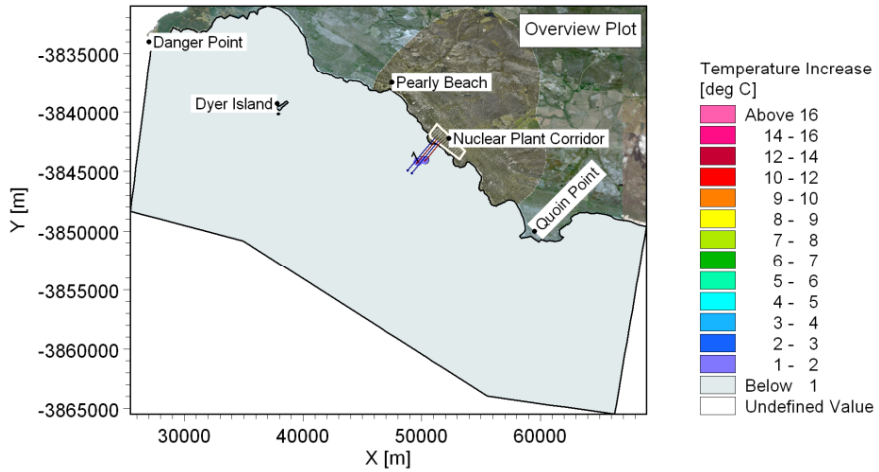

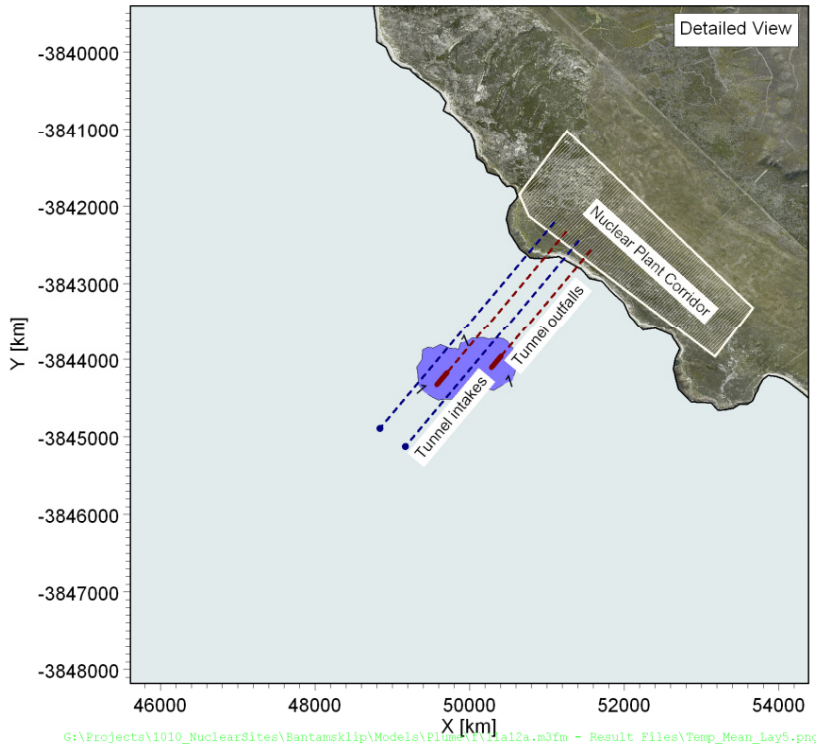

G:\Projects\1010_NuclearSites\Bantamsklip\Models\Plume\Ba12a.m3fm - Result Files\Temp_Mean_Lay5.png

Mean Increase in Temperature Near Seabed

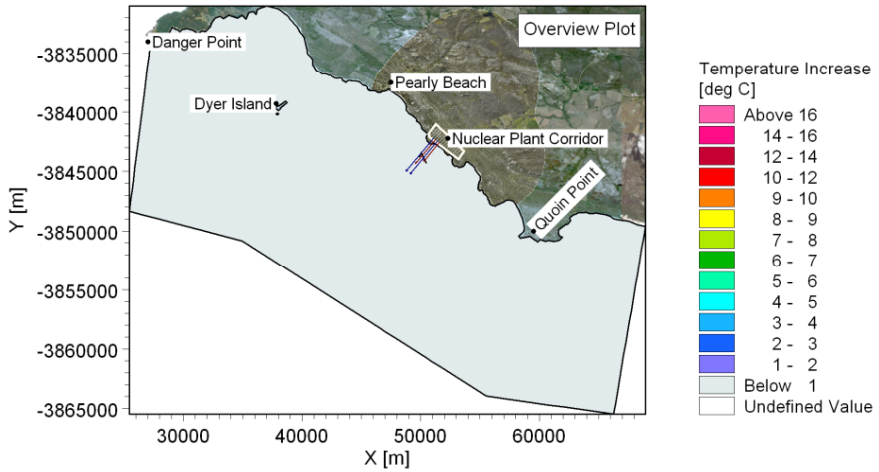

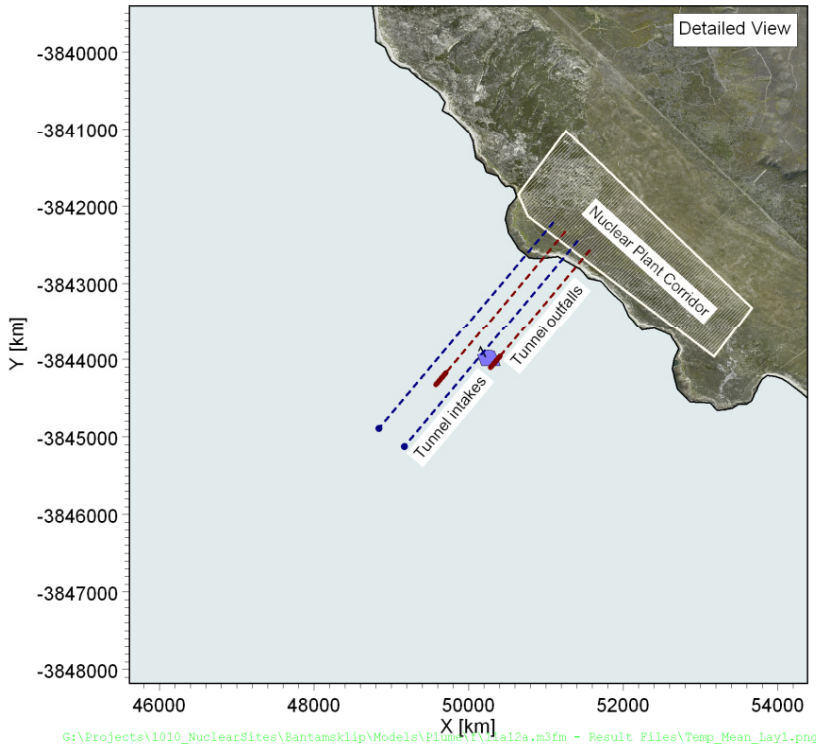

G:\Projects\1010_NuclearSites\Bantamsklip\Models\Plume\Ba12a.m3fm - Result Files\Temp_Mean_Lay1.png

Title: **Thermal plume modelling: Mean increase in temperature due to power station. Layout 1: Offshore tunnel intake (45 m depth) and offshore tunnel outfall (25 m depth). Power output: 4000 MWe.**

Figure No. **9.23**

Maximum Increase in Temperature Near Water Surface

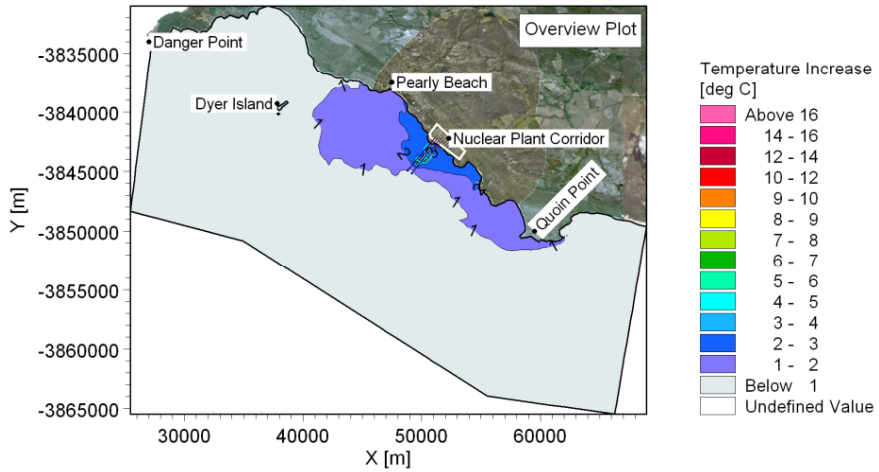

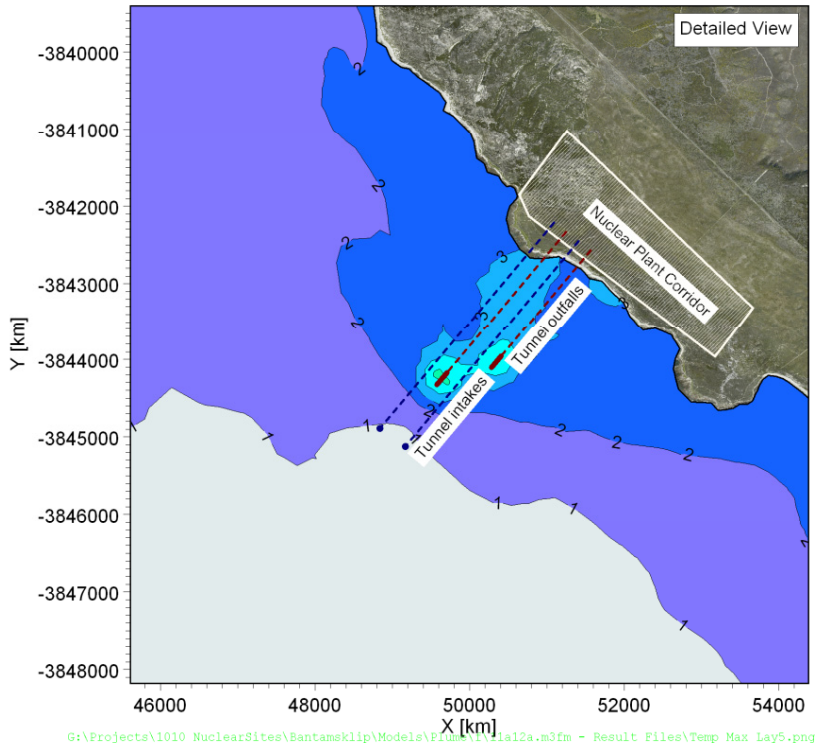

G:\Projects\1010_NuclearSites\Bantamsklip\Models\Plume\T1a1a12a.m3fm - Result Files\Temp_Max_Lay5.png

Maximum Increase in Temperature Near Seabed

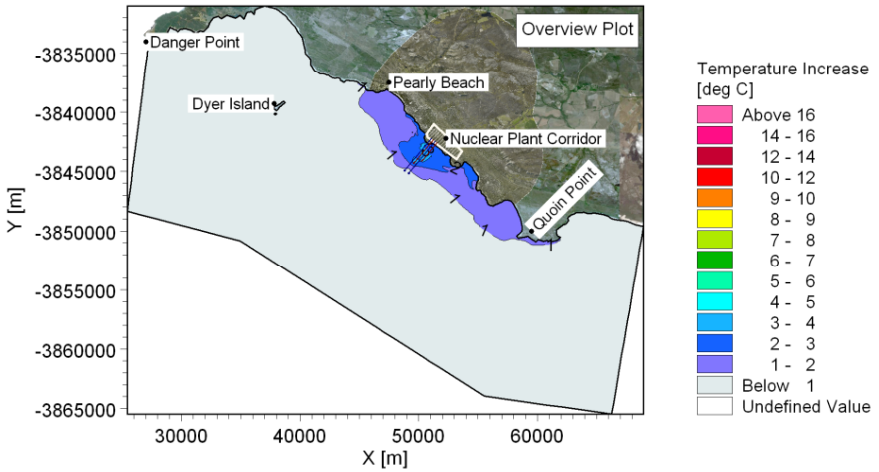

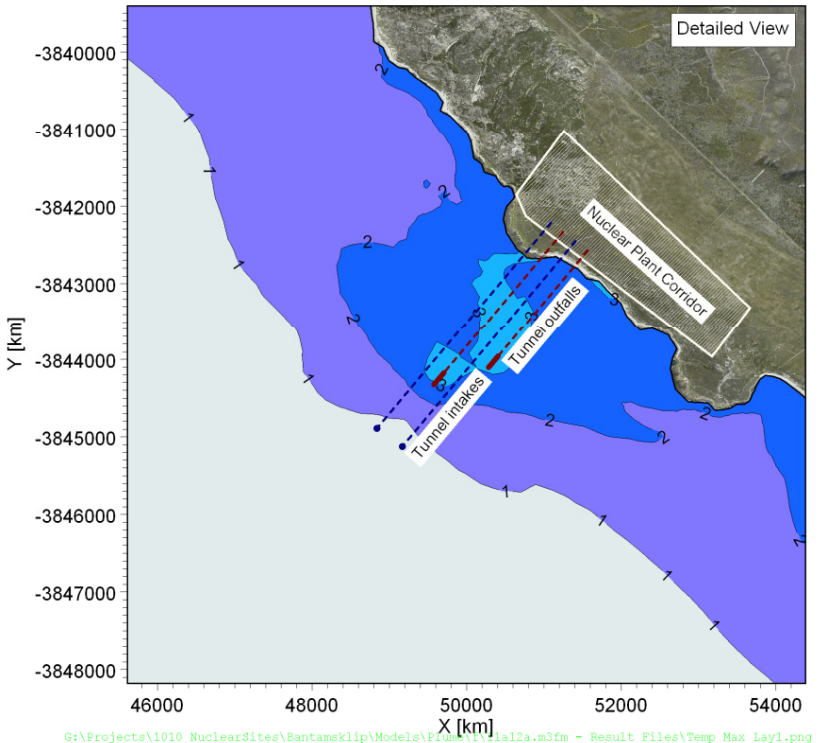

G:\Projects\1010_NuclearSites\Bantamsklip\Models\Plume\T1a1a12a.m3fm - Result Files\Temp_Max_Lay1.png

Title: **Thermal plume modelling: Maximum increase in temperature due to power station. Layout 1: Offshore tunnel intake (45 m depth) and offshore tunnel outfall (25 m depth). Power output: 4000 MWe.**

Figure No. **9.24**

Mean Increase in Temperature Near Water Surface

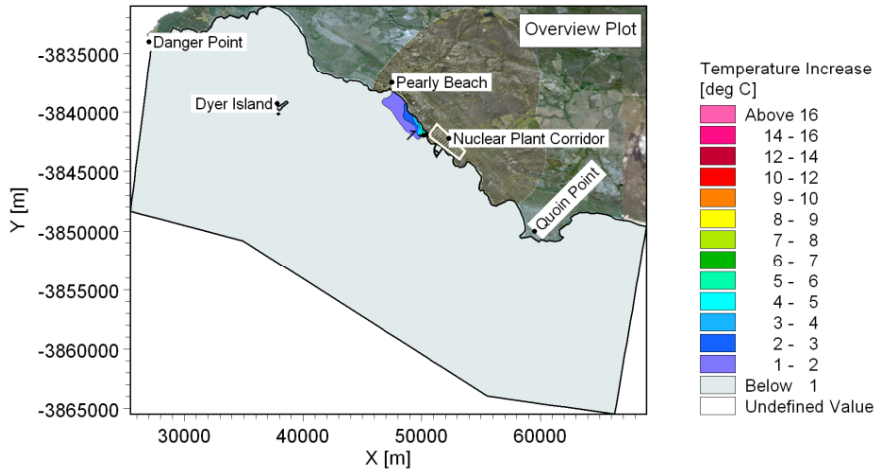

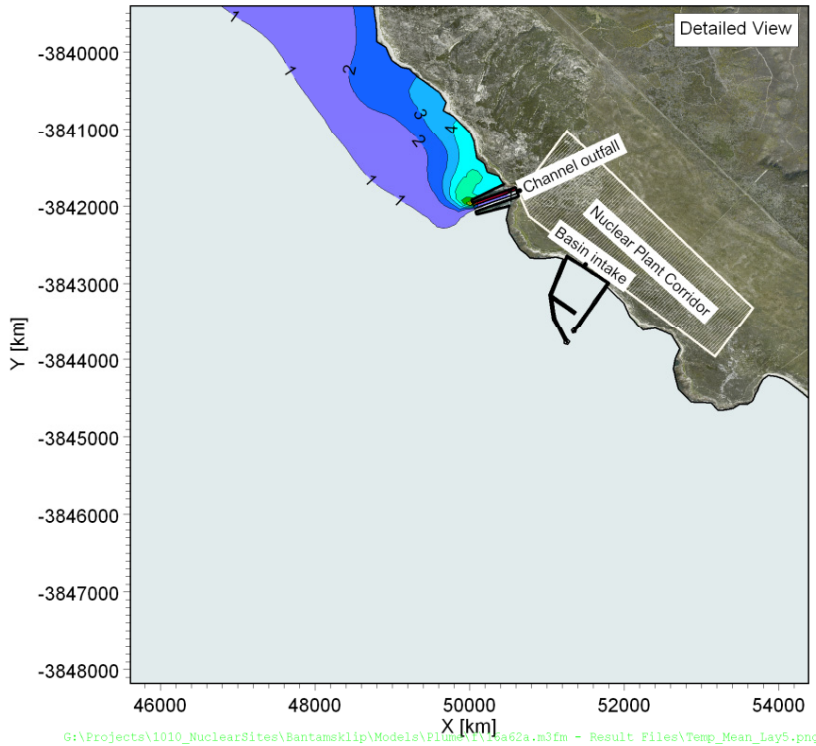

G:\Projects\1010_NuclearSites\Bantamsklip\Models\Plume\1_2a62a.m3fm - Result Files\Temp_Mean_Lay5.png

Mean Increase in Temperature Near Seabed

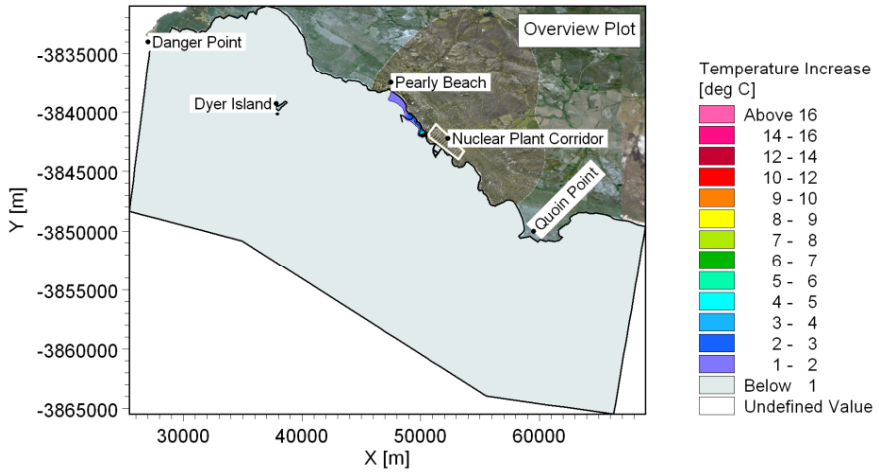

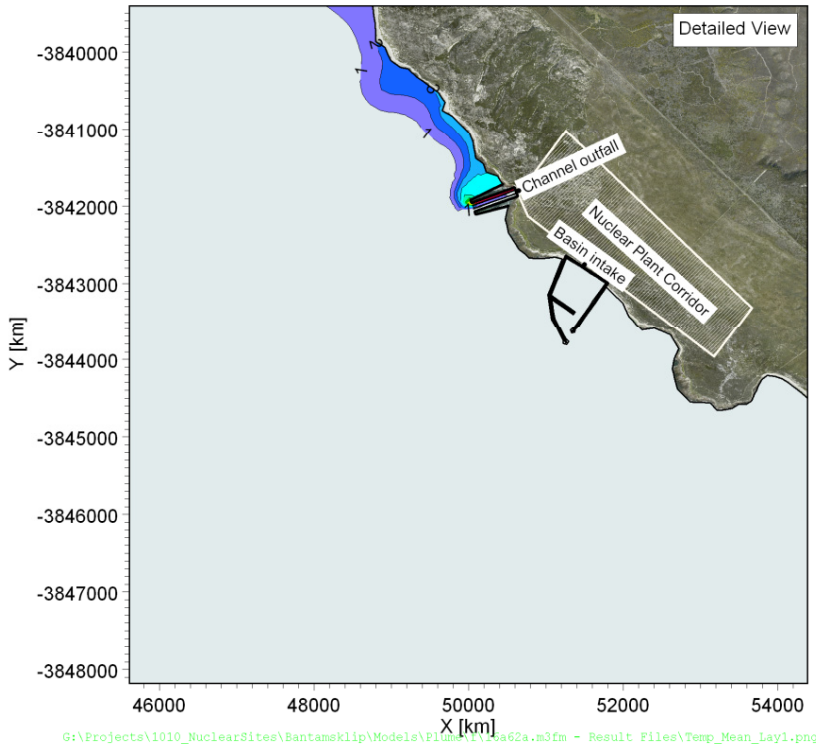

G:\Projects\1010_NuclearSites\Bantamsklip\Models\Plume\1_2a62a.m3fm - Result Files\Temp_Mean_Lay1.png

Title: **Thermal plume modelling: Mean increase in temperature due to power station. Layout 6: Basin intake and nearshore channel outfall (5 m depth). Power output: 4000 MWe.**

Figure No. **9.25**

Maximum Increase in Temperature Near Water Surface

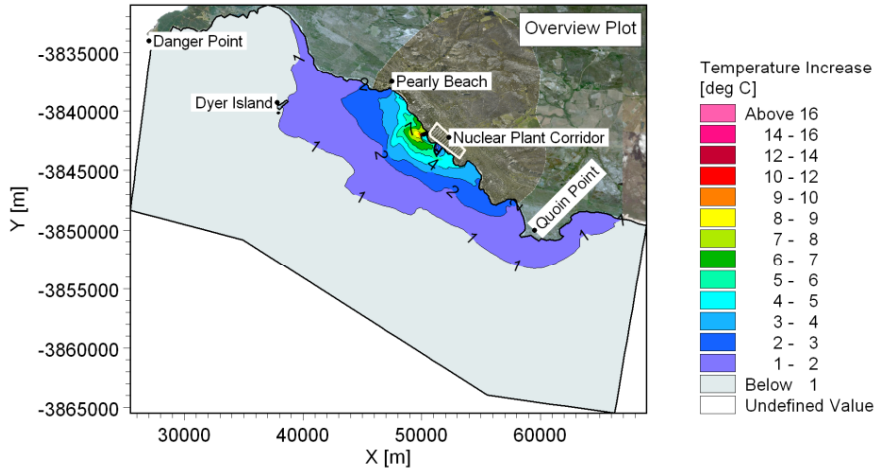

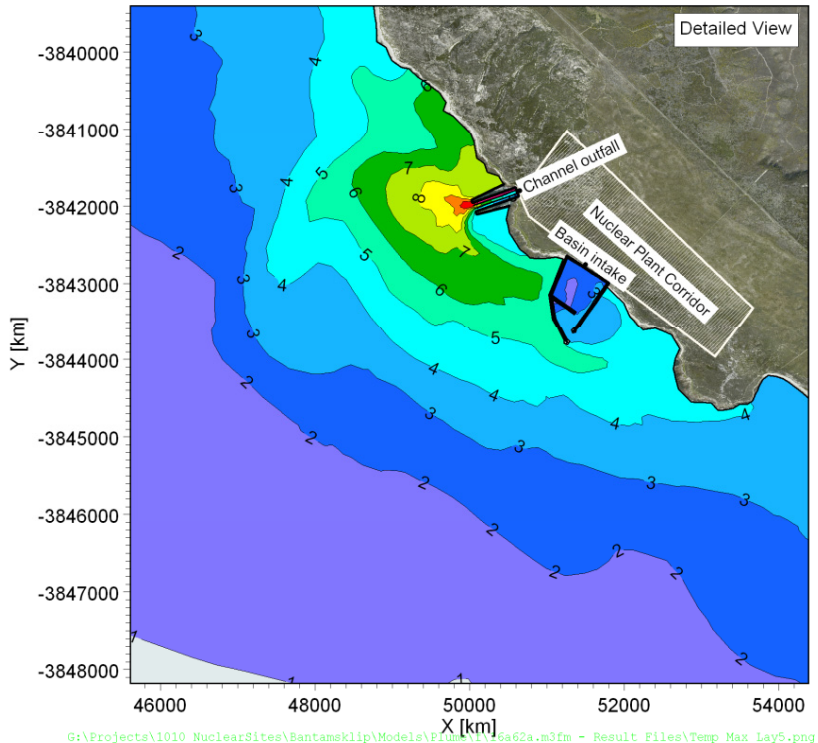

G:\Projects\1010_NuclearSites\Bantamsklip\Models\Plume\1156a62a.m3fm - Result Files\Temp_Max_Lay5.png

Maximum Increase in Temperature Near Seabed

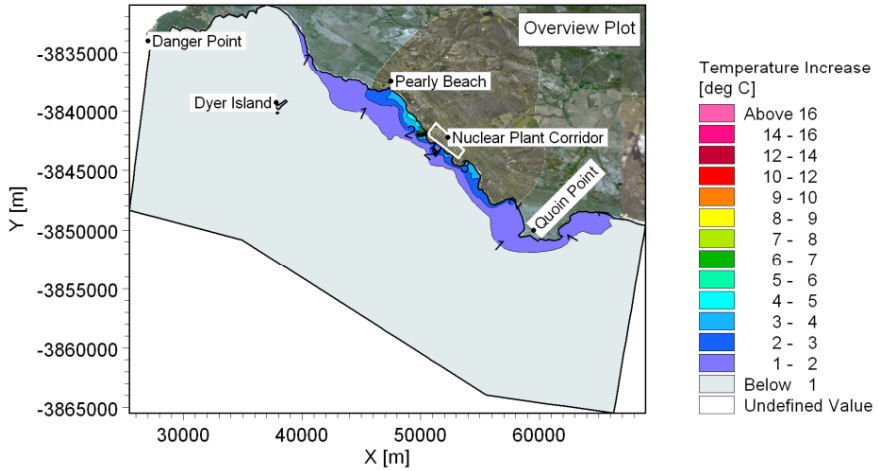

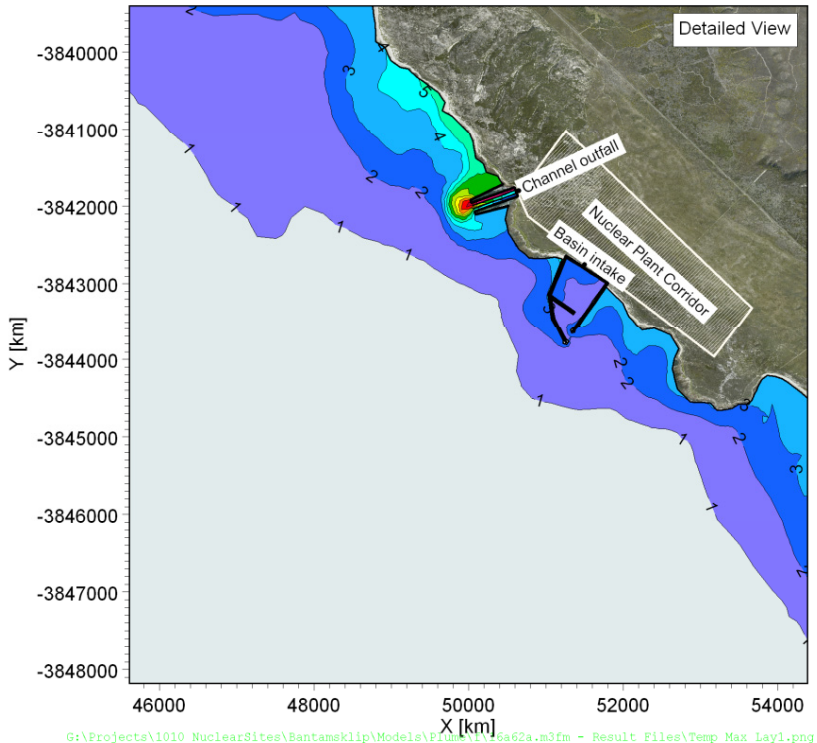

G:\Projects\1010_NuclearSites\Bantamsklip\Models\Plume\1156a62a.m3fm - Result Files\Temp_Max_Lay1.png

Title: **Thermal plume modelling: Maximum increase in temperature due to power station. Layout 6: Basin intake and nearshore channel outfall (5 m depth). Power output: 4000 MWe.**

Figure No. **9.26**

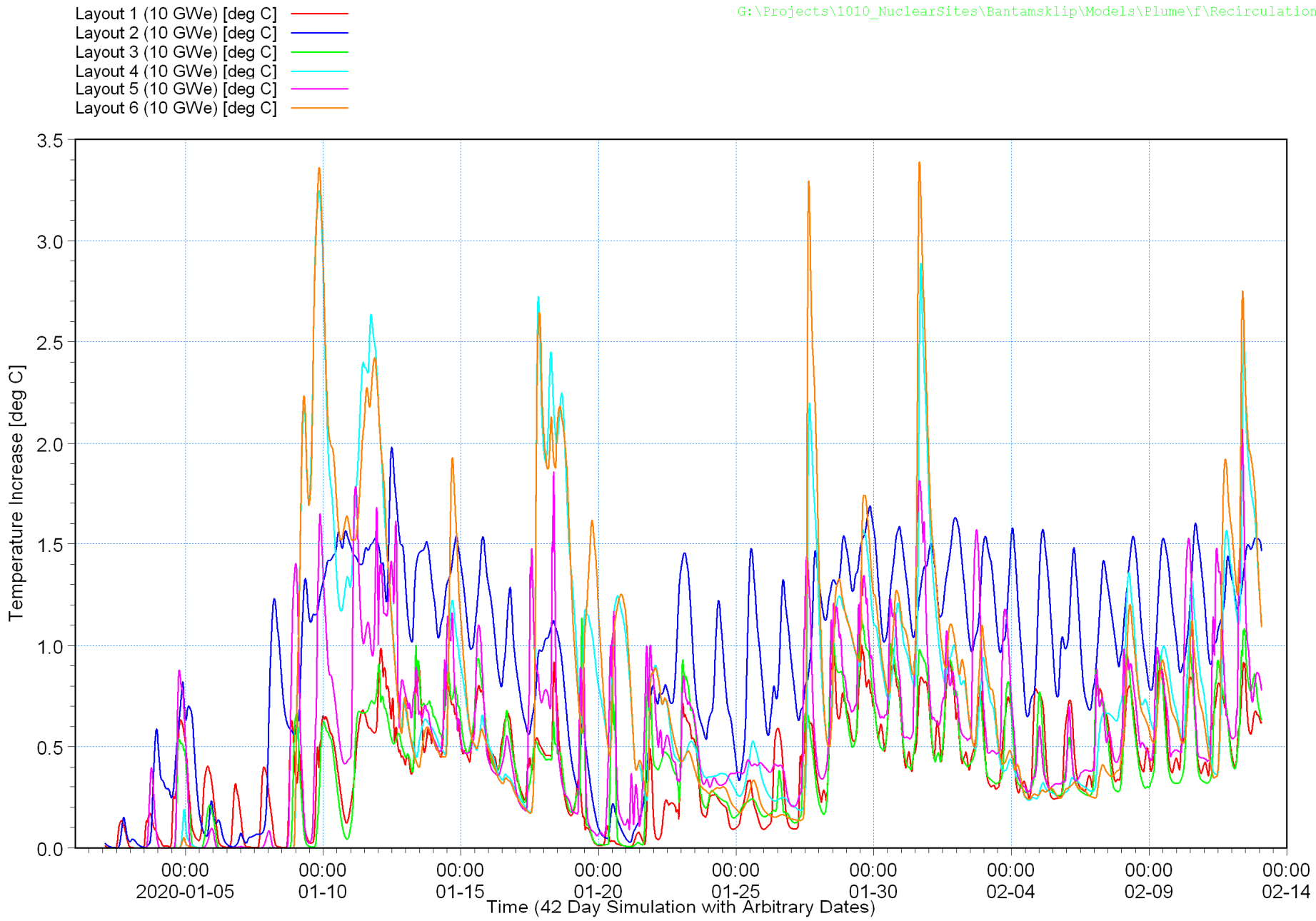

Title:

Thermal plume modelling: time-series of recirculation results showing the increase in temperature at the intakes for the various layouts and power outputs modelled.

Figure No.

9.27

G:\Projects\1010_NuclearSites\Bantamsklip\Data\Lwandle\Sediment\Bantamsklip_D50.png

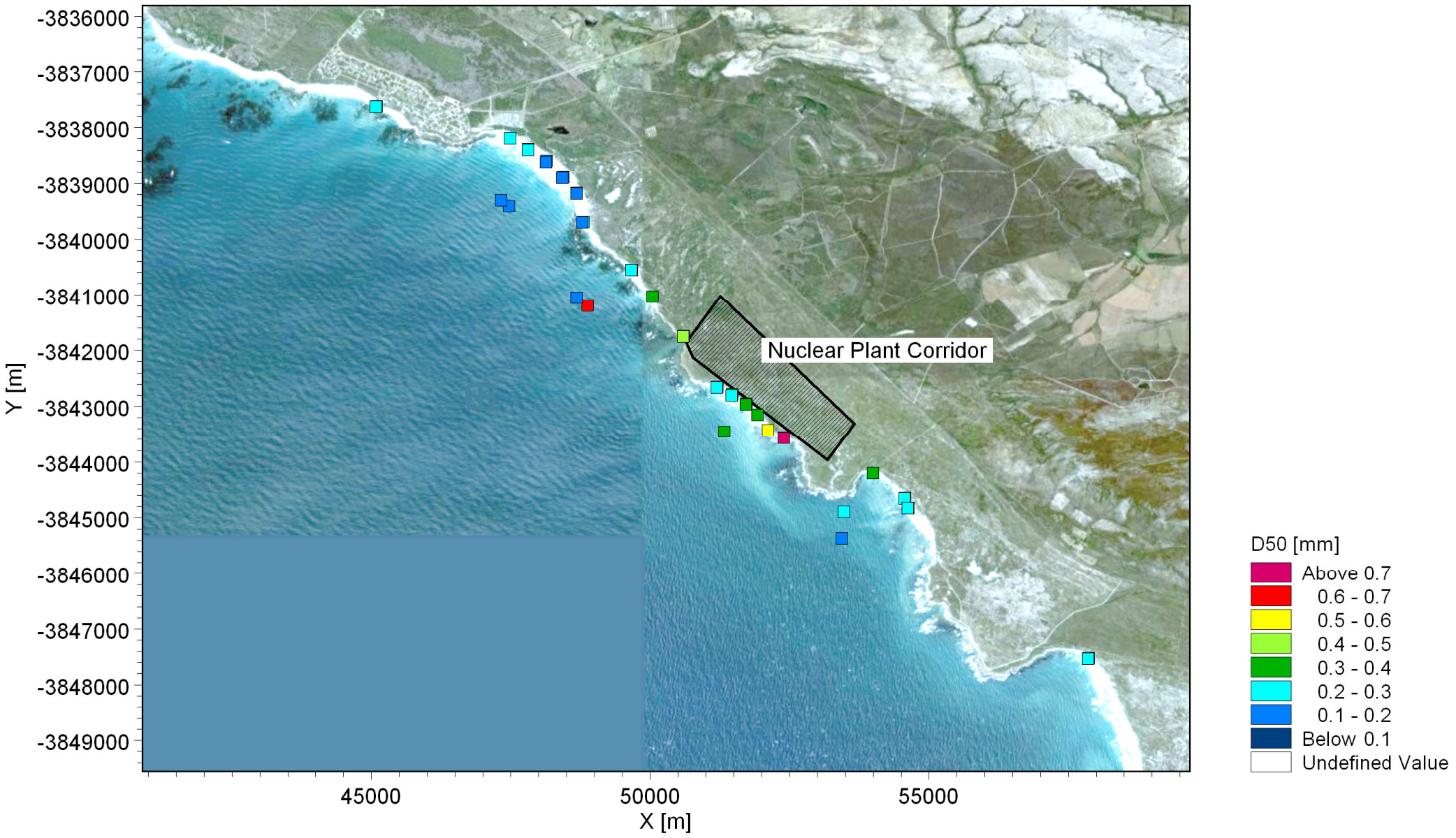

Title:

Sediment transport modelling.
Measured D_{50} grain size.

Figure No.

10.1

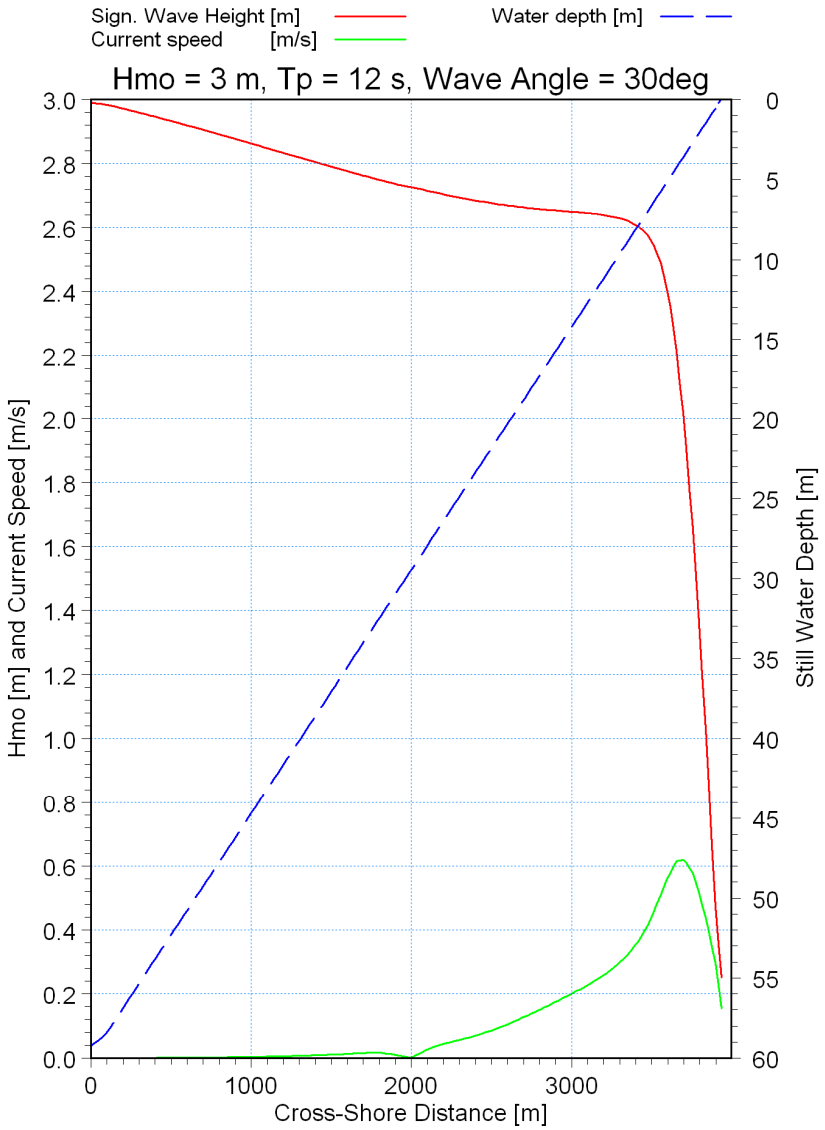

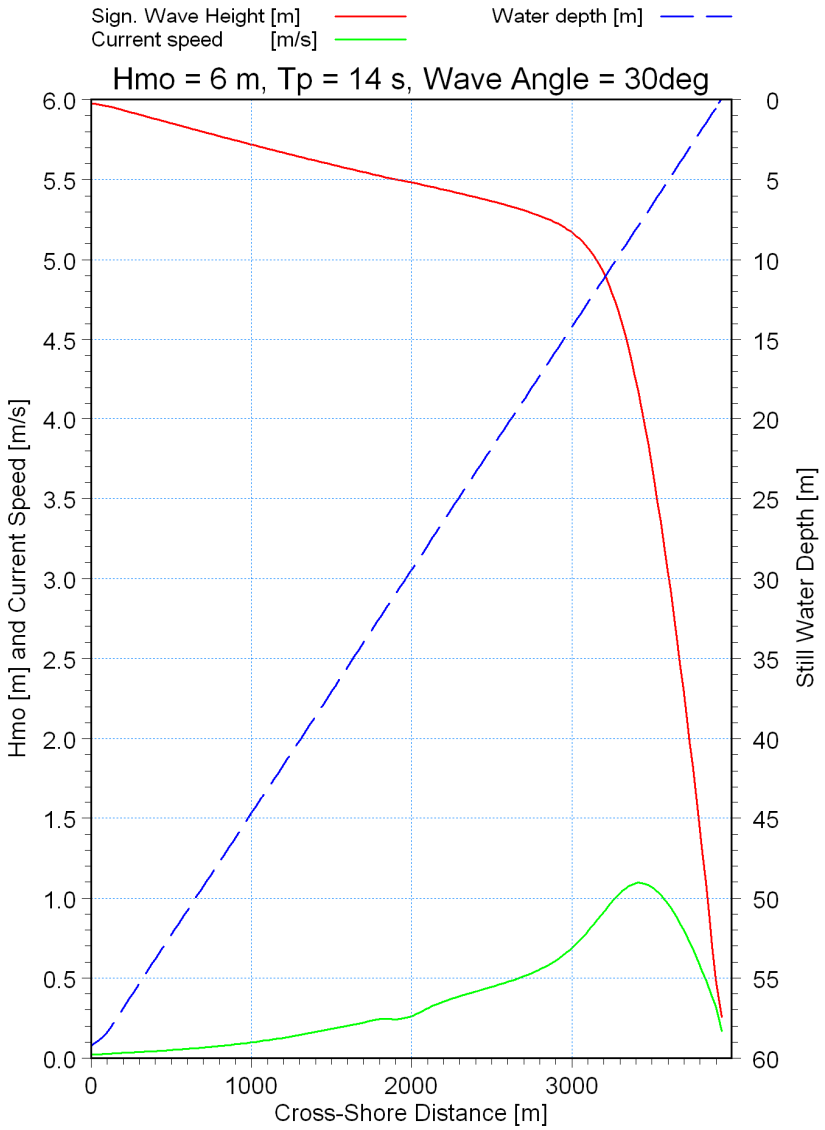

Title:

Sediment transport modelling.
Testing of wave and current modules in a simplified model comprising a uniform 1:67 beach slope with a wave approaching 30° from normal.

Figure No.
10.2

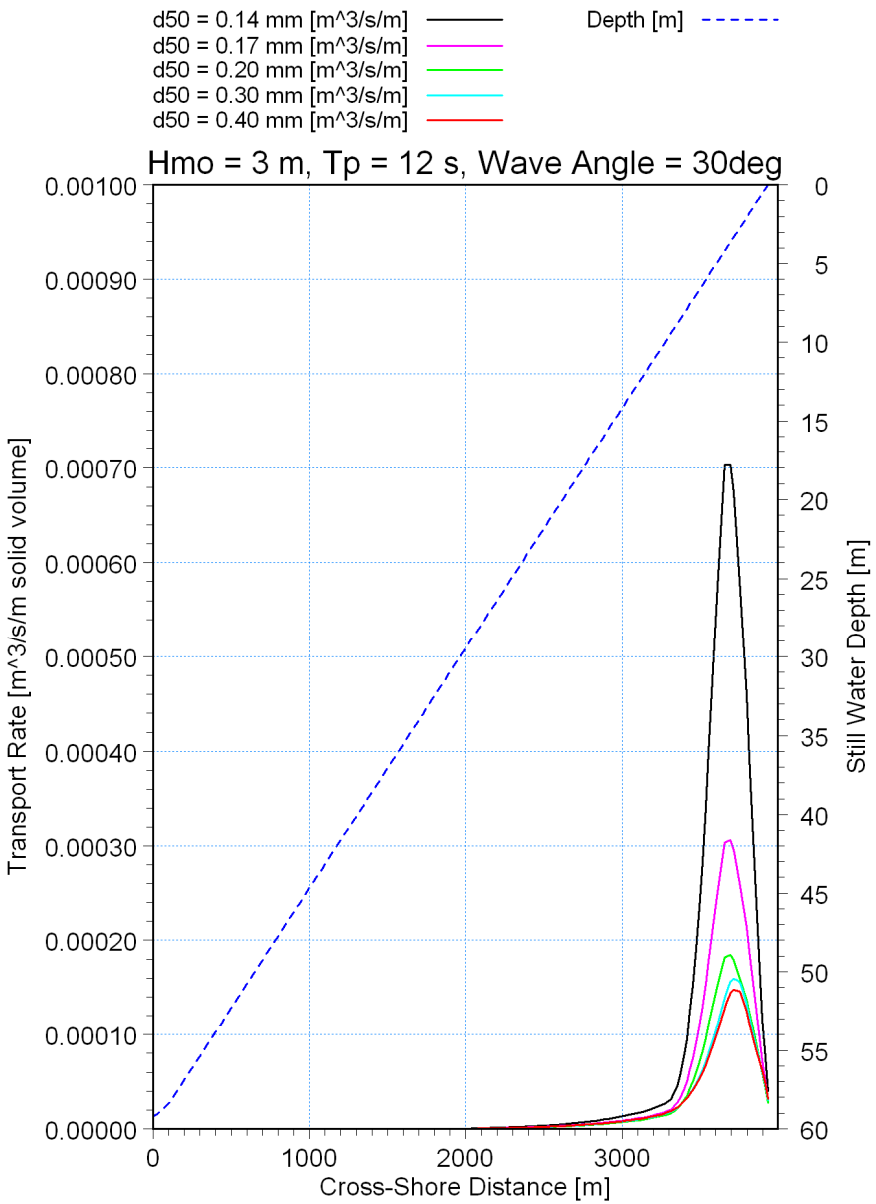

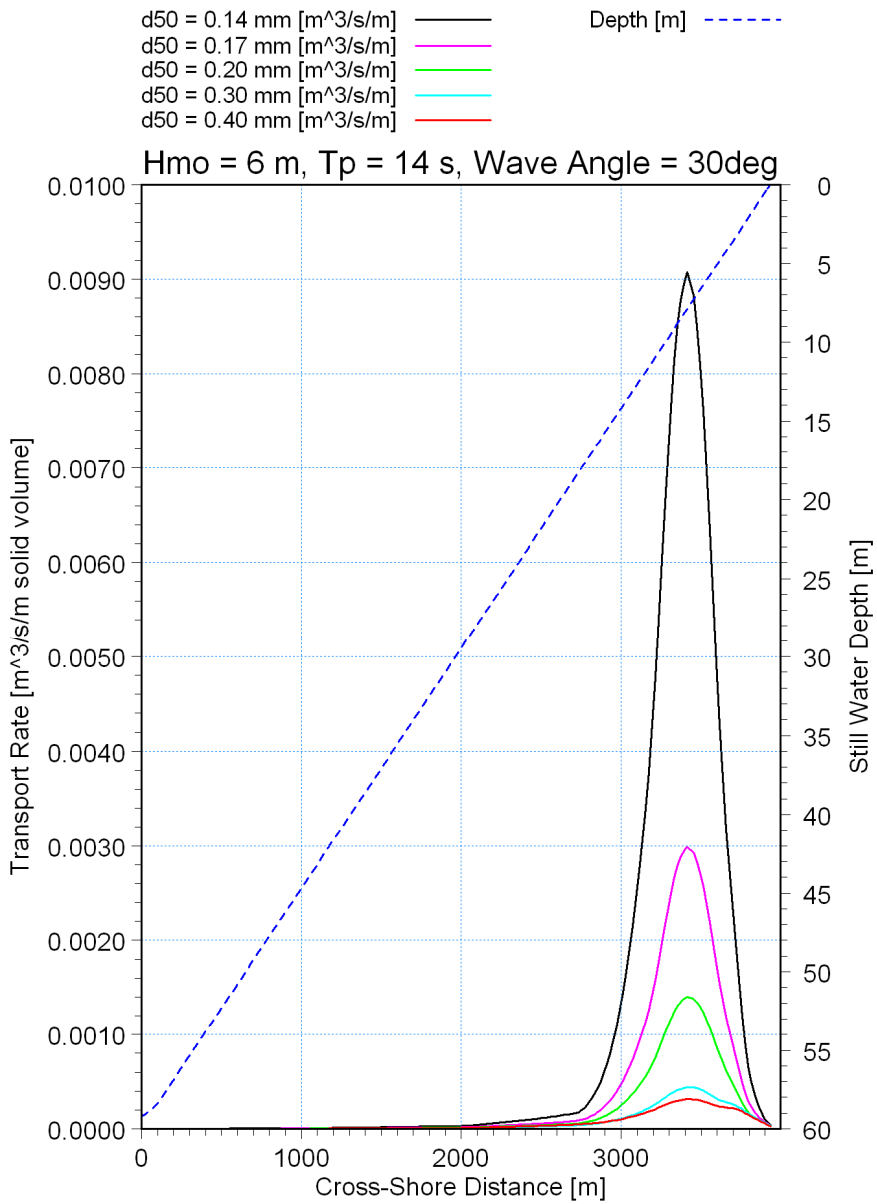

Title:

Sediment transport modelling.
Testing of the coupled wave, current and sediment transport model for a simplified case with a uniform 1:67 beach slope and a wave approaching 30° from normal.

Figure No.
10.3

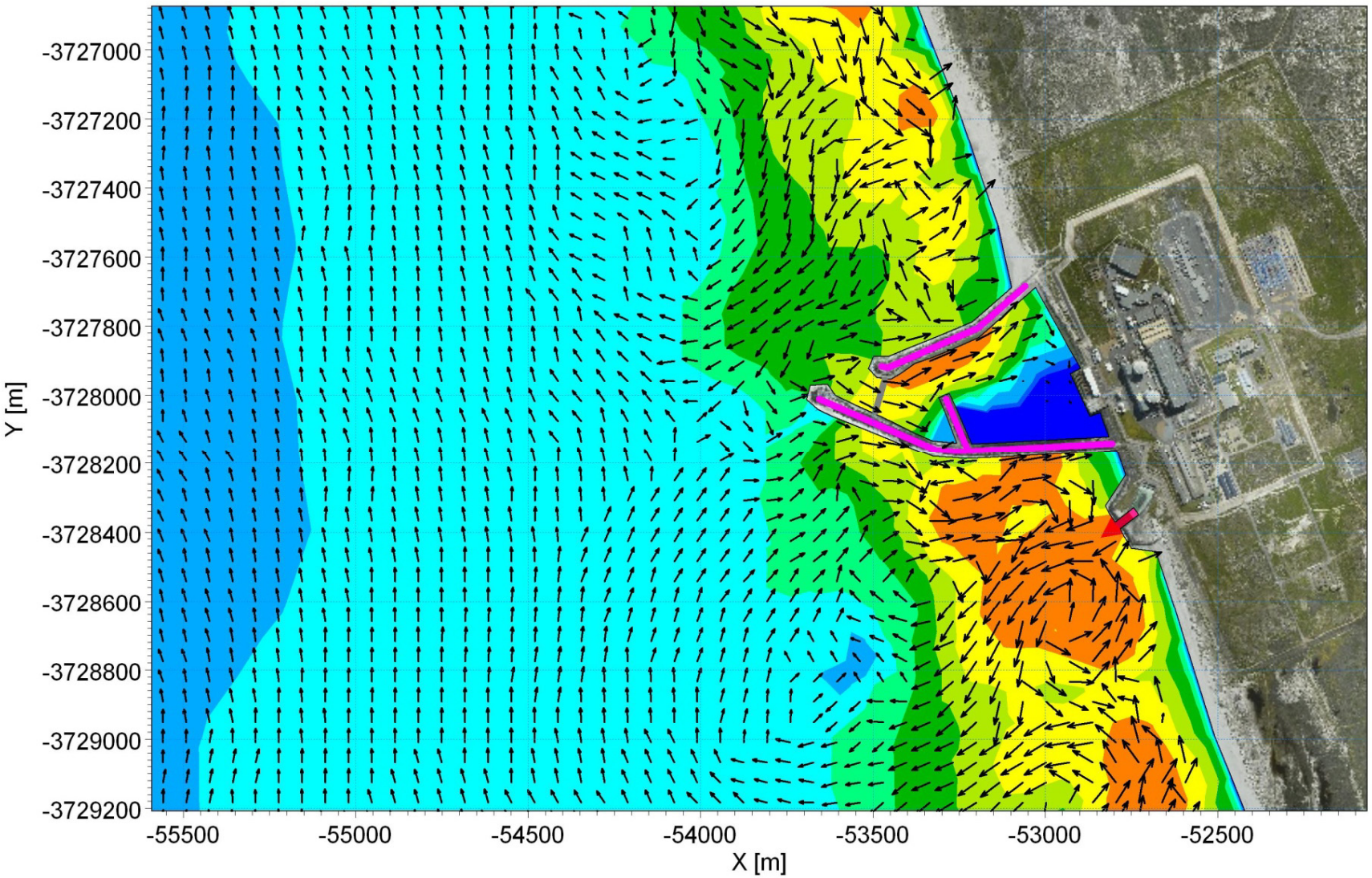

Both contour scale and vector length show sediment transport rates using a logarithmic scale.

Gray line across basin entrance used to estimate transport into basin.

Net Transport [m^3/year/m bulk volume]

- Above 20000
- 10000 - 20000
- 5000 - 10000
- 2000 - 5000
- 1000 - 2000
- 500 - 1000
- 200 - 500
- 100 - 200
- 50 - 100
- 20 - 50
- 10 - 20
- Below 10
- Undefined Value

Title:

Sediment transport modelling: Model calibration.
Sediment transport entering the intake basin at the existing Koeberg power station.

Figure No.

10.4

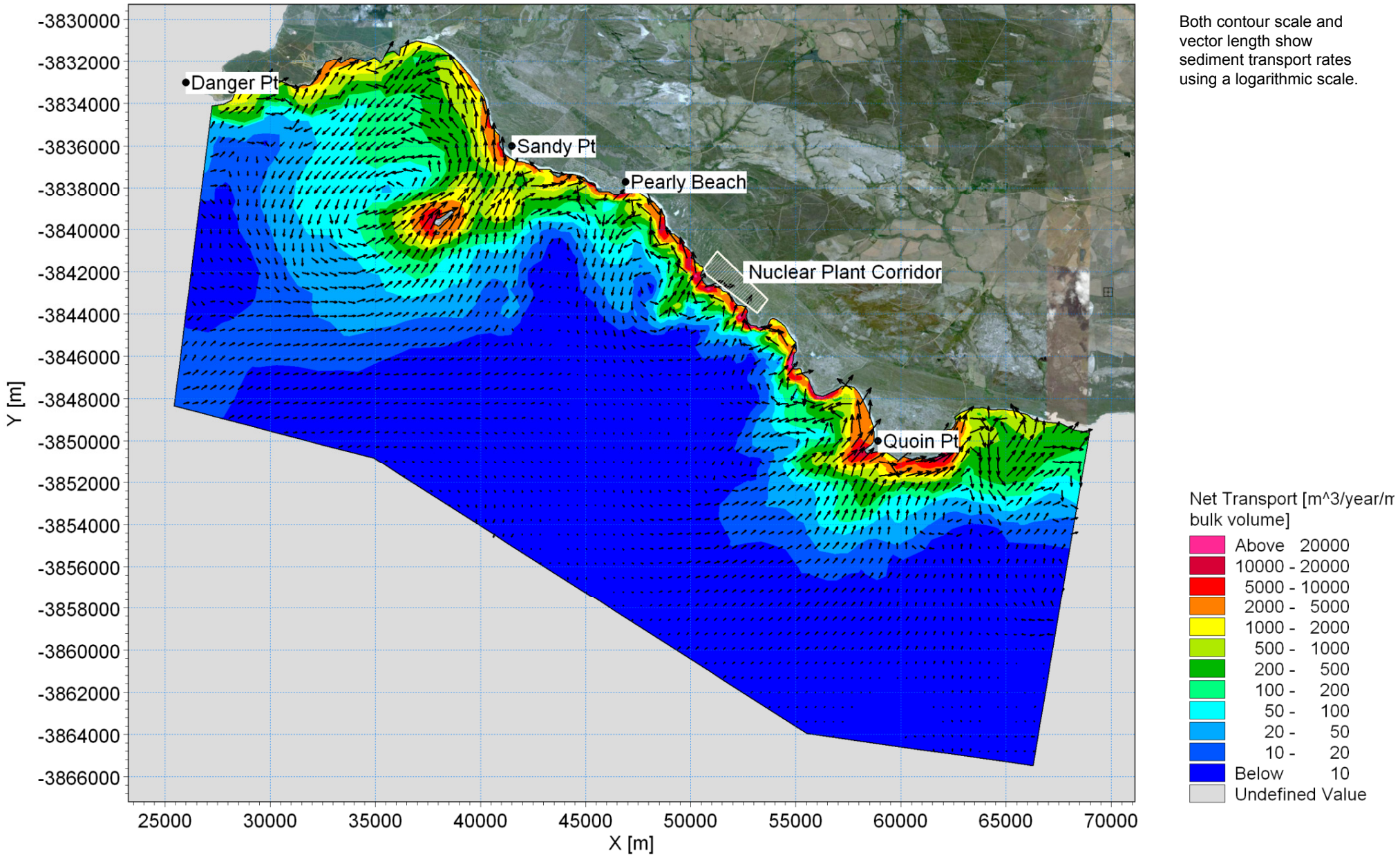

Both contour scale and vector length show sediment transport rates using a logarithmic scale.

Net Transport [m^3/year/m bulk volume]

Above	20000
10000 -	20000
5000 -	10000
2000 -	5000
1000 -	2000
500 -	1000
200 -	500
100 -	200
50 -	100
20 -	50
10 -	20
Below	10
Undefined Value	

G:\Projects\1010_NuclearSites\Bantamsklip\Models\Sediment2D\100b\Postprocess\AnnualTransport.png

Title: **Sediment transport modelling: Potential net sediment transport rate. Layout 1: Offshore tunnel intake and offshore tunnel outfall. D_{50} = 0.2 mm Overview plot.**

Figure No. **10.5**

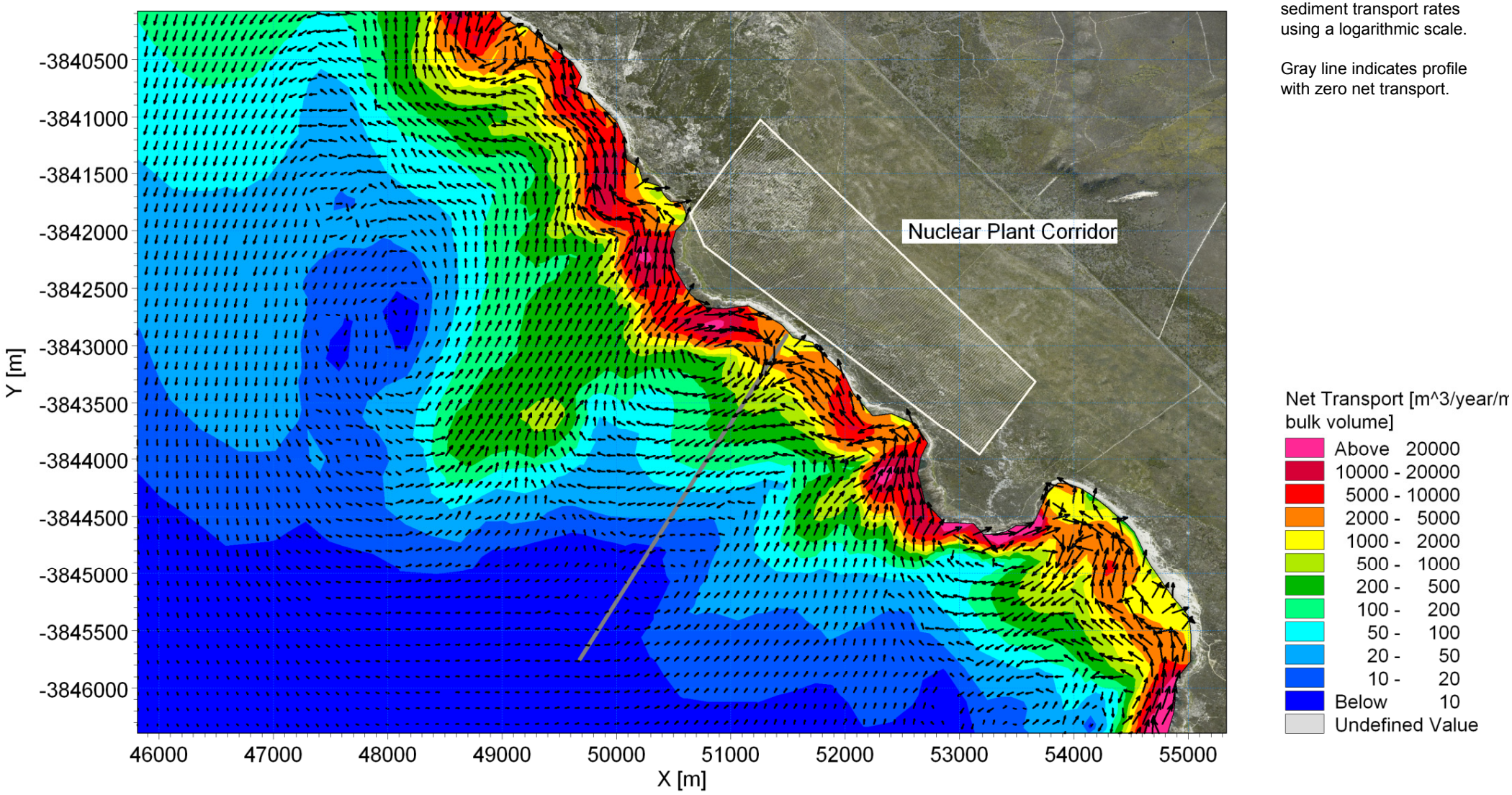

Title: **Sediment transport modelling: Potential net sediment transport rate. Layout 1: Offshore tunnel intake and offshore tunnel outfall. D_{50} = 0.2 mm Detailed view.**

Figure No. **10.6**

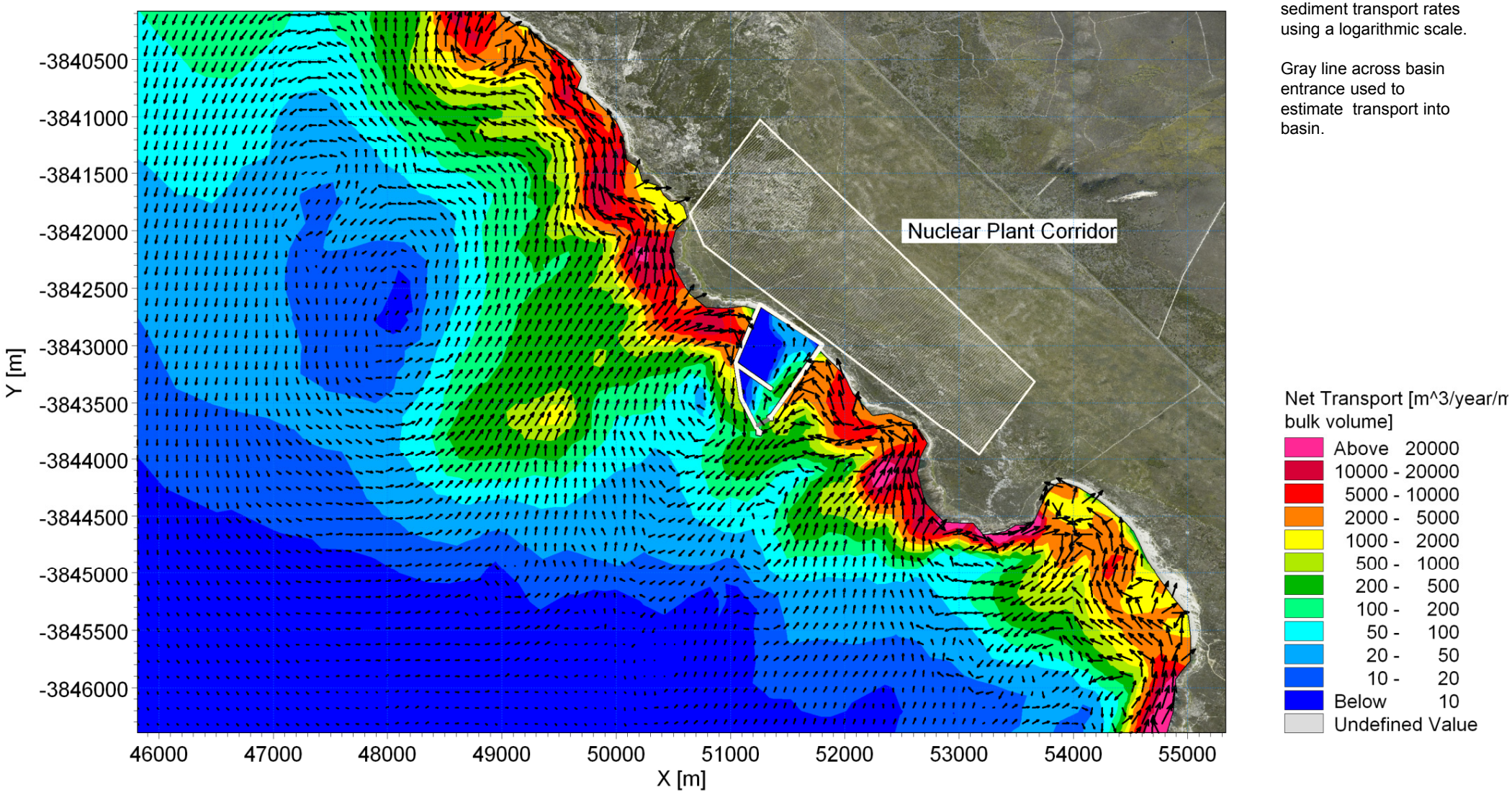

Both contour scale and vector length show sediment transport rates using a logarithmic scale.

Gray line across basin entrance used to estimate transport into basin.

G:\Projects\1010_NuclearSites\Bantamsklip\Models\Sediment2D\221b\Postprocess\AnnualTransport_Zoom.png

Title: **Sediment transport modelling: Potential net sediment transport rate. Layout 2: Basin intake and offshore tunnel outfall. D_{50} = 0.2 mm Detailed view.**

Figure No. **10.7**

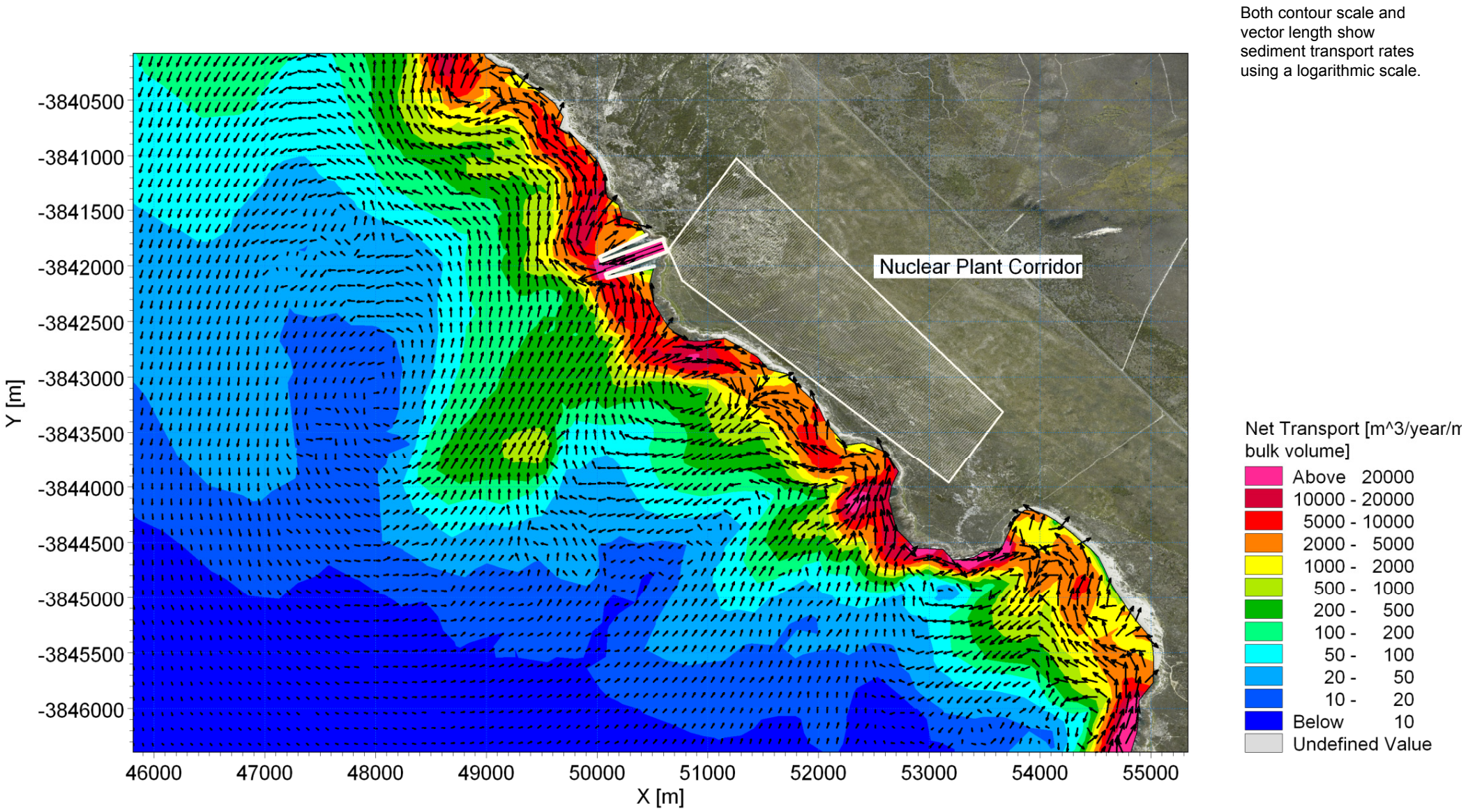

Title: **Sediment transport modelling: Potential net sediment transport rate. Layout 5: Offshore tunnel intake and nearshore channel outfall. D_{50} = 0.2 mm Detailed view.**

Figure No. **10.8**

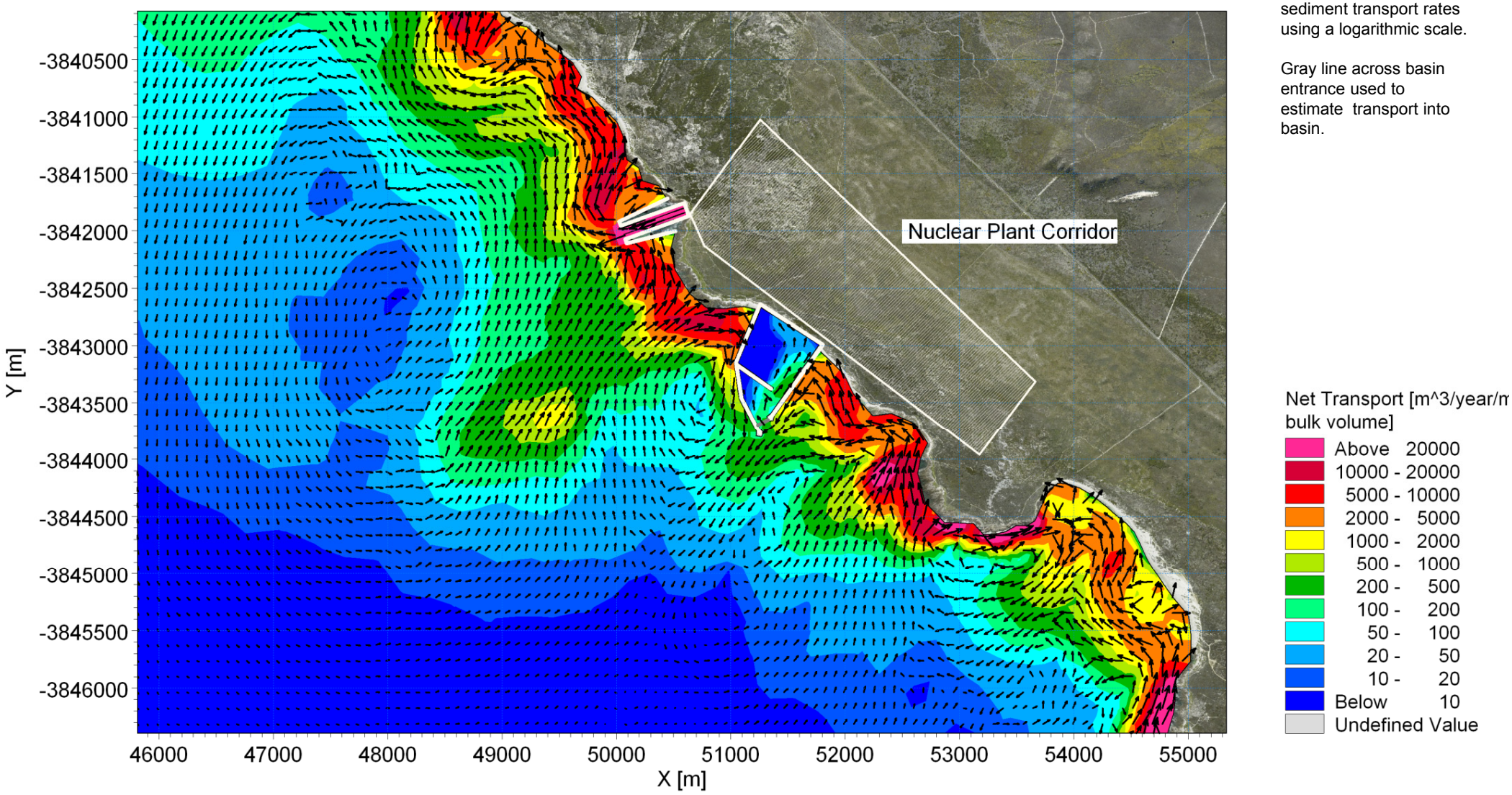

	Title: **Sediment transport modelling: Potential net sediment transport rate. Layout 6: Basin intake and nearshore channel outfall. D_{50} = 0.2 mm Detailed view.**	**Figure No.** **10.9**

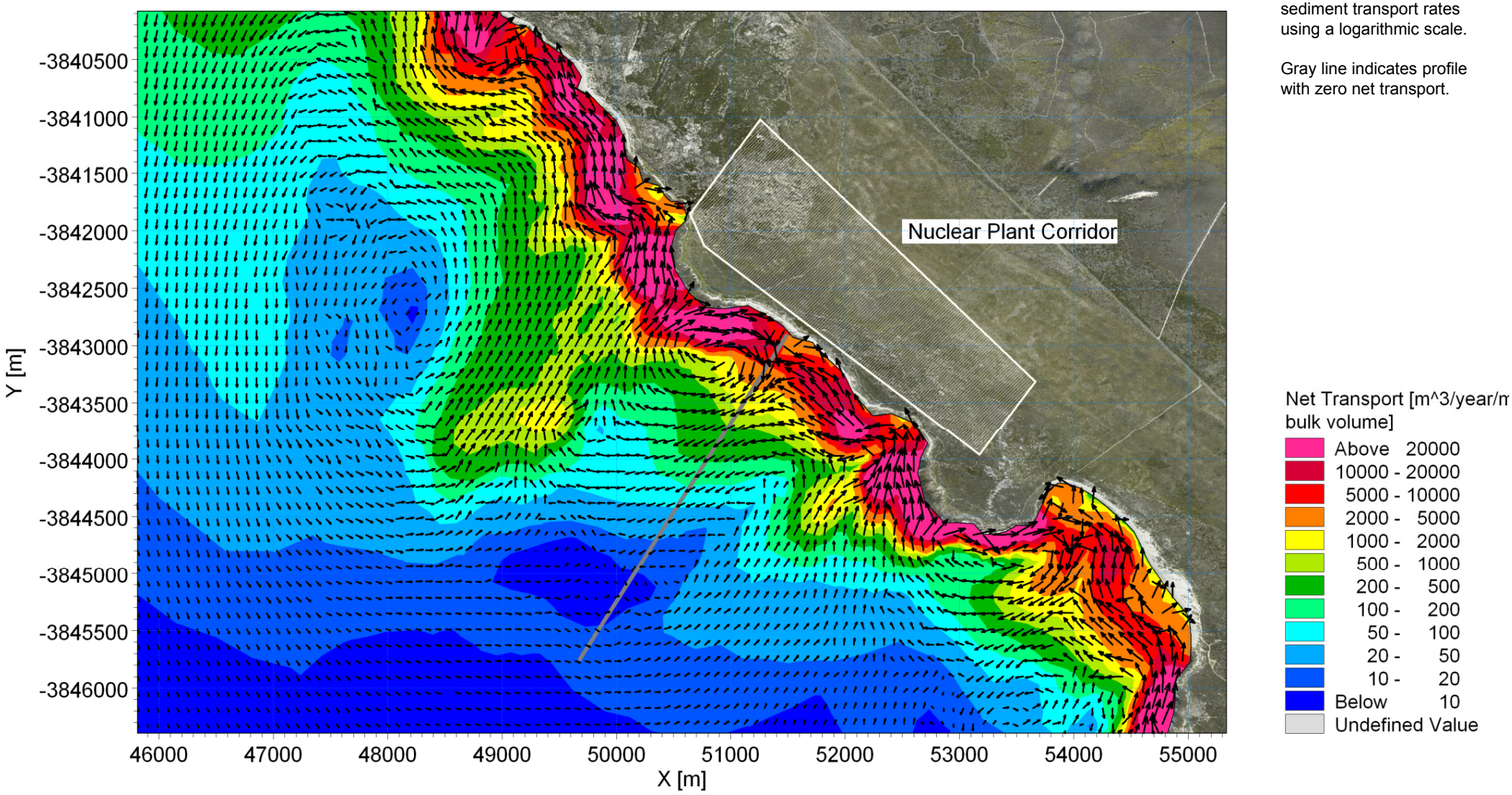

Both contour scale and vector length show sediment transport rates using a logarithmic scale.

Gray line indicates profile with zero net transport.

G:\Projects\1010_NuclearSites\Bantamsklip\Models\Sediment2D\100a\Postprocess\AnnualTransport_Zoom.png

Title: **Sediment transport modelling: Potential net sediment transport rate. Layout 1: Offshore tunnel intake and offshore tunnel outfall. D_{50} = 0.15 mm Detailed view.**

Figure No. **10.10**

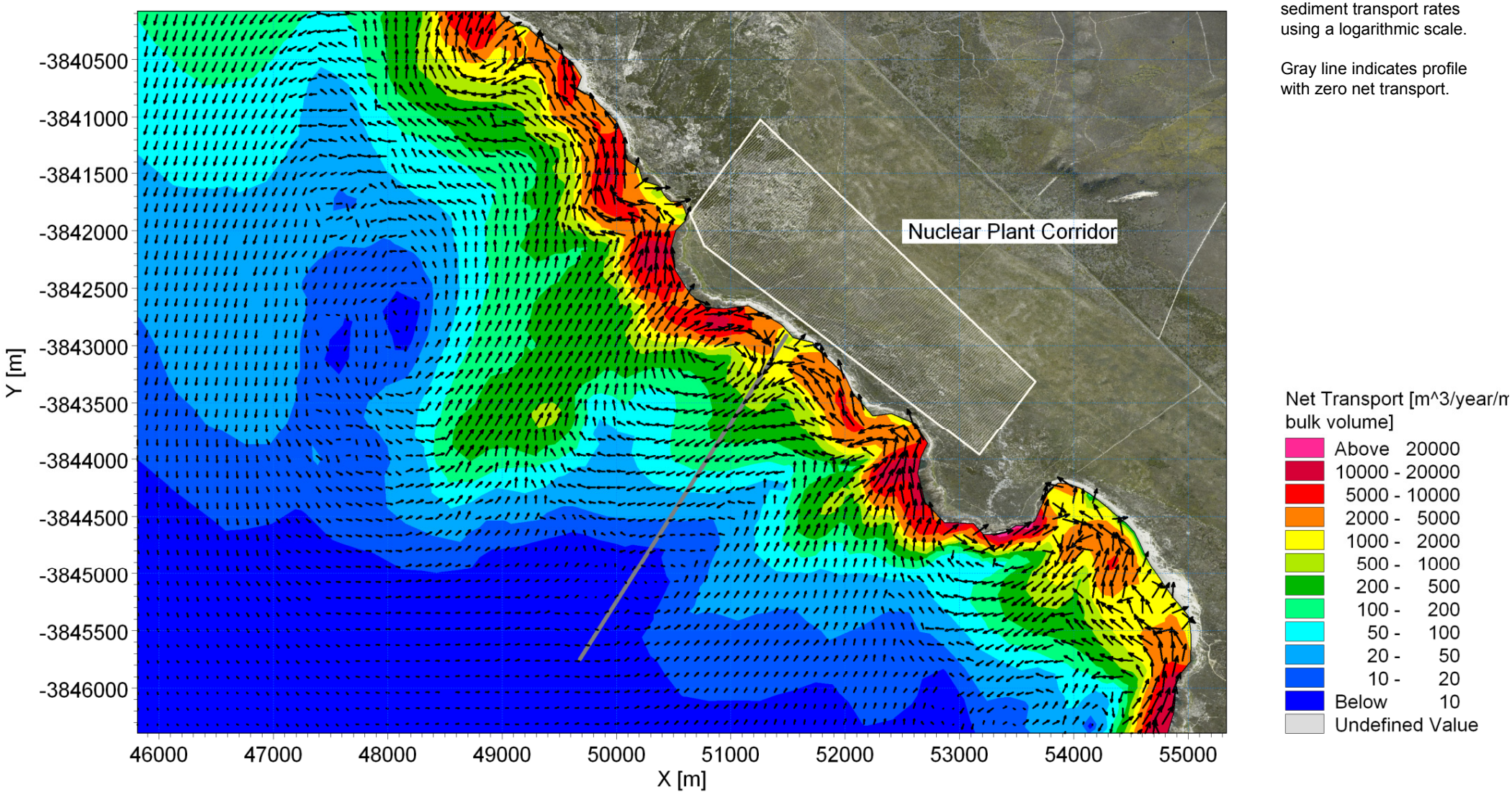

	Title: **Sediment transport modelling: Potential net sediment transport rate. Layout 1: Offshore tunnel intake and offshore tunnel outfall. D_{50} = 0.3 mm Detailed view.**	**Figure No.** **10.11**

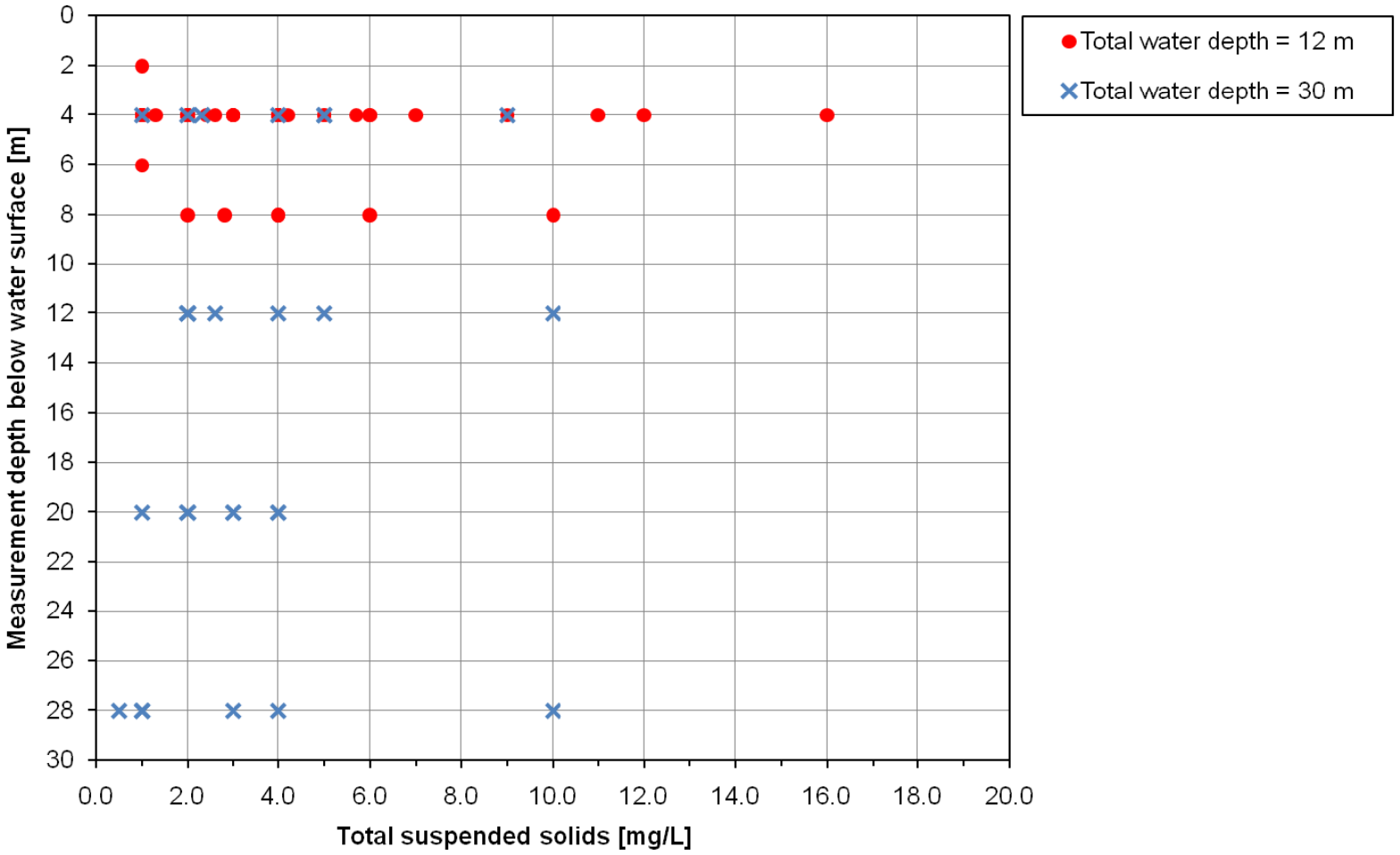

	Title: **Measured total suspended solids.**	**Figure No.** **10.12**

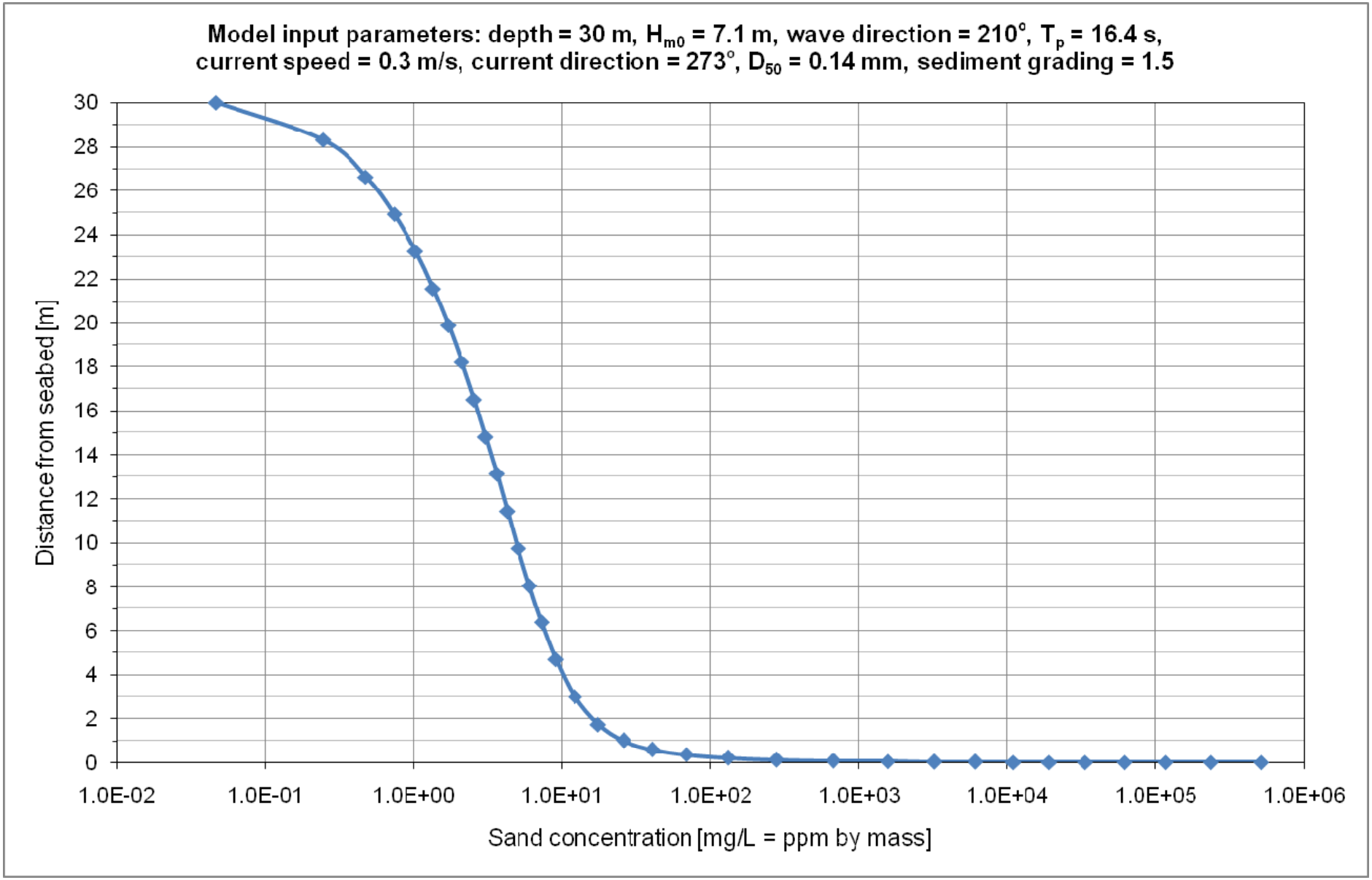

	Title: **Example of modelled vertical profile of suspended sand concentration.**	**Figure No.** **10.13**